

**PRODUCTION AND CHARACTERISATION  
OF HYDROXYAPATITE / MULTI-WALLED  
CARBON NANOTUBE COMPOSITES**

**Ashley Ann White**



**Clare College**

**University of Cambridge**

November 2009

**A thesis submitted for the degree of**

***Doctor of Philosophy***



# PREFACE

This thesis is the result of my own work and includes nothing which is the outcome of work done in collaboration, except where specifically indicated in the text and acknowledgements. The research was conducted at the Department of Materials Science and Metallurgy at the University of Cambridge between October 2005 and October 2009, under the supervision of Prof. Serena Best. This thesis is not substantially the same as any that I have submitted for a degree or diploma or other qualification at any other university. No part of this thesis has already been or is being concurrently submitted for any such degree, diploma or other qualification.

In accordance with the Degree Committee of the Faculty of Physics and Chemistry, this dissertation does not exceed 60,000 words.

Ashley White

November 2009



*To Bogdan Wojtsekhowski, for believing that high school students have better things to do than measure the dimensions of 1000 lead glass bricks,*

*and*

*To Michael Ayers, for giving me the opportunity to spend the coldest summer of my pre-Cambridge life playing with the coolest material in the world.*



# ACKNOWLEDGEMENTS

I would like to thank many people for their support and assistance with this research and in preparing this report. Firstly, thank you to my supervisor, Serena Best, and my advisors, Ian Kinloch and Alan Windle, for their continued support over these four years. I am particularly grateful to Serena for her tireless assistance in the final stages of writing the thesis.

Many thanks must go to all my group members, past and present – anyone for whom I've made a birthday cake – and to all the technicians who have provided equipment training and fixed all the things I've broken over the years. Particular thanks must go to Dominik Eder for many useful discussions, and to Jennifer Shepherd and Marcelo Motta for assistance in revising the thesis, among other things. I would also like to acknowledge the assistance of Sebastian Pattinson and Ian Kinloch in providing transmission electron microscopy images.

I would like to recognise the organisations which provided me Ph.D. funding – the Marshall Aid Commemoration Commission, the Cambridge Overseas Trust, and the National Science Foundation.

Finally, thank you to my parents, particularly my mother, for giving me a goal to strive towards. And thank you to Jack Dudley and many others at Virginia Tech who made it possible for me to do and accomplish more in the last nine years than I imagined I'd do in a lifetime.



# ABSTRACT

Hydroxyapatite (HA) is a biologically active ceramic that is used in surgery to replace bone. While HA promotes bone growth along its surface, its mechanical properties are not sufficient for major load-bearing medical devices. Carbon nanotubes (CNTs), as one of the strongest and stiffest materials available, have the potential to strengthen and toughen HA, thus expanding the range of clinical uses for the material. Furthermore, studies have suggested that the nanotubes themselves possess some bioactive properties. This work sought to develop and characterise HA-CNT composites in four main areas: 1) production and characterisation of green materials, 2) investigation of appropriate sintering atmospheres, 3) evaluation of mechanical properties, and 4) assessment of biological response to *in vitro* cell culture.

HA was synthesised by a precipitation reaction between  $\text{Ca(OH)}_2$  and  $\text{H}_3\text{PO}_4$ , and multi-walled CNTs were produced by chemical vapour deposition. Composites were produced by adding the CNTs to the  $\text{Ca(OH)}_2$  solution as the HA was precipitating. Both as-made (nCNTs) and acid-treated CNTs (fCNTs) were used to make composites with loadings of 0.5 – 5 wt.% CNTs. The resulting slurry was shear mixed and then processed to make a powder. The powder was then uniaxially pressed into tablets of ~45% theoretical density. Characterisation of the green material with XRD and FTIR found that the primary phase was HA which was well hydroxylated. The powder particles were found to have a bimodal size distribution, and all materials had similar surface areas, as determined by BET. Composites made with fCNTs were found to have a better dispersion of CNTs in the HA matrix and better interaction between the HA and CNTs compared with nCNT composites.

CNTs oxidise at the high temperatures needed to sinter HA, yet water is necessary to prevent dehydroxylation and decomposition of the HA. Using 5 wt.% fCNT composite, fourteen sintering atmospheres were investigated to determine their effect on phase purity, hydroxylation, sintered density, and remaining CNT content after sintering. An atmosphere of  $\text{CO} + \text{H}_2$  bubbled through ice water resulted in optimal properties. Additionally, it was found that increasing the gas flow rate and the number of samples sintered in one batch increased CNT retention. However, this came at the expense of the density of the sintered samples, as composites with a higher CNT content were more porous.

To optimise the composite microstructure for mechanical studies, six different sintering time / temperature profiles were examined to determine their effect on density (balanced with CNT retention) and grain size. HA and both nCNT and fCNT composites with CNT loadings of 0.5, 1, 2 and 5 wt.% were produced using the optimised atmosphere and profile, and then tested to determine tensile strength (using diametral compression) and hardness, and to look for evidence of toughening. It was found that CNTs had little reinforcing effect; instead, mechanical behaviour results were mainly attributed to differences in porosity, due at least in part to the CNTs' presence.

The *in vitro* cellular response to the materials was examined by culturing human osteoblast-like cells on HA and nCNT (0.88 wt.%) and fCNT (3.3 wt.%) composites for 12 days. Cells were found to attach and grow well on HA and the nCNT composite, with slightly enhanced response on the composite. The fCNT composite, on the other hand, showed a decrease in cell viability between days 1 and 12. These results were mainly attributed to the effects of a lower local pH due to remnant acid on the fCNTs and differences in material characteristics, such as CNT loading and surface roughness.

This systematic study of the production and properties of HA-CNT composites has resulted in improved understanding of the production and processing of these materials and the effects of a wide range of sintering atmospheres on their characteristics. Additionally, it has yielded interesting preliminary results of their mechanical reinforcement potential and biological behaviour.



# TABLE OF CONTENTS

<b>PREFACE.....</b>	<b>III</b>
<b>ACKNOWLEDGEMENTS.....</b>	<b>VII</b>
<b>ABSTRACT .....</b>	<b>IX</b>
<b>TABLE OF CONTENTS.....</b>	<b>XI</b>
<b>LIST OF ABBREVIATIONS.....</b>	<b>XVII</b>
<b>1 INTRODUCTION AND AIMS.....</b>	<b>1</b>
<b>2 LITERATURE REVIEW .....</b>	<b>4</b>
2.1 Bone replacement materials.....	4
2.1.1 Bone structure .....	5
2.1.2 Natural replacement materials .....	6
2.1.3 Synthetic replacement materials .....	6
2.2 Hydroxyapatite.....	7
2.2.1 Structure and properties.....	7
2.2.2 Synthesis methods.....	9
2.2.3 Processing and heat treatment.....	10
2.2.4 Improving hydroxyapatite.....	12
2.3 Carbon nanotubes .....	13
2.3.1 Structure and properties.....	13
2.3.2 CNT synthesis .....	15
2.3.3 CNT functionalisation .....	16
2.3.4 Biological properties .....	18
2.4 Ceramic composites .....	20
2.4.1 Composite Mechanics.....	21

2.4.2	HA composites.....	22
2.4.3	Ceramic-CNT composites.....	25
2.4.4	HA-CNT composites.....	28
2.5	Summary and project design.....	36
<b>3</b>	<b>PREPARATION, PROCESSING AND CHARACTERISATION OF GREEN MATERIALS.....</b>	<b>37</b>
3.1	Material synthesis.....	38
3.1.1	Hydroxyapatite synthesis.....	38
3.1.2	Carbon nanotube synthesis.....	39
3.1.3	Composite synthesis.....	41
3.1.4	Tablet formation.....	42
3.2	Material characterisation methods.....	43
3.2.1	Physical characterisation.....	43
3.2.2	Physicochemical characterisation.....	45
3.2.3	Electron microscopy.....	46
3.3	Material characterisation results.....	47
3.3.1	Carbon nanotube characterisation.....	47
3.3.2	Physical properties.....	54
3.3.3	Physicochemical properties.....	62
3.3.4	Tablet characteristics.....	68
3.4	Summary.....	70
3.4.1	Material synthesis.....	70
3.4.2	Material characterisation.....	70
<b>4</b>	<b>INVESTIGATION OF SINTERING ATMOSPHERES.....</b>	<b>72</b>
4.1	Background.....	73
4.1.1	CNT oxidation.....	73

4.1.2	HA dehydroxylation and decomposition .....	73
4.1.3	The water-gas reaction: A compromise? .....	77
4.2	Behaviour in standard atmospheres.....	79
4.2.1	CNT behaviour .....	79
4.3	Atmosphere investigations .....	82
4.3.1	Experimental methods.....	82
4.3.2	Characterisation Methods .....	83
4.3.3	Results.....	86
4.3.4	Physical properties.....	92
4.3.5	The white layer phenomenon.....	105
4.3.6	Choosing an atmosphere for further study .....	109
4.4	Optimisation of sintering conditions.....	111
4.4.1	Methods .....	112
4.4.2	Results.....	112
4.5	Summary .....	115
<b>5</b>	<b>PRELIMINARY ASSESSMENT OF MECHANICAL PROPERTIES.....</b>	<b>118</b>
5.1	Background .....	118
5.1.1	Properties influencing mechanical behaviour .....	118
5.1.2	Measurement techniques for fracture strength and toughness .....	120
5.1.3	Theory of mechanical testing techniques used.....	121
5.2	Methods .....	125
5.2.1	Optimisation of sintering profile.....	125
5.2.2	Mechanical testing.....	126
5.3	Results.....	128
5.3.1	Optimisation of sintering profile.....	128
5.3.2	Mechanical testing.....	133

5.3.3	Fracture surfaces.....	139
5.4	Discussion.....	141
5.4.1	Effect of sintering profile on phase purity and hydroxylation.....	141
5.4.2	Effect of sintering profile on CNT loss .....	141
5.4.3	Effect of sintering profile on density.....	142
5.4.4	Mechanical properties.....	143
5.5	Summary .....	145
<b>6</b>	<b>IN VITRO STUDIES .....</b>	<b>147</b>
6.1	Background .....	147
6.1.1	Stages of cellular growth .....	147
6.1.2	Proliferation assays .....	148
6.1.3	Influence of material characteristics on cellular response .....	149
6.2	Methods .....	150
6.2.1	Sample preparation.....	150
6.2.2	Cell seeding .....	151
6.2.3	Cell proliferation by alamarBlue assay.....	152
6.2.4	Cell proliferation by CyQUANT assay.....	153
6.2.5	Statistical analysis.....	153
6.3	Results.....	154
6.3.1	alamarBlue assay .....	154
6.3.2	CyQUANT assay .....	156
6.3.3	Material characterisation.....	158
6.4	Discussion.....	162
6.4.1	Comparison of alamarBlue and CyQUANT results .....	162
6.4.2	Possible role of CNT-dye and CNT-culture medium interactions .....	162
6.4.3	Possible role of catalyst residues .....	163

6.4.4	Possible role of CNT-induced pH changes .....	163
6.4.5	Possible role of material characteristics.....	164
6.4.6	Additional observations .....	165
6.5	Summary .....	166
<b>7</b>	<b>CONCLUSIONS.....</b>	<b>168</b>
<b>8</b>	<b>FUTURE OUTLOOK.....</b>	<b>171</b>
8.1	Improvement through better CNTs.....	171
8.2	Heat treatment techniques .....	172
8.3	Mechanical properties .....	172
8.4	Biological properties .....	173
	<b>REFERENCES .....</b>	<b>175</b>
	<b>PUBLISHED PAPERS</b>	



# LIST OF ABBREVIATIONS

BET	Brunauer-Emmett-Teller
CMC	Ceramic matrix composite
CNT	Carbon nanotube
CTE	Coefficient of thermal expansion
CVD	Chemical vapour deposition
DIW	Deionised water
fCNT	Functionalised carbon nanotube
FTIR	Fourier transform infrared spectroscopy
HA	Hydroxyapatite
HIP	Hot isostatic pressing
MWNT	Multi-walled carbon nanotube
nfCNT	Non-functionalised carbon nanotube
SDT	Simultaneous DSC/TGA
SEM	Scanning electron microscope/microscopy
SPS	Spark plasma sintering
SWNT	Single-walled carbon nanotube
TCP	Tricalcium phosphate
TD	Theoretical density
TEM	Transmission electron microscope/microscopy
TGA	Thermogravimetric analysis
TTCP	Tetracalcium phosphate
XRD	X-ray diffraction



# 1 INTRODUCTION AND AIMS

The development and improvement of synthetic materials for *in vivo* biological applications is highly desirable as an alternative to allografts and autografts. Hydroxyapatite (HA) has been widely investigated as a bone replacement material due to its biologically active characteristics stemming from its chemical similarity to the mineral component of bone. While HA has the ability to promote bone growth along its surface, its mechanical properties, particularly its strength and toughness, are insufficient for major load-bearing applications. Reinforcing HA with a second phase offers a possibility to overcome these limitations.

An ideal reinforcing material would provide mechanical integrity to the composite without negatively impacting its biological properties. Carbon nanotubes (CNTs), considered one of the strongest and stiffest materials available, have excellent potential to accomplish this. As high aspect ratio fibres of nanoscale diameters (1-100 nm) and microscale lengths (0.001-6 mm), CNTs have a large surface area over which to interact with a matrix material. Furthermore, the surface of the CNTs can be functionalised to improve that interaction.

Already, CNTs have shown potential for reinforcing polymers, and to some degree metals and ceramics, as well. Several publications have addressed HA-CNT composites, specifically, but studies thus far have lacked a cohesive view of all aspects of the composites, which encompass production, processing, densification techniques, mechanical behaviour, and biological behaviour. Special attention must be given to the biological impact of the CNTs' presence, as current research is conflicting as to whether CNTs might induce a cytotoxic response or perhaps even improve cellular processes.

This study sought to investigate HA / multi-walled CNT composites in four main areas, with the following objectives in mind:

- 1) Production and characterisation of green materials
  - a. Techniques for combining HA and CNTs
  - b. Effect of CNT functionalisation on the homogeneity of the composite and CNT interaction with the HA matrix

- c. Characterisation of the green (unsintered) powders, including phase purity, hydroxylation, surface area, and particle size
  - d. Characterisation of uniaxially-pressed green tablets, including appearance and density
- 2) Investigations of sintering atmospheres
- a. Understanding the processes of CNT oxidation and HA dehydroxylation and decomposition in a range of sintering atmospheres
  - b. Characterisation of materials sintered in different atmospheres, including phase purity, hydroxylation, density, CNT loading / loss, and appearance
  - c. Effect of sintering gas flow rate, sample number, and sample type on the properties of sintered composites
- 3) Evaluation of mechanical properties
- a. Optimisation of sintering profile to yield materials expected to give optimal mechanical properties
  - b. Characterisation of sintered materials containing both as-made and functionalised CNTs with a range of loadings, including phase purity, hydroxylation, density, and CNT loading / loss
  - c. Testing of tensile strength (by diametral compression), hardness, and toughness (by indentation crack length) of both HA and composites
- 4) Preliminary investigation of biological response using *in vitro* cell culture
- a. Effect of both as-made and functionalised CNTs on human osteoblast-like response
  - b. Influence of other material characteristics on cell response

This dissertation begins with an overview of literature (Chapter 2) on bone replacement materials, particularly HA, as well as CNTs, before considering in more depth HA composites, ceramic-CNT composites, and HA-CNT composites. Chapters 3 through 6 address the four primary objectives outlined above. Chapter 3 provides the methods used to synthesise green HA and the composites, the techniques used to characterise these materials, and the characterisation results. Chapter 4 begins with background information about CNT and HA behaviour at high temperatures before moving into the experimental section, which details the investigation of fourteen sintering atmospheres. The methods

and results of investigations to optimise the sintering profile, based on the resulting microstructure, are detailed in Chapter 5. The chapter then moves forward to describe the mechanical properties of the HA and composites of various loadings. Chapter 6 then covers some preliminary studies of *in vitro* cell culture work on sintered materials. Finally, Chapter 7 brings together the results of Chapters 3 through 6 to provide some conclusions, and Chapter 8 provides suggestions for future study of HA-CNT composites.

## **2 LITERATURE REVIEW**

The purpose of this literature survey is to give a broad background relating to bone replacement materials (particularly HA), CNTs, and ceramic-matrix composites, along with a more in-depth examination of recent publications on HA-CNT composites. Detailed information relating to processing techniques and characterisation; heat treatment chemistry, thermodynamics, and kinetics; mechanical property-structure relationships and testing techniques; and biological techniques and characterisation will be included in the relevant experimental chapters (3-6).

This review first covers the nature of bone and the types of materials currently in use and under development that can replace bone and aid in its repair. As one of the most promising synthetic materials and a main component of this research project, an overview of HA comprises the next section. Background on CNTs, the filler material chosen to reinforce hydroxyapatite to make a composite material in this study, is then given. Next, the properties of ceramic-matrix composites are discussed, with particular emphasis on their mechanical properties. A more in-depth look is then taken at recent literature on ceramic-matrix composites using CNTs for reinforcement, with a particular focus on work done thus far on HA-CNT composites. The final section summarises some of the gaps in current understanding of HA-CNT composites, which has largely served to outline the goals of this Ph.D. work.

### ***2.1 Bone replacement materials***

Bone is the hard connective tissue that forms the rigid skeleton of most vertebrate animals. Its main functions are to physically support the body, protect internal organs, and aid in cell formation, calcium metabolism, and mineral storage. While it is known for its ability to regenerate after disease or injury, bone replacement materials can be used to aid in this process, providing mechanical support as the bone is remodelled and providing an additional source of chemical elements which the body can use to heal more quickly. In some situations, involving the injury or disease of a large amount of bone, it may be more practical to use a substitute material that will remain permanently intact in the body. In this case, adoption by the surrounding tissue, rather than regeneration, is the main goal.

For this to succeed, the implant should be as structurally, chemically, and mechanically similar to the bone it is replacing as possible.

### 2.1.1 Bone structure

Bone is a composite material, consisting of 10% water, 20% organic material, and 70% mineral matter, by weight (Shi *et al.* 2006). The organic component consists mainly of type I collagen fibrils a few nanometres in diameter. The remainder of the organic material is made up of a cement-like substance and a cellular component, comprised of osteocytes, osteoblasts, and osteoclasts, which aid in dissolution, deposition, and nourishment of the bone, respectively. The inorganic, mineral component is a calcium-deficient carbonate-substituted apatite containing calcium and phosphate ions, similar in structure and composition to HA ( $\text{Ca}_{10}(\text{PO}_4)_6(\text{OH})_2$ ) (LeGeros *et al.* 1993).

Figure 2.1 (Lakes 1993) shows the hierarchical structure of bone. Bone mineral crystals are arranged between the ends of collagen fibrils, which are then arranged into sheets called lamellae. The morphology of the mineral crystals is generally agreed to be plate-like, with dimensions on the scale of 10s to 100s of angstroms. The collagen lamellae are either arranged in concentric circles, called tubular Haversian systems, or in sheets. These sheets form the spongy cancellous (trabecular) bone found inside the structure and at bone ends. The Haversian system configuration, on the other hand, leads to the dense, cortical form of bone, which comprises 80% of bone mass and surrounds the cancellous bone.

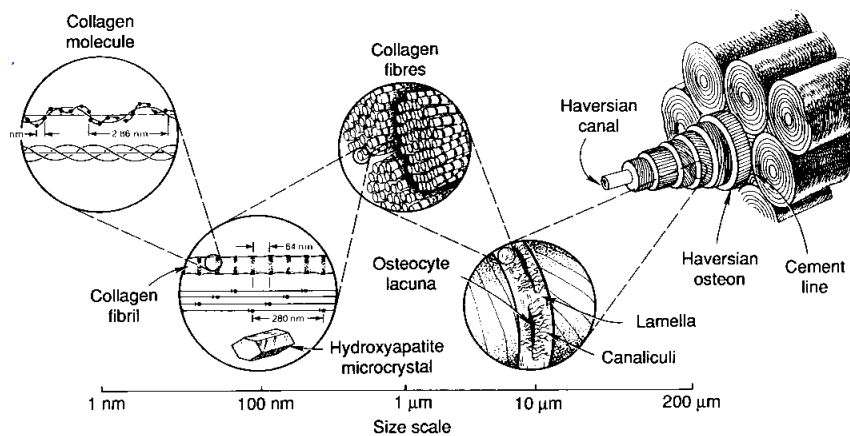


Figure 2.1: Hierarchical structure of bone (Lakes 1993).

### **2.1.2 Natural replacement materials**

When bone is lost due to injury or illness, bone grafts are introduced to perform both a mechanical and biological role, serving to restore skeletal integrity, fill voids, and enhance bone repair. As of the year 2000 more than 2.2 million bone graft procedures were being performed annually worldwide. Ninety percent of these procedures used natural bone from autografts (the patient's own bone) or allografts (from a cadaver), while only 10% used synthetic materials (Lewandrowski *et al.* 2000).

Natural bone is the optimal replacement choice, as it carries with it the entire bone structure, consisting of both inorganic and organic components, but there are serious drawbacks to using it in bone graft procedures. Autografts involve a second incision to harvest the replacement tissue. This requires additional healing at the donation site and can involve long-term post-operative pain. Allografts carry with them the risk of viral infection, immune system rejection, and resorption due to immunological responses. Additionally, donor material is not always readily available. It is for these reasons that the development of suitable synthetic materials is desirable.

### **2.1.3 Synthetic replacement materials**

Synthetic materials are an increasingly popular alternative to natural replacement materials. However, no existing synthetic material can effectively mimic both the biological and mechanical properties of natural bone. Synthetic materials currently used and under development include polymers, metals, and ceramics, and cover a wide range of bioaffinities, from the so-called 'bioinert' to bioresorbable. At one end of the spectrum, the body reacts to bioinert materials (perhaps better termed 'biologically inactive', as suggested by Hench (1991)), such as alumina, by producing a fibrous capsule around the implant. As the body offers no means of chemical bonding, bioinert materials must attach to bone with cement or through bone growth into surface irregularities of the material. At the other end of the spectrum, bioresorbable materials, such as tricalcium phosphate (TCP), degrade over time and are slowly replaced by natural tissue. While bioresorbable materials would seem ideal in many ways, the degradation process can adversely affect the mechanical integrity of the material and the stability of the biomaterial/natural tissue

interface, thus compromising the implant-bone system during the resorption and replacement process. It is also difficult to match the resorption rate of the biomaterial to the repair rate of the body tissue. Bioactive materials, as intermediate between the two extremes, elicit a biological response at the material interface and bond with the surrounding tissue, yet avoid degradation. For load-bearing implants intended to remain intact in the body for extended periods of time, this class of synthetic replacement materials should be promising. Bioactive ceramics include bioactive glasses (*e.g.* Bioglass<sup>®</sup>), bioactive glass-ceramics (*e.g.* A-W glass ceramic), and HA, the matrix material of choice for this study.

## 2.2 Hydroxyapatite

HA is very similar in composition to the mineral phase of bone, and is thus, chemically, an excellent material to use in bone replacement materials. Clinically, it has been used in dental and orthopaedic applications in bulk form, as a filler, and as a coating for more than 30 years (Suchanek *et al.* 1998). However, poor mechanical properties have thus far prevented it from being used in major load-bearing devices.

### 2.2.1 Structure and properties

HA is a polycrystalline calcium phosphate ceramic with a hexagonal crystal structure (Figure 2.2). It is part of the  $P6_3/m$  space group, characterised by a six-fold c-axis perpendicular to three equivalent a-axes at  $120^\circ$  angles to each other. Calcium cations ( $Ca^{2+}$ ) and phosphate anions ( $PO_4^{3-}$ ) are arranged around columns of monovalent hydroxyl anions (OH) (Posner *et al.* 1958; Kay *et al.* 1964). It is this network of phosphate groups that provides the skeletal framework and gives the structure its stability.

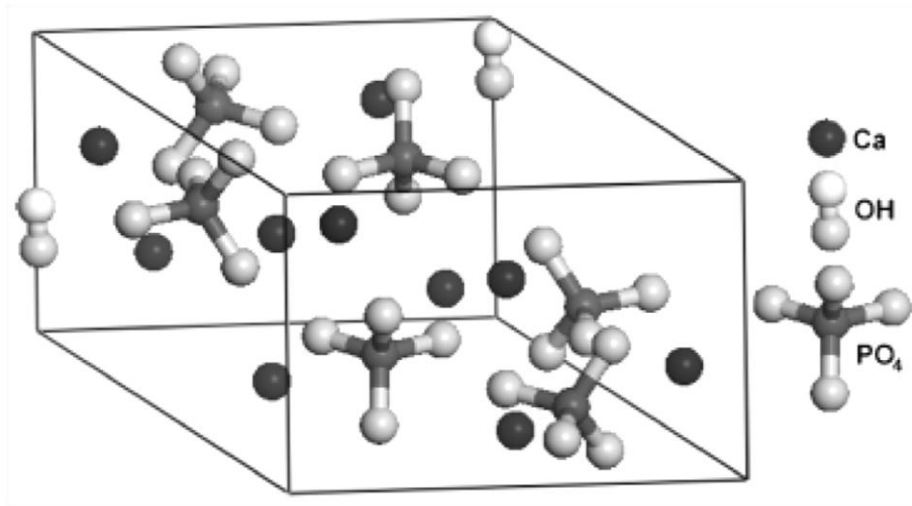


Figure 2.2: Unit cell of hydroxyapatite (Chappell 2006).

HA's composition and crystal structure, being similar to that of the mineral component of bone, are the most important factors to its *in vitro* biological response. Best *et al.* (1997) identified four factors that influence cellular response: 1) Ca/P ratio, 2) trace element impurities, 3) ceramic handling properties, and 4) sintering characteristics. In particular, the bioactivity of the ceramic is very sensitive to the Ca/P ratio. Synthesis conditions, such as pH and reaction rate, and sintering conditions can affect the Ca/P ratio. Stoichiometric HA has a Ca/P of 1.67 and is characterised as 'bioactive', as it forms a stable bond of carbonated apatite at the HA/bone interface through a process of dissolution, precipitation, and ion exchange. *In vivo* studies have confirmed this bond, showing that failure typically occurs in the bone or HA, but not at the HA/bone interface (Hong *et al.* 1992).

While HA has excellent bioactivity, its poor mechanical properties compared with bone have hindered its use in clinical applications. Dense HA has a compressive strength four times that of cortical bone, yet a significantly lower tensile strength and fracture toughness (Table 2.1). It must be noted, however, that even among studies of dense, phase-pure HA, the values reported for mechanical properties vary widely due to differences in sample preparation and measurement techniques. Even with this consideration, HA does not match the mechanical behaviour of natural bone and thus cannot be used in major load-bearing applications in its present form. Additionally, it is

worth noting that the Young's modulus of HA far exceeds that of cortical bone. This may be a concern, as a phenomenon known as 'stress shielding' prevents bone from being loaded properly when it is in contact with an implant material of higher elastic modulus. In this case, the implant takes most of the load and, as a result, the surrounding bone tissue remodels itself with weaker mechanical properties. This can, in turn, cause a breakdown in the implant material-bone interface, resulting in the mechanical failure of the implant-bone system.

Table 2.1: Mechanical properties of bone and hydroxyapatite.

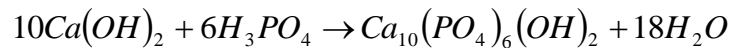
	<b>Cortical Bone</b>	<b>Cancellous Bone</b>	<b>Dense HA</b>
Compressive strength (MPa)	100-230	2-12	430-920 <sup>a-c</sup>
Flexural/Tensile strength (MPa)	50-150	10-20	17-110 <sup>b-e</sup>
Fracture toughness (MPa·m <sup>1/2</sup> )	2-12	NA <sup>*</sup>	1 <sup>a,f</sup>
Young's modulus (GPa)	7-25	0.5-4	108-117 <sup>a</sup>

<sup>\*</sup>NA = not available in the literature; a (deWith *et al.* 1981); b (Denissen *et al.* 1985); c (Jarcho *et al.* 1976); d (Akao *et al.* 1981); e (Wang, P. E. *et al.* 1993); f (vanAnduyt *et al.* 1995). Values for bone are typical of those reported in literature.

### 2.2.2 Synthesis methods

Several methods for synthesising HA have been employed over the past few decades. One of the first techniques was to hydrothermally produce HA by exposing fluorapatite (Ca<sub>10</sub>(PO<sub>4</sub>)<sub>6</sub>F<sub>2</sub>) to high pressures and temperatures (Levitt *et al.* 1969). Other methods include the hydrothermal exchange of coral (Roy *et al.* 1974), solid state reaction between TCP and tetracalcium phosphate (TTCP) or TCP and CaO, and wet chemical methods, including aqueous precipitation (Clark 1955; Hayek *et al.* 1963; Akao *et al.* 1981), hydrolysis (LeGeros 1974), and sol-gel processing (Gross *et al.* 1998; Jillavenkatesa *et al.* 1998; Weng *et al.* 1998; Liu, D. M. *et al.* 2001; Bezzi *et al.* 2003; Vijayalakshmi *et al.* 2006).

By far the most common and simplest method to produce large quantities of HA is by aqueous precipitation. This technique involves a wet chemical reaction between calcium and phosphate precursors under controlled temperature and pH. Typical precursors include diammonium hydrogen phosphate ((NH<sub>4</sub>)<sub>2</sub>HPO<sub>4</sub>) with calcium nitrate (Ca(NO<sub>3</sub>)<sub>2</sub>); calcium carbonate (CaCO<sub>3</sub>) with orthophosphoric acid (H<sub>3</sub>PO<sub>4</sub>); and calcium hydroxide (Ca(OH)<sub>2</sub>) with H<sub>3</sub>PO<sub>4</sub>. The last reaction proceeds as shown below:



In order to make a stoichiometric product and help to ensure HA's bioactive properties, the relative amounts of reactants must be carefully measured to give a Ca/P ratio of 1.67. Other important parameters include the rate at which the acid is added and the pH of the reaction. The pH for this reaction must be kept above 10.5 by the addition of ammonium hydroxide solution (Bouyer *et al.* 2000). In the case of Ca(OH)<sub>2</sub> and H<sub>3</sub>PO<sub>4</sub>, if the acid solution is added too quickly, the pH drops below the dissociation constant, leading to incomplete dissociation of H<sub>3</sub>PO<sub>4</sub> and a calcium-deficient HA (Osaka *et al.* 1991; Bouyer *et al.* 2000). Using the same precursors, Bouyer *et al.* found that the temperature of the reaction was critical to the morphology and surface area of the final product, with low temperatures (35°C) giving a needle-like morphology and high surface area, and high temperatures (80°C) giving more spherical crystals and a lower surface area, while Osaka *et al.* found that a lower temperature also yielded smaller crystals.

### 2.2.3 Processing and heat treatment

Once a suspension of HA particles is created from a wet chemical reaction, it is generally filtered and the resulting filter cake processed. A common method by which to do this is to dry and grind the cake into a powder. It has been shown that the final sintered product is dependent on the quality of the initial powder. Some important factors in powder processing are the fineness of the powder, its surface area, the shape of the particles, and their size distribution. Smaller particles have been shown to promote sintering and spherical particles have been shown to enhance processing by packing more densely (Bowen 1980). After the HA is ground into a powder, it can be pressed to form a monolithic material.

In order to obtain a dense material, normally defined as  $<5\%$  porous, it must undergo sintering. Solid state sintering is the method by which powder particles coalesce to form a dense bulk material at high temperatures below the melting point of the material. Driven by a reduction in surface area and lowering of the surface free energy by elimination of solid-vapour interfaces, particles in contact first form necks. These necks then increase in size as the porosity between the powder particles decreases, and grain boundaries form between the extended areas of contact between the particles, eventually resulting in a smaller, denser material (Figure 2.3).

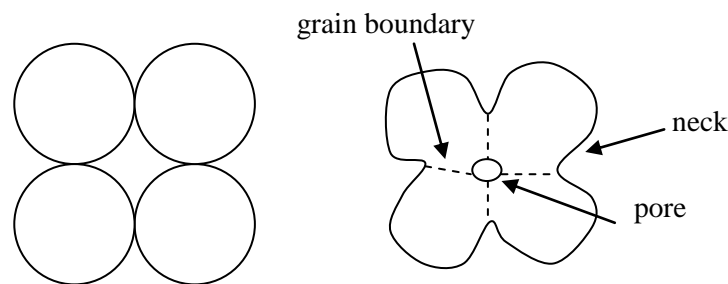


Figure 2.3: Densification of powder particles during solid state sintering. Green material (left) and sintered material (right).

A higher degree of sintering will tend to improve mechanical properties, since any porosity will induce cracking and eventually catastrophic failure. Several factors affect the degree of sintering and the density of the final sample, including: powder properties; sample preparation; phase purity of the raw material; and sintering temperature, atmosphere, and heating rate. Several papers cover the effects of powder properties on sintering, to which the reader is referred for more information (Kendall 1989; Best *et al.* 1997; Gibson *et al.* 2001; Patel *et al.* 2001). The way in which the sample is prepared, such as the method of compaction and pressure applied has also been studied (Gibson *et al.* 2001). This step can be particularly crucial in the process, as pressed powder tablets are prone to delamination and capping defects which reduce the mechanical properties and can cause cracking.

One of the first steps typically involved in heat treatment of the powder is calcining, or heating at temperatures below the material's melting point to bring about thermal decomposition or a phase transition. However, a study by Patel *et al.* (2001), using the

same synthesis and processing techniques as used in this study, showed that calcining at temperatures of 700-900°C had no influence on the final sintered density of the HA. The study also showed that hardness increased with increasing sintering temperature and that a high chemical purity and surface area powder improved sinterability.

To achieve a fully-sintered final structure, it is important that phase changes do not occur during heating (Kendall 1989). To prevent phase changes during heat treatment for HA, it is particularly important to have a Ca/P ratio of 1.67, as slight deviations from this can lead to the formation of  $\alpha$ - and  $\beta$ -TCP and TTCP. If the stoichiometric ratio is maintained, then HA should be stable up to temperatures of 1300°C and no phase changes should occur (Gibson *et al.* 2001). Other possible phase changes include any residual  $\text{Ca(OH)}_2$  decomposing to form CaO and dehydroxylation at high temperatures, forming oxyhydroxyapatite ( $\text{Ca}_{10}(\text{PO}_4)_6(\text{OH})_{2-2x}\text{O}_x\text{V}_x$ , where  $\text{V}_x$  is a hydroxyl vacancy) (Bouyer *et al.* 2000). As these phases have different solubilities than HA, they will also behave differently *in vivo*. The details of these potential phase changes will be discussed in more detail in Chapter 4.

A study by Gibson *et al.* (2001) compared sintering in lab-produced HA to commercially-purchased HA. The HA in the research presented in this dissertation was produced by the same method as the 'lab HA' in the Gibson study. The authors found that while 'lab HA' had a lower green density than commercial HA, it had a higher sintered density. The onset of sintering occurred in the lab HA at relatively low temperatures of 800-900°C, indicated by a sharp increase in density. They also found that the sintered density was independent of green compaction pressure and that varying the sintering time from 1-8 hours did not have much effect on the final density. It was found, however, that a higher ramp rate gave a small increase in sintered density, although a rate of greater than  $10^\circ\text{C min}^{-1}$  resulted in the appearance of TCP in the final product.

### 2.2.4 Improving hydroxyapatite

After decades of research on HA, its preparation and properties (including physical, physicochemical, mechanical, biological, and heat treatment behaviour) are well understood. What is clear is that HA's main limitation is its poor mechanical properties.

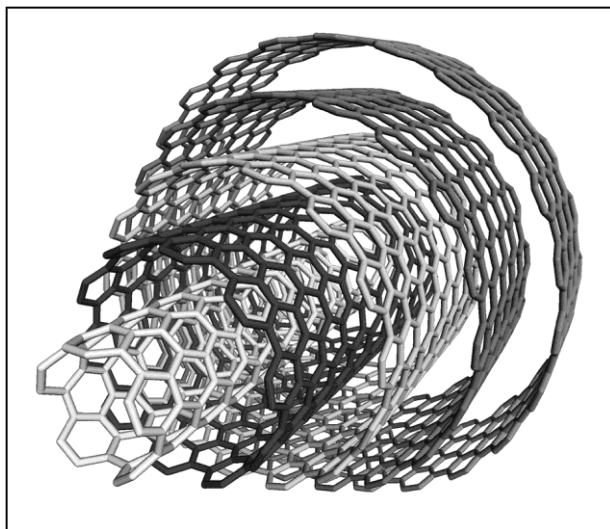
Since CNTs entered the world materials stage nearly 20 years ago, their mechanical properties have been touted as some of the best available. Their strength and stiffness, combined with their small size and large interfacial area, suggest they may have great potential as a reinforcing agent for HA.

## 2.3 Carbon nanotubes

The observation of the  $C_{60}$  fullerene by Smalley and co-workers at Rice University in 1985 began a new chapter in carbon chemistry (Kroto *et al.* 1985). Dubbed buckminsterfullerene, or ‘buckyballs’, after the architect R. Buckminster Fuller who was known for his geodesic dome designs,  $C_{60}$  is a closed, convex structure of 60 carbon atoms arranged in hexagons and pentagons, similar to a football. Six years after the discovery of buckyballs, Iijima observed an elongated form of  $C_{60}$  that came to be known as the carbon nanotube (Iijima 1991). It should be noted that there are various references to nanotube structures from the 1950s onwards, but Iijima was key in relating CNTs to  $C_{60}$ .

### 2.3.1 Structure and properties

A CNT consists of a rolled-up graphene sheet with hemispherical, half-fullerene endcaps. Single-walled nanotubes (SWNTs) have just one graphene sheet, while multi-walled nanotubes (MWNTs) consist of many graphene sheets rolled up within one another and



arranged concentrically, like Russian dolls, with an interlayer distance of  $\sim 0.34$  nm (Figure 2.4). SWNTs generally have diameters of 0.7-2 nm, while MWNTs have diameters of 2-100 nm or more. Their lengths range from several microns to several millimetres. Some of the most interesting properties of CNTs are low density, a thermal conductivity twice that of diamond,

Figure 2.4: Schematic of a MWNT (courtesy of Thomas Swan & Co., Ltd., Consett, Durham, U.K.). thermal stability in vacuum up to

2800°C, and 1000 times the current carrying capacity of copper wires. Additionally, they have excellent mechanical properties due to the strength of the carbon sp<sup>2</sup> bonds. The large aspect ratio (length/diameter) of the CNTs may allow full advantage of these mechanical properties to be taken due to the large interfacial area. Additionally, the nature of their surface chemistry allows them to be functionalised for specific applications. Many interesting applications stem from these properties. For instance, CNTs could be used as nanoprobe in high-resolution imaging, nanolithography, nanoelectrodes, drug delivery, sensors, and field emitters. Additionally, it has been suggested that they would be ideal for use in energy production and storage (Tasis *et al.* 2006). And, if used as a filler in composites, their mechanical properties could be transferred to the matrix material.

While CNTs have excellent mechanical properties, they vary widely depending on the production method used to grow the nanotubes, the number of defects in the structure, and whether the nanotubes are SWNTs or MWNTs. It is also very difficult to measure accurately the mechanical properties of CNTs due to their small size. One should also keep in mind that mechanical property values, especially for SWNTs, will be inexact, given the difficulties in measuring the cross-sectional area of the CNT.

The tensile strength of MWNTs has been measured experimentally to be 11-63 GPa, with no dependence on outer wall diameter (Yu, M. F. *et al.* 2000). The elastic modulus of CNTs is estimated at greater than 1 TPa, based on the in-plane elastic modulus of graphite. This value has been confirmed experimentally on arc-grown CNTs by using atomic force microscopy (Falvo *et al.* 1997; Wong *et al.* 1997). However, CNTs produced by chemical vapour deposition (CVD) are known to contain many more defects than arc-grown CNTs, drastically affecting their mechanical properties. For instance, Salvetat *et al.* (1999) measured the modulus to be ~1 TPa for arc-grown CNTs, yet only 10-50 GPa for CVD-produced CNTs. Arc-grown CNTs, however, are prohibitively expensive to produce in the quantities necessary for bulk composite reinforcement.

The mechanical behaviour of CNTs in composites is more complicated. Whether or not the strength and stiffness of CNTs can be transferred to the matrix depends on the amount of interfacial bonding between the two phases, which is affected by the CNTs' wettability

and interfacial area. (Too good of an interface, however, would make the ceramic too brittle.) Additionally, CNTs can buckle and remain twisted and curved in the matrix, meaning the interfacial area may not fully be taken advantage of (Ajayan 1999). It is also suggested that SWNTs might serve as better fillers than MWNTs (Lau *et al.* 2002). Firstly, SWNTs have a higher aspect ratio and greater surface area than MWNTs, allowing for more interfacial bonding. Secondly, while the outer shells of MWNTs can bond with the matrix material, the inner shells can rotate and slide freely, being held only by weak van der Waals forces. The drawback is that SWNTs are much harder to synthesise in large quantities and to process, compared with MWNTs. Another advantage of CNTs as a filler was reported by Ruoff and Lorents, who showed that fracture can occur via collapse of the inside hollow of the CNT, providing extra absorption energy and increased toughness when used in composites (Ruoff *et al.* 1995). Thostenson *et al.* (2001) provide a more detailed review on the characteristics affecting carbon nanotube composites and current research in the area. Even if the synthesis method and type of CNT limits the mechanical properties and the ability to transfer them to the composite, the composite material still has an excellent chance of enhancement.

### 2.3.2 CNT synthesis

There are three main methods for synthesising CNTs: arc discharge, laser ablation, and CVD. The arc discharge method was used by Iijima when he observed what came to be known later as carbon nanotubes (Iijima 1991). It is known for giving very pristine CNTs, but they are accompanied by many nanoparticles and have a yield of only about 2% after purification. Laser ablation can also give high-quality CNTs, but like the arc discharge method, the yield is low when compared with CVD.

CVD is the most widely used method and is known for yielding a great quantity of CNTs at low cost. It involves the catalytic decomposition of hydrocarbons on nano-sized metal particles, such as Fe, Co, Ni, Cu, Mo, or Pt. The higher the reaction temperature used, the higher the degree of graphitisation and the fewer the defects in the CNT structure. However, while CVD does yield a great quantity of CNTs compared with other methods, the CNTs made with this method have the highest number of defects, including

topological defects, rehybridisation, and incomplete bonding (Liu, Z. J. *et al.* 2001). As mentioned previously, these defects reduce the mechanical integrity of the CNTs.

### 2.3.3 CNT functionalisation

To enjoy the optimal properties of CNTs for many applications, including composites, they need to be functionalised to improve both their dispersibility and wettability. There are three main methods by which CNTs can be functionalised: covalent functionalisation by attaching functional groups to CNT ends, sidewalls, and defect sites; noncovalent functionalisation, which involves wrapping individual CNTs with various species of polymers, surfactants, or biomolecules; and endohedral filling, using the inner cavity of the CNT for doping. Several journal reviews cover the topic of CNT functionalisation extensively (Hirsch 2002; Niyogi *et al.* 2002; Lin, T. *et al.* 2003; Tasis *et al.* 2006).

Chemical oxidation is by far the most common method of functionalising CNTs, both enhancing their reactivity and enabling them to disperse better in water, ethanol, and other solvents. Typical oxidisers include  $\text{HNO}_3$ ,  $\text{H}_2\text{SO}_4$ ,  $\text{KMnO}_4$ ,  $\text{OsO}_4$ , and  $\text{RuO}_4$ . This method attaches a wide variety of functional groups, including carboxyl (-COOH), carbonyl (-C=O), and hydroxyl (-OH) groups, to the CNT ends and sidewall defects, while also purifying the nanotubes, ridding them of any amorphous carbon, nanoparticles, and catalyst residues. Purification occurs because amorphous carbon is highly disordered and has many active dangling atomic sites and weak C-C bonds, making it more reactive. Also, nanoparticles tend to have a more curved structure with higher conformational strain, making them more reactive (Yu, R. *et al.* 1998). For the same reasons, however, CNT tips and defects are also more reactive; thus, oxidation tends to attack and remove nanotube ends first, and then attacks any defects from synthesis, attaching functional groups at those locations. Opening the tips also allows removal of catalyst residues from the CNT interior, although not all metal particles will be removed in this way. Oxidation also tends to peel off layers of graphene in MWNTs, thus the outer diameter of the CNTs maybe become smaller, or, alternately, the inner layers may peel off. In fact, as outer layers have a lower curvature, and thus lower strain energy, they are more likely to persist than inner layers. Additionally, different helicities may cause different layers to oxidise at different rates (Yao *et al.* 1998). Sonicating the acid/CNT mixture during

functionalisation can increase the reaction and also create more defects in the CNTs, offering more sites for functional group attachment. However, this can also shorten the CNTs and weaken them mechanically. So while load transfer efficiency in composites from the matrix material to the CNTs can be improved by functionalisation, it can also weaken the CNTs, creating a trade-off in properties.

Liu, Z. J. *et al.* (2001) performed a detailed study of the effects of oxidation by nitric acid on the structure of MWNTs synthesised by CVD and compared the results to those from studies on the oxidation of MWNTs synthesised by the arc vapour method. Studies on MWNTs created by the arc vapour method show that oxidation begins at the more reactive tips of the CNTs and gradually moves towards the central parts of the tubes, successively removing graphite layers and thinning the CNTs (Ajayan *et al.* 1993). In contrast, Liu, Z. J. *et al.* found that oxidation of MWNTs created by CVD tended to exaggerate pre-existing defects, corroding the outer and inner surfaces of the CNTs. Additionally, they showed, through high-resolution transmission electron microscopy, that 80% of the tips opened and that the CNTs were shortened.

Oxidising CNTs also provides an avenue for further chemical modifications. For example, Eitan *et al.* (2003) functionalised CNTs with  $-COOH$  groups, to which epoxy resin was then attached to aid in interfacial bonding in polymer composites. Kiricsi *et al.* (2003) reported that carboxyl groups can be converted to carbonyl chloride groups by reacting the oxidised CNTs with  $SOCl_2$ , which creates a material reactive to amines, so that virtually any functional group can be generated. Work by Zhao, B. *et al.* (2005) focused on finding functional groups that would successfully attract calcium cations for the mineralisation of HA. The CNTs were first oxidised, then further functionalised with phosphonate and sulphonic acid groups, and finally combined with a small amount of  $CaCl_2$  and  $Na_2HPO_4$  solutions and left to mineralise for periods ranging from 30 min. to 14 days. Results showed that the carboxylic acid groups from the oxidation were not particularly effective in nucleating HA, but the further-functionalised CNTs with phosphonate and sulphonic groups were.

Some studies have suggested that conventional acid treatments do not covalently attach chemical groups to the ends and sidewalls of CNTs, but rather attach oxidation debris

(fulvic acids) to the surfaces by non-covalent  $\pi$ - $\pi$  stacking (Fogden *et al.* 2008; Wang, Z. W. *et al.* 2009). Functional groups may then attach to these debris rather than to the CNTs themselves. In the case of composites, where some bonding between the matrix and CNT is desired, a weak bond between the CNT and functional groups may mean that the matrix is not strongly attached to the CNT, but rather only to functional groups attached to debris. One way to avoid this is to base-wash the CNTs after acid treatment.

As mentioned previously, other types of functionalisation include non-covalent functionalisation and endohedral functionalisation. Noncovalent functionalisation is an alternative to covalent functionalisation that is far less damaging to the CNTs, plus it can still increase solubility and enable the CNTs to interact chemically with the matrix material. This method takes advantage of weaker interactions, such as hydrogen bonding,  $\pi$ - $\pi$  stacking, electrostatic forces, van der Waals forces, and hydrophobic and hydrophilic interactions to attach DNA and proteins to sidewalls or to wrap polymer chains around the CNTs. Endohedral functionalisation stores molecules such as fullerenes, nitrogen, metals, and metal salts.

### 2.3.4 Biological properties

If CNTs are to be incorporated into composite materials for medical applications, evidence of their potential bioactivity and/or toxicity is essential. Depending on the dissolution rate of the matrix material *in vivo*, CNTs could be released into the body, possibly inducing a harmful response. On the other hand, the presence of CNTs in the composite may have no detrimental effects, and could even enhance its bioactive properties.

A study by George *et al.* (2006) tested the response of MWNTs to human lung epithelial cells, osteoblast-like cells, and primary osteoblast cells. They found that these cells attached and survived on MWNTs, though not with as much proliferation as the flat control substrate. They also suggested that the dimensions and spacing of CNTs may be key to determining subsequent cell spreading and proliferation. A study by Price *et al.* (2003) showed that carbon nanofibres produced by CVD with diameters of 60-200 nm promoted osteoblast adhesion, both on their own and when combined with polycarbonate

urethane. Zanello *et al.* (2006) compared osteoblast proliferation and bone formation on functionalised and non-functionalised CNTs. They found that rat osteosarcoma ROS 17/2.8 cells grew best on the surfaces of as-prepared SWNTs and neutrally-charged polyethylene glycol-functionalised SWNTs, followed by negatively-charged oxidised SWNTs (SWNTs-COOH), and zwitterionic poly(aminobenzene sulfonic acid)-functionalised SWNTs. While the lowest growth was found on as-prepared MWNTs and MWNTs-COOH, they suggest this was due in part to loss of MWNTs into the solution because of decreased attachment to the glass substrate. Their findings also suggest that the electrical activities of the osteoblast membrane are maintained, and  $\text{Ca}^{2+}$  channel functions enhanced, in cells grown on neutral CNTs. Additionally, they determined that cell shape and possibly cell differentiation can be controlled by the use of SWNTs or MWNTs. There have also been indications that CNTs can induce the formation of type I collagen by fibroblasts and osteoblasts (Chlopek *et al.* 2006).

A review of CNT biocompatibility reports that shorter fibres ( $< 7 \mu\text{m}$ ) show no toxicity (Smart *et al.* 2006). Long fibres ( $> 17 \mu\text{m}$ ), on the other hand, are difficult for macrophages to phagocytose, leading to the chronic release of inflammatory mediators and contributing to fibrosis (Ye *et al.* 1999). Shorter fibres are easily phagocytosed and cleaved by macrophages (Donaldson *et al.* 1992). However, there are still discrepancies in toxicity reports, which the review suggests are most attributable to a variation of CNT dispersion from study to study. In addition, several *in vitro* studies have shown that functionalising CNTs, thus improving their aqueous dispersibility, improves their biocompatibility and their toxicity profile *in vitro* (Pantarotto *et al.* 2004; Sayes *et al.* 2004; Sayes *et al.* 2006). Finally, an *in vivo* study found no severe inflammatory response, such as necrosis, tissue degeneration, or neutrophil infiltration, when oxidised SWNTs and MWNTs were intravenously administered to rats (Singh *et al.* 2006). Instead of being retained in organs, such as the heart, liver, and spleen, electron microscopy showed that both types of CNTs were excreted intact in urine.

Another concern is the toxicity of any catalyst particles that may remain in CVD-produced CNTs, even after post-synthesis treatments to remove them. Two studies have found CNT toxicity to be independent of the amount of catalyst particle remaining (Lam *et al.* 2004; Flahaut *et al.* 2006). Flahaut *et al.* point out that the metal particle is

encapsulated by graphene layers and would thus not influence the toxicity. However, there is a concern that catalyst particles may be released from the CNT interior, particularly in the case of CNTs damaged by functionalisation.

Overall, there is a noticeable lack of consistency in studies reporting on the biological and toxicological properties of CNTs. CNT concentrations vary widely, as do assessment techniques and, in the case of *in vivo* studies, the methods by which CNTs are introduced to the animal. While reports of both biological and toxicological effects vary, the majority of studies thus far suggests that not only can CNTs serve a mechanical role, but they can also stimulate bone regeneration and are non-toxic *in vivo* when functionalised to be more easily dispersed in water.

### ***2.4 Ceramic composites***

Ceramics are preferred over other classes of materials in many applications due to their low density, high rigidity and hardness, and low sensitivity to corrosion. Their main drawback, however, is brittleness. Metals, with a structure that allows for high mobility of structural defects which inhibits crack propagation, are thus often used in applications in which ceramics cannot be. In the field of biomaterials, hip implants (typically made of a titanium alloy) are one example.

Ceramic materials tend to fail, often catastrophically, by brittle fracture. Cracks form and quickly propagate through the material in a direction perpendicular to the applied load, resulting in sudden material failure. With crystalline ceramics, such as HA, crack growth is usually through grains and along specific crystallographic planes. Thus, in order to prevent catastrophic, brittle fracture of ceramic materials, crack propagation must be hindered. One method of accomplishing this is to reinforce the ceramic matrix with a particulate or fibrous second phase. By incorporating high stiffness, high strength CNTs, it is hoped both the toughness and tensile strength of the ceramics can be improved, making them less brittle and allowing them to be used in a wider range of applications.

### 2.4.1 Composite Mechanics

One of the main purposes of creating ceramic-matrix composites (CMCs) is to improve the ceramic's fracture toughness, or, in other words, its ability to resist fracture when a crack is present. Low strength in tension compared with compression is a main problem with brittle ceramics. In tension, even the slightest flaw, such as a surface or interior crack, internal pore, or grain corner, will amplify the applied stress. Thus, as the two go hand-in-hand, an improvement in toughness generally leads to improvements in strength and stiffness, as well (Matthews *et al.* 1994).

The reinforcing phase in a ceramic serves to impede crack growth. This can be accomplished by a number of methods, including: deflecting crack tips, forming bridges across crack faces, absorbing energy during pull-out, and causing a redistribution of stresses in regions adjacent to crack tips (Xia *et al.* 2004). In addition to the reinforcing material's mechanical properties, its morphology is critical. The higher the aspect ratio of the reinforcing material, the better the reinforcement. It is for this reason that long, thin fibres with high aspect ratios reinforce better than particulates, which generally have an aspect ratio of about 1.

Another consideration in CMCs is the thermal properties of the reinforcement. Firstly, the reinforcement must be able to withstand the high temperatures involved in ceramic processing. Secondly, differences in coefficients of thermal expansion (CTE) between the matrix and the reinforcement can lead to thermal stresses on cooling, causing cracks in the matrix (Matthews *et al.* 1994).

In addition to hindering the propagation of cracks through the matrix, the reinforcement should also bear much of the applied load. The magnitude of the interfacial bond between the fibre and the matrix determines how well the weak matrix transmits stress to the strong fibres (Wagner *et al.* 1998). However, while a bond between the matrix and reinforcement must exist for the purpose of stress transfer, it should not be so strong that it prevents toughening mechanisms, such as debonding and fibre pull-out (Peigney 2003).

Other factors to consider in the CMC are the volume fraction of the reinforcing phase, the orientation of the reinforcement, and the homogeneity of the overall composite. To a

degree, higher volume fractions of reinforcement tend to improve mechanical properties. Continuous, aligned fibres best prevent crack propagation, with the added advantage/disadvantage of anisotropic behaviour. Additionally, a uniform dispersal of the reinforcing phase is also desirable, as it gives the material homogeneous properties. Ultimately, the properties of a CMC depend upon its density, phase composition, and defect structure.

### 2.4.2 HA composites

Over the last twenty years, a wide variety of materials has been studied as possible reinforcing phases for HA, including particles, fibres, and whiskers. While mechanical properties sometimes improved with the addition of these phases, problems were often found with matrix-CNT reactions or mismatches in thermal expansion coefficients. Additionally, large amounts of the reinforcing phase were sometimes required, and these phases tend to be much less biologically active compared with HA, thus possibly resulting in reduced bioactivity for the composite compared with HA. This section discusses a few HA composite studies in detail.

Much HA composite work has examined HA-zirconia composites. Zirconia, as a biologically inactive material, is expected to improve the mechanical properties of HA without inducing any negative biological effects. Two issues have pervaded HA-zirconia composite research: reactions between the two phases, resulting in secondary phases which reduce the mechanical properties, and decomposition of the HA, seemingly induced by the presence of zirconia. Both Rao *et al.* (2002) and Wu *et al.* (1988) found poor sinterability due to reactions between HA and zirconia when pressureless sintering in air. Other authors, using reinforcing phases such as tetragonal zirconia polycrystal (Takagi *et al.* 1992), yttria-partially-stabilised zirconia (Li, J. *et al.* 1996), and magnesia-partially-stabilised zirconia (Delgado *et al.* 1999), found the main problem lay in the decomposition of HA to TCP when pressureless sintered in air. To combat this, Takagi *et al.* and Li *et al.* used hot isostatic pressing (HIP) and found no decomposition. Delgado *et al.*, on the other hand, used a flowing wet O<sub>2</sub> atmosphere and found no decomposition at temperatures as high as 1250°C. Takagi *et al.* and Delgado *et al.* also measured the mechanical properties of their composites. Takagi *et al.* found a 20% increase in strength

and 100% increase in toughness in their composite compared with HA, while Delgado *et al.* found approximately a 50% increase in both strength and toughness.

A wide variety of other particulate and fibre reinforcements has also been investigated. Other particulates have included Al<sub>2</sub>O<sub>3</sub>, C, SiC, SiO<sub>2</sub>, ZrO<sub>2</sub>, and 316L stainless steel (Ruys, A. J. *et al.* 1995), silver (Zhang *et al.* 1997), and Ni<sub>3</sub>Al combined with Al<sub>2</sub>O<sub>3</sub> (Choi *et al.* 1998). Choi *et al.*'s work chose Ni<sub>3</sub>Al for its chemical inertness and good fracture toughness and Al<sub>2</sub>O<sub>3</sub> for its chemical inertness and good strength. The composites were sintered with hot pressing. The authors found that a Ni<sub>3</sub>Al reinforcement alone in an HA matrix induced microcracks due to differences in CTEs, while Al<sub>2</sub>O<sub>3</sub> on its own increased strength at 20 vol.%, but not toughness. A combination of the two reinforcing phases with HA, however, gave a composite with a 100% increase in strength and a 230% increase in fracture toughness compared with HA. The authors did admit, though, that the biocompatibility of Ni<sub>3</sub>Al remained in question. Zhang *et al.*'s work chose silver particulates for reinforcements due to the ductility of silver combined with its biological inertness and anti-bacterial properties. At 30 vol.% silver the authors found an increase in fracture toughness from 0.70 to 2.45 MPa·m<sup>1/2</sup>, which they attributed to both crack deflection and bridging, and at 10 vol.% silver they found a peak increase in strength, from 38.8 MPa for pure HA to 100.7 MPa for the composite.

Ruys *et al.*'s work took an extensive look at six particulate additives (listed previously). After several investigations in which they found that any reinforcing phase caused the HA to decompose when sintering in air (Ruys *et al.* 1992; Ruys *et al.* 1993; Ruys *et al.* 1994), they decided to try to oppose dehydration (leading to decomposition) by both a 'thermodynamic effect' of sintering in a moist atmosphere of O<sub>2</sub> and H<sub>2</sub>O and a 'physical effect' of a pressurised Ar atmosphere (1 MPa). The authors found that including H<sub>2</sub>O in the atmosphere significantly suppressed decomposition in composites with all reinforcing phases (with the exception of C, which was oxidised), while the pressurised atmosphere was ineffective at preventing decomposition. Interestingly, they also found that HA sintered in a wet O<sub>2</sub> reached only 92% theoretical density, while in air it reached 99% density.

Other authors have looked into fibre reinforcements, such as alumina and various metals. Knepper *et al.* (1997) investigated titanium, alumina and 316L stainless steel fibres. The fibres were 10-50  $\mu\text{m}$  in diameter and 0.15-1.5 mm in length. With the steel fibres, the authors were not able to densify the composite, as the fibres formed a mesh network and held the structure open, resulting in a composite of only 56% theoretical density. Similarly to the particulate composites, it was found that the HA decomposed when the composites were sintered in air, but it remained phase pure when hot isostatically pressed. XRD showed that the HA transformation to TCP was highly dependent on: 1) the type of fibre, 2) the matrix:fibre ratio and 3) the atmosphere and gas pressure while processing. They also found that the relative density of the HA composites was lower compared with pure HA sintered under the same conditions. De With *et al.* (1989) used uniaxial hot pressing to sinter their fibre-reinforced composites. In preliminary investigations, they looked at alumina, titanium, and 316L stainless steel fibres, as Knepper *et al.* did. However, they found that in the case of alumina and titanium the fibres caused microcracking in the HA matrix, presumably due to differences in CTEs, and in the case of steel fibres, the steel reacted with the HA matrix, even when sintering was performed in a  $\text{N}_2$  atmosphere. The two fibres they had success with were made from Hastelloy X (containing Ni, Cr, Mo and Fe) and FeCr alloy (containing Fe, Cr and Al). At 20 vol.% the authors found that strength increased approximately two-fold and toughness six-fold for both types of composites. It should be noted, however, that no verification that the HA matrix remained phase pure after sintering was reported.

Finally, other composites have included high density polyethylene with HA (HAPEX<sup>TM</sup>) (Bonfield *et al.* 1981; Wang, M. *et al.* 2001) and biological glasses with HA (Tancred *et al.* 2001). In the case of a polyethylene-HA composite, while the toughness and strain-to-failure is higher than that of HA and the elastic modulus is similar to bone, the composite's tensile strength is still far inferior to that of bone. The maximum value of tensile attained in Wang and Bonfield's 2001 study was 23 MPa at 40 vol.% HA in polyethylene. Biological glasses, on the other hand, can improve both the toughness (substantially) and tensile strength (moderately) of HA, but only when large amounts of bioglass are used. In a study by Tancred *et al.* (2001) they found the best mechanical properties at 25 wt.% bioglass in HA, which gave a more than two-fold increase in

fracture toughness and a 30% increase in fracture strength compared with pure HA. It is worth noting that both of these composites had a large amount of additional phases (60 vol.% polyethylene and 25 wt.% biological glass), which could alter the biological response of the composite significantly compared with HA.

### 2.4.3 Ceramic-CNT composites

There are several obstacles and considerations to take into account when using CNT fillers in composites. One is the wettability of the CNT surface, which relates to interfacial bonding and, ultimately, the load transfer from the CNTs to the matrix material. It is suggested, however, that interfacial bonding not be too strong, as some fibre pull-out allows energy to be absorbed in breaking the fibre-matrix bonds (Peigney 2003). A second factor is the CNT dispersion. A uniform dispersion is necessary to give homogeneous properties throughout the composite. However, in CNTs this is particularly difficult due to their high aspect ratio which makes them hard to mix. One can imagine something similar to achieving a homogeneous mixture of peas and spaghetti.

Several different methods can be used to disperse nanotubes in a matrix. Physical blending involves using a method like shear mixing to distribute CNTs throughout the matrix material and is commonly used with polymer-CNT composites. In-situ formation involves either synthesising the CNTs in a preformed matrix material or synthesising the matrix material around the CNTs. Chemical functionalisation of CNTs can more easily disperse them and improve interfacial bonding.

Another concern is that ceramics must be densified by sintering for many applications, because any pores will act as cracks and impair mechanical properties. Sintering of ceramics takes place at high temperatures and CNTs oxidise and burn in air at temperatures above about 650°C. Thus special atmospheres or techniques must be used in order to successfully incorporate CNTs into ceramic matrices. Secondly, CNTs tend to inhibit matrix grain growth during heat treatment, preventing full densification of the material (Peigney 2003). Processing-induced changes in the matrix, such as that just mentioned, may actually have greater effects on the mechanical properties of the composite material than the presence of CNTs (Curtin *et al.* 2004).

Pressureless sintering is a common and relatively simple and cheap method for achieving dense HA, involving standard high-temperature furnaces and allowing a wide range of geometries for the end product. However, the issue of CNTs holding open the HA matrix is particularly problematic with this method, since it involves no external pressure. Other possible methods of sintering include hot uniaxial pressing, hot isostatic pressing (HIP), and spark plasma sintering (SPS). Hot pressing gives the advantage of being able to sinter at lower temperatures (LeGeros *et al.* 1993) and to continually fill in pores throughout the sintering process. However, the equipment for this method is more expensive and the end product has limited geometry. Additionally, HIP, which uses gaseous pressures at high temperatures, can achieve greater density and higher compressive strength than uniaxial pressing (LeGeros *et al.* 1993). In addition to its greater expense, it also involves individually sealing each specimen in a metal or ceramic casing. SPS is gaining popularity as it can very quickly sinter ceramics to nearly full density. This method involves a high-temperature plasma that is momentarily generated in gaps between powder particles by electrical discharge during on-off DC pulsing under pressure. While sintering times are very fast (several minutes), the main limitation of this technique is that it is most successful for small samples and is geometrically limited.

It is also suggested that SWNTs might serve as better fillers than MWNTs for a few reasons (Lau *et al.* 2002). Firstly, SWNTs have a higher aspect ratio and greater surface area than MWNTs, allowing for more interfacial bonding. Secondly, while the outer shells of MWNTs can bond with the matrix material, the inner shells can rotate and slide freely, being only held by weak van der Waals forces. The drawback is that SWNTs are prohibitively expensive to produce in large quantities, while MWNTs can be synthesised in high quantities and at a lower cost. A more detailed review on the characteristics affecting CNT composites and current research in the area is available (Thostenson *et al.* 2001).

As many of the issues involved in creating HA-CNT composites are present in other ceramic-CNT composites, examining studies on other ceramic-CNT composites can give an idea of the potential CNTs might have for reinforcing HA. By far the most common ceramic matrix in which to include CNTs is alumina. However, there is a wide range of methods to incorporate CNTs into the alumina matrix. The work of An *et al.* (2003) and Peigney *et al.* (2000; 2002) involved growing CNTs in-situ in an alumina powder. An *et*

*al.* grew CNTs by CVD on an alumina powder containing varying amounts of iron catalyst. The resulting composite powder was then hot pressed at 1800°C in Ar. The CNTs were found to inhibit grain growth in these composites, leading to only small improvements in mechanical properties. A maximum microhardness was found at 4 wt.% CNT loading and it was observed that if the CNT content was over 10 wt.%, mechanical properties were worse than pure alumina due to poor cohesion between the CNTs and the matrix.

Similarly, Peigney *et al.* grew CNTs on an  $\text{Al}_{2-2x}\text{Fe}_x\text{O}_3$  powder and hot pressed the resulting composite at 1475°C in vacuum. They then performed three-point bend tests on the composites to measure fracture strength and used a single-edge notch beam method to measure fracture toughness. They observed that there was a smaller quantity of CNTs after hot pressing and that there was no correlation between CNT loading and mechanical properties and that overall the mechanical testing results were inconclusive. A study by the same group two years later involved a similar powder preparation technique, but then used high-temperature extrusion in a graphite die under vacuum to align the CNTs. No mechanical testing results were presented for these composites, however.

Both Siegel *et al.* (2001) and Zhan *et al.* (2003) reported more significant toughness improvements in alumina. Siegel *et al.* found a 24% increase in a composite made by hot pressing MWNTs and nano-alumina powder, while Zhan *et al.* found an improvement in fracture toughness of SWNT-alumina over pure dense alumina even when the porosity of the composite was 14%. Zhan *et al.* used SPS to sinter a powder mixture of alumina and SWNTs at a temperature of 1150°C, achieving theoretical densities of 100% in the best cases. Using crack lengths emanating from Vickers hardness indentations, the highest toughness of the composites was estimated at  $9.7 \text{ MPa}\cdot\text{m}^{1/2}$ , which is three times that of pure nanocrystalline alumina. A year later, Wang *et al.* (2004) repeated Zhan's experiment and compared it with alumina-graphite fibre composites, finding similar results to those using CNTs. They concluded that SWNTs do not play a unique role in determining the contact-mechanical response of the composites. They also pointed out that the Vickers hardness measurements used by Zhan *et al.* were indirect measurements of toughness. By performing a direct measurement by single-edge V-notched beam test,

Wang showed that the composites were not, in fact, tough, but rather contact-damage resistant.

One of the first ceramic/CNT composites was that of Balazsi *et al.* (2003) who created a silicon nitride/CNT composite by HIPing a powder mixture at 1700°C in nitrogen at pressures ranging from 2-20 MPa. The authors compared composites with CNTs to ones with carbon black, graphite, and carbon fibres. They found that at lower pressures the CNTs survived and connected  $\beta$ -Si<sub>3</sub>N<sub>4</sub> grains. They also found that the CNTs showed a 15-37% increase in mechanical properties compared with the other carbon fillers. However, pure silicon nitride had the best properties, as the carbon fillers prevented the material from fully densifying.

Better densification results were achieved by Ma *et al.* (1998) with a silicon carbide/CNT composite. By hot pressing in Ar at 2000°C and a pressure of 25 MPa, 95% theoretical density was achieved. Additionally, a 10% improvement in bending strength and fracture toughness was found compared with pure silicon carbide. It has been suggested that poor homogeneity of the composite prevented further improvements in mechanical properties (Peigney 2003).

More encouraging are the results of G.Y. Li *et al.* (2005) from mechanical testing on a cement-oxidised CNT composite. Using 0.5 wt.% oxidised MWNTs in Portland cement, increases in compressive strength of up to 19% and flexural strength of up to 25% were observed. Additionally, specimens containing MWNTs had less porosity and a smaller total pore volume, indicating that the CNTs acted as a filler of voids. The authors suggest that some interfacial bonding took place from a O-Ca-O bond between the functionalised CNTs and the cement, however there was no direct evidence of this. Additionally, the Li *et al.* study only required drying the composite, rather than high temperature densification. Many of the other authors observed a loss of CNTs during the sintering process, which could have been detrimental to the mechanical properties.

### 2.4.4 HA-CNT composites

As HA requires improved mechanical properties to be used in a wider range of biomedical applications, and some success has been found with other ceramic-CNT

composites, combining HA and CNTs is a logical next step. A review paper on HA-CNT composites by this author details the progress until 2007 made with these materials (White *et al.* 2007). Those early publications, along with more recent work, are discussed below.

#### 2.4.4.1 HA-CNT composite coatings

Four groups have investigated the possibility of adding CNTs to HA coatings to improve their strength and bonding for application in coating metal prostheses. A summary of their studies is provided in Table 2.2 (at the end of the chapter). Among the four groups, three different techniques have been used to apply the coating. The first group to publish on the topic was Chen *et al.* They investigated the hardness, elastic modulus, phase composition, and wear resistance of composite coatings applied by laser surface alloying. As described in two very similar papers from (2005) and (2006) they ball milled HA powder with MWNTs at loadings of 5, 10, and 20 wt.% and used laser surface alloying to apply the coating to a Ti-6Al-4V substrate. The hardness and elastic modulus were evaluated by nanoindentation with a Berkovich tip. They found that CNTs were still present in the coating after application, but that HA had decomposed to form TTCP,  $\beta$ -TCP and CaO, and that the MWNTs had reacted with the substrate to form TiC. They found that both hardness and elastic modulus increased with increasing loading of MWNTs, although the modulus increased to a lesser extent compared with the hardness. Their third paper (2007) investigated the wear resistance of their coatings using a scratch test. They found an improvement of wear resistance with addition of MWNTs to the coating.

The work of Balani *et al.* investigated the wear resistance (2007b) and *in vitro* reaction of human osteoblast cells (2007a) to plasma-sprayed HA-CNT coatings. HA powder and 4 wt.% MWNTs were milled together for 18 hours and then plasma sprayed onto a Ti-6Al-4V substrate. Wear performance was tested in simulated body fluid (SBF) by abrasion with a ZrO<sub>2</sub> pin. The authors found that the MWNTs increased the wear resistance of the coatings, which they attributed to the MWNTs' ability to connect splats, restrict the separation of adjacent splats, and reduce the release of wear debris by pinning HA islands by stretched MWNTs. They also cultured human osteoblasts on the coatings for three days and found that cells attached and grew well.

Two groups have reported HA-CNT coatings applied by electrophoretic deposition. C. Lin *et al.* (2008) ultra-sonicated 20 and 30 wt.% acid-treated MWNTs with an HA powder and deposited the coating on Ti using electrophoretic deposition. They then attached an epoxy resin coating to the specimens to aid in testing the bonding strength between substrate and coating. XRD showed that HA retained its phase purity after deposition. They also verified that CNTs remained in the structure and reported a supposed “high density” of the coating, although no evidence of this was shown. Results showed an increase in bonding strength of 69% for 20 wt.% MWNTs and 72% for 30 wt.% MWNTs over a pure HA coating. The authors also examined the *in vitro* response of the coatings to MG63 osteoblast-like cells. After three days’ culture, they found that the cells attached and grew well on the composite.

The second publication to report electrophoretic deposition of HA-CNT coatings was that of Kaya (2008). The author synthesised nano-HA powders by sol-gel technique and mixed them ultrasonically with acid-treated MWNTs at 0.5, 1 and 2 wt.%. Following electrophoretic deposition on Ti-6Al-4V substrates, the coatings were heat treated at 600°C for 2 hours in flowing nitrogen. Kaya found that coating thicknesses above 25 µm led to microcracks in the coatings’ surfaces after heat treatment, which the author attributed to effects from the differences in thermal expansion between the Ti alloy and the coating. The elastic modulus, hardness, and interlaminar shear strength of the coatings compared with pure HA was also reported. The author found the best mechanical properties at a loading of 2 wt.%. Nanoindentation was used to evaluate the modulus and hardness, and an increase from 15 GPa to 178 GPa was found for modulus and an increase from 4.88 GPa to 36.44 GPa was found for hardness. Interlaminar shear strength values were found to increase from 0.7 MPa for HA to 2.76 MPa for the 2 wt.% coating.

While the mechanical data reported for HA-CNT coatings is promising for improving the performance of coated metal prostheses, concern still remains regarding the effect the CNTs might have if released from the coating *in vivo*. Chen *et al.* reported that their method of coating resulted in decomposition of the HA. While Balani *et al.* did not report the phase composition of their coating after application, plasma spraying is well known to cause decomposition of HA. As these degradation products are known to be much more soluble and have a much higher dissolution rate *in vivo* compared with HA, it seems

likely CNTs would be released into the body. While the method used by Lin *et al.* did not result in decomposition, a concern in all cases is wear particles. Both Chen *et al.* and Balani *et al.* reported increased wear resistance with the addition of CNTs; however, some wear particles could still be released from the coating, and with their high surface area would be more easily dissolved than the bulk coating. Additionally, wear particles can result in inflammatory reactions, which could affect the response of the body to the presence of CNTs. Thus, before these coatings can be used *in vivo*, the biological response to CNTs must be much better understood than at present.

#### 2.4.4.2 Bulk HA-CNT composites

The first known publication on HA-CNT composites was in 2004 by L. Zhao *et al.* The authors combined both sodium dodecyl sulphate (SDS)-treated MWNTs and nitric acid-treated MWNTs in solution with  $\text{Ca}(\text{NO}_3)_2$ , followed by the addition of  $(\text{NH}_4)_2\text{HPO}_4$  to form HA. The resulting precipitate was then dried and hot pressed at  $1200^\circ\text{C}$  for 20 hours. The authors examined the composite material with TEM and proclaimed a 'homogeneous coverage' of HA on MWNTs had been achieved. Comparing the micrographs with images typical of CNT coatings of, for example, titania, the coverage seems by no means homogenous. However, there does seem to at least be some aggregation of HA particles around the CNTs and possible bonding in places. Improvements in compressive strength are reported, from 63 MPa for pure HA to 87 MPa for SDS-functionalised MWNTs and 102 MPa for nitric acid-functionalised MWNTs, though the authors offered no analysis of strengthening mechanisms to account for these results.

H. Li *et al.* (2008) tried a novel approach by adding an iron catalyst directly to the HA and then growing the CNTs *in situ*. The HA/Fe composite was synthesised by adding  $\text{Fe}(\text{NO}_3)_3 \cdot 9\text{H}_2\text{O}$  to HA, then adding NaOH, yielding  $\text{Fe}(\text{OH})_3/\text{HA}$ . The material was then calcined in nitrogen to make  $\text{Fe}_2\text{O}_3/\text{HA}$ , which was then sprayed onto a quartz substrate. The CNTs were then grown *in situ* with a mixture of  $\text{CH}_4$  and  $\text{N}_2$  carrier gases. The resulting powder was pressed in a mould at 500 MPa and sintered at  $1000^\circ\text{C}$  for 2 hours in vacuum, followed by a second press at 1.2 GPa. The authors found a 226% increase in

toughness compared with pure HA, to  $2.35 \text{ MPa}\cdot\text{m}^{1/2}$ , as measured by crack length from a Vickers indentation and a 49% increase in fracture strength, to 79 MPa.

While an interesting approach, the most obvious problem is the large amount of iron incorporated into the composite, as iron has been shown to have toxic effects *in vivo*. The authors report that at a loading of 2 wt.% CNTs, there was 1.5 wt.% Fe. Additionally, a lot of key characterisation is missing from this work. No information is given on the characteristics of the HA powder compared to the composite powder and no density information is presented for either type of material before or after sintering. If there were substantial differences in either of these properties, they alone could account for the mechanical data rather than the addition of CNTs. Additionally, there is only XRD characterisation of the HA powder before sintering. Considering that the material has been sintered at high temperature in vacuum, it seems doubtful that it is still HA, as HA is known to dehydroxylate and decompose at high temperature in vacuum.

The only publication to date to report sintering of HA-CNT composites by pressureless sintering was by A. Li *et al.* Their composites were made by first synthesising HA in a precipitation reaction, followed by ultrasonic dispersion in SDS, then later adding 3 wt.% MWNTs which had previously been dispersed in water and SDS. The resulting powder was uniaxially, then isostatically pressed and then sintered in vacuum and argon at  $1100^\circ\text{C}$  for 3 hours. HA was sintered in air for comparison. The authors measured bending strength and toughness and also characterised the materials with XRD. Additionally, they embedded both the HA-CNT composite and an HA-ZrO<sub>2</sub> composite in rat muscle and measured the response at intervals over 14 days.

The XRD analysis showed that the HA sintered in air decomposed slightly, forming a small amount of  $\beta$ -TCP. The composite, sintered in vacuum and in argon, decomposed to form a mixture of HA,  $\alpha$ -TCP, and Ca<sub>2</sub>P<sub>2</sub>O<sub>7</sub>. As different atmospheres were used for the two materials, it is unclear whether the additional decomposition for the composite was more due to sintering in a water-free atmosphere or to the presence of CNTs. The mechanical testing found that bending strength and toughness were better in composites sintered in vacuum than in argon, with a toughness increase over HA of 100% for the composites sintered in argon and 200% for those sintered in vacuum. The authors also

noted there was not much interfacial bonding between the HA and CNTs when sintering in argon and that the materials had a high porosity. Unfortunately, no density values for any materials were reported, so it is unclear whether differences in density may have had some effect on mechanical properties or whether the CNTs alone were responsible. There was also no confirmation that the composites retained the entire 3 wt.% of CNTs following sintering. The biological studies showed the composites were not toxic to rats and had better histocompatibility than the HA-ZrO<sub>2</sub> composites.

Xu *et al.* (2009) reported the mechanical properties and response of osteoblast-like cells to HA-CNT composites densified by spark plasma sintering. HA powder and 2 vol.% MWNTs were dry mixed, then consolidated using spark plasma sintering at 7.5 MPa for 3 minutes at temperatures ranging from 900-1200°C with a ramp rate of 100°C/min. Hardness and Young's modulus were evaluated by Berkovich nanoindentation, and osteoblast-like cells were cultured for 2 and 4 days. The authors confirmed by XRD and FTIR that the HA had largely remained intact during the sintering process, although a small amount had decomposed to β-TCP. They also confirmed that some amount of CNTs was still present. The mechanical property results were reported as simply showing an increase in hardness and modulus over HA, though no numerical values are reported. They also report an increase in cellular response to the composites compared with HA alone.

The work of Kealley *et al.* (2006; 2008) reports the only decrease in mechanical properties with the addition of CNTs in the literature. The authors added 2 wt.% MWNTs with graphite impurities *in situ* while HA was precipitating. The material was then calcined and hot isostatically pressed (HIPed) at 100 MPa and 900°C in argon. The hardness of the material was measured by Vickers microhardness and the toughness was measured from nanoindentation from a Berkovich tip. Results showed the hardness decreased compared with pure HA while the toughness remained the same. While the 2006 paper reports the CNTs were evenly distributed in the matrix, the 2008 paper shows microscopy images with clumps of CNTs. The authors then later attributed the decrease in mechanical properties to the presence of graphite clumps. Additionally, the densification was reported as 'excellent', although no numerical values were given to justify this claim.

Other work involving hot pressing was reported by Meng *et al.* (2008). HA was made by the precipitation method and then calcined at 900°C. Thin, short MWNTs were acid-treated then mixed at 2.4, 6, 7, 11, and 25 vol.% with the HA powder. The material was then hot pressed at 1200°C for 30 minutes at 28 MPa in nitrogen. The authors confirmed that the HA remained phase pure during heat treatment, and found an improvement in flexural strength of 28% and toughness, as evaluated by indentation fracture, of 50%, both at a loading of 7 vol.%. At loadings higher than this value, the authors found that mechanical properties decreased. No density or porosity values were reported.

Overall, the work thus far on HA-CNT composites suffers from a lack of thorough characterisation. Relative density and/or porosity values are rarely reported and grain size has not been examined at all, both of which are known to affect mechanical properties. Thus, it is not readily evident how much of the mechanical data reported is due to differences in microstructure of the composite compared with HA and how much is due to any effects from the CNTs. Additionally, often times the phase purity of the HA after heat treatment is not examined. As HA can easily dehydroxylate and decompose at the high temperatures required for sintering, it may well be that the material being reported is in fact no longer HA, but rather another calcium phosphate phase that may behave differently from HA *in vivo*. Finally, while the presence of CNTs following heat treatment is often confirmed by microscopy, the amount of CNTs remaining has not been reported in any HA-CNT publication. Rather, it seems to be assumed by the authors that all CNTs remain intact. While this may be less of a concern at very high pressures in a sealed environment, it seems less sure in the case of other heat treatment techniques.

In terms of sintering techniques, only one paper thus far has investigated pressureless sintering. The authors did so in an argon atmosphere and in vacuum, and found that the composites decomposed. No post-sintering CNT loading values were reported, so it is not known if the Ar and vacuum atmospheres fully prevented oxidation. Also, as no density values were reported, whether pressureless sintering is capable of densifying HA-CNT composites is unknown. Hot pressing and SPS are more frequently used and seem relatively successful. However, as mentioned earlier, much characterisation is missing from these studies.

Table 2.2: Summary of publications on HA-CNT bulk composites (top) and coatings (bottom).

Author	Dispersion Method	Loading	Functionalisation	Sintering Method/Application	Mechanical Properties	Biological Properties
Kealley	<i>In situ</i>	2 wt.%	Acid treatment	HIP	Decrease in hardness; no effect on toughness	Not reported
A. Li	Ultrasonication	3 wt.%	SDS	Vacuum and pressureless in Ar	Better properties with vacuum. Toughness increased 100% (Ar) and 200% (vac.)	Not toxic to rats <i>in vivo</i> . Better histocompatibility than HA-ZrO <sub>2</sub> composites
H. Li	<i>In situ</i> growth of CNTs in HA	2 wt.%	None	Vacuum at 1000°C	226% increase in toughness; 49% increase in fract. strength	Not reported
Meng	Dry mixing	2.4, 6, 7, 11, 25 vol.%	Acid treatment	Hot pressing	50% increase in toughness; 28% increase in flexural strength at 7 vol.%	Not reported
Xu	Dry mixing	2 vol.%	None	SPS	Increase in hardness and modulus	Increase in osteoblast response at 2, 4 days
L. Zhao	<i>In situ</i>	2 wt.%	SDS and acid treatment	Hot pressing	Increase in compressive strength: oxidised by 38% and SDS by 62%	Not reported
Balani	Dry milling	4 wt.%	None	Plasma spraying	Improvement in wear resistance	Osteoblasts grew well
Chen	Dry milling	5, 10, 20 wt.%	None	Laser surface alloying	Hardness and modulus increased with increasing loading; improved wear resistance	Not reported
Kaya	Ultrasonication	0.5, 1, 2 wt.%	Acid treatment	Electrophoretic deposition	1087% increase in modulus; 647% increase in hardness;	Not reported
Lin	Ultrasonication	20, 30 wt.%	None	Electrophoretic deposition	Increase in bonding strength – 69% (20 wt.%), 72% (30 wt.%)	Osteoblast-like cells attached and grew well

## 2.5 Summary and project design

While HA's chemical similarity to bone makes it an excellent choice for a bone graft material, its poor mechanical properties prevent its use in major load-bearing situations. CNTs' long, thin geometry, small size, high interfacial area, and excellent mechanical properties make them good candidates to reinforce HA.

Previous attempts to strengthen HA have resulted in degradation of the HA, microcracking from differences in thermal expansion coefficients, and have required large amounts of reinforcing phases to achieve the desired mechanical results. CNTs may be able to achieve the results with smaller amounts of material and less cracking (due to their very small size).

Studies on HA-CNT composites thus far have found some improvements in mechanical properties and have occasionally reported very brief biological results. However, none of these investigations has been very extensive. Often mechanical properties and *in vitro* or *in vivo* studies are mentioned in the last few sentences of a publication and are presented without any analysis. Additionally, no study thus far has reported a full characterisation of the materials, which should include phase purity, hydroxylation, density, and CNT loading after heat treatment, among other things. Almost all current research has also relied on more expensive or geometrically limiting sintering methods, compared with pressureless sintering, to achieve good densities and to prevent CNT oxidation and reactions with the HA matrix.

The aim of this Ph.D. work was to present a cohesive view of the potential these composites may have by filling in gaps in the literature. This can best be achieved by thorough characterisations and comprehensive studies which look at all key aspects (heat treatment, mechanical properties, and biological properties) for material produced in the same manner. Additionally, as pressureless sintering has only been briefly reported once and is an industrially-friendly sintering technique, focus was placed on developing the composites using this heat treatment method.

### 3 PREPARATION, PROCESSING AND CHARACTERISATION OF GREEN MATERIALS

This chapter details the development and characterisation of the green (un-sintered) composite materials, from the synthesis of the raw constituents to the formation of composite tablets from pressed powders. All raw materials – HA, CNTs, and composites – were synthesised in house. Figure 3.1 outlines the procedure used for making the green tablets, which is explained in more detail in this chapter.

Carbon nanotubes were synthesised by chemical vapour deposition (CVD) and, in the case of composites, were added to the solution of precipitating HA. The resulting slurry was then filtered, shear mixed, dried, ground, milled, and sieved, yielding a fine powder. The powder was then pressed into tablets to create the final green samples.

The green material was characterised by a number of different methods. The raw materials' morphology was examined by electron microscopy; phase purity and hydroxylation were analysed by X-ray diffraction (XRD) and Fourier transform infrared spectroscopy (FTIR); and thermogravimetric analysis (TGA) was used to evaluate CNT quality and purity. The powder was then characterised to determine surface area, particle size, CNT loading (post-processing), and bulk density.

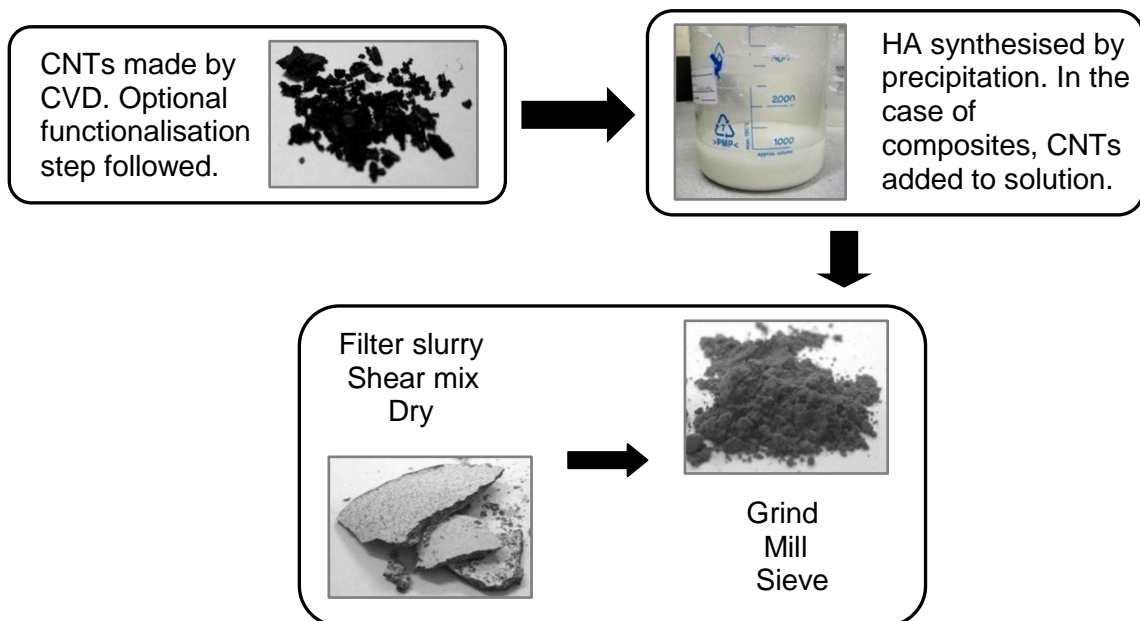
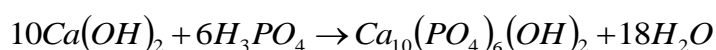


Figure 3.1: Green material synthesis outline.

## 3.1 Material synthesis

### 3.1.1 Hydroxyapatite synthesis

Hydroxyapatite was synthesised by the aqueous precipitation of calcium hydroxide,  $\text{Ca}(\text{OH})_2$ , and orthophosphoric acid,  $\text{H}_3\text{PO}_4$ , at room temperature (21-24°C) according to the reaction shown below:



The relative amounts of reactants were calculated to maintain a Ca/P ratio of 1.67, corresponding to phase pure HA.

The reaction was performed by the following method, illustrated by the schematic in Figure 3.2. First, 1-2 litre quantities of 0.5 M (37.046 g L<sup>-1</sup>) aqueous solution of  $\text{Ca}(\text{OH})_2$  (98.0+% purity, Acros Organics) and 0.3 M (34.588 g L<sup>-1</sup>) aqueous solution of  $\text{H}_3\text{PO}_4$  (85% assay, Acros Organics) were prepared with deionised water (DIW). After stirring for 30 minutes, the  $\text{H}_3\text{PO}_4$  solution was added, drop-wise, to the  $\text{Ca}(\text{OH})_2$  solution over a period of 3-4 hours. The pH was kept above 10.5 throughout the reaction by the addition of ammonium hydroxide ( $\text{NH}_4\text{OH}$ ) solution. During the precipitation both solutions were stirred, and the final suspension continued to stir for 1 hour after the last of the  $\text{H}_3\text{PO}_4$  solution was added. The suspension was then covered with plastic film and left to age at ambient temperature overnight.

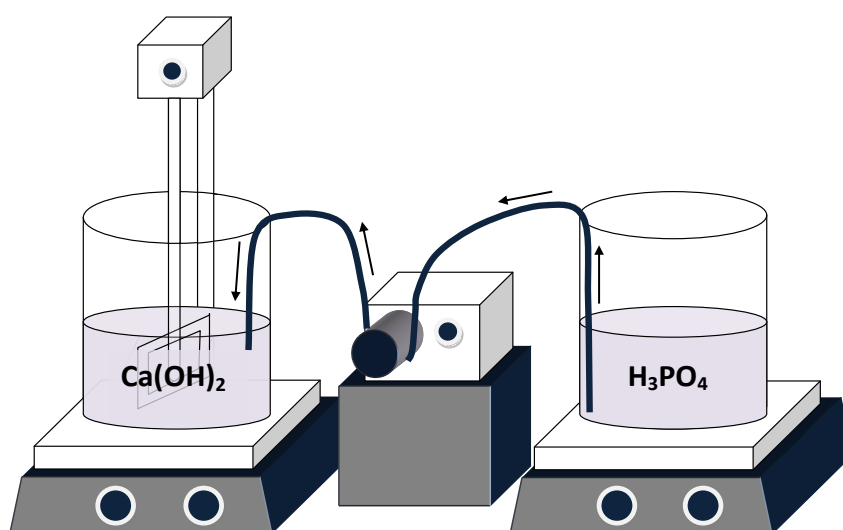


Figure 3.2: Schematic of HA production set-up.

The following day, the majority of the ammonia solution was decanted from the top of the beaker, leaving the HA precipitates that had settled to the bottom during the ageing process. Next, the precipitate slurry was filtered under vacuum using a large funnel and filter paper (Fisher Scientific, QL100, 240 mm). The filter cake was then washed with DIW, filtered for a second time, and placed in a drying cabinet at 80°C overnight. Approximately 50 g of HA was synthesised for each litre of starting Ca(OH)<sub>2</sub> solution.

### ***Processing***

After drying overnight, the filter cake was ground with a mortar and pestle. The resulting powder was then poured into polyethylene bottles along with alumina milling media (10 and 12 mm in diameter), so that approximately one-third of the container was filled with powder, one-third with milling media, and one-third was left empty. The powder was then milled for 48 hours.

Following milling, the powder was sieved on a vibrating table, and any particles smaller than 75 µm in diameter were separated out and considered fully processed. The remaining powder was milled a further 24 hours. Once again, powder particles smaller than 75 µm were separated out, and then mixed with the other fully-processed powder.

### **3.1.2 Carbon nanotube synthesis**

The multi-walled carbon nanotubes (MWNTs) used in the composites were grown by CVD. Ferrocene (98%, Aldrich) served as the source for the iron catalyst and toluene (99.5+%, Aldrich) as the primary carbon source. The MWNTs were grown directly on a quartz reaction tube in a two-stage horizontal tube furnace in an Ar atmosphere (Figure 3.3). A 4 wt.% ferrocene in toluene solution was prepared and injected into the first stage of the furnace, maintained at 180°C, at a rate of 5.6 mL hr<sup>-1</sup> for 4 hours. The vaporised reactants were then carried by the Ar gas at a flow rate of 2.4 L min<sup>-1</sup> to the second stage of the furnace, maintained at 760°C, where ferrocene decomposed to form the iron catalyst and the subsequent MWNT growth occurred. Upon completion of the MWNT synthesis, the quartz tube was allowed to cool overnight. The CNTs were then scraped off the inside of the tube in a glove box. Yields were ~5-7 g per batch. After characterisation to ensure an acceptable quality of the CNTs, material from five batches was mixed

together for use in the composites. This mixing step was included to minimise the effects of any batch variation.

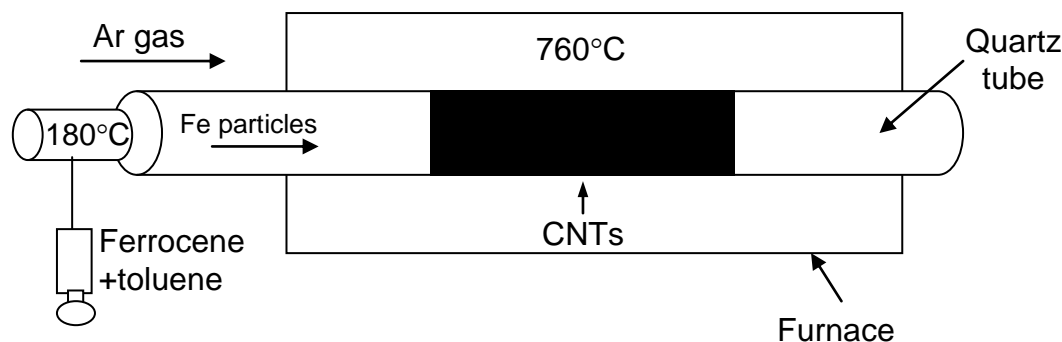


Figure 3.3: Schematic of CNT growth set-up.

### ***Carbon nanotube functionalisation***

To encourage interaction between the HA and MWNTs and to improve the dispersion of the nanotubes, the MWNTs were acid treated to functionalise the ends and wall defects with  $-\text{COOH}$  and  $-\text{OH}$  groups. MWNTs for functionalisation were taken from the mixed CNT batch and were ultra-sonicated in a 3:1 volume ratio of sulphuric (95+%, Fisher Scientific) to nitric acid (70% assay, Fisher Scientific). For each batch, 2.5 g of MWNTs was sonicated with 400 mL of acid in a round-bottomed, glass flask. The functionalisation took place over two days. The mixture was sonicated for 6 hours the first day, left to sit overnight, then sonicated an additional 6 hours the following day. At the end of the second day, the acid and MWNTs were combined with 600 mL DIW and left overnight.

On the third day, the functionalised CNTs (fCNTs) were filtered and washed with DIW. The mixture was filtered under vacuum with a porosity 4 (10-16  $\mu\text{m}$  pore size) borosilicate sintered glass filter. After each filtration, 1 litre of DIW was added to the filtered CNTs. Filtration continued until the filtered solution had a pH of  $\sim 7$  (usually after seven filtrations). While the pore size of the filter was relatively large, especially compared with the filter membranes normally cited for this purpose in the literature, only a very minimal amount of CNTs was found to have passed through the filter. As most of

the fCNTs were more than 16  $\mu\text{m}$  in length, they would have to have been very well dispersed and oriented fairly vertically to pass through the filter.

Following filtration, the fCNTs were placed in a loosely covered container in an oven at 120°C overnight to dry. No significant difference in mass was observed before and after functionalisation, suggesting that any loss in mass due to CNTs passing through the filter or removal of amorphous carbon and catalyst particles was balanced by the added mass of the functional groups.

### **3.1.3 Composite synthesis**

Composite materials were made by an *in-situ* precipitation method, similar to the method used to synthesise HA. Composites with both as-made CNTs (nCfCNTs) and fCNTs with loadings of 0.5, 1.0, 2.0 and 5.0 wt.% were produced.

First, the amount of CNTs needed for each batch was calculated with a loading relative to the expected amount of HA (e.g. 2.04 g of CNTs was used for a batch expected to produce 100 g of HA and a 2 wt.% composite, as the total mass of the composite would be 102.04 g). The CNTs were then added to 750 mL of DIW. The mixture was first shaken on a vibrating table for 30 minutes to break up any large clumps, then ultrasonicated an additional 15 minutes to break up smaller clumps. The CNT mixture was then added to the solution of  $\text{Ca}(\text{OH})_2$  and allowed to stir for 30 minutes before addition of the  $\text{H}_3\text{PO}_4$  solution began to allow the  $\text{Ca}^{2+}$  ions to interact with the negatively-charged functional groups on the fCNTs. This step was also included when making composites containing nCfCNTs. In the case of composite synthesis, the amount of DIW in the  $\text{Ca}(\text{OH})_2$  solution was reduced by 750 mL so that the total amount of DIW in the solution once the CNTs had been added would be the same as when synthesising pure HA.

The remainder of the synthesis was carried out as described in Section 3.1.1:  $\text{H}_3\text{PO}_4$  was added drop-wise to the mixture of  $\text{Ca}(\text{OH})_2$  and CNTs over a period of 3–4 hours, the entire suspension was then stirred an additional hour, left to age overnight, and filtered under vacuum the following day. At this point, rather than dry the filter cake right away, it was first shear mixed for 15 minutes to achieve a more homogeneous mixture of HA and CNTs under more viscous conditions. This procedure most notably improved the composites with nCfCNTs, as nCfCNTs do not disperse well in water and thus are more

susceptible to clumping during the *in-situ* precipitation process. After shear mixing, the material was dried overnight.

### ***Processing***

The dry composite material was processed in a similar way to the pure HA material. First, it was ground by mortar and pestle, milled for 48 hours, then sieved to separate out particles less than 75 µm. The remaining larger powder particles were then milled for an additional 24 hours, unless otherwise noted, sieved, and all powder less than 75 µm was combined and considered fully processed. After characterisation to ensure phase purity and hydroxylation of each batch, batches of the same loading and CNT type were combined to minimise batch variation.

#### **3.1.4 Tablet formation**

For the purpose of heat treatment investigations, mechanical testing, and evaluation of biological properties, the powders were pressed into tablets. A variety of pressing conditions were tested, and what follows are the methods which resulted in the most consistent and robust samples.

The tablets were formed by uniaxially pressing the powder in a 13 mm evacuable steel or tungsten carbide pellet die. A suspension of magnesium stearate ( $\text{Mg}(\text{C}_{18}\text{H}_{35}\text{O}_2)_2$ ) in ethanol was applied as a lubricant to the sample-contacting surfaces of the pellets and the die walls. Unless otherwise noted, 0.8 g of powder was pressed at pressures of 55 – 110 MPa (700 – 1500 kg force for the 13 mm tablets) under vacuum and held for 2 minutes before releasing the pressure and ejecting the tablet. It was observed that important factors for preventing tablet delamination and capping included the application of lubricant, the 2-minute hold time, and also very slowly applying and releasing the pressure.

## 3.2 Material characterisation methods

The following characterisation methods were used to examine the green materials described in this chapter. They were also used throughout the study to assess the material properties and will be referenced in later chapters.

### 3.2.1 Physical characterisation

#### 3.2.1.1 Density

The density of the tablets was calculated from measurements of tablet dimensions and mass. Archimedes' method was not used as the samples contained open porosity (even after heat treatment, in some cases). To calculate the percentage of theoretical density (% TD), the measured density was compared to the theoretical density of HA ( $3.16 \text{ g cm}^{-3}$ ) for the pure HA samples and the calculated theoretical density of the composite samples, taking into account the loading of CNTs and using a density of  $2.00 \text{ g cm}^{-3}$  for the MWNTs. The following formula was used:

$$\% TD = \frac{\rho_{sample}}{L_{CNTs} \times 2.00 \frac{g}{cm^3} + (1 - L_{CNTs}) \times 3.16 \frac{g}{cm^3}} \times 100\%$$

where  $L_{CNTs}$  is the weight percent loading of CNTs in the sample and  $\rho_{sample}$  is the measured density of the sample. Throughout the text, the % TD will be referred to as the 'density'.

#### 3.2.1.2 Powder packing density

The difference in ability of the powder particles to pack efficiently was measured as the 'powder packing density'. Three grams of powder were placed in a graduated cylinder which was then agitated on a vibrating table at an amplitude of  $1.20 \text{ mm g}^{-1}$  for 2 minutes. The volume after agitation and the mass of the powder were used to calculate the packing density. Two measurements were taken and the results were averaged.

### ***3.2.1.3 Specific surface area***

Specific surface area was measured by the Brunauer-Emmett-Teller (BET) method using a Micromeritics Tristar 3000. Eight partial pressures were taken and used to calculate the surface area. Samples were prepared by outgassing in N<sub>2</sub> at 180°C for at least two hours.

### ***3.2.1.4 Particle size distribution***

The distribution of powder particle sizes was measured using a Mastersizer 2000 (Malvern Instruments). To prepare samples for measurement, approximately 0.5 g of powder was ultra-sonicated in 800 mL of water for 2 min. Measurements were made over the size range of 0.02 – 2000 µm. Reported values are the means of three measurements taken for each sample.

### ***3.2.1.5 Carbon nanotube loading***

To determine the loading of CNTs post-processing (green materials) and post-sintering, hydrochloric acid (HCl) was used to dissolve the HA, leaving only the CNTs and any related carbonaceous material. The remaining CNTs were then filtered from the solution and weighed. Approximately 0.5 g of powder (in the case of sintered tablets, a section of tablet was ground) was weighed and added to 50 mL of 2.0M HCl solution. The mixture was then ultra-sonicated for 5 minutes to allow the HA to fully dissolve. The solution was then filtered through polytetrafluoroethylene (PTFE) filters (0.2 µm pore size, Sartorius Biolab) and washed with 100 mL DIW. The filter was then dried in a vacuum oven at 80°C for one hour, and the mass of the filter before and after the addition of CNTs was compared. The loading of CNTs was then calculated as the ratio of the mass increase of the filter to the mass of the powder.

### ***3.2.1.6 Carbon nanotube morphology***

The length and diameter of the CNTs was measured by examination in SEM. Approximately 1 mg of CNT was dispersed in 5 mL of ethanol and a drop of the suspension was placed on an aluminium SEM stub to dry. Diameters of 100 CNTs were measured for each batch, and reported values are means ± standard deviation. The length values were also taken from SEM images. The lengths of at least 20 individual CNTs were averaged.

### **3.2.1.7 Thermogravimetric analysis**

Thermogravimetric analysis (TGA) was carried out on samples to determine if any weight loss (indicating oxidation or decomposition) occurred over the evaluated temperature range. Measurements were made in a variety of atmospheres using a TA Instruments TGA Q500 (for samples up to 1000°C) and a TA Instruments SDT Q600 (for samples up to 1200°C). The specific atmosphere and the heating and cooling profile are indicated with the presentation of results for each sample.

## **3.2.2 Physicochemical characterisation**

### **3.2.2.1 X-ray diffraction**

X-ray diffraction (XRD) was used to determine the phase composition of the samples. Of particular interest was whether or not the HA was phase pure or if there were impurities present, such as tricalcium phosphate (TCP), tetracalcium phosphate (TTCP), or calcium oxide (CaO). Powder diffraction patterns were measured on a Bruker D8 Gen 10 using a CuK $\alpha$  line (40 kV, 40 mA, 0.5° divergence slit, and 0.5° antiscatter slit). The data was recorded using a step size of 0.01° and a 0.02 second dwell time. Measured diffraction patterns were compared to powder diffraction files from the JCPDS database. Quantitative estimations of phase composition were made using the semi-quantitative feature in the X'Pert Highscore Plus (PANalytical, the Netherlands, v2.2b) software. Before analysing, a minimal amount (~0.01 mm) of material was ground off the top layer of each tablet to remove any residual material from the lubricant used when forming the tablets.

### **3.2.2.2 Fourier transform infrared spectroscopy**

Fourier transform infrared spectroscopy (FTIR) spectrographs were taken to investigate the functional groups present in the samples. In particular, this technique is useful for detecting small amounts of dehydroxylation of HA, which is difficult to detect with techniques such as XRD. Potassium bromide (KBr) pellets were prepared with approximately 200 mg of KBr and 2 mg sample. The KBr and sample were first ground, then dried in a vacuum oven at 120°C for two hours, and finally pressed into tablets of 13 mm diameter at 12 tons for 10 minutes under vacuum. A Bruker Optik Tensor 27

spectrometer was used at a resolution of  $4\text{ cm}^{-1}$ , covering the wavenumber range of  $4000\text{-}400\text{ cm}^{-1}$  in absorbance mode.

### **3.2.3 Electron microscopy**

#### ***3.2.3.1 Scanning electron microscopy***

Samples were studied using SEM to examine microstructural characteristics, CNT dimensions, HA/CNT interaction, and fracture surfaces. Samples were prepared by mounting on an aluminium stub with carbon tape and sputter coating with Pt for 50 seconds with a deposition current of 60 mA. Samples containing only CNTs were not coated. A JEOL 6340 FEG SEM was used with an acceleration voltage of 5 kV and a working distance of 6 mm in most cases.

#### ***3.2.3.2 Transmission electron microscopy***

CNTs and HA-CNT interaction were observed with transmission electron microscopy (TEM) using a JEOL 200CX TEM with an acceleration voltage of 200 kV. Samples were prepared for TEM by dispersing a small amount of powder (or ground) material in ethanol, placing a few drops of the suspension on a holey carbon-coated copper grid, and allowing it to dry.

### 3.3 Material characterisation results

#### 3.3.1 Carbon nanotube characterisation

##### 3.3.1.1 Morphology

Examining the CNTs with SEM provides an overview of their morphology and quality. Figure 3.4 shows both nfCNTs (a and b) and fCNTs (c and d), demonstrating that in both cases the CNTs have a high aspect ratio, are randomly oriented, and are entangled. As produced, the carpets were well aligned, as seen in Figure 3.5. However, ultra-sonication to prepare the samples for SEM and to functionalise them (in the case of fCNTs) broke up the carpets and led to entanglements.

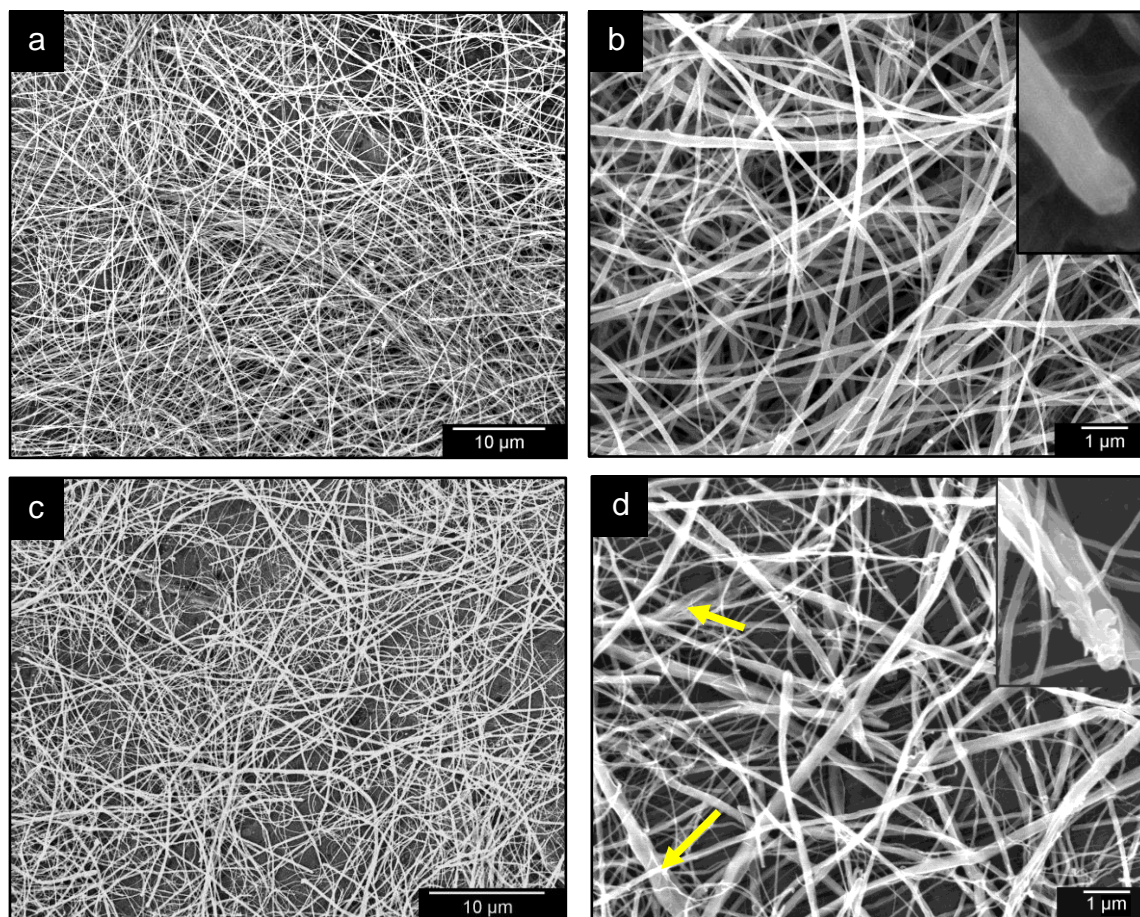


Figure 3.4: SEM micrographs showing nfCNTs (a) and (b) and fCNTs (c) and (d). Insets compare quality of CNT tips. Yellow arrows indicate 'unzipped' regions of CNTs.

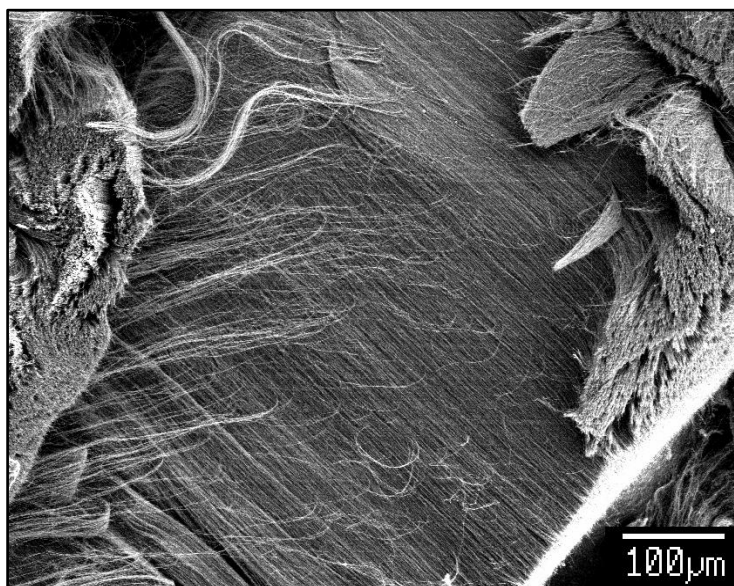


Figure 3.5: SEM micrograph of as-made MWNT carpet.

At low magnification (Figure 3.4 a and c), the functionalisation process does not seem to have altered the morphology of the CNTs. However, upon closer examination (b and d) small differences become more apparent. The insets compare high magnification images of the CNT tips, which are expected to be more susceptible to functionalisation due to the higher strain induced by the curved end structure (Liu, Z. J. *et al.* 2001). Figure 3.4(b) shows a fairly smooth tip, while Figure 3.4(d) shows a damaged functionalised tip. Figure 3.4(d) also reveals ‘un-zipped’ nanotubes, in which the graphene sheets have begun to unroll from the ends inward. The arrows identify two such nanotubes.

While the diameters of CNTs can easily be measured by examining SEM images, measuring the lengths is not as straightforward. The CNTs were so long and entwined it was rarely possible in the case of nfCNTs or fCNTs to identify any entire individual CNT. In the case of nfCNTs, which are formed as aligned carpets, the length of the CNTs can be estimated as the length of the carpet (Figure 3.5), giving a value of 0.6 mm. This value should be considered an upper limit of length, however, as not all CNTs may grow for the entire length of the carpet. It is also possible that a carpet may consist of the starts and stops of growth of several CNTs. Occasionally, it was possible to identify a few entire individual CNTs at the edge of an entanglement, and thus a length could be

measured. It is likely, however, that this is a lower estimate of the length, as no entire CNTs of similar lengths could be found inside an entanglement, despite it being possible to follow along the length of many CNTs through the part visible in the image. It is possible that these individual CNTs were distinguishable at the edge of entanglements because their short length made it easier for them to untangle and become separated from the larger bundle.

Results from the diameter measurements are provided in Table 3.1. The batches are labelled nf1-nf6 and f1-f6 to identify separate synthesis batches and functionalisation batches, respectively (all made with the same conditions). Each diameter reported in the table was based on 100 measurements. The standard deviations were large in both cases, thus more information can be gained from a distribution plot of CNT diameters.

Table 3.1: Average diameters of nfCNT and fCNT batches

Batch	Average Diameter (nm)	Batch	Average Diameter (nm)
1nf	69 ± 46	f1	61 ± 27
2nf	73 ± 52	f2	51 ± 26
3nf	98 ± 67	f3	70 ± 47
4nf	52 ± 32	f4	60 ± 45
5nf	81 ± 47	f5	83 ± 42
6nf	91 ± 52	f6	82 ± 53

Figure 3.6 shows the distribution of diameters for each batch of nfCNTs(a) and fCNTs(b). It can now be seen more clearly that the diameter values were distributed across a very wide range. For nfCNTs the range was 15-230 nm, while the range for fCNTs was 10-235 nm. In Figure 3.6(a) it is difficult to discern any clear difference between the batches. The average value peaks at about 35 nm, with a high percentage of CNT diameters falling at the lower end of the scale, and then a wide distribution across larger diameters. Figure 3.6b shows a similar distribution, with a peak just before 50 nm and a wide distribution across larger diameters, although it should be noted that there appear to be fewer of the widest CNTs in the case of fCNTs than for nfCNTs. When the average distributions are

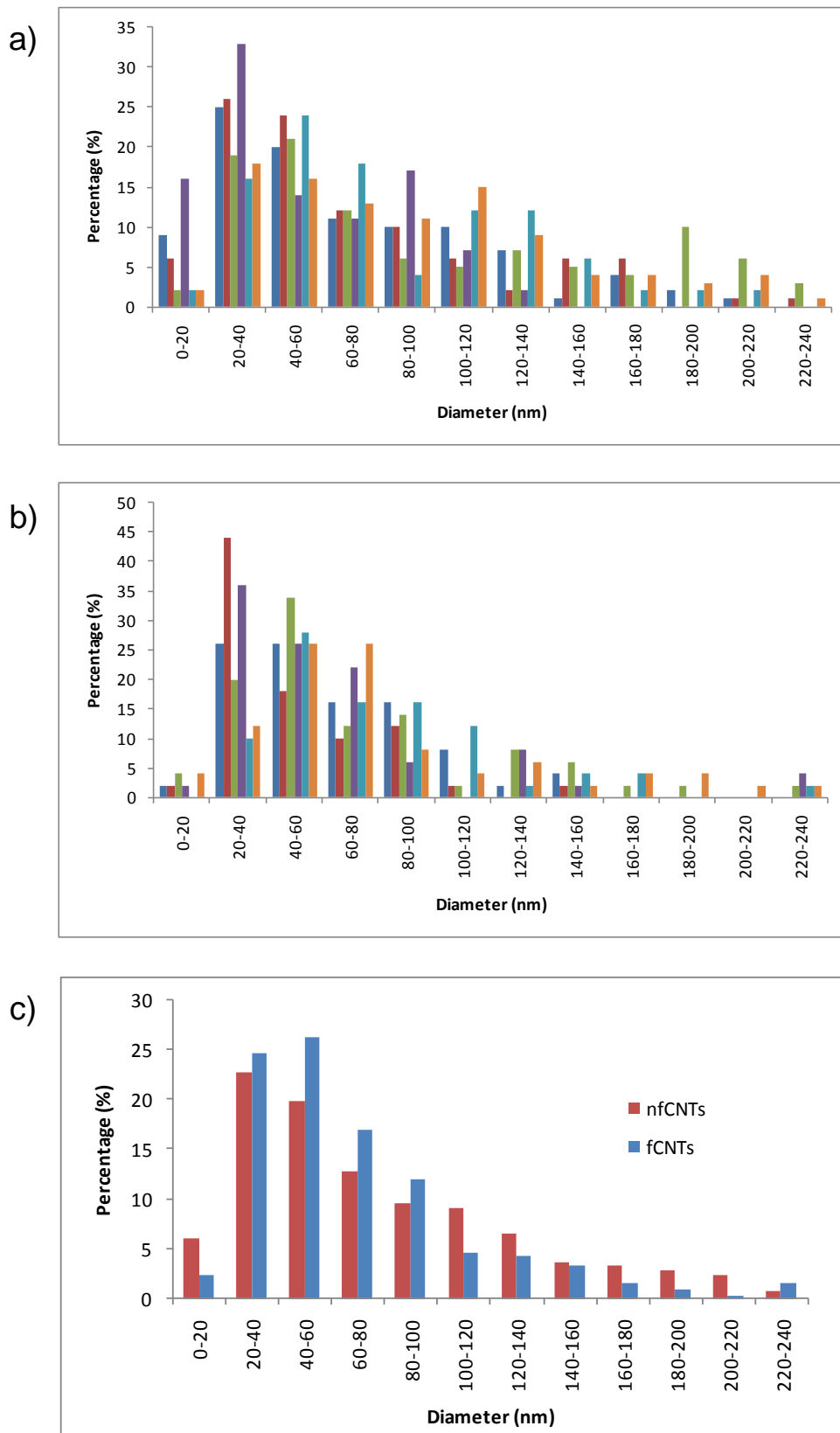


Figure 3.6: Distribution of CNT diameters for nfcCNTs (a), fcCNTs (b), and comparing average values for nfcCNTs and fcCNTs (c). For (a) and (b) each colour represents a different batch.

plotted on the same scale, as shown in Figure 3.6(c), it can be observed that the distributions are, indeed, very similar, although there are fewer very large diameter fCNTs.

Table 3.2 shows a summary of CNT morphology measurements. It includes the distribution of diameters at  $d_{0.1}$ ,  $d_{0.5}$ , and  $d_{0.9}$  as well as lengths and an estimate of aspect ratio. The diameter values are based on 600 measurements in each case, while the individual length values are based on 20 measurements. The aspect ratio was calculated from the extremes of diameter and length in each case to give a range of values.

Table 3.2: Summary of CNT morphology measurements and calculations.

	$d_{0.1}$ (nm)	$d_{0.5}$ (nm)	$d_{0.9}$ (nm)	$L$ ( $\mu\text{m}$ ) (carpet)	$L$ ( $\mu\text{m}$ ) (individual)	<b>Aspect ratio (L/d)</b>
<b>nfCNTs</b>	18	48	150	600	$63 \pm 40$	$10^2$ - $10^4$
<b>fCNTs</b>	22	52	125	NA *	$27 \pm 10$	$>10^2$

\*NA = not applicable

The aspect ratios were in the same range for both nfCNTs and fCNTs, although the ratio is likely larger for nfCNTs, in general, as nfCNTs will not have been shortened by ultrasonication during the functionalisation process.

### ***3.3.1.2 Oxidation behaviour***

TGA was used to 1) understand the oxidation behaviour of CNTs at high temperatures, 2) distinguish between the behaviour of nfCNTs and fCNTs, and 3) compare the extent of functionalisation of different batches of fCNTs by examining their relative susceptibility to oxidation. Also, since all of the batches were functionalised following the same procedure, TGA could be used for quality control. Figure 3.7 shows the oxidation behaviour of six batches of fCNTs and the mixed batch of nfCNTs.

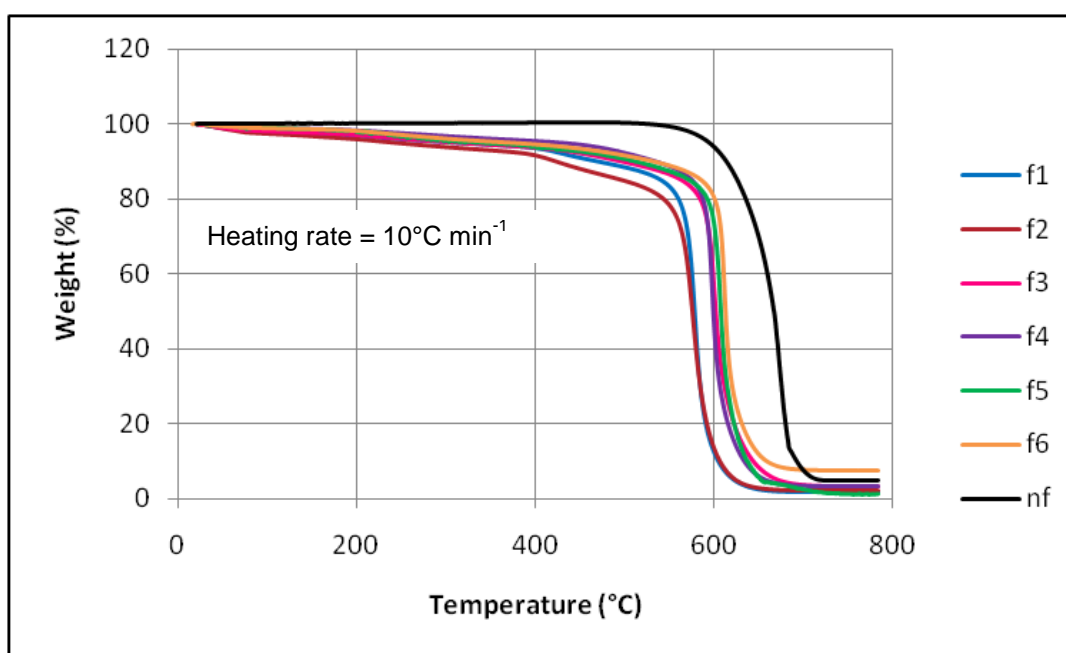


Figure 3.7: TGA comparing six fCNT batches and mixed nfCNT batch.

From Figure 3.7 the peak burnout temperature of nfCNTs occurred at a much higher temperature (674°C) than for the fCNT batches (average 595°C). Additionally, an initial weight loss of 15-20% occurred prior to peak burnout in the fCNTs compared with virtually no prior weight loss in the nfCNTs. The weight loss for fCNTs can be separated into several stages. Up until 250°C, the weight loss can be attributed to adsorbed water. Since fCNTs are hygroscopic, they adsorb water from the atmosphere, unlike the hydrophobic nfCNTs. From 250°C to about 400°C, the functional groups begin to oxidise. Then, from 400°C to 550°C, any fCNTs severely damaged by the functionalisation process are oxidised before the burnout becomes much more significant and quick at higher temperatures. On the other hand, nfCNTs are hydrophobic, do not have functional groups and have higher and more uniform quality compared with fCNTs, thus weight loss occurs over a much narrower temperature range. Additionally, this oxidation occurs at a much higher temperature because the nfCNTs contain far fewer defects than the fCNTs, as they have not undergone the damaging functionalisation process.

As all of the fCNT curves seem similar and distinct from the nfCNT curve, it can be estimated that they have all been functionalised to a similar extent. However, the curves

for f1 and f2 do stand out as seeming to be more damaged, and thus more functionalised, due to their lower peak oxidation temperature. This may be due to them having both been functionalised on the day new bottles of acid were opened. The acid was most reactive at this point, so may have functionalised the CNTs more extensively.

Finally, the role of residual iron content of the CNTs should be examined. It could be expected that any remaining mass at the end of peak oxidation is iron oxide residue from catalyst particles. It would also be expected that some of this residue would be removed during the functionalisation process, in which the ends of the CNTs are opened, thus providing the opportunity for the catalyst particle to be released. However, as the data show, not all of the iron seems to be removed. Visual evidence of this can be seen in a TEM image of a fCNT (Figure 3.8) which shows a residual encapsulated catalyst particle which appears to have been protected from the acid treatment by layers of carbon.

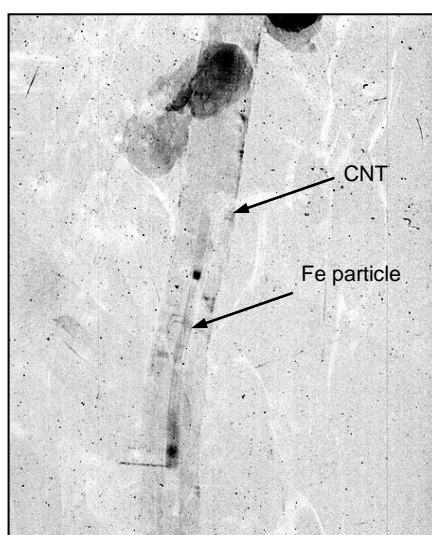


Figure 3.8: TEM image of a residual Fe particle in a fCNT.

Table 3.3 shows the peak oxidation temperature for each batch as well as the amount of iron oxide residue and the amount of iron remaining at the end of the run (calculated from the assumption that all residue is  $\text{Fe}_2\text{O}_3$ ). With the exception of f6, a significant portion of

Table 3.3: Peak oxidation temperature and wt.% residual Fe oxide and Fe in CNT batches.

Batch	Peak oxidation temp. (°C)	Fe <sub>2</sub> O <sub>3</sub> (wt.%),	Fe (wt.%)
f1	578	1.6	1.1
f2	576	2.0	1.4
f3	600	3.3	2.3
f4	598	3.3	2.3
f5	607	1.2	0.8
f6	612	7.5	5.3
nf, mixed	674	5.0	3.5

the iron seems to have been removed from each batch. The f6 batch, however, appears to be anomalous as there should not be any reason for more residue to be present in a functionalised batch compared with the nfcCNTs.

### 3.3.2 Physical properties

#### 3.3.2.1 Homogeneity

The degree of homogeneity in the composite materials is dependent on how well CNTs are dispersed in the HA matrix. This can be observed both in the appearance of the material to the naked eye and in high-magnification SEM images. Two factors were observed to affect the homogeneity most distinctly: whether or not the CNTs were functionalised and the technique used to combine the CNTs and HA.

In initial studies into the best production method for the composites, shear mixing an HA slurry with CNTs was compared with the *in-situ* precipitation technique in which CNTs are added to the solution as the HA precipitates. Additionally, nfcCNTs were compared with fcCNTs. The SEM images in Figure 3.9 best summarise the findings.

The left-hand images show that composites prepared with nfcCNTs result in an inhomogeneous dispersion of HA and CNTs, regardless of the preparation technique,

while the right-hand images show that composites containing fCNTs have a more homogeneous dispersion of HA and CNTs. In terms of dispersion, no real difference was observed between the top and bottom rows of images, and thus from it would appear the shear mixing and *in-situ* precipitation techniques produce materials with similar degrees of homogeneity.

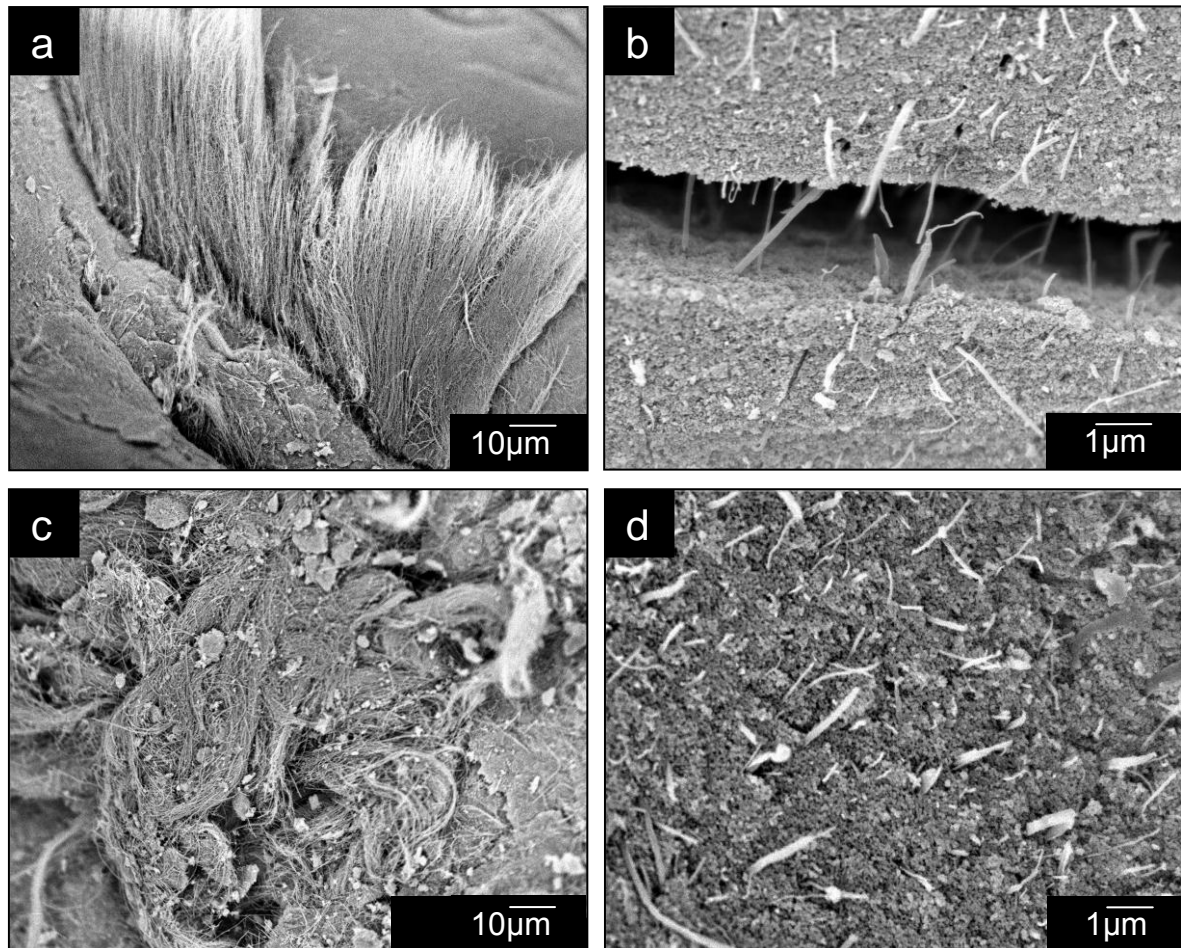


Figure 3.9: SEM images comparing preparation techniques and nfcCNTs vs. fcCNTs. (a) mixed, nfcCNT; (b) mixed, fcCNT; (c) *in-situ*, nfcCNTs; (d) *in-situ*, fcCNTs.

More striking in this respect are the differences that can be seen with the naked eye. It was observed on a macro level that shear mixing helped to achieve a more homogeneous dispersion of CNTs. Due to this observation and observations discussed in Section 3.3.3.3 on interaction, the preparation technique for the composites was developed as outlined in Section 3.1.3, wherein the *in-situ* technique is used, followed by shear mixing, thus combining the benefits of both methods.

### 3.3.2.2 CNT loading post processing

To examine the effect processing might have on CNT loading and to validate the measurement method described in Section 3.2.1.5, the CNT loading of some of the composite powders was measured. Figure 3.10 compares the post-processing CNT loadings over a range of expected pre-processing loadings for powders with particle size  $>75 \mu\text{m}$  and  $<75 \mu\text{m}$ .

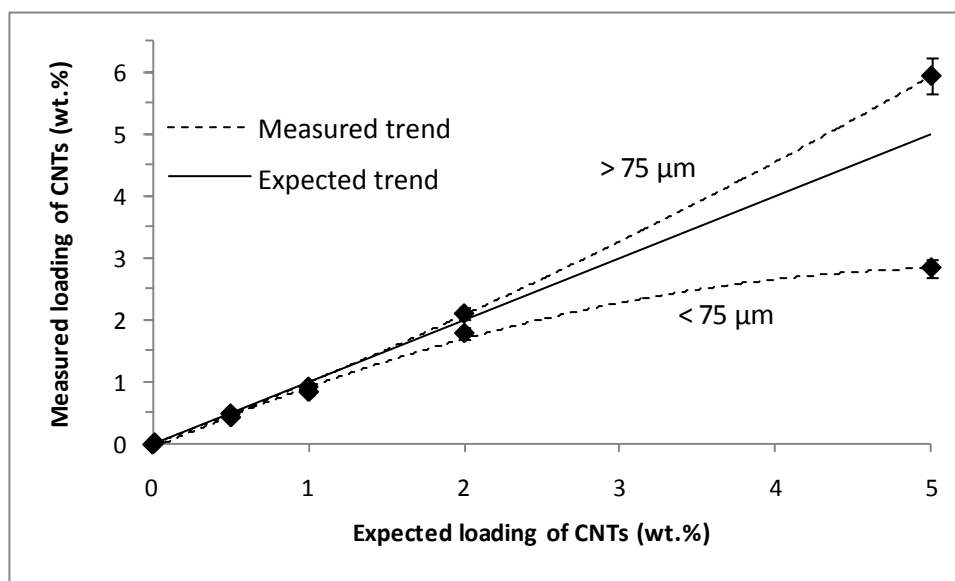


Figure 3.10: Plot of relationship between measured CNT loading post processing and the expected loading, based on the original amount of CNTs incorporated into the material. The solid line shows the expected trend, while the dotted lines show the measured trends.

The plot shows that the ‘fully-processed’ powders with particle size  $<75 \mu\text{m}$  contained fewer CNTs than did the powders whose particle size remained  $>75 \mu\text{m}$ . This trend of deviation from the expected loadings was exaggerated at higher CNT loadings. These data suggest that ball milling was not as effective at reducing the particle size at high CNT loadings; thus, the CNTs became segregated, with fewer CNTs remaining in the smaller diameter particles and more remaining in the larger diameter particles. It is important to note that fully-processed powders expected to contain 5 wt.% CNTs may actually contain only about half that loading.

As controls, the CNT loading of fCNTs and HA were measured. The fCNT sample showed a 97 wt.% loading, while HA showed 0.01 wt.%. Additionally, a Teflon filter was

submitted to the same acid filtration, but without any material, and no weight change was observed. Thus, this method of measurement appears to be accurate within a reasonable degree of error.

### ***3.3.2.3 Powder properties***

The size (diameter) of powder particles has been shown to be directly related to compaction (green density) and the ultimate sintered density of ceramics (Kendall 1989). Figure 3.11 shows the distribution of particle sizes, as measured by particle size analysis, while Table 3.4 gives specific values at different points along the distribution curve ( $d_{0.1}$ ,  $d_{0.5}$ ,  $d_{0.9}$ ). The samples are labelled according to  $xnf$  or  $xf$ , where  $x$  is the loading of CNTs (either 0.5, 1, 2, or 5 wt.%) and the composites are made with nfcNTs or fcNTs, respectively. In the case of 5f, multiple batches were made, and these are notated by 5f-1, 5f-2, 5f-3, 5f-3,2, and 5f-bio. The 5f-3,2 batch was the same material as the 5f-3 batch, but milled for 96 hours.

Figure 3.11 shows that all the powders had a bimodal distribution of sizes with peaks at similar values, although the ratio of volume percents for the two peaks varied significantly among the different materials, which is reflected in the values. HA showed the most even distribution of particles between the two modes. It also had the lowest diameter values for each mode, with an average particle size of 10  $\mu\text{m}$ . The 5f powder, on the other hand, while still bimodal, had the highest relative volume percent of larger particles to smaller particles compared with the other materials, with an average particle size of 22  $\mu\text{m}$ .

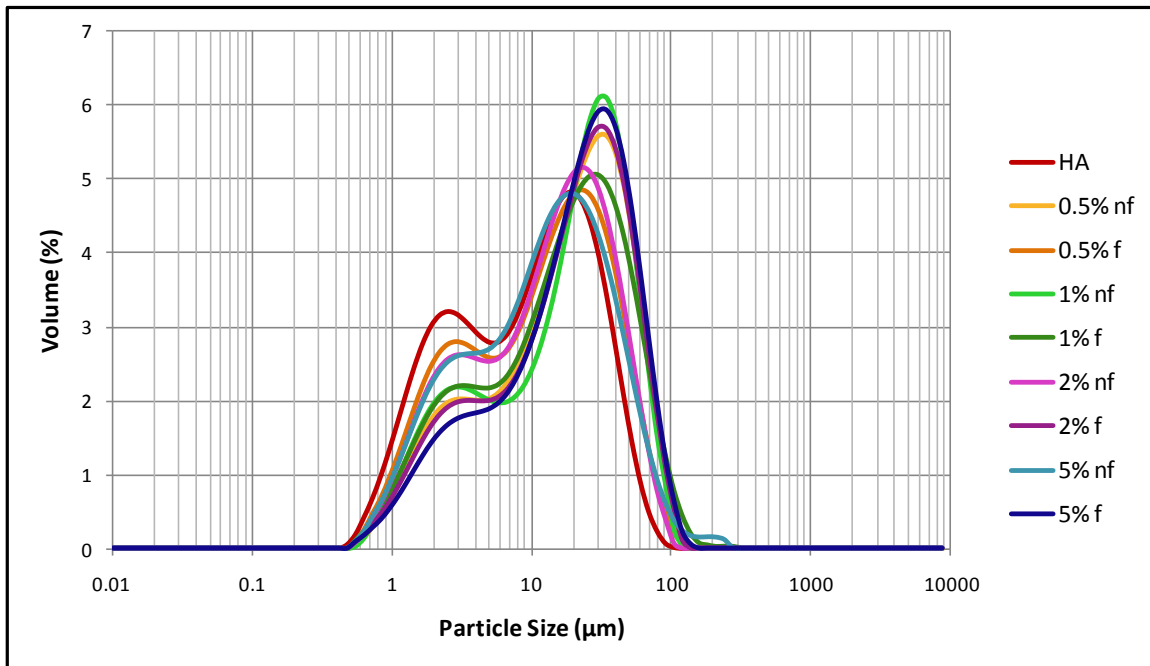


Figure 3.11: Particle size distribution of HA and composite powders.

Table 3.4: Summary of particle size distribution of HA and composite powders.

Sample	$d_{0.1}$ ( $\mu\text{m}$ )	$d_{0.5}$ ( $\mu\text{m}$ )	$d_{0.9}$ ( $\mu\text{m}$ )
HA	1.7	10	37
0.5nf	2.5	20	58
1nf	2.3	21	57
2nf	2.1	14	46
5nf	2.1	13	48
0.5f	2.0	14	47
1f	2.3	18	61
2f	2.6	21	60
5f-1	2.9	22	62
5f-2	2.9	26	97
5f-3	3.1	27	75
5f-3,2	2.7	25	80
5f-bio	3.0	21	82

The general trend in the nfCNT composite powders appears to be decreasing particle size with increasing CNT loading, while for the fCNT composites the particle size increased with decreasing CNT loading. This could be explained by differences in homogeneity in the samples and the distribution of CNTs within the powders at different loadings for different types of composites. In the case of nfCNT powders, the bundled CNTs act as defects; the more CNTs are in the sample, the more defects are present, and thus it becomes easier to break apart powder particles as the loading of CNTs increases. In the case of fCNT powders, however, the CNTs are more evenly distributed, and thus an increase in CNT loading may reinforce the individual powder particles, toughening them and making them more difficult to break apart. Indeed, it was observed when grinding the powders by hand, that it was most difficult to grind the 5f materials, while it was relatively much easier to grind any of the nfCNT composite materials.

Figure 3.12 shows SEM images of the powders. The powder particles appear from the SEM images (a-c) to have two main sizes which are similar to those shown in the particle size analysis. While the particles are fairly round, they have irregular edges and so are not as smooth as particles generally observed for some calcined powders. Images (d) and (e) show the distribution of CNTs in the powders. There is no clear distinction between the nfCNT and fCNT composites, but CNTs can be more clearly observed extending from the edges of the powder particles (e) in these higher magnification images and in some cases CNTs seem to join together particles (d).

Table 3.5 gives an overview of several properties of the powders: bulk packing density, average particle size, and surface area. Considering the surface area, it can be seen that the values of the HA and composite powders ranged from 67-95 m<sup>2</sup> g<sup>-1</sup>, with most values between 88-90 m<sup>2</sup> g<sup>-1</sup>. It was noted that the values for 5f-2 and 2f were particularly low, though it was not readily evident why this might be. The CNTs, in comparison, had much lower surface area values of 31 m<sup>2</sup> g<sup>-1</sup> for nfCNTs and 45 m<sup>2</sup> g<sup>-1</sup> for fCNTs. The fCNTs may have a higher value of surface area due to a greater concentration of defects, and functional groups on the surface of the CNTs.

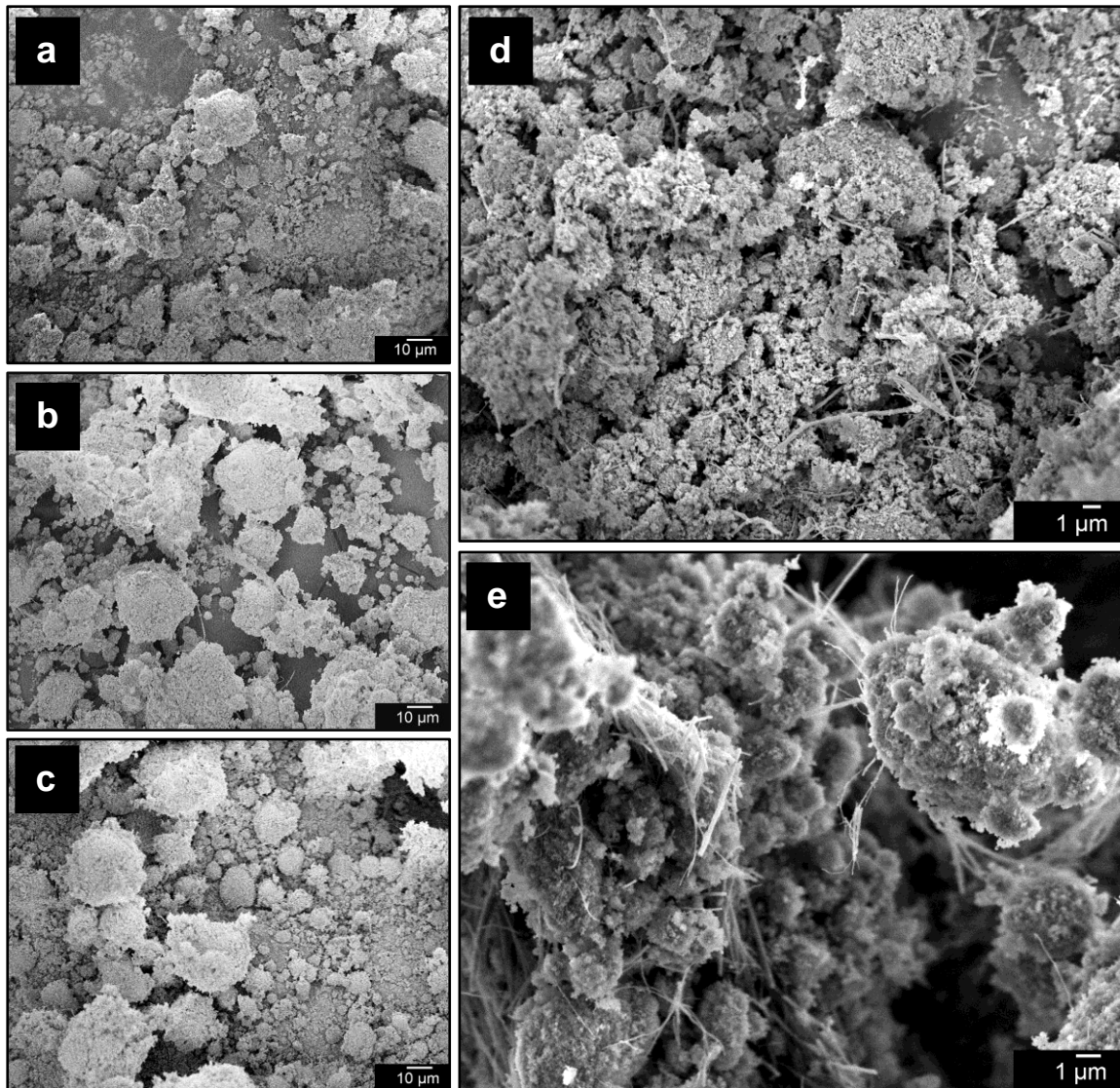


Figure 3.12: SEM images of powder particles. (a) HA; (b) 5nf; (c) 5f; (d) 5nf; (e) 5f.

The bulk density data shows a general trend of decreasing density with increasing loading of CNTs. However, this trend is more dramatic for the nfcNT composites compared with the fcNT composites. In fact, nfcNT composite particles pack significantly more tightly for nfcNT composites at lower loadings compared with fcNT composites. Interestingly, the bulk density of pure HA was slightly lower than that of 0.5nf. The general trend of decreasing density with increasing CNT loading is to be expected. As more CNTs are

added to the composites, sticking out of each particle, it becomes more difficult to achieve tight packing. The bulk density data does not seem to correlate in any way with the average particle size.

Table 3.5: Summary of green powder properties.

<b>Material</b>	<b>Bulk Density (g cm<sup>-3</sup>)</b>	<b>Average Particle Size (µm)</b>	<b>Surface Area (m<sup>2</sup> g<sup>-1</sup>)</b>
HA	0.64	10	85
0.5nf	0.66	20	93
1nf	0.60	21	88
2nf	0.45	14	89
5nf	0.37	13	88
0.5f	0.53	14	90
1f	0.53	18	95
2f	0.50	21	70
5f-1	0.49	22	88
5f-2	NM	27	67
5f-3	NM	26	82
5f-3,2	NM	25	91
5f-bio	NM	21	86
nfCNTs	0.33	NM	31
fCNTs	1.0	NM	45

\*NM = not measured

### **3.3.3 Physicochemical properties**

Physicochemical characterisation was carried out on both the HA and composite powders. XRD was used to determine the composition of the materials to ensure phase purity. FTIR was used to determine the level of hydroxylation of the material. Finally, the composite samples were examined for evidence of chemical interaction between the HA and CNTs.

#### **3.3.3.1 Phase purity**

Results of XRD analysis are shown in Figure 3.13. Sample patterns from each formulation are shown after sintering in wet Ar. Additionally, the pattern for green HA is shown. The measured patterns were analysed and compared to powder diffraction files (PDFs). The primary phase in all cases was matched as hydroxyapatite (PDF 9-432, shown in blue), and in many cases there was also a small amount of  $\beta$ -tricalcium phosphate (PDF 9-169, shown in red). The main peak for graphite in CNTs, which occurs at  $2\theta = 26.6^\circ$  was not observed as too many CNTs burned out of the samples due to oxidation from water in the atmosphere.

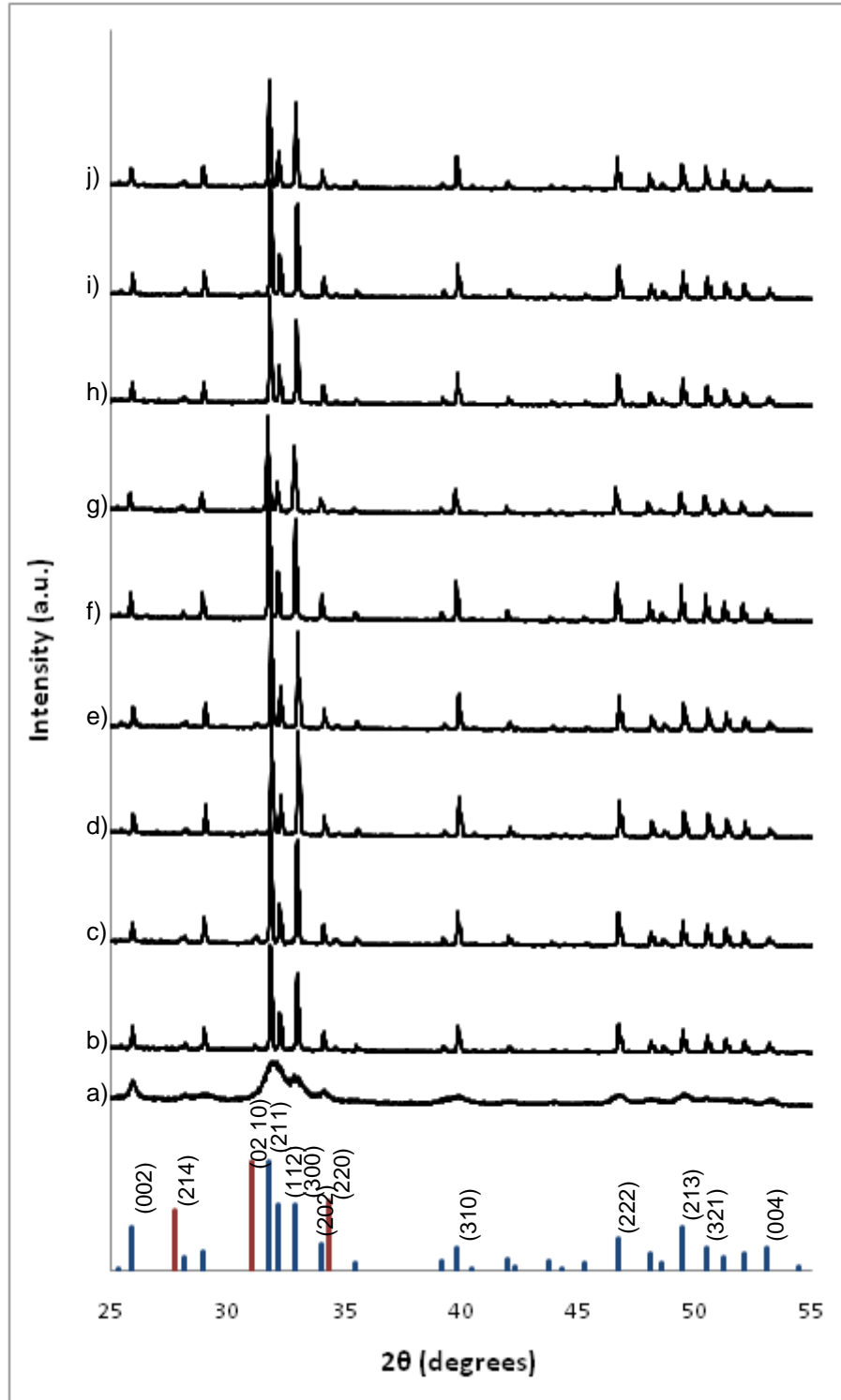


Figure 3.13: XRD patterns of HA and composite materials. (a) green HA, (b) HA sintered at 1200°C, (c)-(f) 0.5%, 1%, 2%, 5wt.% nCNTs, (g)-(j) 0.5%, 1%, 2%, 5wt.% fCNTs. Reference patterns for HA (blue) and  $\beta$ -TCP (red) shown at bottom.

### 3.3.3.2 Hydroxylation

The extent of hydroxylation of each green batch was examined using FTIR. This data is particularly important when comparing the hydroxylation of sintered materials, which can easily become dehydroxylated during heat treatment. FTIR was performed on each batch of material. Figure 3.14 shows example scans for each type of material, and Table 3.6 gives the expected and observed locations of the main peaks attributed to HA. All peaks were present and in the expected location. Both the –OH stretch peak and –OH libration shoulder were observed in each material, although the libration peak, in particular, became more obscured with increased CNT loading. This is to be expected as CNTs absorb infrared radiation.

Table 3.6: FTIR peak assignments for HA.

<b>Peak</b>	<b>Wavenumber (cm<sup>-1</sup>), expected</b>	<b>Wavenumber (cm<sup>-1</sup>), observed</b>
OH stretch	3572	3572-3573
Adsorbed H <sub>2</sub> O	1640; 3450	1634-1645; 3700-2500
CO <sub>3</sub> <sup>2-</sup>	875; 1460	872-873; 1418-1421
PO <sub>4</sub> <sup>3-</sup> (ν <sub>1</sub> )	962	956-958
PO <sub>4</sub> <sup>3-</sup> (ν <sub>3</sub> )	1046; 1087	1031-1033; 1102-1104
PO <sub>4</sub> <sup>3-</sup> (ν <sub>4</sub> )	565; 606	566-567; 604-605
OH libration	630	636-637

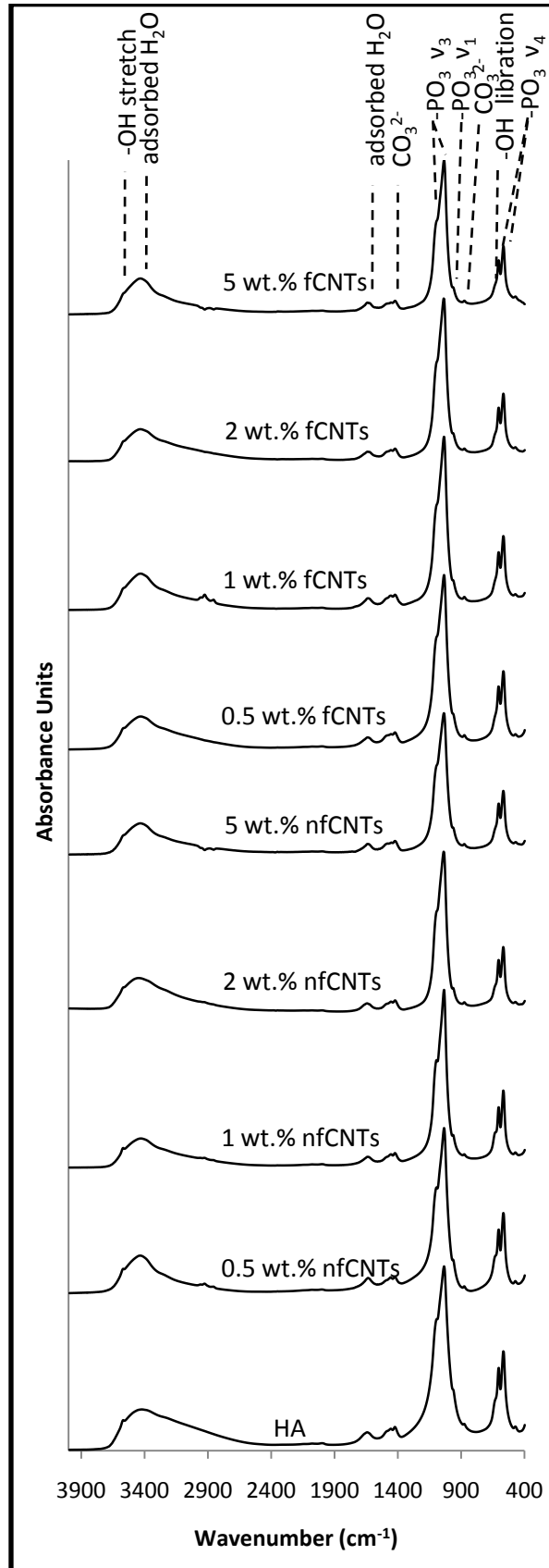


Figure 3.14: FTIR scans of green materials.

### **3.3.3.3 Interaction**

The degree of interaction between HA and CNTs was investigated using SEM and TEM. Figure 3.15 shows some representative micrographs of the composites, comparing the degree of interaction between HA and nfCNTs (a-c) and HA and fCNTs (d-f). In Figure 3.15(a) CNT-shaped holes can be seen in the HA matrix where the nfCNTs appear to have separated from the matrix, demonstrating that the degree of interaction between the two phases was quite low. Figure 3.15(b) shows a TEM micrograph of a few nfCNTs and a number of HA particles. In this case, there is no particular evidence that the HA particles are attracted to the nfCNTs; they seem to simply be mixed. Figure 3.15(c) is a closer view of a nfCNT in one of the composite materials in which no HA particles can be seen in the vicinity of the CNT. In contrast, Figure 3.15(d-f) show that fCNTs illicit a much higher degree of interaction with HA. HA particles appear to be adhering to the fCNTs in Figure 3.15(d), and in Figure 3.15(e), HA appears to surround and engulf a small bundle of fCNTs. With functionalisation, the CNTs also seem to be able to attract HA crystals, as shown in Figure 3.15(f). While the interaction is not enough to be really termed a ‘coating’, there appears to be a large degree of attraction between the fCNTs and HA. While this phenomenon was not observed along the entire length of a fCNT, almost always HA particles were attracted to the ends of fCNTs and occasionally along significant lengths of a fCNT, as shown in Figure 3.15(f).

The observation that attraction occurs most often at the ends of fCNTs matches with what theory and observation suggest about the location of functional groups. Functionalisation tends to break open the ends of CNTs, where the strain is highest, and attach functional groups firstly there (Yu, R. *et al.* 1998). Anywhere else there is a defect in the CNT structure, then functional groups can also attach there. Since the functional groups known to be added in chemical oxidation by sulphuric and nitric acid, such as –OH and –COOH, are negatively charged, it has been proposed that the positively-charged calcium ions would be attracted to these functional groups during the precipitation process, and thus form HA particles adhering to a CNT (Zhao, L. P. *et al.* 2004).

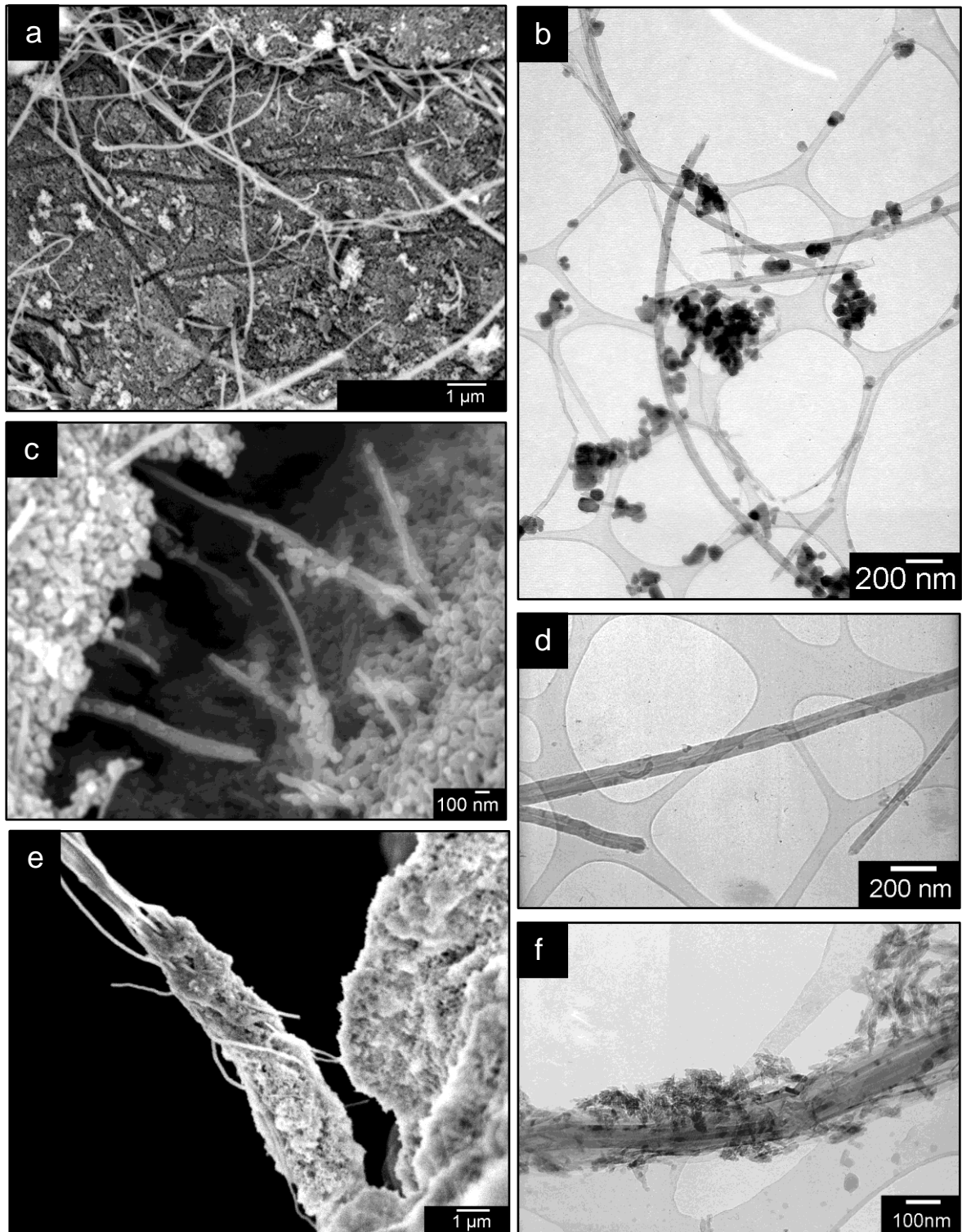


Figure 3.15: Micrographs demonstrating interaction between HA and CNTs. nFCNT composites (a,b,d); fCNT composites (c,e,f).

### 3.3.4 Tablet characteristics

#### 3.3.4.1 Appearance

The tablets ranged in colour from white (HA) to black (5f) with various shades of grey in between. Selected images of the tablets are shown in Figure 3.16. As CNT loading increased, the tablets became increasingly dark. An interesting observation, however, is that nfCNT composite tablets were lighter for a given loading of CNTs than the fCNT tablets. This is possibly due to differences in the homogeneity of the materials.

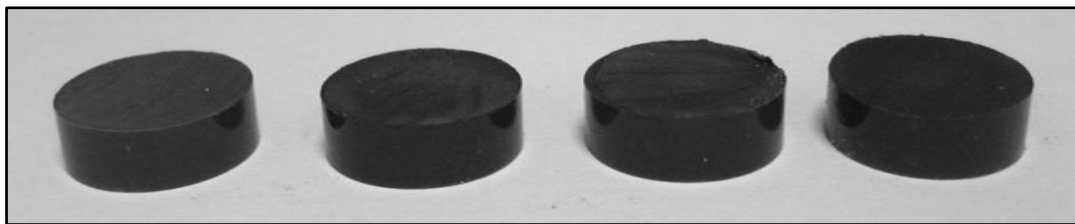


Figure 3.16: Green tablets of fCNT composite. CNT loading increases and colour darkens from left to right.

#### 3.3.4.2 Pressing characteristics

As green density may have an effect on the final sintered density of HA tablets, the pure HA, 5nf and 5f powders were pressed at a range of pressures and the resulting green density was calculated by measuring the dimensions of the tablets and their mass. The results are shown in Table 3.7 and Figure 3.17. Each data point is based on an average of at least four samples.

Table 3.7: Green tablet density (%TD) for a given pressure (MPa) under uniaxial loading. X = tablet failed under load; --- = material not tested under given pressure.

Pressure (MPa) /Material	HA	5nf	5f-1	5f-2	5f-3
55	44.5 ± 0.4	---	---	---	---
75	45.9 ± 0.4	43.0 ± 0.5	42.8 ± 0.5	45.9 ± 0.6	42.2 ± 0.4
90	47.1 ± 0.6	44.6 ± 0.1	45.2 ± 0.3	---	---
110	49.6 ± 0.4	45.3 ± 1.1	46.7 ± 0.1	---	46.8 ± 0.4
150	X	47.4 ± 0.1	49.5 ± 0.3	---	---
185	X	48.5 ± 0.8	50.3 ± 0.1	---	---

The trends in the results can be better viewed in Figure 3.17, which plots density vs. pressure. It can easily be seen that the green density increases with uniaxial loading for a given powder. In general, it was observed that HA had a higher green density at a given pressing pressure than composite powders at the same pressure, and that, at higher pressures, 5f-1 powder resulted in a higher density than 5nf. Thus, it appears that 5nf cannot reach the same high green density as HA, and that 5f-1 requires nearly 70% more pressure to achieve the same density as HA. This corresponds to the bulk density data from section 3.3.2.3, thus the mechanisms for these differences are likely the same; namely, that CNTs protruding from the powder particles interfere with packing.

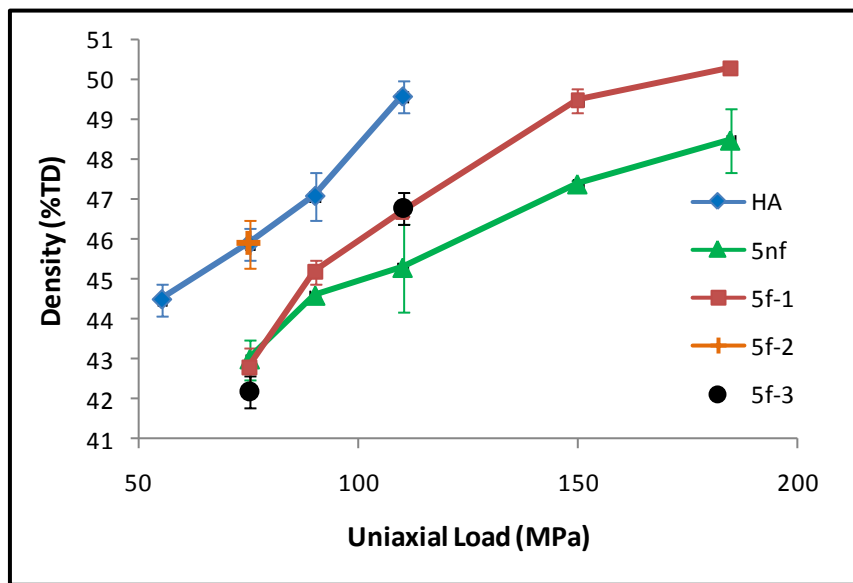


Figure 3.17: Density vs. uniaxial load for green tablets.

Additionally, it was found that HA tended to delaminate, resulting in tablet failure, at pressures above 110 MPa. The composites, on the other hand, only delaminated and failed at pressures above 185 MPa. Thus, the limit of green density was found to be 49.6% for HA, 48.5% for 5nf and 50.3% for 5f-1. An additional observation is that the 5f-2 powder resulted in a much higher density for the same pressure than 5f-1 or 5f-3 and an equivalent density to HA. A final observation related to handlability is that the fCNT composite powder more often resulted in a well-formed tablet compared with nCNT composite powders. This seems most likely due to differences in the homogeneity of the

powders; namely, that bundles of CNTs still present in the nfcCNT composite powders acted as defects which resulted in the failure of the tablets.

### **3.4 Summary**

#### **3.4.1 Material synthesis**

HA was synthesised by a precipitation reaction between  $\text{Ca(OH)}_2$  and  $\text{H}_3\text{PO}_4$ . MWNTs were synthesised by CVD with ferrocene as the catalyst source and toluene as the carbon source. Composites were synthesised by adding MWNTs to the  $\text{Ca(OH)}_2$  solution as the HA was precipitating. The resulting slurry was then filtered, further shear mixed, then dried, ground and milled to form a fine powder. The powder was then pressed into tablets. Composite materials were made with both nfcCNTs and fcCNTs, which had been acid treated with a mixture of sulphuric and nitric acid.

#### **3.4.2 Material characterisation**

Characterisation of the CNTs revealed a wide distribution of diameters that was similar for both nfcCNTs and fcCNTs. The aspect ratio of the CNTs was estimated to be between  $10^2$ - $10^4$ , and on the shorter end for fcCNTs, which would have been shortened during ultrasonication as part of the functionalisation process. fcCNTs were also found to be more damaged, demonstrated by ‘un-zipped’ ends and a lower oxidation temperature compared with nfcCNTs.

Composites made with fcCNTs were found to be more homogeneous than those with nfcCNTs, as the former are dispersible in water while the latter are not. Powders of HA and the composites were found to have a bimodal distribution of particle sizes and a fairly spherical morphology. The materials were found to be largely phase pure, though some contained a small amount of  $\beta$ -TCP. The materials were also found to be hydroxylated. More interaction was found between HA and fcCNTs than between HA and nfcCNTs, likely resulting from the negative charge on the fcCNTs that would attract calcium cations during the precipitation process.

The colour of the material was observed to be darker with increasing CNT loading, although the fcCNT composites were darker in colour than the nfcCNT composites for the

same loading due to differences in homogeneity. A good green density could be achieved in the case of all powders, although it was found that more pressure was required to reach the same green density for composites as compared with pure HA. At pressures higher than those required to achieve a green density of ~48-50%, the tablets tended to delaminate.

## **4 INVESTIGATION OF SINTERING ATMOSPHERES**

Perhaps the greatest obstacle to successfully making HA-CNT composites is the choice of appropriate sintering conditions. Particularly in the case of pressureless sintering, the sintering atmosphere is key, as it must enable the composite to retain both the CNTs and the hydroxyl (OH) groups of HA at the high temperatures required for full densification of the material. To keep HA's OH groups, the atmosphere must contain water, but this will, in turn, oxidise the CNTs. While hot pressing or hot isostatic pressing may largely circumvent this problem by applying enough pressure to prevent oxidising reactions or dehydroxylation, the processing is more complex and expensive compared with pressureless sintering (deGroot *et al.* 1990). Spark plasma sintering, with its extremely high sintering rates and applied pressure, is another alternative, yet it is geometrically limited (Nygren *et al.* 2004). Thus, the goal of this portion of the project was to investigate atmospheres for use in pressureless sintering that might allow retention of both CNTs and OH groups, while providing enough densification for improved mechanical properties over HA alone.

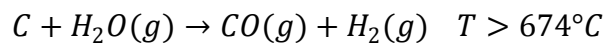
The first part of this chapter will explain the issue of balancing CNT oxidation against HA dehydroxylation and decomposition and detail the requirements for a successful sintering atmosphere. The experimental methods and results then follow and are divided into three sections. The first part examines the typical behaviour of HA and HA-CNT composites in more common sintering atmospheres through TGA and SDT study. The second part consists of a detailed study of fourteen sintering atmospheres and their effects on various properties of the composites, such as CNT retention, density, phase purity, and hydroxylation. Using the optimal atmosphere from the second part, the final section examines the effects of additional variables, such as flow rate and number of samples, on the characteristics of the sintered material.

## 4.1 Background

To understand how to design an atmosphere that might allow the retention of CNTs and OH groups, the competing reactions of CNT oxidation and HA dehydroxylation and decomposition must be examined.

### 4.1.1 CNT oxidation

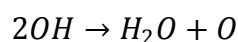
CNTs may be oxidised by a number of reactions in the type of atmospheres that are standard for HA sintering, such as air and moist Ar or N<sub>2</sub>. For example:



As the TGA data from Figure 3.7 showed, the reaction between CNTs and air occurs quickly and over a narrow temperature range. The reaction rate between CNTs and water tends to be slower, but depending on the rate of porosity closure of the composite material compared with CNT consumption, all the CNTs in a composite might easily be consumed by water during sintering. It should also be noted that these reaction temperatures are theoretical values (from software Outokumpu, HSC Chemistry, v.4.1). From TGA it has already been shown (Section 3.3.1.2) that some of the functionalised CNTs (fCNTs) used in this study begin to oxidise between 550-600°C, while non-functionalised CNTs (nfCNTs) begin to oxidise at about 650°C.

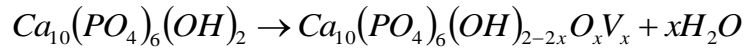
### 4.1.2 HA dehydroxylation and decomposition

Dehydroxylation of HA occurs at elevated temperatures, beginning at temperatures as low as 900°C in air and 850°C in a water-free atmosphere (Wang, P. E. *et al.* 1993). When OH groups are removed from the HA structure, two OHs combine to form one molecule of water, leaving one oxygen atom in the lattice:



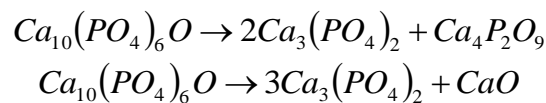
When HA begins to dehydroxylate, it forms oxyhydroxyapatite (OHA), which has a similar crystal structure to HA, but contains vacancies. A completely dehydroxylated HA which has not yet decomposed is called oxyapatite (OA; Ca<sub>10</sub>(PO<sub>4</sub>)<sub>6</sub>O). Trombe *et al.*

(1978) were the first to demonstrate the existence of OA and OHA and to characterise them. OHA forms according to:



where  $V_x$  is a hydrogen vacancy. In a moist atmosphere (in which water is explicitly added), it should be possible to sinter HA up to a temperature of 1300°C without dehydroxylation or decomposition (Wang, P. E. *et al.* 1993). This temperature is based on experimental results by Wang *et al.* and is a typical value reported in the literature when gas is bubbled through water at room temperature (partial pressure of water = 17.5 mmHg). However, in theory, it should be possible to sinter HA with a Ca/P ratio of precisely 1.67 to temperatures of up to 1475°C before decomposition begins, provided that the partial pressure of water in the sintering atmosphere is 500 mmHg (deGroot *et al.* 1990). In the case of ‘pressureless’ sintering, assuming atmospheric pressure of 760 mmHg, achieving this partial pressure of water means bubbling through water very close to boiling.

If HA becomes completely dehydroxylated during sintering, forming OA, its crystal structure changes, as OA is not a stable phase. Two outcomes are stoichiometrically possible: OA may decompose to a mixture of TTCP and TCP ( $\beta$ -TCP at temperatures below ~1200°C and  $\alpha$ -TCP at higher temperatures), or it may decompose to a mixture of TCP and CaO by the following reactions:



Small deviations in the Ca/P ratio of the starting material also can result in the formation of these secondary phases. This can be seen in the phase diagram displayed in Figure 4.1. A material with  $Ca/P > 1.67$  will decompose to form either HA + CaO, HA + TTCP, or TCP + TTCP, depending on the partial pressure of water in the atmosphere and the sintering temperature. A material with  $Ca/P < 1.67$  can form either a mixture of TCP + HA or TCP + TTCP, again depending on the amount of moisture and the temperature. If the partial pressure of water in the atmosphere is 500 mmHg, then  $T_1$  and  $T_2$  will be 1360°C and 1475°C, respectively. If the partial pressure of water is less, then  $T_1$  and  $T_2$

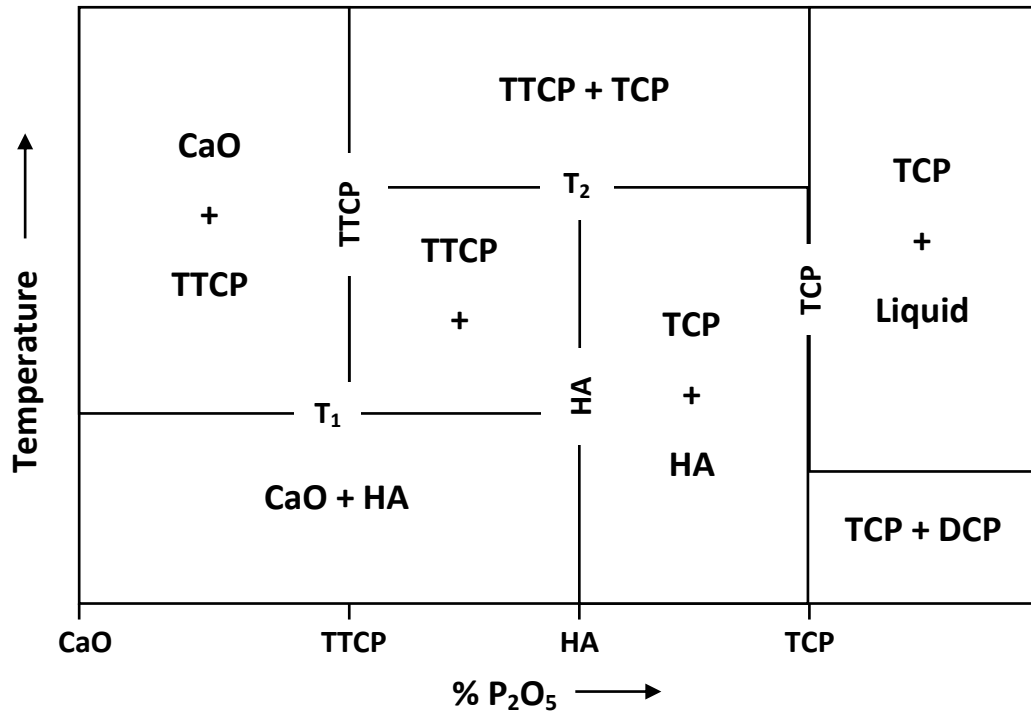


Figure 4.1: Phase diagram of the CaO-P<sub>2</sub>O<sub>5</sub> system at high temperatures. DCP = dicalcium phosphate (monetite). Partial pressure of water = 500mmHg. Adapted from de Groot *et al.* (1990).

will be lowered, potentially substantially. If no water is present, HA cannot form at all, and so the material will be a mixture of TCP + TTCP for all sintering temperatures (deGroot *et al.* 1990). An earlier paper by de Groot (1980) gave a more lenient practical range of Ca/P ratios and resulting phases, saying that, ‘all materials with a Ca/P ratio of 1.5–1.7 sintered at temperatures of 1000-1300°C, with no explicit exclusion of water, will be apatitic.’

Experimentally, when considering a compacted tablet that is densifying as these reactions proceed, the material may easily be a mixture of HA, OHA, TCP, and TTCP, for example, at a given time. Diffusion of water into and out of the tablet will be slowed by densification and eventually prevented altogether when porosity has been eliminated. Thus, different regions of the tablet may have very localised atmospheres with varying amounts of water. The heating rate can also affect the final density and phase purity of the material. Higher ramp rates can give a higher final density, but a rate greater than 10°C min<sup>-1</sup> has been shown to result in decomposition (Gibson *et al.* 2001). An additional concern with HA-CNT composites is that since CNTs oxidise at temperatures above 650°C, the choice becomes either losing the CNTs or dehydroxylating the HA. Even in

dry atmospheres, dehydroxylation produces water, which can then interact with the CNTs.

#### 4.1.2.1 Impact on *in vivo* properties

For use in biological applications, it is important to prevent the dehydroxylation and decomposition of HA as different calcium phosphate phases have different biological properties. *In vitro* studies have shown that solubility increases in the order: HA < oxy-HA <  $\beta$ -TCP < TTCP <  $\alpha$ -TCP  $\ll$  CaO, although the solubilities vary somewhat depending on the solvent used (aqueous vs. a variety of buffers) (Klein *et al.* 1990; Dorozhkin 2009). However, de Groot *et al.* (1990) and Klein *et al.* (1990) acknowledge that *in vitro* studies do not necessarily accurately reflect the *in vivo* behaviour of the materials. While  $\alpha$ - and  $\beta$ -TCP have been found to resorb faster *in vivo* than HA (Keller *et al.* 1987), TTCP has been shown to develop intimate bone contact, similar in behaviour to HA, perhaps due to its high calcium content (Klein *et al.* 1991). However, TTCP has been investigated very little compared with TCP and HA.

Additional factors which impact the *in vivo* behaviour are the degree of crystallinity and surface area of the material (deGroot *et al.* 1990). More amorphous materials will have a higher dissolution rate than their crystalline counterparts, and powders and porous materials will dissolve more quickly than dense monoliths. Additionally, even small amounts of microporosity in a fairly dense monolith can have a significant impact, as exposed necks between particles may have poor crystallinity compared with the bulk ceramic.

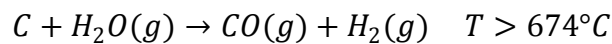
#### 4.1.2.2 Characterisation

To characterise phase composition and dehydroxylation, two techniques should be used in parallel. XRD is best suited to determine the phase composition of the material, while FTIR will most easily show dehydroxylation. As the OHA has the same crystal structure as HA, evidence of dehydroxylation in XRD can only be seen by slight shifts in  $2\theta$  values as the lattice contracts with the loss of OH groups. In FTIR this is more easily observed by a decrease in intensity of the OH peaks at  $3572\text{ cm}^{-1}$  and  $633\text{ cm}^{-1}$ . FTIR may also show evidence of decomposition, although it is more difficult to determine precisely the decomposed phases and their amounts compared with XRD. Additional phosphate

vibration peaks may appear for the phosphate groups in the other calcium phosphate phases, while other peaks may weaken to shoulders.

### 4.1.3 The water-gas reaction: A compromise?

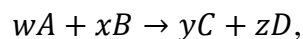
Faced with the loss of either CNTs or OH groups from the composites with the standard atmospheres, alternatives should be considered. One possibility lies in the reaction between CNTs and water:



This reaction is more commonly known as the ‘water-gas reaction’ from its industrial origins in creating a cooking and heating gas by pouring water over hot coals. While this reaction normally proceeds in the forward direction at high temperatures, Le Chatelier’s principle offers the possibility of shifting the equilibrium of the reaction if the concentration of the products is increased, thus potentially retaining carbon (the CNTs) and the water needed to keep HA’s OH groups:



To better understand the thermodynamics of the reaction and how possible it may be at a given temperature to preserve the OH groups and the CNTs, the equilibrium constant can be plotted against temperature. When the reaction is of the form



the equilibrium constant can be calculated by the following formula:

$$K_{eq} = \frac{[C]^y [D]^z}{[A]^w [B]^x}$$

$K < 1$  forward direction     $K = 1$  equilibrium     $K > 1$  backward direction

where  $K_{eq}$  is the equilibrium constant;  $[A]$ ,  $[B]$ ,  $[C]$ , and  $[D]$  are the concentrations (or activities) of species  $A$ ,  $B$ ,  $C$ , and  $D$  from the reaction equation; and  $w$ ,  $x$ ,  $y$ , and  $z$  are molar coefficients from the reaction equation. The value of  $K_{eq}$  will determine if the reaction is in equilibrium or if it will proceed in the forward or backward direction. In the case of  $C + H_2O \leftrightarrow CO + H_2$ , the molar coefficient of all species is 1; in the case of

gases, the concentrations become the partial pressures of the gases; and the activity of a solid material ( $C$ ) is 1. Thus, the equilibrium constant can be represented by:

$$K_{eq} = \frac{[CO]^1[H_2]^1}{[C]^1[H_2O]^1} = \frac{[CO][H_2]}{[1][H_2O]} = \frac{p_{CO} \cdot p_{H_2}}{p_{H_2O}}$$

where  $p_{CO}$ ,  $p_{H_2}$ , and  $p_{H_2O}$  are the partial pressures of CO, H<sub>2</sub>, and H<sub>2</sub>O, respectively. The equilibrium constant varies with temperature, and in the case of the water-gas reaction, the equilibrium constant is positive and increases exponentially at temperatures higher than 674°C. Figure 4.3 shows a graph of  $K_{eq}$  vs. temperature for the water-gas reaction. Using the value for  $K_{eq}$  at 1200°C, further calculation reveals that  $p_{CO}$  and  $p_{H_2}$  at this temperature are 0.4997 atm (379.8 mmHg) and  $p_{H_2O}$  is a very minimal  $6 \times 10^{-4}$  atm (0.456 mmHg). While the partial pressure of water at this temperature seems very low, and thus would not necessarily prevent much dehydroxylation, it should be kept in mind that these are theoretical values based on the system being in equilibrium, which may be far from reality experimentally.

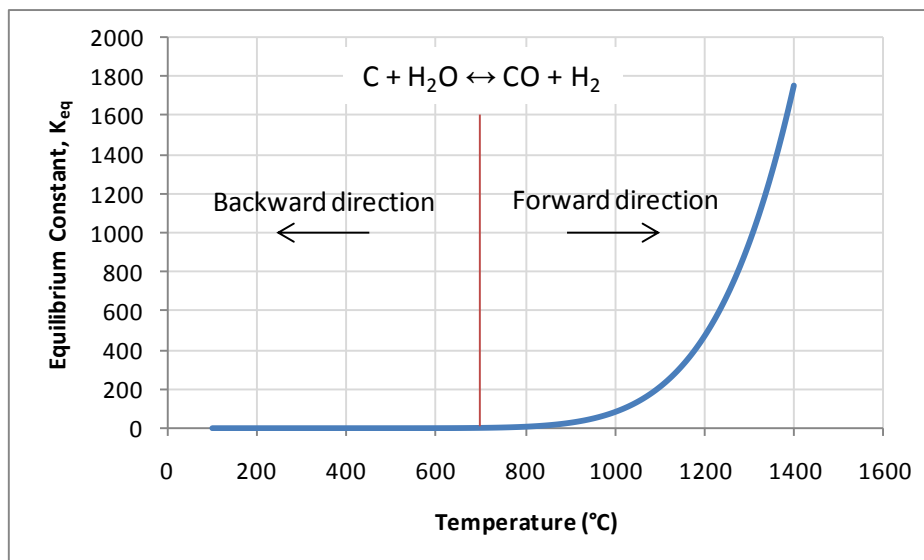


Figure 4.3: Equilibrium constant vs. temperature for the water-gas reaction. Values calculated using the software Outokumpu, HSC Chemistry v.4.1.

## 4.2 Behaviour in standard atmospheres

The vast majority of publications involving HA sintering have used either air or an inert gas (such as nitrogen or argon) bubbled through water as the sintering atmosphere. Despite evidence that HA dehydroxylates and decomposes without the presence of water, some studies have used dry inert atmospheres to sinter HA composites in order to prevent reactions with the secondary phase. This section will examine the behaviour of CNTs, HA, and composites in these ‘standard’ sintering atmospheres.

### 4.2.1 CNT behaviour

To examine the behaviour of CNTs in different atmospheres, TGA and SDT were used to determine the profile of mass loss relative to temperature, as described in Section 3.2.1.7. HA and composite behaviour were compared for a range of atmospheres. The samples analysed were in powder form. A heating rate of  $10^{\circ}\text{C min}^{-1}$  was used for TGA, while SDT was set to simulate a sintering profile run, with a ramp rate of  $5^{\circ}\text{C min}^{-1}$  to  $1200^{\circ}\text{C}$ , a two-hour dwell, and ramp down at  $5^{\circ}\text{C min}^{-1}$ .

The mass-temperature profiles of HA and 5 wt.% fCNT (5f) composite are shown for a dry Ar atmosphere in Figure 4.4. Generally, the shape of the two curves was similar, with two distinct regions of mass loss during heating – one between room temperature and about  $500^{\circ}\text{C}$  and the second from about  $700 - 1200^{\circ}\text{C}$ . The first mass loss can be attributed to adsorbed water, while the second can be attributed to dehydroxylation (Liao *et al.* 1999; Wang, T. *et al.* 2004). During the dwell at  $1200^{\circ}\text{C}$ , a small mass increase was observed in both samples, the cause of which is unclear. A similar increase has been observed before, but only when HA was heated in a water-free atmosphere and then dwelled and cooled in a moist atmosphere, and thus was attributed to rehydroxylation (Trombe *et al.* 1978). During cooling, a slight increase in weight was observed. Despite the experiment being carried in dry Ar, this may still be due to rehydroxylation, as weight gain due to rehydroxylation during cooling has been observed even in vacuum (Trombe *et al.* 1978).

From room temperature to approximately  $750^{\circ}\text{C}$ , the HA and 5f experienced the same amount of weight loss, although with slightly different rate profiles. Above  $820^{\circ}\text{C}$ , the differences in behaviour were more significant. Between  $700 - 1200^{\circ}\text{C}$ , the HA lost

approximately 1.8% of its mass, while the 5f composite experienced a 3.1% mass loss. A mass loss of 1.8% can be attributed to complete dehydroxylation, which should have a theoretical mass loss of 1.79%, while the additional mass loss in the 5f sample may be due to CNT oxidation due to water produced by the dehydroxylation process. Both of these phenomena were observed in the atmosphere study discussed in the next section, and will be described in more detail.

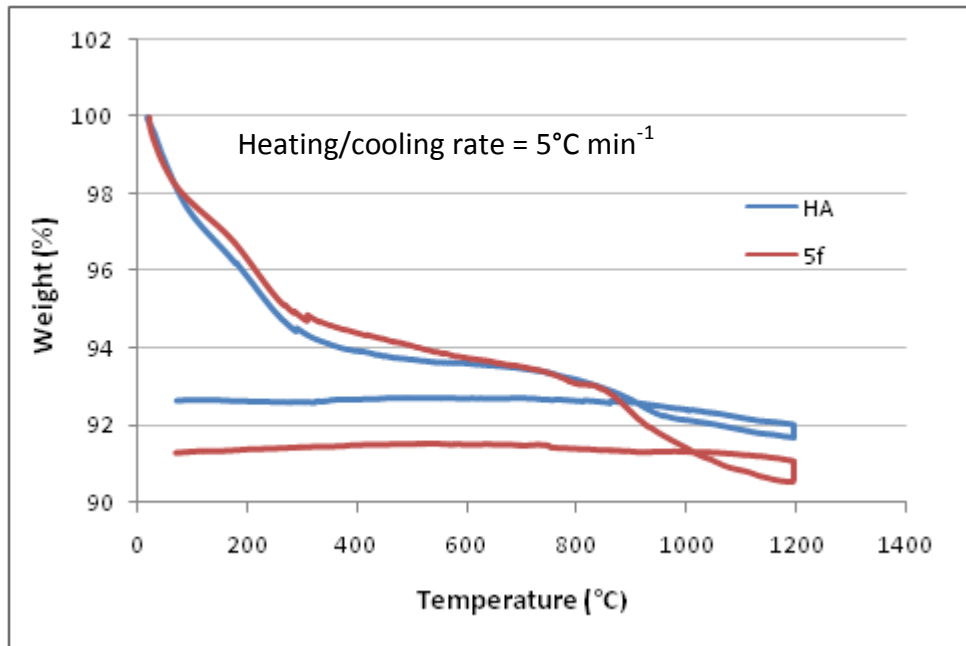


Figure 4.4: Sintering profile of HA and 5f in dry Ar.

Figure 4.5 compares several different atmospheres up to 1000°C. The oxidation of fCNTs in air from Figure 3.7 is also shown as a reference. Note that the data have been normalised for 100% mass at 200°C. All of the materials showed a nearly identical rate of weight loss up to 500°C. Above this temperature, the different atmospheres resulted in markedly different behaviour. The graph compares two atmospheres for the composites – air and nitrogen bubbled through water at room temperature. Between 520°C and 710°C the 5f composite in air lost 5.5% of its mass, which is approximately equal to the loading of CNTs. While this mass loss began at the same temperature as the mass loss in the fCNTs sample, the mass loss ended at a temperature approximately 35°C higher than the fCNTs alone, possibly because the incorporation of the CNTs into HA as a composite slows the rate of oxidation. Above 710°C the 5f material in air experienced a gradual, additional weight loss of 0.4%, possibly due to partial dehydroxylation.

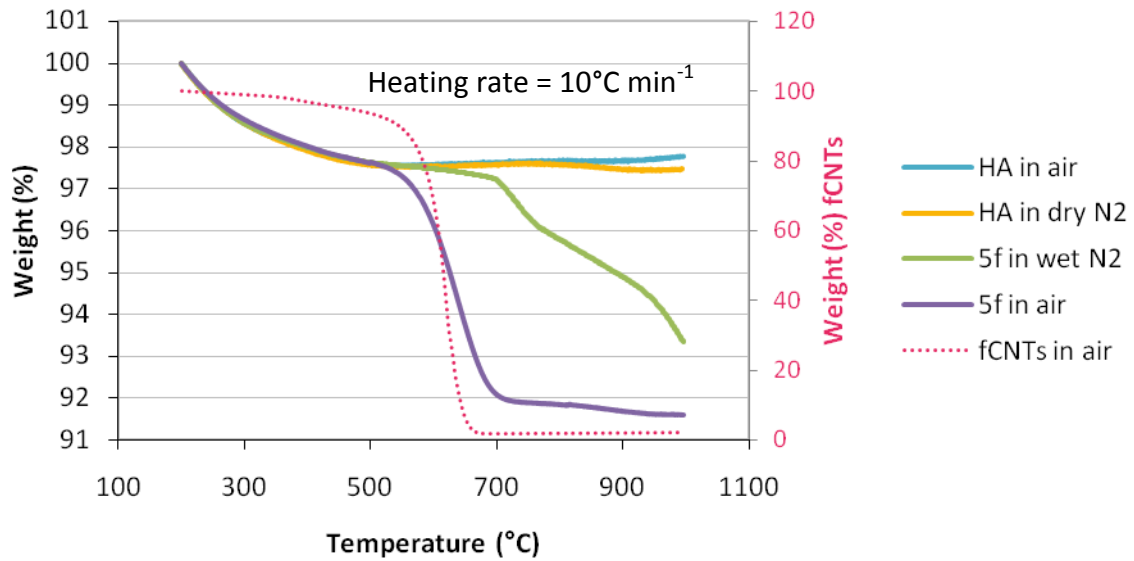


Figure 4.5: Mass-temperature profile of HA and 5f in air, dry nitrogen, and wet nitrogen, with fCNTs for comparison.

The profile of the 5f composite in wet nitrogen is quite different. This sample did not experience any significant weight loss past 500°C until nearly 700°C. The rate of mass loss was fairly high between 700 – 770°C, slightly lower between 770 – 950°C, and then higher again from 950 – 1000°C. As this sample was heated in a wet atmosphere, it seems unlikely that much dehydroxylation, if any, would have occurred, especially at these relatively low temperatures. Thus, it is possible that the different rates of loss are attributable to different degrees of interaction between the CNTs and water at a given temperature. Most importantly, it should be noted that oxidation of CNTs occurred at a temperature nearly 150°C higher in wet nitrogen than in air. The total mass loss between 600 – 1000°C was 4.3%. Thus, compared with 5f in air, the mass loss in wet nitrogen from 500 – 1000°C was 20% less.

The profiles for HA in air and dry nitrogen are nearly identical until 800°C. Above this temperature, the HA in air gained a slight amount of mass, whereas the HA in nitrogen lost a small amount of mass. It is not clear why the HA in air would have gained mass, but the HA in dry nitrogen may have lost weight due to some dehydroxylation.

### **4.3 Atmosphere investigations**

From observing the behaviour of HA and composite materials in standard atmospheres, it is clear that the composition of the atmosphere has a strong effect on both the CNT retention and hydroxylation of the final product. While the wet nitrogen atmosphere seemed to preserve more CNTs and more OH groups than the air atmosphere, a significant amount of CNTs was still oxidised. It is also not clear what effect the composition of the atmosphere may have on other characteristics, such as density. Thus, a more detailed study was undertaken to investigate a wider range of atmospheres and to more fully characterise the effect of each atmosphere on the final sintered material.

#### **4.3.1 Experimental methods**

Fourteen sintering atmospheres were investigated in this study, including standard atmospheres and atmospheres based on the water-gas reaction (described in Section 4.1.3). Four tablets of 0.8 g each of 5f composite were sintered with the following profile: ramp up at  $5^{\circ}\text{C min}^{-1}$  to  $1200^{\circ}\text{C}$ , hold for two hours, and ramp down at  $5^{\circ}\text{C min}^{-1}$  to room temperature. The ramp rate was set at  $5^{\circ}\text{C min}^{-1}$  as this rate has been shown to be low enough to avoid HA decomposition (Gibson *et al.* 2001), but is still relatively high compared with standard rates of  $\sim 1 - 2.5^{\circ}\text{C min}^{-1}$  and thus should minimise the amount of time the material is at temperatures high enough to cause CNT oxidation. Heat treatments were carried out in a tube furnace with either a quartz, mullite, or alumina tube (length = 1.5 m, inner diameter = 10 cm), unless otherwise noted. The tablets were placed on an alumina tray which was positioned in the centre of the furnace, and the samples were arranged in two rows of two, with all tablets touching one another.

The number of experiments necessitated the use of three different batches of material. Table 4.1 summarises the characterisation results of these batches, as described in Chapter 3. Some of the more promising atmospheres were tested more than once.

Table 4.1: Characteristics of 5f batches used in sintering studies.  
H = HA;  $\beta$  =  $\beta$ -TCP

Batch	CNT Loading (wt.%)	Surface Area ( $\text{m}^2\text{g}^{-1}$ )	$d_{0.5}$ ( $\mu\text{m}$ )	Phases Present
5f-1	$3.3 \pm 0.2$	82	22	H
5f-2	$4.8 \pm 0.2$	67	26	H
5f-3	$3.7 \pm 0.2$	88	27	H, <5% $\beta$
5f-3,2*	$5.3 \pm 0.3$	91	25	H, <5% $\beta$

\*5f-3 and 5f-3,2 were the same material, but 5f-3,2 was ball milled for an additional 24 hours.

It is apparent from Table 4.1 that the batches have a large variability in CNT loadings. Additionally, 5f-2 has a much lower surface area than the other batches and the 5f-3 batches have a small amount of  $\beta$ -TCP, indicating that its Ca/P ratio was likely slightly lower than the stoichiometric value of 1.67.

Descriptions and detailed methods for each of the fourteen atmospheres are shown in Table 4.2. Atmospheres which are indicated 'NF' for non-flowing were not completely closed, as gas could freely expand out of the furnace during heating and contract during cooling. The pressure for all sintering experiments was atmospheric pressure.

## 4.3.2 Characterisation Methods

### 4.3.2.1 Physical characterisation

The physical characterisation of the materials included observations of appearance, measurements of CNT loading after sintering, and measurements of density before and after sintering.

#### 4.3.2.1.1 Appearance

The appearance of the tablets was observed both before and after sintering. Differences in colour and uniformity of colour throughout a tablet between the green and sintered materials were noted, and the tablets were photographed.

#### 4.3.2.1.2 CNT loading

CNT loading was measured as described in Section 3.2.1.5, by crushing a tablet into a powder with a mortar and pestle, dissolving the calcium phosphate phases with HCl,

Table 4.2: Detailed methods for each of the fourteen heat treatment atmospheres investigated.

Notation	Atmosphere	Flow Rate (L min <sup>-1</sup> )	Details
H/W(NF)	H <sub>2</sub> + H <sub>2</sub> O	NF	After flushing with Ar, H <sub>2</sub> bubbled through H <sub>2</sub> O was switched on long enough to fill tube, then switched off for remainder of experiment. During cooling, bubbler was immersed in ice to minimise water uptake.
A/W	Ar + H <sub>2</sub> O	0.5	Flowing Ar bubbled through water.
H(NF)	H <sub>2</sub>	NF	After flushing with Ar, H <sub>2</sub> switched on long enough to fill tube, then switched off for remainder of experiment.
A	Ar	0.5	Flowing Ar.
A/W (boiled)	Ar + H <sub>2</sub> O (boiled)	0.5	Flowing Ar bubbled through water which had previously been boiled to remove dissolved O <sub>2</sub> .
H	H <sub>2</sub>	0.8	Flowing H <sub>2</sub> between 710°C - 1200°C during both heating and cooling. System flushed with Ar at beginning and end of experiment.
CO	CO	0.4	Same as H, but with CO.
CO/H	CO + H <sub>2</sub>	0.8	Same as H, but with flowing CO (0.5 L min <sup>-1</sup> ) and H <sub>2</sub> (0.5 L min <sup>-1</sup> ).
CO/H/W (ice)	CO + H <sub>2</sub> + H <sub>2</sub> O (ice)	0.8	Same as CO/H, but gas flowed through water bubbler immersed in ice.
Air	Air	NF	No flow, experiment carried out in box furnace.
A/W(ice)	Ar + H <sub>2</sub> O (ice)	0.5	Same as A/W, but bubbler immersed in ice.
H/W(ice)	H <sub>2</sub> + H <sub>2</sub> O (ice)	0.5	Same as H, but bubbler immersed in ice.
CO/H/W	CO + H <sub>2</sub> + H <sub>2</sub> O	0.8	Same as CO/H/W(ice), but bubbler at room temperature.
CO/W	CO + H <sub>2</sub> O	0.4	Same as CO, but bubbled through water.

\*NF = non-flowing; p<sub>H<sub>2</sub>O</sub> (ice) = 5 mmHg; p<sub>H<sub>2</sub>O</sub> (room temperature) = 17.5 mmHg

and filtering the CNT-containing solution. The mass difference between the filter before and after filtration was then measured, and the CNT loading was calculated based on the mass of composite powder added to the HCl, assuming all additional mass on the filter was CNTs. The percentage of CNTs lost during sintering was then calculated based on the CNT loading measured for each green batch (listed in Table 4.1) and the CNT loading

measured for the sintered material. Only one measurement was made for each heat treatment experiment in most cases, due to limitations in the amount of material available. On three occasions, the loading of two samples from the same experiment were measured and found not to vary by more than about 5%. Thus, an error of  $\pm 5\%$  is reported for each measurement as an estimation of the expected variability. Additionally, the sample measured was always taken from the same relative location in the furnace to minimise any positional variations in CNT loading.

#### 4.3.2.1.3 Density

The density of the tablets both before and after sintering was calculated from measurements of tablet dimensions and mass. Archimedes' method was not used because some samples were porous enough that liquid absorbed into the interior of the tablet would have affected the measurements. The percentage of theoretical density (% TD) was calculated as described in Section 3.2.1.1 assuming the calcium phosphate phases were all HA. In the case of decomposed samples, the reported % TD value will tend to be an underestimate, as the other calcium phosphate phases have a lower density than HA.

#### 4.3.2.2 Physicochemical characterisation

Physicochemical characterisation of the materials was used to determine the phases present and assess whether any degradation or dehydroxylation had occurred. A combination of XRD and FTIR was used to examine most accurately the crystal structure and determine the level of hydroxylation of the material. Both XRD and FTIR analysis were performed as described in Section 3.2.2. XRD analysis was carried out on the tablet surfaces. A minimal amount of material (~0.1 mm) was ground off the top layer of each tablet to remove any residual material from the lubricant used when making the green tablets. The relative amounts of each phase were determined using the semi-quantitative feature of the X'Pert Highscore Plus (PANalytical, the Netherlands, v.2.2b) software. The phases were matched to JCPDS powder diffraction files (HA: 01-089-6440;  $\beta$ -TCP: 01-86-1585;  $\alpha$ -TCP: 01-70-0364; TTCP: 00-25-1137; CaO: 01-77-2010). For FTIR analysis, the tablets were ground into a fine powder, a small amount of which was incorporated into KBr discs.

### **4.3.3 Results**

A summary of the atmosphere investigation results is presented in Table 4.3. The following sections will discuss the results of the material characterisation for each atmosphere.

#### **4.3.3.1 Phases and hydroxylation**

A first step in identifying a suitable heat treatment atmosphere is to determine whether or not the atmosphere results in decomposition and/or dehydroxylation of the material. The results of XRD characterisation are shown in Figure 4.6, while the plots for FTIR are presented in Figure 4.7. The results are summarised in Table 4.3.

##### *4.3.3.1.1 X-ray diffraction analysis*

Several atmospheres resulted in decomposition of the material as shown in XRD. Five different combinations of phases were observed:

- |                              |   |
|------------------------------|---|
| 1) HA + CaO                  | H(NF), CO/H/W(ice) 5f-1, H/W(ice) 5f-2, and CO/H/W 5f-2 |
| 2) TTCP + $\alpha$ -TCP      | A   |
| 3) TTCP + HA + $\alpha$ -TCP | H   |
| 4) TTCP + HA + CaO           | CO, A/W(ice), CO/W                                      |
| 5) HA + $\beta$ -TCP         | CO/H/W 5f-3   |

According to the phase diagram in Figure 4.1, HA + CaO should result when the Ca/P ratio of the material is slightly more than 1.67 and water is present in the atmosphere. The second combination, TTCP +  $\alpha$ -TCP, can result either when the sintering temperature is extremely high with or without water in the atmosphere, or, at lower sintering temperatures such as 1200°C, only when very little water is present. The combination of TTCP + HA +  $\alpha$ -TCP would then seem to result from either localised differences in the partial pressure of water or an incomplete phase transition with a material which has a Ca/P ratio > 1.67. The fourth combination, TTCP + HA + CaO, would then result from similar circumstances, but with a Ca/P ratio < 1.67. Finally, the fifth combination of phases, HA +  $\beta$ -TCP, would result from having a Ca/P ratio slightly lower than 1.67 and some water present in the atmosphere.

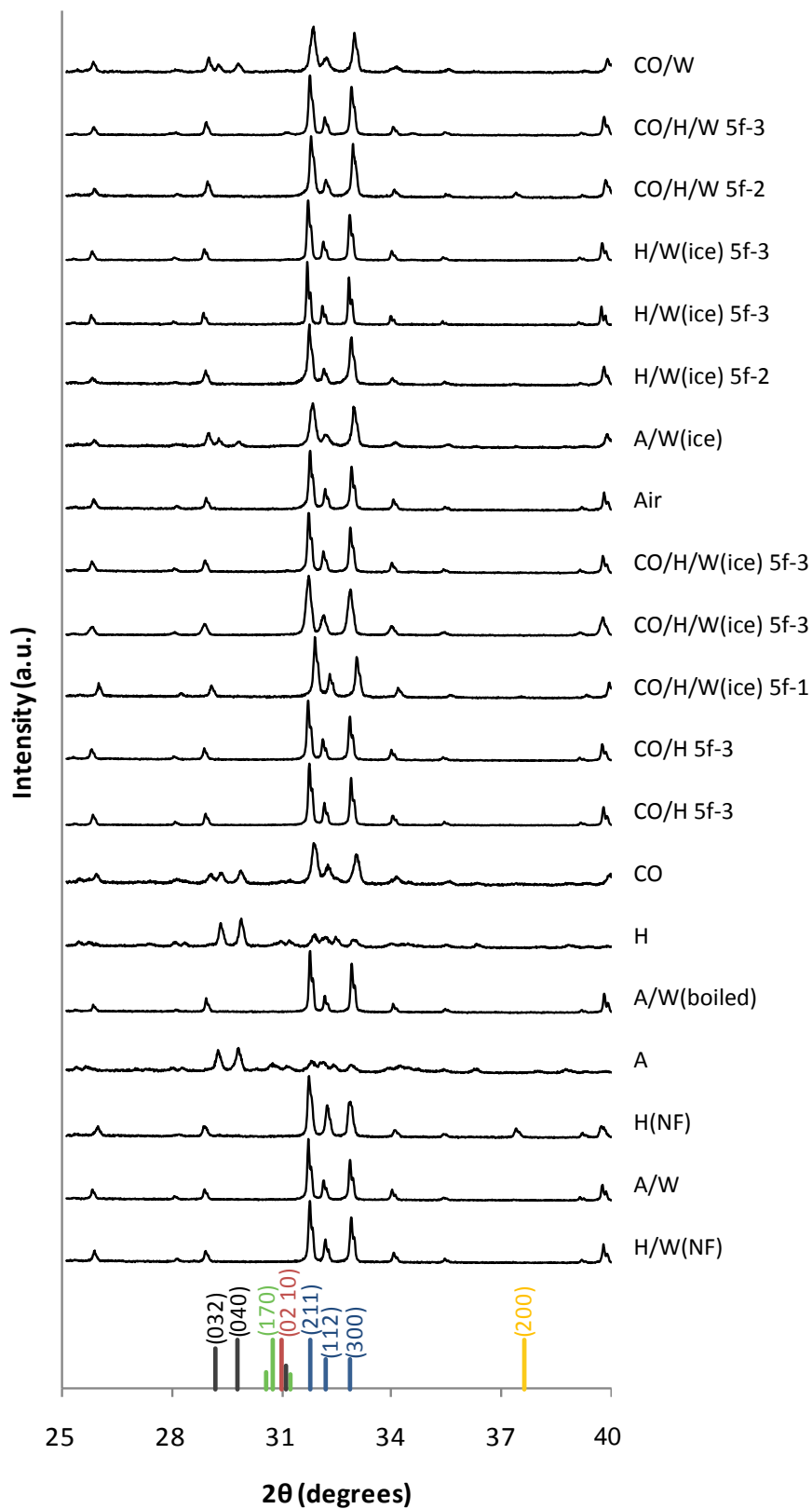


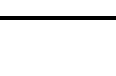
Figure 4.6: XRD traces for different heat treatment atmospheres, performed on surfaces of 5f tablets sintered at 1200°C. HA = blue; B-TCP = red; a-TCP = green; TTCP = black; CaO = gold.

#### 4. Investigation of Sintering Atmospheres

Table 4.3: Summary of heat treatment results. NF = non-flowing; H = HA; O = CaO; T = TTCP;  $\alpha$  =  $\alpha$ -TCP;  $\beta$  =  $\beta$ -TCP.

Atmosphere	Batch	Appearance of Tablet	Tablet Picture	CNT Loading (wt.%)	CNT Loss (%)	XRD	FTIR	Green Density (% TD)	Final Density (% TD)	Adjusted Density (% TD)
<b>H/W(NF):</b> H <sub>2</sub> + H <sub>2</sub> O (NF)	5f-1	White layer, black inside		0.22 ± 0.01	93%	HA	Some OH loss	41.8 ± 0.1	95.8 ± 0.1	
<b>A/W:</b> Ar + H <sub>2</sub> O	5f-1	White layer, black inside		1.7 ± 0.08	50%	HA	Significant OH loss	42.0 ± 0.0	92.3 ± 2.0	
<b>H(NF):</b> H <sub>2</sub> (NF)	5f-1	Uniformly black		1.6 ± 0.08	52%	HA (95%), O (5%)	Complete OH loss	42.2 ± 0.2	88.8 ± 1.8	88.4 ± 1.8
<b>A:</b> Ar	5f-1	Uniformly black		2.0 ± 0.10	40%	T (65%), $\alpha$ (35%)	Decomposition	43.7 ± 0.5	85.9 ± 0.4	90.6 ± 0.4
<b>A/W(boiled):</b> Ar + H <sub>2</sub> O (boiled)	5f-2	White coating, black inside		1.2 ± 0.06	75%	HA	Significant OH loss	51.6 ± 0.2	87.5 ± 0.2	
<b>H:</b> H <sub>2</sub>	5f-1	Uniformly black		2.1 ± 0.10	37%	T (75%), $\alpha$ (25%)	Decomposition	42.7 ± 0.3	85.6 ± 0.5	89.7 ± 0.5
<b>CO:</b> CO	5f-1	Uniformly black		1.4 ± 0.07	58%	HA (61%), T (37%), O (2%)	Decomposition	42.0 ± 0.5	86.1 ± 0.1	87.1 ± 0.1
<b>CO/H:</b> CO + H <sub>2</sub> , flowing	5f-3	Medium grey coating, dark grey inside		1.7 ± 0.08	54%	HA	Good OH retention	44.3 ± 0.5	82.8 ± 0.9	
	5f-3	Medium grey coating, dark grey inside		1.7 ± 0.09	54%	HA	Good OH retention	44.1 ± 0.2	81.9 ± 0.4	
<b>CO/H/W(ice):</b> CO + H <sub>2</sub> + H <sub>2</sub> O (ice)	5f-1	Thin medium grey coating, black inside		1.5 ± 0.07	55%	HA (97%), O (3%)	Significant OH loss	42.5 ± 0.5	91.6 ± 0.6	91.4 ± 0.6

4. Investigation of Sintering Atmospheres

	5f-3	Light grey coating, dark grey inside		$1.4 \pm 0.07$	62%	HA	Some OH loss	$47.3 \pm 0.1$	$86.3 \pm 0.7$	
	5f-3	Light grey coating, medium grey inside		$0.47 \pm 0.02$	87%	HA	Some OH loss	$43.9 \pm 0.2$	$89.8 \pm 0.3$	
<b>Air:</b> Air (NF)	5f-1	Uniformly pale blue		$0.10 \pm 0.01$	97%	HA	Excellent OH retention	$42.8 \pm 1.3$	$96.2 \pm 0.5$	
<b>A/W(ice):</b> Ar + H <sub>2</sub> O (ice)	5f-2	White coating, black inside		$1.5 \pm 0.08$	55%	HA (67%), T (32%), O (2%)	Decomposition	$46.4 \pm 1.0$	$87.9 \pm 0.3$	$87.8 \pm 0.3$
<b>H/W(ice):</b> H <sub>2</sub> + H <sub>2</sub> O (ice)	5f-2	Dark grey coating, black inside		$1.3 \pm 0.07$	61%	HA (97%), O (3%)	Significant OH loss	$46.5 \pm 0.3$	$92.2 \pm 0.2$	$92.0 \pm 0.2$
	5f-3	Uniformly medium grey		$0.30 \pm 0.02$	92%	HA	Some OH loss	$45.3 \pm 0.4$	$89.1 \pm 0.8$	
	5f-3	Light grey coating, dark grey inside		$0.53 \pm 0.03$	86%	HA	Some OH loss	$47.6 \pm 0.1$	$89.1 \pm 1.0$	
<b>CO/H/W:</b> CO + H <sub>2</sub> + H <sub>2</sub> O	5f-2	Dark grey coating, black inside		$1.3 \pm 0.07$	61%	HA (96%), O (4%)	Complete OH loss	$48.3 \pm 1.8$	$87.5 \pm 3.0$	$87.2 \pm 3.0$
	5f-3	Pale grey coating, medium grey inside		$0.45 \pm 0.02$	88%	HA (96%), β (4%)	Significant OH loss	$50.6 \pm 0.1$	$95.4 \pm 0.7$	$95.5 \pm 0.7$
<b>CO/W:</b> CO + H <sub>2</sub> O	5f-2	Medium grey coating, black inside		$1.6 \pm 0.08$	52%	HA (54%), T (43%), O (3%)	Slight decomposition	$46.3 \pm 0.2$	$89.2 \pm 0.5$	$90.2 \pm 0.5$

Out of all the atmospheres, the one which caused the highest degree of decomposition was A – dry flowing Ar. This atmosphere should have been the ‘driest’ of all the atmospheres, as it contained no added water and did not contain H<sub>2</sub> or CO, which would be expected to suppress the water-gas reaction to some extent, keeping some degree of water and OH groups in the system. The next highest degree of decomposition came from H, CO, A/W(ice), and CO/W. With the exception of CO/W, this result also seems to fit with theory. H and CO contained no added water, but should have retained some partial pressure of water in the system due to the thermodynamics of the water-gas reaction. A/W(ice) – Ar bubbled through ice water – should also contain only a minimal amount of water, as the vapour pressure of ice water is very small ( $p_{\text{H}_2\text{O}} = 5 \text{ mmHg}$ ). The level of decomposition for CO/W was unexpected, however, as it contained added water.

The degree of decomposition for H(NF), CO/H/W(ice) 5f-1, H/W(ice) 5f-2, and CO/H/W was very small and, theoretically, should have resulted from slight deviations in the Ca/P ratio. However, while each batch should have had a uniform Ca/P ratio, the only batch which seemed to result consistently in a small amount of CaO (Ca/P > 1.67) or  $\beta$ -TCP (Ca/P < 1.67) was 5f-2, which formed a small amount of CaO in all but one case. Atmospheres tested with the 5f-1 batch, if they did decompose, tended to decompose into phases which should result from Ca/P > 1.67. The one case in which samples from a 5f-3 batch decomposed (CO/H/W), they decomposed to form a small amount of  $\beta$ -TCP, indicating a Ca/P < 1.67. This is not unexpected, as the characterisation of the batches discussed in Chapter 3 showed that 5f-3 contained a ~5%  $\beta$ -TCP when sintered in wet Ar. So, while samples, when they did decompose, consistently decomposed for a particular batch to form a small amount of either CaO or  $\beta$ -TCP, they did not always undergo decomposition. This would suggest that either the Ca/P ratio was not uniform for a batch, or that the composition of the atmosphere can influence the decomposition product.

##### *4.3.3.1.2 FTIR analysis*

By examining the FTIR data the level of hydroxylation can be determined. Plots of the FTIR data are shown in Figure 4.7. Table 4.4 shows the changes expected in an FTIR plot from each phase. In the case of decomposition to phases such as TTCP and  $\alpha$ -TCP, the FTIR data tend to match the XRD data. The only exception was that the amount of decomposition shown in XRD for CO/W did not seem as extensive in FTIR.

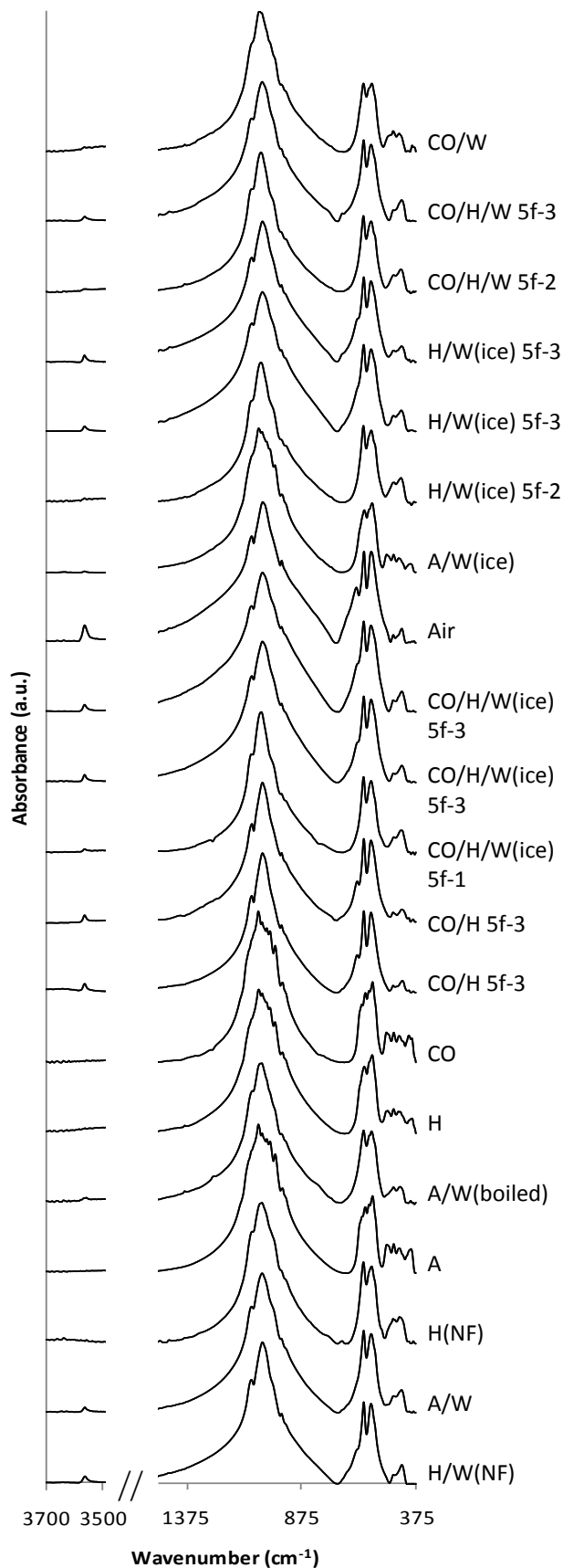


Figure 4.7: FTIR traces for heat treatment atmospheres, performed on sintered, then ground 5f material.

Table 4.4: Evidence of secondary calcium phosphate phases in FTIR.

Phase	Evidence in FTIR
OHA <sup>a,b</sup>	<ul style="list-style-type: none"> <li>Disappearance/weakening of OH librational mode at <math>633\text{ cm}^{-1}</math>, followed by OH lattice stretching peak at <math>3572\text{ cm}^{-1}</math></li> <li>Disappearance/weakening of <math>\nu_1</math> peak at <math>960\text{ cm}^{-1}</math> and appearance of shoulders at <math>970</math> and <math>945\text{ cm}^{-1}</math></li> <li>Appearance of <math>\nu_2</math> modes at <math>474</math> and <math>434\text{ cm}^{-1}</math></li> </ul>
$\alpha$ -TCP <sup>a</sup>	<ul style="list-style-type: none"> <li>Absence of OH peaks</li> <li>Disappearance of <math>\nu_1</math> peak and appearance of peaks at <math>970</math> and <math>945\text{ cm}^{-1}</math></li> <li>Presence of <math>\nu_2</math> modes at <math>474</math> and <math>434\text{ cm}^{-1}</math></li> </ul>
TTCP <sup>c</sup>	<ul style="list-style-type: none"> <li>Absence of OH peaks</li> <li>Splitting of <math>\nu_3</math> (<math>980</math>-<math>1100\text{ cm}^{-1}</math>) and <math>\nu_4</math> (<math>550</math>-<math>620\text{ cm}^{-1}</math>) vibrations due to lowering of symmetry from hexagonal (HA) to monoclinic (TTCP)</li> <li>Stronger presence and splitting of <math>\nu_2</math> (<math>350</math>-<math>500\text{ cm}^{-1}</math>) modes</li> </ul>
CaO <sup>d</sup>	<ul style="list-style-type: none"> <li>Presence of peak at <math>3640\text{ cm}^{-1}</math> due to OH in <math>\text{Ca}(\text{OH})_2</math> formed during adsorption of water by CaO</li> </ul>

<sup>a</sup>(Radin *et al.* 1992) <sup>b</sup>(Trombe *et al.* 1978);  
<sup>c</sup>(Sargin *et al.* 1997); <sup>d</sup>(Slosarczyk *et al.* 1987)

The FTIR data indicate the extent of dehydroxylation for each heat treatment atmosphere. In the summary table (Table 4.3) the FTIR results for each atmosphere are listed either as ‘decomposition,’ to indicate a significant amount of secondary phases, or some degree of dehydroxylation is listed. ‘Some OH loss’ is listed if the OH libration peak at  $633\text{ cm}^{-1}$  has been reduced to a shoulder, the intensity of the OH lattice stretching peak at  $3572\text{ cm}^{-1}$  and  $\nu_1$  mode at  $960\text{ cm}^{-1}$  have also been reduced, and weak peaks  $\nu_2$  peaks have appeared. ‘Significant OH loss’ is listed if the OH libration peak has completely disappeared, the intensity of the OH stretching peak and  $\nu_1$  have further decreased, shoulders have begun to appear around  $970$  and  $945\text{ cm}^{-1}$ , and the  $\nu_2$  peaks have intensified. When no OH peaks are evident, ‘complete OH loss’ is listed. ‘Good OH retention’ and ‘excellent OH retention’ are listed, depending on peak intensity, when the  $\nu_2$  peaks are minimal, the  $\nu_1$  peak is clear with no evidence of additional shoulders appearing, and both the OH libration and stretching peaks are present.

Generally, the level of hydroxylation of the sintered material fit well with the expected amount of water in the sintering atmosphere. However, CO/H/W and CO/W yielded unexpected results in this regard. While CO/H, which only incorporated water that might be present based on the water-gas reaction, resulted in no decomposition and ‘good OH retention’, CO/H/W and CO/W, both of which explicitly included water, in addition to what might result from the thermodynamics of the water-gas reaction, experienced a great deal of dehydroxylation and, in the case of CO/W, some decomposition.

### **4.3.4 Physical properties**

#### **4.3.4.1 CNT loading**

At high temperatures, CNT loss in an HA-CNT composite can originate from two sources – oxidation by reactive species in the sintering atmosphere and oxidation by water formed during dehydroxylation of the HA. When considering the atmospheres tested in this study, reactive species were present in the sintering atmosphere due to impurities in the gases (with the exception of Air) and water added to the atmosphere by bubbling the gases through water. The amount that each of these components may contribute to CNT loss can be calculated, although there are many assumptions made and sources of error in the calculations that may not result in an entirely accurate explanation of CNT loss.

Nonetheless, the calculations can provide useful insight which can partially explain CNT loss for different atmospheres.

#### 4.3.4.1.1 Are CNTs still present after sintering?

The presence of CNTs was verified by examining in SEM and TEM material left on the filter when the CNT loading measurements were made on an CO/H/W(ice) sample. Figure 4.8 shows an SEM (a) and TEM (b) micrograph of the material. While the material has still retained the basic CNT shape, the CNTs appear to be very damaged, quite short, and many are unrolled.

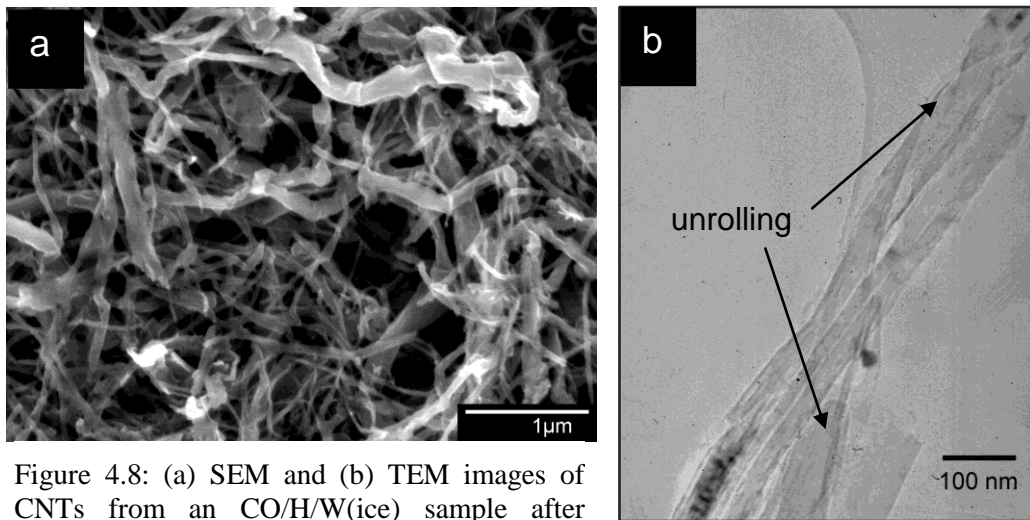


Figure 4.8: (a) SEM and (b) TEM images of CNTs from an CO/H/W(ice) sample after sintering.

#### 4.3.4.1.2 CNT loss due to gas impurities

The first step in calculating the amount of CNTs oxidised due to gas impurities is to determine the number of moles of gas which pass through the furnace during a heat treatment run at temperatures high enough to cause CNT oxidation. This can be determined by the following equation:

$$n_{gas} = \frac{r_{flow} t}{22.4}$$

where  $n_{gas}$  is the number of moles of gas,  $r_{flow}$  is the flow rate,  $t$  is the time, and 22.4 is the number of litres occupied by a mole of gas, assuming standard temperature and pressure. The time above critical temperatures was calculated in the case of flowing Ar atmospheres as above 570°C, which is the approximate temperature at which fCNT

oxidation begins, according to Figure 3.7, and in the case of other atmospheres as above 710°C, which is the temperature at which the gas flow was turned on during the heating stage and turned off during the cooling stage. The mass of CNTs consumed by oxidation can then be calculated as:

$$m_C = n_{gas} V_{imp} R_{C/imp} M_C$$

where  $m_C$  is the mass of carbon,  $n_{gas}$  is the moles of gas,  $V_{imp}$  is the volume concentration of the oxidising impurity,  $R_{C/imp}$  is the molar ratio of carbon to the impurity as dictated by the reaction equations (listed in Section 4.1.1), and  $M_C$  is the molar mass of carbon. The values for  $V_{imp}$  were obtained from the gas suppliers, and are listed in Table 4.5. The impurities O<sub>2</sub>, CO<sub>2</sub>, and H<sub>2</sub>O were considered the only oxidising species in these calculations. The calculation results are listed in Table 4.6.

Table 4.5: Gas impurities, as provided by suppliers.

Gas	Purity	O <sub>2</sub> (ppm)	N <sub>2</sub> (ppm)	CO <sub>2</sub> (ppm)	THC (ppm)	H <sub>2</sub> O (ppm)
Ar* (BOC)	99.998%	4	8	2	2	4
H <sub>2</sub> (Air Products)	99.9996%	0.5	2	0.5	0.1	1
CO (BOC)	99.8%	100	500	400	100	5

\*Impurity values were not specified beyond “total impurities 20 ppm maximum.” These numbers are based on scaling the impurity values in the next most pure Ar available from the same company.

#### 4.3.4.1.3 CNT loss due to dehydroxylation of HA

Dehydroxylation results from two OH groups combining to form one water molecule, leaving one oxygen atom in the HA crystal structure. As water can oxidise carbon, the amount of CNTs with which this water could potentially react should be taken into account. This can be calculated by:

$$m_C = m_{HA} \left( \frac{M_{H_2O}}{M_{HA}} \right) R_{C/H_2O} \left( \frac{M_C}{M_{H_2O}} \right) = m_{HA} \left( \frac{M_C}{M_{HA}} \right)$$

where  $m_C$  is the mass of carbon,  $m_{HA}$  is the mass of HA,  $M_{H_2O}$ ,  $M_{HA}$ , and  $M_C$  are the molar masses of water, HA, and carbon, respectively, and  $R_{C/H_2O}$  is the molar ratio of carbon to

Table 4.6: Calculations of CNT loss due to dehydroxylation and impurities.

Atmosphere	Flow Rate (L min <sup>-1</sup> )	Batch	CNT loss (%)	Oxidation (%)			CNT loss, un- accounted (%)
				Impur.	DH	Impur. + DH	
<b>H/W(NF):</b> H <sub>2</sub> + H <sub>2</sub> O (NF)	NF	5f-1	93	Neg.	36	36	57
<b>A/W:</b> Ar + H <sub>2</sub> O	0.5	5f-1	50	1.3	36	37	13
<b>H(NF):</b> H <sub>2</sub> (NF)	NF	5f-1	52	Neg.	36	36	16
<b>A:</b> Ar	0.5	5f-1	40	1.3	36	37	3
<b>A/W(boiled):</b> Ar + H <sub>2</sub> O	0.5	5f-2	75	0.9	25	26	49
<b>H:</b> H <sub>2</sub>	0.8	5f-1	37	0.3	36	36	1
<b>CO:</b> CO	0.4	5f-1	58	39	36	75	-17
<b>CO/H:</b> CO + H <sub>2</sub> , flowing	0.8	5f-3	54	35	32	67	-13
		5f-3	54	35	32	67	-13
<b>CO/H/W(ice):</b> CO + H <sub>2</sub> + H <sub>2</sub> O	0.8	5f-1	55	39	36	75	-20
		5f-3	62	35	32	67	-5
		5f-3	87	35	32	67	20
<b>Air:</b> Air (NF)	NF	5f-1	97	100	36	>100	-3
<b>A/W(ice):</b> Ar + H <sub>2</sub> O (ice)	0.5	5f-2	55	0.9	25	26	29
<b>H/W(ice):</b> H <sub>2</sub> + H <sub>2</sub> O (ice)	0.5	5f-2	61	0.1	25	25	36
		5f-3	92	0.2	32	32	60
		5f-3	86	0.2	32	32	54
<b>CO/H/W:</b> CO + H <sub>2</sub> + H <sub>2</sub> O	0.8	5f-2	61	27	25	52	9
		5f-3	88	35	32	67	21
<b>CO/W:</b> CO + H <sub>2</sub> O	0.4	5f-2	52	27	25	52	0

\*DH = dehydroxylation; Impur. = impurities; Neg. = negligible; NF = non-flowing

water (equal to 1) as dictated by the reaction listed in Section 4.1.1. This calculation assumes that the HA is completely hydroxylated to begin with and is completely dehydroxylated during the heat treatment process, and that all water produced reacts with the CNTs to oxidise them. It also does not take into account that part of the mass of HA (if taken as a room temperature mass prior to any heat treatment) will include some adsorbed water. While this adsorbed water should come off at temperatures below those

which should oxidise CNTs and be removed from the system in the case of a flowing gas atmosphere, it will mean an overestimation of the true mass of the HA and thus an overestimation of the relative amount of CNTs oxidised by water formed from dehydroxylation. The results of this calculation are listed in Table 4.6. Note that, unlike CNT loss due to gas impurities, the amount of oxidation caused by dehydroxylation will be independent of the amount of material in the furnace. Therefore, the percentage of CNT loss will only depend on the initial loading of CNTs in any given batch.

#### 4.3.4.1.4 CNT loss due to added water

A third contribution to CNT oxidation comes from the added water in moist atmospheres. Water was added to the atmospheres by bubbling gas through water, and the amount of water added to the gas should depend on the temperature of the water in the bubbler, as the vapour pressure of water varies with temperature. At a temperature of 20°C, the concentration of water in the gas can be calculated as follows:

$$\frac{g \text{ H}_2\text{O}}{L \text{ gas}} = \frac{M \times P}{R \times T \times 1000} = \frac{18 \frac{g}{mol} \times 17.535 \text{ mmHg} \times 133.3 \frac{Pa}{mmHg}}{8.31 \frac{J}{K \cdot mol} \times 293 \text{ K} \times 1000 \frac{L}{m^3}} = 0.01728 \frac{g}{L}$$

where  $M$  is the molar mass of water,  $P$  is the vapour pressure of water at the given temperature,  $R$  is the gas constant, and  $T$  is the temperature. This assumes that the water fully saturates the gas. The amount of carbon that will be oxidised can then be calculated by (using A/W – Ar + H<sub>2</sub>O as an example):

$$\begin{aligned} m_C &= r_{flow} t \left( \frac{g \text{ H}_2\text{O}}{L \text{ gas}} \right) R_{C/H_2O} \left( \frac{M_C}{M_{H_2O}} \right) = 0.5 \frac{L}{min} \times 372 \text{ min} \times 0.01728 \frac{g}{L} \times 1 \left( \frac{12}{18} \right) \\ &= 2.14 \text{ g} \end{aligned}$$

At 0°C (vapour pressure = 4.579 mmHg, concentration of water in gas = 0.00451 g L<sup>-1</sup>) the amount of carbon consumed will be 0.56 g. While the amount of carbon consumed at 0°C is far less than that consumed at 20°C, both amounts exceed the mass of CNTs in the samples, which was between 0.10 – 0.15 g, depending on the batch used. As there were still CNTs remaining after sintering in the moist atmospheres, either the gas was not fully saturated by the water or not all of the water interacted with the material.

#### 4.3.4.1.5 Analysis of CNT loss in different atmospheres

To give an idea of how much CNT oxidation due to gas impurities and dehydroxylation could be explained by calculations, Table 4.6 lists the predicted values of CNT loss for each heat treatment experiment. The right-most column lists the difference between the observed CNT loss and the calculation. Note that the oxidation from added water vapour is not included in the table calculations.

##### CNT loss in atmospheres without explicitly-added water

As the right-most column shows, these calculations only partially account for CNT loss. A few atmospheres are more straightforward than others, in this respect. The air atmosphere is the most basic, as the CO<sub>2</sub> and O<sub>2</sub> in the air in the furnace, even when not flowing, are easily enough to oxidise all the CNTs in the samples. Ar should be the next most straightforward, as it does not involve any added water and contains only inert gas and its impurities. As the material sintered in Ar was found to have decomposed and, thus, to have dehydroxylated, the full oxidation contribution from dehydroxylation can be expected to be fairly accurate. And, as the table shows, adding the contribution from gas impurities and dehydroxylation explains the CNT loss within a reasonable amount of error.

The explanation of results for the other dry atmospheres (H(NF), H, CO, and CO/H) may be slightly more complicated, as they involve CO and/or H<sub>2</sub>, which play a role in the water-gas reaction. Particularly interesting is the difference in CNT loss between H(NF), which lost 52% of the CNTs, and H(flowing), which lost 37%. As both samples showed complete dehydroxylation, then the entire amount of oxidation due to dehydroxylation should be taken into account. Since the impurity content of the H<sub>2</sub> was relatively low, the flowing vs. non-flowing atmosphere should make little difference to that part of the calculation. The calculation for H matches the experimental value very well. H(NF), however, lost more CNTs. One possible explanation is the following. As the system was not completely sealed, water formed from dehydroxylation may have oxidised some CNTs, forming CO and H<sub>2</sub> in the process. As the furnace heated, the CO and H<sub>2</sub> products would have been pushed out of the furnace, as the gas expanded. Once at a cooler temperature, the CO and H<sub>2</sub> could have reacted to form water and amorphous carbon, which might have condensed on the cool end of the furnace tube or in tubing. When the

furnace began to cool, the water could then have been sucked inside the furnace to react once again with the CNTs.

The CO calculation overestimated the CNT loss compared with the experimental value. As the sintered material had decomposed, it seems likely that the dehydroxylation component fully contributed to oxidation. The impurity component could be an overestimate, however, as at some point some degree of closed porosity should have formed (despite the somewhat low sintered density of the composites), making access to the CNTs more difficult. The amount by which the CNT loss is overestimated is equal to approximately half the calculated value for the impurity calculation, suggesting that gas access to the CNTs could have become much more difficult during the dwell at 1200°C, which is when porosity closure should be at its peak. Indeed, it may be that the impurity component is overestimated in all cases, but Ar and H<sub>2</sub> have such small amounts of impurities relative to CO that the overestimate is not noticeable.

For CO/H, again, the calculation overestimates the CNT loss, and by approximately the same amount as for CO. Thus, it could be that the impurity value is once again an overestimation. However, XRD and FTIR showed that the end material was well-hydroxylated HA, thus bringing into question if any oxidation occurred due to dehydroxylation. If the system was in thermodynamic equilibrium, then a small amount of water would have been present at all temperatures, thus suppressing dehydroxylation. However, the partial pressure of water in this system is extremely low by 1200°C (0.11 mmHg), suggesting a large amount of dehydroxylation would occur.

CO/H differs from atmospheres H(NF), H, and CO in that it contains both CO and H<sub>2</sub>. While Le Chatelier's principle suggests that an increase in either or both species on one side of an equation will shift the equilibrium towards the opposite side (in this case, either CO or H<sub>2</sub> or the combination might suppress dehydroxylation and the reaction of CNTs with water), Figure 4.9 shows that the thermodynamic situation is a bit more complex.

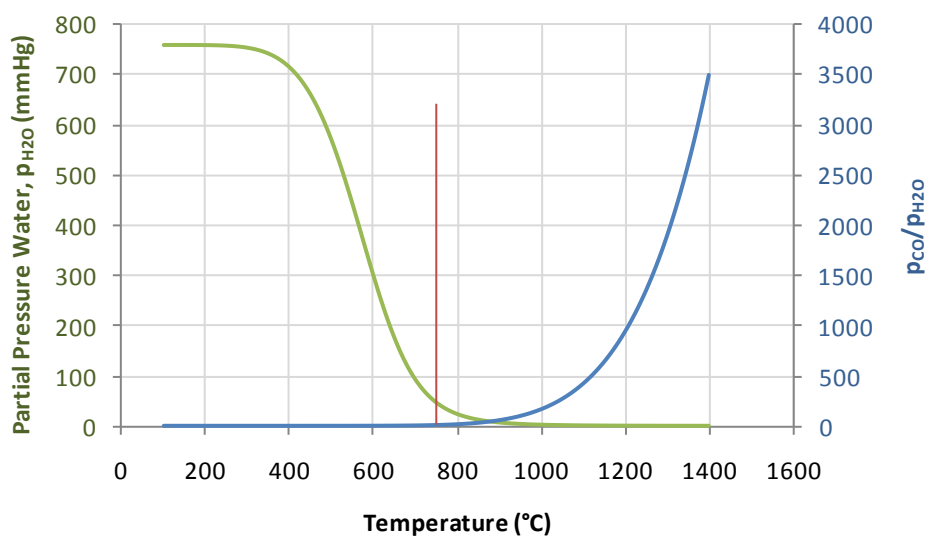


Figure 4.9: Change in partial pressures of gases with temperature for the water-gas reaction.

Figure 4.9 plots the partial pressures of the gases involved in the water-gas reaction with temperature. As temperature increases, the partial pressure of water tends to decrease. As the temperature decreases during the ramp down, more water will be present in the system. If the material is dehydroxylated by the end of the dwell at 1200°C, then CO and H<sub>2</sub> will tend to react to provide the necessary amount of water to fulfil thermodynamic equilibrium, and this water could serve to rehydroxylate the material during the cooling stage. However, in the case of an atmosphere of just CO or H<sub>2</sub>, while the heating stage may be similar to an atmosphere of CO + H<sub>2</sub> the cooling stage will be different. If the material has dehydroxylated and the resulting water has either reacted with the CNTs or been carried away by the flowing gas, then during the ramp down, only one of the two components necessary to form more water will be present, and therefore the material cannot be rehydroxylated. This would result in either a dehydroxylated or decomposed material, as was the result for H(NF), H, and CO. With CO/H, on the other hand, as both components necessary to make additional water were present, then the resulting material was more hydroxylated. It is unclear whether this new water could reach the interior of the tablet, just as it seems possible that gas impurities may no longer be able to reach the interior of the tablet due to closed porosity. It should be noted, however, that the CO/H samples had the lowest density of any samples (~82%), and thus may not have had a large

degree of closed porosity, making rehydroxylation more possible than for denser materials.

CNT loss in atmospheres with explicitly-added water

CNT loss in atmospheres with explicitly added water is more difficult to account for. In most cases it is unclear how much of the CNT loss was due to water and how much was due to impurities, as at some stage closed porosity likely prevented some oxidation from the impurities and water. Looking first at the three atmospheres containing Ar and added water (A/W, A/W(boiled), and A/W(ice)), a clear difference in CNT loss can be seen. A/W(boiled), which contained water which had previously been boiled to remove dissolved oxygen, was expected to have a slightly lower CNT loss than A/W, if any difference was observed. The trend, however, was the opposite, as A/W lost 50% of its CNTs and A/W(boiled) lost 75%. The calculations for A/W(ice), which was Ar bubbled through ice water, showed a CNT loss of 55%. Since the vapour pressure of water near freezing temperature is much lower than at room temperature, the contribution of CNT loss due to added water should be lower for A/W(ice). As this is the case when compared with A/W(boiled) but not with A/W, then another factor must be contributing. Both A/W(boiled) and A/W(ice) (which follow the expected trend) used samples from the 5f-2 batch of material, while A/W used the 5f-1 batch. Thus, some differences may be attributable to batch variations.

Making a comparison between the two atmospheres containing H<sub>2</sub> and water (H/W(NF) and H/W(ice)) is more difficult, as one was non-flowing and the other was flowing. For H/W(NF), the material was still somewhat hydroxylated, so not even the full CNT loss for dehydroxylation would be expected, yet even without that consideration, impurities and dehydroxylation still leave a CNT loss of 57% to explain. Calculating the volume of the furnace tube (volume of gas) and the amount of water expected to be incorporated into that volume when the gas is bubbled through at room temperature (from Section 4.3.2.1.2) shows that the resulting CNT oxidation will cause a CNT loss of ~60%, which should account for the remainder of the unexplained CNT loss. In examining the data from H/W(ice) (H<sub>2</sub> + H<sub>2</sub>O ice), a larger CNT loss would be expected compared with H (dry H<sub>2</sub>), due to oxidation by added water, and, indeed, this seems to be the case. Once again, however, the matter of batch variation arises, as the three H/W(ice) experiments

yielded very different results. The two experiments which used 5f-3 had an 86% and 92% CNT loss, which is the same within experimental error, while the experiment which used 5f-2 had only a 61% loss for the same conditions. It could be that the different batches (which have somewhat different surface areas and particle sizes) may sinter at slightly different temperatures and rates, meaning that the ability of water to penetrate into the sample is altered, depending on the degree of sintering and closed porosity at a given time.

CO/W (CO + H<sub>2</sub>O) yielded somewhat unexpected results compared with the other atmospheres. The FTIR and XRD data show some degree of decomposition and no hydroxylation, thus it seems reasonable to estimate a CNT loss in line with full dehydroxylation. As observed for CO, it seems possible that the full amount of impurities may not contribute to CNT loss, due to the onset of closed porosity. Yet the loss of CNTs when water is included in the atmosphere is 6% less than when water is not. Again, the reason may be effects from batch variation, as CO used 5f-1 and CO/W used 5f-2. Thus, it is unclear for CO/W how much loss is attributable to oxidation by added water and how much is due to impurities.

The final two atmospheres left to examine for CNT loss are CO/H/W(ice) (CO + H<sub>2</sub> + H<sub>2</sub>O ice) and CO/H/W (CO + H<sub>2</sub> + H<sub>2</sub>O). Looking at the data for multiple experiments done with each atmosphere, it again appears that batch variation may be playing a role in the degree of sintering, and thus the extent to which impurities and added water contribute to CNT oxidation. One would expect a greater CNT loss from CO/H/W than from CO/H/W(ice), as more water should be incorporated into the atmosphere when bubbled through at room temperature than near freezing. Particularly interesting are the results from the second and third experiment for CO/H/W(ice) and the second experiment of CO/H/W, all of which used the 5f-3 batch. The CNT loss for the third experiment of CO/H/W(ice) was similar to that of the second experiment of CO/H/W. On the other hand, the second two experiments for CO/H/W(ice), which used the same batch, differed quite a lot in their CNT loss. It seems, in this case, that the green density may play a role in the extent to which impurities and water are able to oxidise the CNTs, as a higher green density may mean an earlier onset of sintering or a greater extent of sintering.

##### Batch variation

Overall, it was observed that experiments performed with the 5f-2 batch resulted in relatively high loadings of CNTs, while those performed with the 5f-3 batch resulted in relatively low loadings. Looking back at the properties of these batches from Table 4.1, the most noticeable difference among the batches is that 5f-2 has a lower surface area than 5f-1 and 5f-3. The mean particle sizes for the batches are also somewhat different. It would be expected that a higher surface area and smaller particle size would mean an earlier onset of sintering; however, if anything, the opposite seems to be true for 5f-2. Another possibility is that the quality of the CNTs varied from one batch to another, and thus the temperature at which oxidation of the CNTs began may have been different. While the CNTs for these materials were taken from one large, mixed batch to minimise differences, the CNTs could have become damaged to different extents during ball milling.

##### **4.3.4.2 Density**

The density values reported in this study are % TD values, based on the theoretical density of HA. The balance of the % TD value (based on 100%) gives the porosity of the sample. As mechanical properties of ceramics correlate strongly with porosity, the % TD value is therefore of considerable value when assessing the relative potential for mechanical improvement for different samples.

The density of the samples both before sintering (green density) and after sintering (final density) is listed in Table 4.3. A third density column in the table represents an adjusted density, taking into account that the theoretical density of many samples will be different from that of HA if they have decomposed. The density values for this column were taken as percentage of theoretical density, with the theoretical density being calculated based on the phase percentages determined by XRD and using the rule of mixtures. The theoretical densities of the phases were taken as: HA = 3.16 g cm<sup>-3</sup>;  $\beta$ -TCP = 3.08 g cm<sup>-3</sup>;  $\alpha$ -TCP = 2.86 g cm<sup>-3</sup>; TTCP = 3.05 g cm<sup>-3</sup>; and CaO = 3.42 g cm<sup>-3</sup>. What this calculation does not take into account is the amount of OHA that might be in a sample. It is difficult to determine a theoretical value for each sample, as a quantitative extent of dehydroxylation was not determined, nor were adjusted lattice parameters for each sample measured. It is presumed that the % TD for dehydroxylated samples should be marginally higher than

that shown in the ‘final density’ column. An additional compounding factor in calculating the % TD is that the XRD measurements were taken near the surface of the sample; however, the phase composition may change in the interior of the sample. Despite these considerations, the adjusted density values may give a more accurate representation of the porosity in the samples.

The green density vs. adjusted final density values do not seem to show any correlation. There is a large spread of green density values (41.8 – 51.6%) and a large spread of final adjusted densities (81.9 – 95.8%), but the higher green density values do not seem to yield the higher final density values, nor the other way around. The number of variables makes it difficult to judge if there is any correlation, as atmosphere composition, material batch, and CNT loading may all affect the final density. Thus, accurate comparisons may only be made when the batch and atmosphere are the same and the CNT loadings are similar. In the case of CO/H, the same batch and nearly identical green densities yielded very similar final densities. For CO/H/W(ice), two of the experiments used the 5f-3 batch but with different green densities (47.3% vs. 43.9%), and the result was fairly different final densities (86.3% and 89.8%, respectively). However, in this case the final CNT loading was quite different (1.4% vs. 0.47%, respectively), so it is difficult to make a comparison.

Under the same sintering conditions and using the same batch, the samples with a higher green density retained more CNTs. This could indicate that the higher green density helped to suppress CNT oxidation. A final comparison can be made for the H/W(ice) atmosphere where, once again, 5f-3 was used with green densities of 45.3% and 47.6%, giving a final density of 89.1% in both cases, which would suggest that green density does not affect final density. However, the CNT loading was slightly different between the two experiments following sintering, with values of 0.30 wt.% and 0.53 wt.%, respectively. Once again, the samples with the higher green density retained slightly more CNTs.

The data were also analysed to determine whether there was any correlation between the final CNT loading and the final density of the samples. In previous studies, CNTs have been shown to prevent full densification of ceramics, particularly when pressure is not used to sinter (Peigney 2003). Figure 4.10 shows a graph of CNT loading vs. final density (adjusted final density, when available), using data points from Table 4.3. The different

batches are represented by different symbols and trendlines are plotted for a particular batch, as some effects have already been noted from batch differences. The 5f-1 batch shows a weak linear correlation between density and CNT loading, with lower CNT loadings giving higher densities. The 5f-3 batch shows a stronger correlation, though with lower density values for a given loading in comparison with 5f-1. The 5f-2 batch, on the other hand, does not seem to show any trend. In general, however, it seems there is at least some loose correlation between the two characteristics, indicating that the CNT loading may play a role in the final sintered density of a sample.

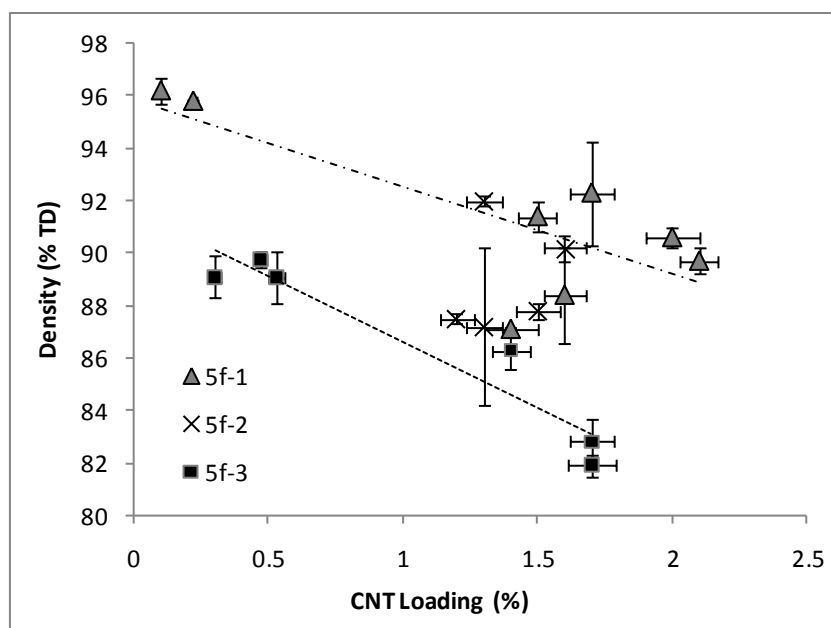


Figure 4.10: Final density vs. CNT loading for sintered samples.

#### 4.3.4.3 Appearance

The most obvious difference between HA and composite materials, when unsintered, is their colour. As noted in Section 3.4.2.1, the colour of the unsintered tablets darkened with increasing loading of CNTs. Thus, it seems reasonable to expect a similar trend in the sintered materials. This colour difference could then serve as a qualitative estimation of the CNT loading after sintering.

The appearance observations for each heat treatment experiment are listed in Table 4.3 with both a description and photograph of one of the samples. As expected, the samples sintered in air, which contained virtually no CNTs after sintering were a very light colour,

although rather than white they were a very pale blue, which can be attributed to manganese impurities in the starting materials (Yubao *et al.* 1993). To a certain extent, the degree of greyness of the samples correlated with the loading of CNTs. Samples described as 'black' or 'dark grey' had relatively high loadings, whereas samples described as 'medium grey' or 'pale grey' had relatively low loadings. Misleading, however, is that most of the samples seemed relatively dark in colour compared with their unsintered counterparts. A sample which contained only about 0.5 wt.% CNTs following sintering might still appear as dark in colour as a green sample with 2 wt.% CNTs, thus at first suggesting that the CNT loading should be much higher than the measured value of 0.5 wt.%. However, an apparent darkening in colour is likely also attributable to a higher density. While a green powder containing 0.5 wt.% CNTs will appear very pale grey, when pressed to about 45% TD it appears a medium grey. Thus, it follows that a medium grey unsintered tablet might appear a dark grey when sintered to a much higher density.

In addition to the general colour of the tablet, it was noted that some tablets had coatings or layers on the outside that were lighter in colour than the interior of the tablets. This would suggest that the outer layers had a lower loading of CNTs than the interior. In Table 4.3, a 'coating' refers to a very thin layer of a lighter colour (< 0.1 mm), whereas a 'layer' refers to a thicker amount (> 0.1 mm). In the cases of H/W(NF) and A/W, the layer was particularly pronounced and white in colour, suggesting virtually no CNTs were present in those areas. All atmospheres which contained either added water or the possibility of producing added water (*i.e.* contained both CO and H<sub>2</sub>) resulted in samples with some degree of coating or layer. All 'dry' atmospheres, on the other hand, were a uniform colour throughout. These observations led to a more in-depth study of these layers.

#### 4.3.5 The white layer phenomenon

The observation of a light-coloured layer on samples when heat treated in some atmospheres suggested further implications warranting more study. Firstly, if a gradient in CNT loading was present, there could be a gradient in other properties. Secondly, since the layer was observed when there was a significant amount of water in the atmosphere, it would imply that water was at least partially responsible for the layer.

#### 4.3.5.1 Phase composition and hydroxylation variation with depth

To examine if the properties of the tablet changed with depth, one 1 g tablet of HA and one 1 g tablet of 5f-3 were sintered in wet Ar according to the conditions described for the A/W atmosphere. This atmosphere was chosen as it produced a noticeable white layer but still a relatively high loading of CNTs in the interior. After sintering, the tablets, which were ~4 mm in thickness, were examined on the top surface and at 1, 2, 3, and 4 mm from the top surface by XRD and FTIR to create a thickness profile. Additionally, the top surface and a fracture surface of similar tablets sintered at 1000°C were examined in SEM.

The results of the XRD and FTIR studies are shown in Table 4.7. The characterisation followed the same methods as the results reported in Table 4.3. A depth of 0 mm refers to the top surface of the tablet, while 4 mm refers to the bottom surface, which was sitting against an alumina substrate.

Table 4.7: XRD and FTIR results of tablet profile performed on HA and 5f sintered in wet Ar.

Depth (mm)	XRD		FTIR	
	HA	5f-3	HA	5f-3
0	HA (96%), β (4%)	HA	Good OH retention	Good OH retention
1	HA (95%), β (5%)	HA (80%), T (15%), α (5%)	Some OH loss	Complete OH loss
2	HA (95%), β (5%)	HA (80%), T (15%), α (5%)	Some OH loss	Small amount of decomposition
3	HA (95%), β (5%)	HA (80%), T (15%), α (5%)	Some OH loss	Small amount of decomposition
4	HA (95%), β (5%)	HA	Some OH loss	Significant OH loss

The results show that there was a variation in phase composition and level of hydroxylation with depth. For the HA tablet, small amounts of β-TCP and dehydroxylation were observed below the top surface of the tablet, while the top surface remained well hydroxylated, with an amount of β-TCP comparable to the characterisation results shown in Chapter 3. The change with depth was more noticeable in the 5f tablet.

While both outside surfaces of the tablet remained HA, according to XRD, the interior decomposed to a mixture of HA, TTCP, and  $\alpha$ -TCP. The decomposed regions matched up to the black coloured regions of the tablet, while the regions which remained HA were part of the white layer. Additionally, the FTIR results showed decomposition in the interior of the tablet, along with significant dehydroxylation on the bottom surface of the tablet. With both the HA and 5f tablets, the bottom surface, which was in contact with the alumina substrate, showed more decomposition and/or dehydroxylation compared with the top surface. This could be due to the top surface of the tablet having more ready access to water in the sintering atmosphere.

#### 4.3.5.2 Density variation with depth

SEM micrographs of a 5f tablet are shown in Figure 4.11. Figure 4.11(a) shows the top surface of the tablet, while Figure 4.11(b) shows a fracture surface, just at the interface between the white and black regions. On the top surface, long, thin holes are evident, which are about the right size and shape to be artefacts from oxidised CNTs. No intact CNTs were observed on the surface. The fracture surface shows the interface of the black and white regions. In the black region, CNTs can still be seen, while in the white region, there appear to be no CNTs. Also of note is that the black region seems much more porous than the white region. In the white region, necking between particles is observed, while in the black region, it does not appear that sintering has yet begun. This supports earlier observations that composites with more CNTs tend to be more porous. As porosity

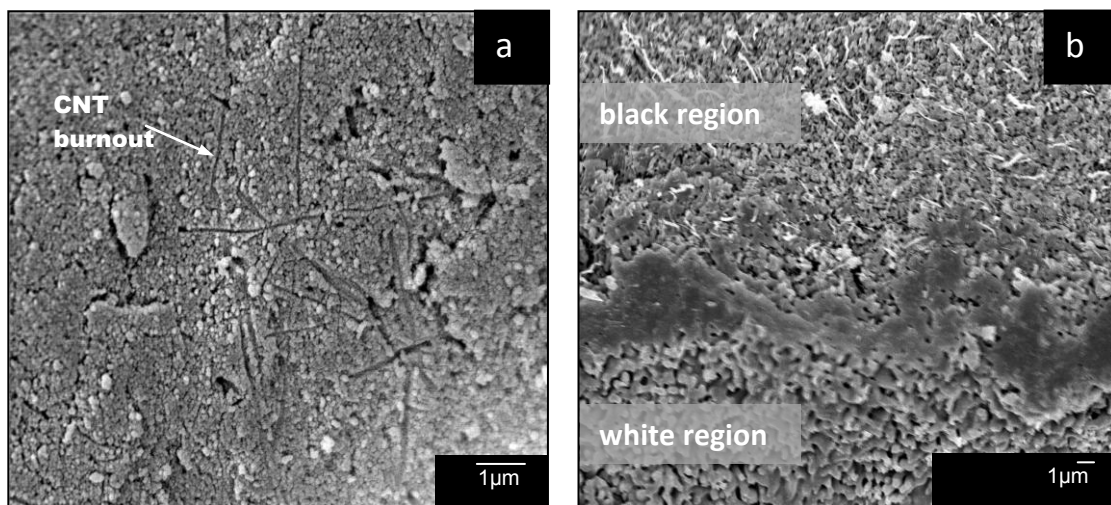


Figure 4.11: SEM micrographs of a 5f (a) surface and (b) white-black interface sintered at 1000°C. The surface image shows holes remaining after CNT oxidation, while the interface image shows CNTs remaining in the black region and no CNTs present in the white region.

is related to mechanical properties, it seems likely that the two regions will have different mechanical properties. Indeed, preliminary tensile strength testing showed that the sample partially failed on the interface between the white and black layers (Figure 4.12(e)). Thus, this interface could be a source of mechanical weakness if present in an implant material. As porosity is related to mechanical properties, it seems likely that the two regions will have different mechanical properties. Indeed, preliminary tensile strength testing showed that samples partially failed on the interface between the white and black layers (Figure 4.12(e)). Thus, this interface could be a source of mechanical weakness if present in an implant material.

#### 4.3.5.3 Origin of the white layer

To investigate if the thickness of the layer changed with sample thickness, three tablets of different masses (0.5 g, 1.0 g, 1.5 g) of 5f were sintered at 1200°C. Figure 4.12(b-d) shows that the white layer thickness does not seem to depend on sample thickness, suggesting that the white layer is caused by oxidising gas trying to pass into the tablet, and that it is a time-dependent reaction unrelated to material mass or geometry. Figure 4.12(a) shows that the white layer is of approximately equal thickness around the entire outer diameter of the tablet.

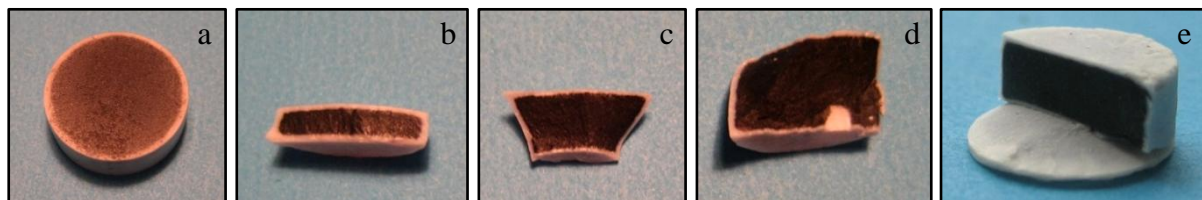


Figure 4.12: Photographs of tablets with white layer. (a) horizontal section, (b) vertical section 0.5 g, (c) vertical section 1.0 g, (d) vertical section 1.5 g, (e) mechanical failure at white-black interface.

From all these characterisations, what is known about samples with a white layer is: 1) the layer appears to be CNT-free due to oxidation of CNTs in the white area, 2) the layer does not vary with sample thickness, thus seems controlled by the outside sintering atmosphere rather than any interior reactions (such as dehydroxylation), and 3) composite samples with a white layer have a variation in phase composition and hydroxylation which is more pronounced than in HA samples. Thus, an overarching theory could be as

follows. At relatively low temperatures (~20 - 650°C) the powder particles are in contact with one another, but not much CNT oxidation has occurred. Between the onset of oxidation due to the water-gas reaction and the onset of sintering (~650 - 1000°C), CNTs begin to burn out of the sample rather evenly, as the porosity allows for easy gas access. Once sintering begins, the particles begin to coalesce and the porosity becomes more closed. As this happens, gas access both into and out of the tablet becomes more difficult. At some stage, the oxidation from water added to the atmosphere becomes more significant than oxidation due to water formed during dehydroxylation, and CNTs more easily oxidise on the outer layer of the tablet. As CNTs tend to inhibit densification, eventually the outer layer becomes CNT-free and nearly all open porosity is eliminated, effectively trapping the interior of the tablet from reaction with the sintering atmosphere. One of two things may happen at this point to cause a variation in phase composition and hydroxylation. Firstly, the entire sample may have already dehydroxylated and only very slowly (due to slow diffusion from the very low open porosity) are the outside layers rehydroxylated by the water in the sintering atmosphere. Secondly, it may be that the material has not completely dehydroxylated when the white layer forms. In this case, dehydroxylation may continue on the interior of the tablet and the resulting water would then oxidise CNTs. As it is very difficult for water to rehydroxylate the interior from the outside, the interior may fully dehydroxylate and then begin to decompose, while the exterior remains hydroxylated.

#### **4.3.6 Choosing an atmosphere for further study**

The goal of these heat treatment investigations was to find a sintering atmosphere that would 1) prevent decomposition, 2) retain HA's OH groups, 3) retain a reasonable amount of CNTs, and 4) result in a low porosity/high % TD. No atmosphere tested was found to meet all of these criteria ideally, particularly as no atmosphere resulted in both a % TD of at least 95% and significant retention of CNTs. Therefore, the atmospheres were compared to choose one which resulted in the best combination of properties that would give the best potential in further studies of mechanical properties and biological properties.

Perhaps the most important criteria to consider first are whether the material remained phase pure decomposed and whether it retained a large amount of OH groups, as other

calcium phosphate phases and OHA have been shown to be more soluble and have a higher dissolution rate than well-hydroxylated HA. Not only would a more soluble material negatively impact the mechanical integrity of an implant material, but in the case of these particular composites, the release of CNTs into the body would be a concern. Thus, any atmospheres which resulted in decomposition or 'complete OH loss' were eliminated from consideration. This included H(NF), A, H, CO, A/W(ice), CO/H/W, and CO/W.

Next, the CNT loading and density were considered. These criteria were somewhat more difficult to assess. Some effects due to batch variation were previously noted, which resulted in some batches giving more consistently higher CNT losses than others. Thus, some consideration was given to the CNT loading relative to other experiments which used the same batch. Additionally, it must be kept in mind that since density will vary some with CNT loading, some comparison should be made between the final densities of batches with similar CNT loadings.

The characterisation of the H/W(NF) samples showed that they had a high density (95.8%), but a very low loading of CNTs (0.22 wt.%). This atmosphere resulted in the largest CNT loss for any atmosphere other than air, and was thus eliminated from further consideration. The A/W(boiled) atmosphere resulted in a material with fairly good CNT retention and density. However, the material was also observed to be particularly friable. Additionally, while the CNT retention and density were fairly good in comparison with all the atmospheres, they were not as good as for some of the other atmospheres which used the 5f-2 batch. The samples sintered with CO/H had one of the best retentions of CNTs, along with excellent OH retention, but because of this they also had by far the lowest density of any of the samples at 82.8 and 81.9%. The air atmosphere was also eliminated from consideration, as it yielded samples with virtually no CNTs after sintering.

The remaining atmospheres – A/W, CO/H/W(ice), and H/W(ice) – all yielded samples with an HA crystal structure, some degree of hydroxylation, a reasonable loading of CNTs (depending on the batch), and a fairly good density compared with similar CNT loadings in other atmospheres. The main problem with A/W was the presence of the white layer, which seemed to accompany a change in phase composition and

hydroxylation with thickness in the tablet and led to differences in mechanical properties between the white and black sections. Aside from that, the properties of the tablets produced in this atmosphere were good compared with other atmospheres. This atmosphere may prove useful in other studies, as the white layer could be ground off (although, with implants of complex geometry this could be time consuming and costly). However, for this study, it was preferred to choose an alternate atmosphere which would not need post-processing.

The differences in the results produced by CO/H/W(ice) and H/W(ice) were subtle, and not completely conclusive. Both produced samples with a wide range of CNT loadings, which seemed to depend partly on the batch used and partly on the green density of the starting material. If it is assumed that comparisons can be most accurately made only between the same batch of material and similar green densities, then a comparison can be made best between the second experiment of CO/H/W(ice) and the third of H/W(ice). In this case, XRD and FTIR gave similar results, but the loading of CNTs after sintering was quite different, with CO/H/W(ice) giving a loading of 1.4 wt.% and H/W(ice) a loading of 0.53 wt.%. At the same time, however, the densities reflected the difference in loading, with CO/H/W(ice) yielding a density of 86.3% and H/W(ice) a density of 89.1%. The third experiment for CO/H/W(ice) showed that a lower CNT loading produced samples with higher densities, and indeed a similar density to the H/W(ice) experiment with a similar CNT loading. Therefore, there was no conclusive difference in the results produced by CO/H/W(ice) and H/W(ice). In the end, CO/H/W(ice) was chosen for further study in the interest of additional investigation of the water-gas reaction.

#### ***4.4 Optimisation of sintering conditions***

The atmosphere investigations in Section 4.3 all used the same flow rate for each atmosphere studied, four samples for each experiment, and were only investigated with 5f material. The purpose of this next set of experiments was to assess the effect of the CO/H/W(ice) atmosphere on different types of material (and if sintering them together in the furnace had any effect), the effect of varying the number of samples sintered at once, and the effect of changing the flow rate of the gas. Optimisation of the sintering profile (ramp rate, dwell time, and dwell temperature) will be addressed in Chapter 5.

#### **4.4.1 Methods**

For the assessment of sintering different materials, four samples each of HA, 5nf, and 5f were sintered in CO/H/W(ice), according to the procedure described in Section 4.3.1. Additionally, one sample of each material (three total) were sintered together with the same conditions to examine if the materials behaved any differently when sintered together compared with separately. To examine the effect the number of samples sintered at once had on the final sintered properties of the materials, 1, 4, and 10 samples of 5f were sintered in separate experimental runs in the CO/H/W(ice) atmosphere. Previous results from the atmosphere investigations were used for the four samples. The effect of flow rate on the properties of the sintered materials was examined by sintering four samples of 5f in the CO/H/W(ice) atmosphere using three different flow rates – 0.2, 0.8, and 1.0 L min<sup>-1</sup>. The materials were all characterised in the same manner as described in Section 4.3.2.

#### **4.4.2 Results**

A summary of the results for all the experiments is shown in Table 4.8. The upper part of the table gives the results for the study of different materials, the middle part shows the results for the variation of sample number study, and the bottom part gives the results for the flow rate study.

##### ***4.4.2.1 Examination of different materials and mixing materials***

Considering the effect of the CO/H/W(ice) atmosphere on sintering HA, both alone and with composite materials, the results show that the material was dehydroxylated and slightly decomposed. The densities in both cases were similar, however the samples which were sintered separately were decomposed more than the HA samples sintered along with the composites. These results would seem to indicate that there was an

Table 4.8: Summary of results of additional variables study.

Batch	Flow Rate (L min <sup>-1</sup> )	Number of Samples	CNT Loading (wt.%)	CNT Loss	XRD	FTIR	Green Density (% TD)	Final Density (% TD)
HA	0.8	4/4*	---	---	HA (88%), $\beta$ (10%), O (2%)	Slight decomposition	45.4 $\pm$ 0.2	93.5 $\pm$ 0.1
5nf	0.8	4/4	0.38 $\pm$ 0.02	87%	HA	Good OH retention	44.8 $\pm$ 0.5	89.8 $\pm$ 0.6
5f-3	0.8	4/4	0.47 $\pm$ 0.02	87%	HA	Some OH loss	43.9 $\pm$ 0.2	89.8 $\pm$ 0.3
HA, mixed	0.8	3/9	---	---	HA (95%), $\beta$ (5%)	Significant OH loss	44.9 $\pm$ 0.4	93.1 $\pm$ 0.2
5nf, mixed	0.8	3/9	1.31 $\pm$ 0.06	54%	HA	Good OH retention	44.9 $\pm$ 0.1	86.2 $\pm$ 0.3
5f-3,2, mixed	0.8	3/9	0.73 $\pm$ 0.04	83%	HA	Good OH retention	44.3 $\pm$ 0.3	84.3 $\pm$ 0.3
5f-3	0.8	1/1	0.25 $\pm$ 0.01	93%	HA (90%), $\beta$ (10%)	Slight decomposition	44.1	93.9
5f-3	0.8	4/4	0.47 $\pm$ 0.02	87%	HA	Some OH loss	43.9 $\pm$ 0.2	89.8 $\pm$ 0.3
5f-3, 2	0.8	10/10	0.77 $\pm$ 0.04	86%	HA	Excellent OH retention	46.5 $\pm$ 0.7	81.7 $\pm$ 0.8
5f-3,2	0.2	4/4	1.23 $\pm$ 0.06	77%	HA (97%), $\beta$ (3%)	Good OH retention	46.8 $\pm$ 0.1	83.9 $\pm$ 0.2
5f-3	0.8	4/4	0.47 $\pm$ 0.02	87%	HA	Some OH loss	43.9 $\pm$ 0.2	89.8 $\pm$ 0.3
5f-3,2	1.0	4/4	2.49 $\pm$ 0.12	53%	HA	Excellent OH retention	47.0 $\pm$ 0.8	77.8 $\pm$ 0.9

\*Notation x/y is x of one type of sample sintered in a batch with y total samples.

insufficient partial pressure of water in the atmosphere to maintain hydroxylation, although it is unclear why the partial pressure of water was sufficient to result in hydroxylated composite materials. It may be that a higher density and greater degree of closed porosity in the HA samples compared with the composites prevented water from reaching the interior of the tablet.

The 5nf samples, both when sintered alone and with the other materials, remained phase pure and well hydroxylated. A lower density was measured for the samples sintered alongside others compared with the 5nf samples sintered alone. As there were fewer CNTs remaining in the samples sintered alone, it is possible that the differences in density were due to the relative amounts of CNTs. The fact that fewer CNTs were lost in the samples sintered alongside other samples may be because there was more material and there were more CNTs in the system over which to spread any oxidation from gas impurities and water.

The 5f samples also remained phase pure in both cases, although they were more hydroxylated when sintered with other samples than when alone. When sintering the materials separately, the 5f and 5nf materials had the same degree of CNT loss. However, when sintered together, the 5f samples experienced a much larger degree of CNT loss compared with the 5nf samples. This may be due in part to the fact that the material sintered alone was 5f-3, while that sintered separately was 5f-3,2. As 5f-3,2 had a longer milling time, the CNTs from this batch may be more damaged. Additionally, fCNTs were previously found to have a lower oxidation temperature than nCNTs, thus it follows that the 5f samples would experience a greater degree of CNT loss than the 5nf material. Additionally, the density of the 5f samples sintered with others was lower than when sintered alone. This may partially be due to batch variation and partially due to the fact that the samples sintered together had a higher loading of CNTs, which might prevent densification.

#### ***4.4.2.2 Variation of number of samples***

When varying the number of samples sintered at once, several properties were found to scale with number. The density, final CNT loading, and CNT loss all correlated to the number of samples, with the density and CNT loss decreasing with increasing number and the final CNT loading increasing with increasing number. The hydroxylation and

phase purity also seemed to scale with sample number. One sample sintered alone was found to slightly decompose, whereas four were somewhat dehydroxylated, but ten were phase pure and well hydroxylated. Again, this may be an effect of density. The samples which were most hydroxylated also had the highest loading of CNTs and the lowest density, so water was more accessible to their structures.

#### ***4.4.2.3 Variation of flow rate***

The results for the flow rate study were somewhat inconclusive, as either the batches used or the green densities seem to have had some effect. Most interestingly, the highest flow rate yielded the lowest loss of CNTs. In theory, the opposite should be expected, as a higher flow rate should introduce more gas impurities and more water into the system, which should result in a high degree of CNT loss. It may be that at higher flow rates the water in the bubbler does not saturate the gas to the same degree, so less water is actually being introduced into the system. As previously observed, the results showed decreasing density with greater CNT retention.

### ***4.5 Summary***

Choosing a sintering atmosphere for composites of HA and CNTs presents a dilemma, as CNTs oxidise at high temperatures, yet water is necessary to prevent dehydroxylation and decomposition of HA. Thus, the purpose of this study was to investigate a wide range of atmospheres that might enable both CNTs and OH groups to be retained.

The results of these sintering atmosphere studies have revealed a complex system which is dependent on many variables. However, by understanding the role of each of these variables, it becomes possible to tailor-make a material with different combinations of properties. Some of the variables which were found to affect key properties (some of which are interrelated) are listed below.

#### **CNT loss**

- Batch variation (from effects of phase purity, green loading of CNTs, milling time, specific surface area, and particle size and shape)
- Green density of samples
- Gas impurities

- Composition of atmosphere

**Final density of sample**

- Loading of CNTs
- Phase purity and hydroxylation

**Phase purity and hydroxylation**

- Composition of atmosphere
- Final density of sample

Several conclusions were drawn from the atmosphere studies, which eventually led to the choice of an atmosphere which resulted in the best combination of properties. Dry atmospheres were found to result in decomposed and dehydroxylated materials. Most materials sintered in wet atmospheres (including CO/H – CO + H<sub>2</sub>, which is expected to create its own water) decomposed less than in dry atmospheres, or not at all, and were hydroxylated to some extent. Some wet atmospheres resulted in a white layer or coating, which was found to be undesirable due to variations in the degree of sintering and phase composition throughout the tablet, which also resulted in mechanical property deficiencies. The optimal atmosphere was chosen as CO/H/W(ice) – CO + H<sub>2</sub> + H<sub>2</sub>O ice.

Further studies were conducted to investigate sintering HA and composites with nfcCNTs in the CO/H/W(ice) atmosphere and to examine the effects of varying the number of samples sintered at once and the flow rate of the sintering gas. HA was found to decompose slightly when sintered in CO/H/W(ice), possibly because it was more dense than the composite samples and thus water was not accessible to its interior. The 5nf material gave similar results to the 5f material. No difference in properties was found when sintering the different types of material together, although it did appear that greater CNT loss may have occurred in the 5f samples compared with the 5nf samples, perhaps because the fCNTs oxidise at lower temperatures. Increasing the number of samples and the flow rate resulted in a higher loading of CNTs and phase pure samples which were well hydroxylated. However, this came at the expense of density, which was lower the more CNTs were present.

There is evidence that having at least a moderate vapour pressure of water throughout the experiment causes the formation of a white layer. In the case of an atmosphere like CO/H/W(ice), it seems possible that the material mostly dehydroxylates during the heating stage of sintering and rehydroxylates from water formed from the atmosphere in the reaction between H<sub>2</sub> and CO during the cooling stage. If the material was not well densified by the time it reached the dwell temperature, then it may have still been possible to rehydroxylate it during the cooling stage. The new challenge then becomes balancing the loading of the reinforcing CNTs with porosity, which is detrimental to mechanical properties.

## **5 PRELIMINARY ASSESSMENT OF MECHANICAL PROPERTIES**

The addition of CNTs to an HA matrix has the potential to both strengthen and toughen HA, enabling it to be used in a wider range of biomedical applications. However, while CNTs are theoretically strong and stiff enough to accomplish this, many variables will determine whether or not this is experimentally practical. In particular, the HA-CNT interaction must be controlled and the microstructure of the material must be optimised to permit strengthening and toughening.

This chapter details preliminary studies of the mechanical behaviour of the HA-CNT composites developed in this work. The microstructure of the material was optimised for properties related to mechanical behaviour by adjusting the time–temperature sintering profile of the composite. Tensile strength was measured by diametral compression, hardness was measured by Vickers indentation, toughening potential was evaluated by indentation crack length, and the fracture surfaces were examined by SEM. A range of CNT loadings from 0.5 – 5 wt.% was used and composites with both as-made CNTs (nfCNTs) and functionalised CNTs (fCNTs) were tested.

### ***5.1 Background***

#### **5.1.1 Properties influencing mechanical behaviour**

To achieve strengthening and toughening of brittle materials using CNTs, two main considerations must be addressed: 1) careful control of the interaction between the HA and CNTs and 2) optimisation of the microstructure of the material. With regards to the first aspect, the HA and CNTs must interact sufficiently for load to be transferred across the HA-CNT interface. On the other hand, the interaction cannot be too strong, so that it is still possible for energy to be absorbed in breaking fibre-matrix bonds through fibre pull-out. The critical fibre length,  $l_c$ , required for effective strengthening and toughening is related to the tensile strength,  $\sigma_t$ , of the fibre and the fibre-matrix interfacial bond strength,  $\tau$ , by:

$$l_c = \frac{\sigma_t d}{2\tau}$$

where  $d$  is the fibre diameter (Hull 1981). Thus, for fibres with high aspect ratios, like CNTs, a large tensile strength to bond strength ratio is required for reinforcement.

Microstructural characteristics, such as porosity and grain size, will also have an effect on mechanical properties. According to Juang *et al.* (1996), for ceramics above 95% theoretical density, grain size is the dominant factor affecting the fracture strength of HA. The Hall-Petch equation relates fracture strength to grain size by the following equation:

$$\sigma_f = \sigma_0 + kd^{-\frac{1}{2}}$$

where  $\sigma_f$  is the fracture strength,  $\sigma_0$  is the strength at which dislocation motion begins,  $k$  is a material constant, and  $d$  is the grain size. Thus, strength increases with decreasing grain size. Below 95% density, Juang *et al.* report that porosity is the dominant factor, and can be related to strength by the Ryshkewitch-Duckworth equation (Duckworth 1953):

$$\sigma_f = \sigma_0 \cdot e^{-bp}$$

where  $\sigma_f$  is the fracture strength,  $\sigma_0$  is the fracture strength at zero porosity,  $b$  is a material constant, and  $p$  is the amount of porosity. This relationship predicts an increase in strength as porosity decreases.

Additionally, the location of the CNTs in the matrix will play a role in determining strength. Firstly, how well the CNTs are dispersed will affect the mechanical properties. A poor dispersion will result in clumps of CNTs that may act as defects rather than reinforcements, while a good dispersion will optimise the interfacial area available for HA-CNT interaction. Also, whether they are located between grains or within grains may affect the properties.

Other factors to consider in how well CNTs may reinforce a brittle material are the differences in the coefficients of thermal expansion between the matrix and CNT, the type of CNT, and the quality of the CNTs. The coefficient of thermal expansion for HA is

approximately  $12 - 17 \times 10^{-6} \text{ }^\circ\text{C}^{-1}$  (Fischer *et al.* 1983; Perdok *et al.* 1987; Babushkin *et al.* 1994), while that of CNTs is much lower ( $-0.5 - 4 \times 10^{-6} \text{ }^\circ\text{C}^{-1}$  for SWNTs (Jiang *et al.* 2004)). During heat treatment, this will place tensile stresses on the matrix, which may cause microcracking. The type of CNT (MWNT vs. SWNT) may affect the mechanical properties, as MWNTs have a much larger diameter than SWNTs, a lower interfacial area, and it is likely that only the outer-most layer of the MWNT will be loaded (Zhan *et al.* 2003). Finally, after processing and heat treatment, the quality of the CNTs may be lowered, which will make them less able to withstand high stresses and resist crack propagation.

### **5.1.2 Measurement techniques for fracture strength and toughness**

Several methods for measuring tensile strength and toughness are commonly used for brittle materials. In place of a tensile test (pulling a specimen apart), brittle materials, like HA, may instead be tested by a variety of bending tests, the most common of which are the three- and four-point bending tests. These tests involve bending a rod of circular or rectangular cross section between either three or four contact points. Careful preparation of specimens is important for this test, as any surface flaws may induce premature failure.

The diametral compression test is an alternative technique which does not require any special material preparation in most cases, as failure tends to initiate in the interior of the sample rather than on the surface. It involves placing a disc on its edge and compressing it between two metal plates. Despite the sample being compressed, failure results from tensile stresses, and so can be used to determine tensile strength.

Such a wide range of measurement techniques also results in a range of mechanical property values. For instance, Driessen *et al.* (1982) tested sintered  $\beta$ -TCP and found that diametral compression testing gave only 30% of the fracture strength value of a three-point bending test, while Ovri and Davies (1987) tested silicon nitride and found that diametral compression gave 40% of the value of a three-point bend test. The discrepancy between methods was attributed to a volume effect, as a higher volume of material (with a higher probability of containing more flaws) is subjected to a tensile load in the diametral compression test compared with the three-point bend test.

Toughness may also be evaluated by a number of different techniques. Some of the more popular are the single-edge notched beam, the Chevron notched beam, and the single-edge V-notched beam. These are carried out in a similar fashion to bending tests, but with a sharp notch of known length placed first in the sample. Like bending tests for strength, surface preparation is important; additionally, the notch geometry must be carefully controlled. A much simpler test involves measuring toughness through crack propagation from a hardness indentation. The length of the cracks emanating from the indentation is indirectly proportional to the toughness of the material. Care should be taken in interpreting toughness values obtained by this method, however, as the values may only be known to  $\pm\sim 50\%$  due to inherent uncertainties involved in determining the calibration coefficient included in the toughness calculation (Kruzic *et al.* 2009). Thus, when comparing materials, a factor of at least 3 is generally needed between values to consider the differences significant. Despite the uncertainty in toughness values obtained by this method, it is easy to obtain a large number of measurements with this technique and it is widely used, particularly for bioceramics. As with tensile testing techniques, variations in toughness testing techniques will also produce variations in measured toughness values.

Due to the statistical nature of failure in brittle ceramics, large numbers of measurements are necessary to obtain accurate values of mechanical properties. Thus, simple tests which can provide a large amount of data for analysis are generally preferred. For this reason, diametral compression was chosen for measuring tensile strength for this study, as specimen geometries are easy to prepare and sample surfaces do not require special preparation. The indentation method was chosen to evaluate toughness, as it requires little sample preparation and provides quick and simple toughness values which are suitable for comparing the behaviour of similar batches of material.

### **5.1.3 Theory of mechanical testing techniques used**

#### **5.1.3.1 Diametral compression**

The diametral compression, or Brazilian disc, test offers a means of testing the tensile strength of brittle materials. Developed independently by both Carniero and Bracellos (1953) and Akazawa (1953), it involves compressing a right circular disc between two flat plates. A biaxial stress state is induced, with a tensile load perpendicular to the loaded

diameter. As fracture tends to initiate internally, careful preparation of the sample surface is not needed. This testing method also avoids complications that would be involved in trying to grip a ceramic material to pull it apart. The tensile strength can be calculated as:

$$\sigma_t = \frac{2P}{\pi Dt}$$

where  $\sigma_t$  is the tensile strength,  $P$  is the load at fracture,  $D$  is the disc's diameter, and  $t$  is its thickness. Since the stresses induced in this test are similar to those experienced by dental and other biomedical implants, this method is particularly appropriate for testing biomaterials, like HA (Thomas *et al.* 1980).

Three modes of failure are typically observed when using this testing method (Thomas *et al.* 1980). When the sample experiences excessively high stresses at the loading lines, it may fail by shear or shatter into many pieces. As this type of failure is not tensile, the strength values of materials which fail in this manner should be discarded. The samples may also fail by tensile mode, in which the sample splits vertically down the centre, or by 'triple-cleft' mode, in which the sample splits symmetrically about the loaded diameter into either three or four pieces (see Figure 5.1). Triple-cleft fractures are induced by secondary fracture after the initial tensile-mode fracture. As both tensile and triple-cleft modes are indicative of tensile failure, the values obtained may be considered tensile strengths.

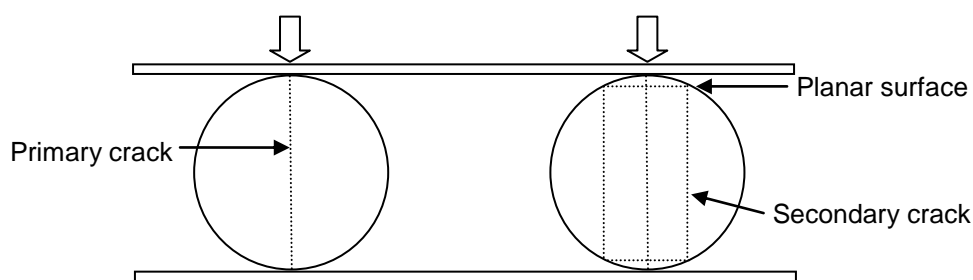


Figure 5.1: Schematic of tensile failures. Tensile mode (left) and triple-cleft mode (right). After Ovri and Davies (1987).

In order to reduce shear failure resulting from point loading, two techniques may be used. The first is to use packing strips, or shims, to distribute the load over a controlled volume. Thin sheets of metal, such as copper, have been found effective in giving reproducible

tensile-mode results (Thomas *et al.* 1980; Ovri *et al.* 1987). A second method, studied by Fahad (1996), involves grinding opposite edges of the sample flat. This work found that for a flat length  $<0.2D$ , the tensile strength value obtained should be accurate.

A volume effect has been noted when using the diametral compression test. Fahad (1996) found that plaster of Paris discs 50 mm in diameter had 87% of the tensile strength of discs 40 mm in diameter and the same thickness. This discrepancy was attributed to a larger volume giving a higher probability of the presence of fracture-inducing flaws. So, just as different measurement techniques may tend to give higher or lower strength values, depending on the volume of material stressed in the technique, sample size differences using the same technique may also yield different values.

### 5.1.3.2 Toughness by indentation

During loading and unloading of a Vickers, or pyramidal, indentation, a penny-shaped crack forms at a critical load. This crack may then expand towards the sample surface, resulting in perpendicular cracks extending out from the corners of the indentation (see Figure 5.2). Additional, lateral, cracks may also form which, given sufficient load, may extend upwards to the sample surface resulting in chipping.

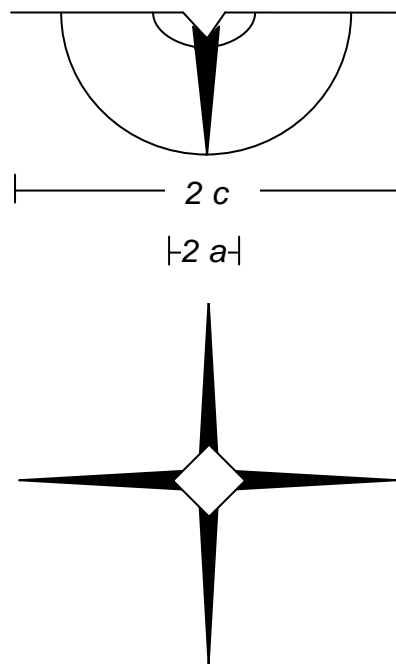


Figure 5.2: Schematic of Vickers-induced indentation fractures. Section view (above) and top view (below). After Antis *et al.* (1981).

The crack length from these indentations was first related to fracture toughness by Palmqvist (1962). Since then, many equations have been developed to calculate the fracture toughness,  $K_c$ , based on the crack length  $c$ . One of the more common relationships is:

$$K_c = \chi \left( \frac{E}{H} \right)^{1/2} \frac{P}{c^{3/2}}$$

where  $E$  is the Young's modulus,  $H$  is the Vickers hardness, and  $\chi$  is a calibration constant (Antis *et al.* 1981).

### 5.1.3.3 Weibull statistics

As the fracture strength of a brittle material is statistical in nature, analysis of the distribution of strength values provides a better understanding of the mechanical behaviour of the material than simply a mean strength value. The Weibull modulus is commonly used as a measure of the distribution of strength values for a brittle material. It is based on Griffith theory, which predicts that brittle fracture will be initiated at the most serious flaw or the 'weakest link.' The probability  $P_s$  that a material with volume  $V$  will survive an applied stress  $\sigma$  is given by:

$$P_s(V) = \exp\left(-V \left[\frac{\sigma}{\sigma_0}\right]^m\right)$$

where  $m$  is the Weibull modulus and  $\sigma_0$  is a normalising parameter. The modulus value reflects the variability in strength, with lower values indicating a wide scatter of fracture stresses and higher values indicating a narrow distribution. Brittle ceramics typically have modulus values ranging from 5 – 25 (Warren 1992). By taking the natural logarithm of this equation twice, the following is obtained:

$$\ln \ln \left( \frac{1}{P_s} \right) = \ln V + m \ln \sigma - m \ln \sigma_0$$

By plotting  $\ln \ln (1/P_s)$  vs.  $\ln \sigma$ , then the slope of the best-fit line is the Weibull modulus,  $m$ .

There are several formulas for estimating the values of  $P_s$ , of which one of the more popular is the ‘median-ranked position’, calculated as:

$$P_s(i) = 1 - \frac{i - 0.3}{n + 0.4}$$

where  $n$  is the number of measurements and  $i$  is the rank of the measurement (Benard *et al.* 1953).

## 5.2 Methods

### 5.2.1 Optimisation of sintering profile

Tablets were sintered using six different sintering time-temperature profiles to determine which yielded the optimal combination of properties, based on low porosity and grain size, along with phase purity and good hydroxylation. Composites containing 2 wt.% CNTs were used for this study to give an intermediate estimate of how CNTs might affect the final sintered properties of the composite materials over a CNT loading range of 0.5 – 5 wt.%.

#### 5.2.1.1 Experimental methods

Three 0.8 g tablets of each material type (HA, 2 wt.% nfCNT composite (2nf), and 2 wt.% fCNT composite (2f)) were sintered in one batch for each of six sintering profiles. The sintering profiles used (dwell temperature and time) were: 1) 1100°C, 3 hours; 2) 1150°C, 2 hours; 3) 1150°C, 3 hours; 4) 1200°C, 15 min.; 5) 1200°C, 1 hour; and 6) 1200°C, 2 hours. The heating and cooling rate for all profiles was 5°C min<sup>-1</sup>.

Samples were sintered using the CO + H<sub>2</sub> + H<sub>2</sub>O (ice) atmosphere as described in Section 4.3.1, with a flow rate of 0.35 L min<sup>-1</sup>. This flow rate was chosen based on scaling down a flow rate of 1.2 L min<sup>-1</sup> to account for the mass of CNTs that would be in the furnace for one batch in this experiment compared with the mass of CNTs that would be used in next part of the experiment to sinter samples for mechanical testing.

### **5.2.1.2 Characterisation methods**

For each of the sintered tablets, the density, phase purity, and hydroxylation were measured, as described in Section 3.2.1. One tablet of each type from each sintering profile was measured to determine CNT loading, as described in Section 3.2.1.5.

The microstructure of each material type for all sintering profiles was examined using SEM. Approximately 1 mm was ground from the surface of each tablet before polishing to 3  $\mu\text{m}$ . Samples were etched with 5% orthophosphoric acid for 10 seconds to reveal grain boundaries. In the case of more dense samples, the grain size was measured by the linear intercept method, drawing horizontal and vertical lines across micrographs and counting  $\sim 100$  grains.

## **5.2.2 Mechanical testing**

### **5.2.2.1 Sample production**

Tablets of 0.8 g each were produced of HA, composites with nfcCNTs (loadings of 0.5, 1, 2 and 5 wt.%), and composites with fcCNTs (0.5, 1, 2 and 5 wt.%). Samples were pressed at varying pressures to give green densities of  $\sim 45\%$ . All composite tablets were sintered in  $\text{CO} + \text{H}_2 + \text{H}_2\text{O}$  (ice) at  $1200^\circ\text{C}$  for 1 hour, with a ramp rate of  $5^\circ\text{C min}^{-1}$  and a flow rate of  $1.2 \text{ L min}^{-1}$ . Five tablets of each of the four loadings of one composite type were sintered together, for a total of 20 samples in each batch. HA tablets were sintered with the same sintering profile, but in  $\text{Ar} + \text{H}_2\text{O}$  and a flow rate of  $0.8 \text{ L min}^{-1}$ , as this atmosphere was found in Chapter 4 to result in less decomposition and dehydroxylation of the HA compared with  $\text{CO} + \text{H}_2 + \text{H}_2\text{O}$  (ice). Ten HA samples were sintered in each batch.

### **5.2.2.2 Sample characterisation**

Each sintered tablet was measured to determine density, and one sample of each loading from each batch was used to determine CNT loading.

### 5.2.2.3 Tensile strength

Tensile strength was measured by diametral compression. Opposite edges of the tablet samples were ground flat to a length of  $\sim 0.2x$  the tablet diameter. The tablets were tested in an Instron Tensile Tester using a crosshead speed of  $0.2 \text{ mm min}^{-1}$ . The tensile strength was calculated from the failure load using the equation from Section 5.1.3.1. Measurements were considered valid when the samples failed in tensile or triple cleft mode. The tensile strengths reported are mean values  $\pm$  standard deviation of 10 measurements for each sample type.

### 5.2.2.4 Indentation measurements

Two specimens of each sample type and loading were used for indentation measurements. Sample surfaces were ground and polished to  $6 \mu\text{m}$  using diamond paste. Vickers microhardness indentations were made with a Mitutoyo MVK-H2 Hardness Testing Machine using a load of 1 kgf (unless otherwise specified) and a duration of 10 seconds. The indentation dimensions were measured to obtain hardness values, which are reported as mean values  $\pm$  standard deviation of 10 measurements for each sample type. Hardness measurements were rejected when the indentation was asymmetrical.

Indentations were then examined under an optical microscope to observe cracks emanating from the indentation corners. The diagonal crack length was measured to give an indication of toughness. Crack lengths were averaged for one sample, and that value was then averaged over five samples to give a mean value  $\pm$  standard deviation. The measurements were considered valid only when secondary cracking and spalling around the hardness indentation were not observed.

### 5.2.2.5 Observation of fracture surfaces and toughening mechanisms

Fracture surfaces from diametrically compressed samples were examined in SEM to observe any differences in fracture mechanisms or evidence of toughening mechanisms. Ground powder from selected samples was also examined in TEM to look for any evidence of HA-CNT interaction.

## **5.3 Results**

### **5.3.1 Optimisation of sintering profile**

The characterisation results of the six time-temperature profiles investigated are shown in Table 5.1 and comprise the CNT loading and loss, phase purity, hydroxylation, and density for each sample type.

#### ***5.3.1.1 Effect of sintering profile on CNT loading and density***

The CNT loading was similar in most of the samples, yielding CNT losses ranging from 71 – 77%. The exceptions to this were 2nf sintered at 1100°C for 3 hours (0.75 wt.%, 58% loss) and the two composite samples sintered at 1150°C for 3 hours (2nf = 0.78 wt.%, 56% loss; 2f = 0.88 wt.%, 58% loss).

Figure 5.3 compares the sintered densities of the three materials for the six sintering profiles. For all sample types, the best density was found at a sintering temperature of 1200°C for 1 hour (HA = 93.8%, 2nf = 89.8%, 2f = 93.4%). The density of HA increased with increasing sintering temperature and time until 1200°C for 1 hour; 1200°C for 2 hours resulted in a slightly lower density. The composite densities followed a similar trend, with the exception of the three samples which had significantly higher loadings and lower CNT losses compared with the other samples.

Table 5.1: Results of the sintering profile optimisation study.

Sintering Profile	Material	CNT Loading (wt.%)	CNT Loss	XRD	FTIR	Sintered Density (% TD)
1100°C, 3 hours	HA	---	---	HA (92%), $\beta$ (8%)	Complete OH loss	81.6 $\pm$ 0.4
	2nf	0.75 $\pm$ 0.04	58%	HA (95%), $\beta$ (5%)	Excellent OH retention	79.8 $\pm$ 0.6
	2f	0.48 $\pm$ 0.02	77%	HA (97%), $\beta$ (3%)	Excellent OH retention	84.9 $\pm$ 0.9
1150°C, 2 hours	HA	---	---	HA (95%), $\beta$ (5%)	Complete OH loss	89.6 $\pm$ 0.4
	2nf	0.52 $\pm$ 0.03	71%	HA (98%), $\beta$ (2%)	Good OH retention	88.2 $\pm$ 0.6
	2f	0.53 $\pm$ 0.03	75%	HA (99%), $\beta$ (1%)	Significant OH loss	91.2 $\pm$ 0.4
1150°C, 3 hours	HA	---	---	HA (95%), $\beta$ (5%)	Complete OH loss	89.7 $\pm$ 0.4
	2nf	0.78 $\pm$ 0.04	56%	HA	Good OH retention	86.3 $\pm$ 0.2
	2f	0.88 $\pm$ 0.04	58%	HA	Significant OH loss	88.8 $\pm$ 0.3
1200°C, 15 min.	HA	---	---	HA (93%), $\beta$ (7%)	Complete OH loss	91.5 $\pm$ 0.5
	2nf	0.47 $\pm$ 0.02	74%	HA	Good OH retention	88.2 $\pm$ 0.4
	2f	0.54 $\pm$ 0.03	74%	HA	Significant OH loss	90.8 $\pm$ 0.5
1200°C, 1 hour	HA	---	---	HA (90%), $\beta$ (10%)	Complete OH loss	93.8 $\pm$ 0.5
	2nf	0.48 $\pm$ 0.02	73%	HA	Slight OH loss	89.8 $\pm$ 0.4
	2f	0.58 $\pm$ 0.03	73%	HA	Significant OH loss	93.4 $\pm$ 0.4
1200°C, 2 hours	HA	---	---	HA (85%), $\beta$ (15%)	Complete OH loss	92.8 $\pm$ 0.1
	2nf	0.44 $\pm$ 0.02	75%	HA	Slight OH loss	88.1 $\pm$ 0.1
	2f	0.62 $\pm$ 0.03	71%	HA	Significant OH loss	89.7 $\pm$ 0.3

$\beta$  =  $\beta$ -TCP; TD = theoretical density

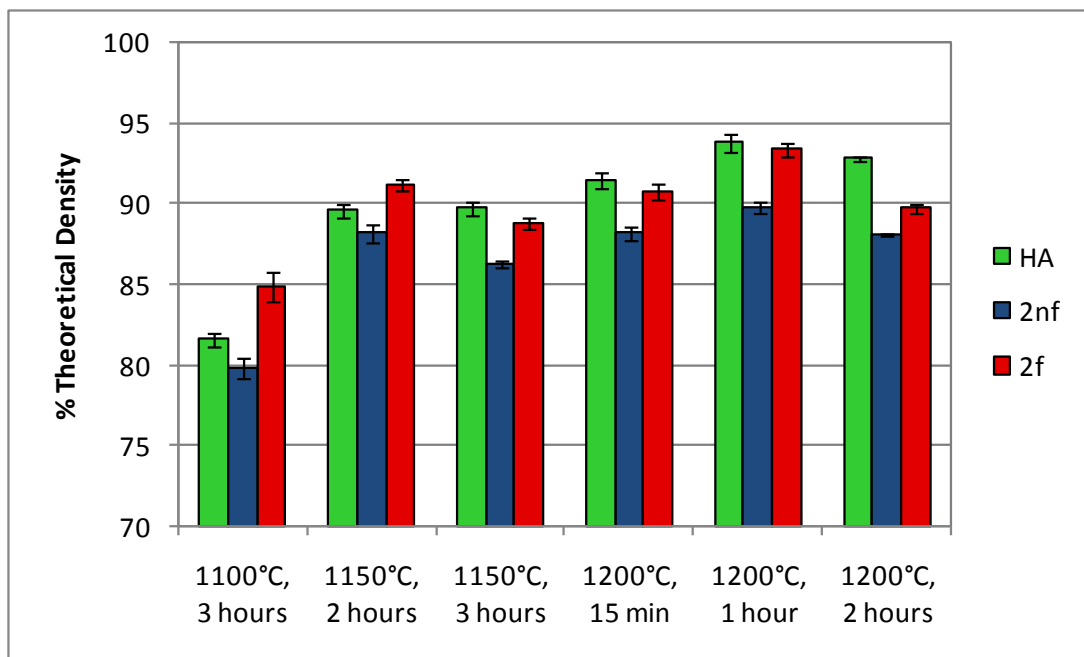


Figure 5.3: Comparison of percent theoretical densities for different materials over a range of sintering times and temperatures.

### 5.3.1.2 Effect of sintering profile on microstructure

The grain size of the samples was found to vary considerably for the different sintering profiles as well as between sample types. The grain structures of the 2nf composites for all six sintering profiles are shown in Figure 5.4. Sintering temperature had the greatest influence on the grain sizes, with higher temperatures yielding larger grain sizes. Sintering time at 1200°C did not appear to have a significant effect on the grain size, which was ~800 nm for all 2nf samples sintered at 1200°C. The microstructure at 1100°C shows a porous material with smaller grains ~400 nm in size. The samples sintered at 1150°C had intermediate grain sizes, although, unlike the samples sintered at 1200°C which all had similar grain sizes, the grain size of the samples sintered for 3 hours was smaller than those sintered for 2 hours.

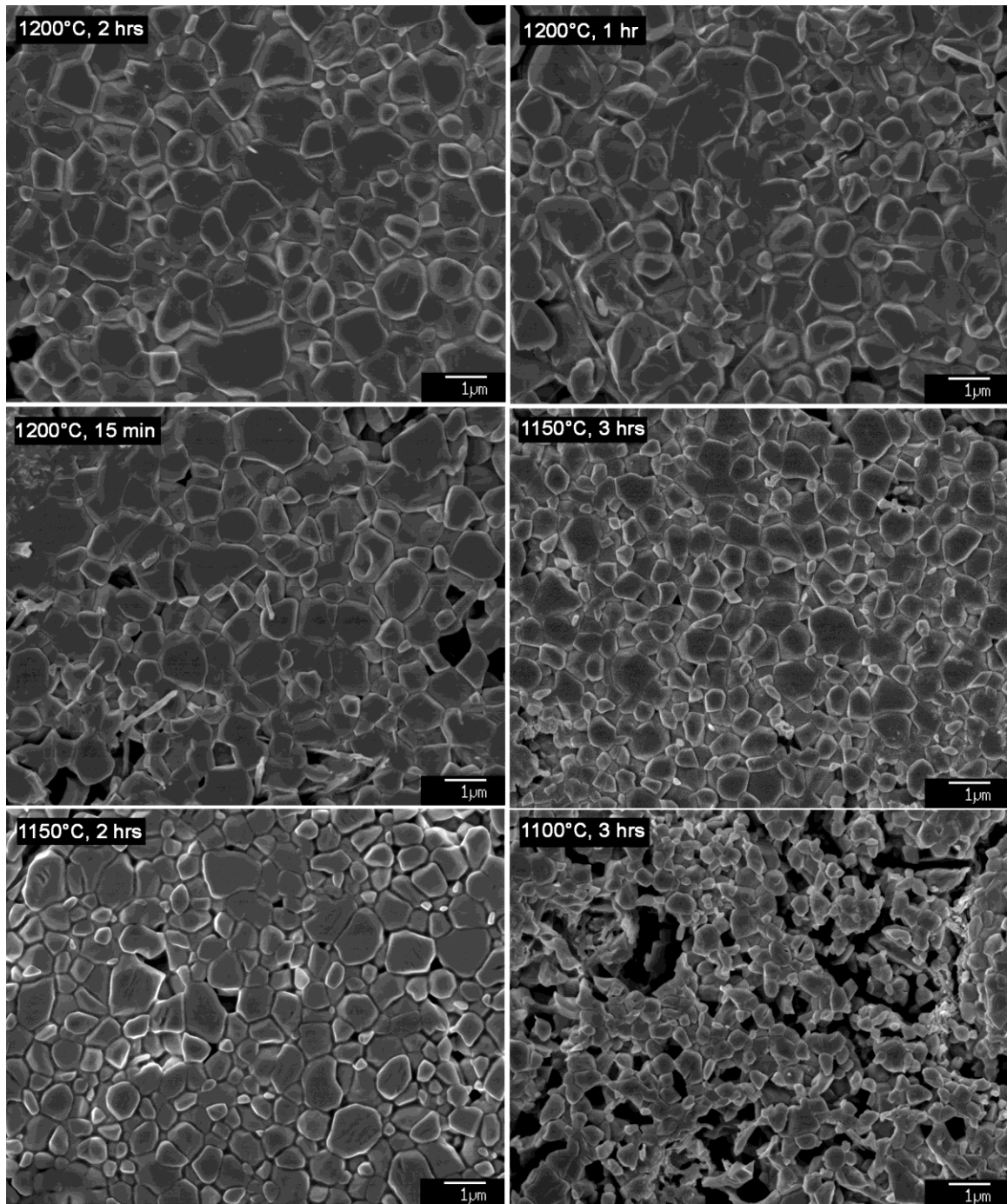


Figure 5.4: Microstructures of 2nf composites for different sintering profiles.

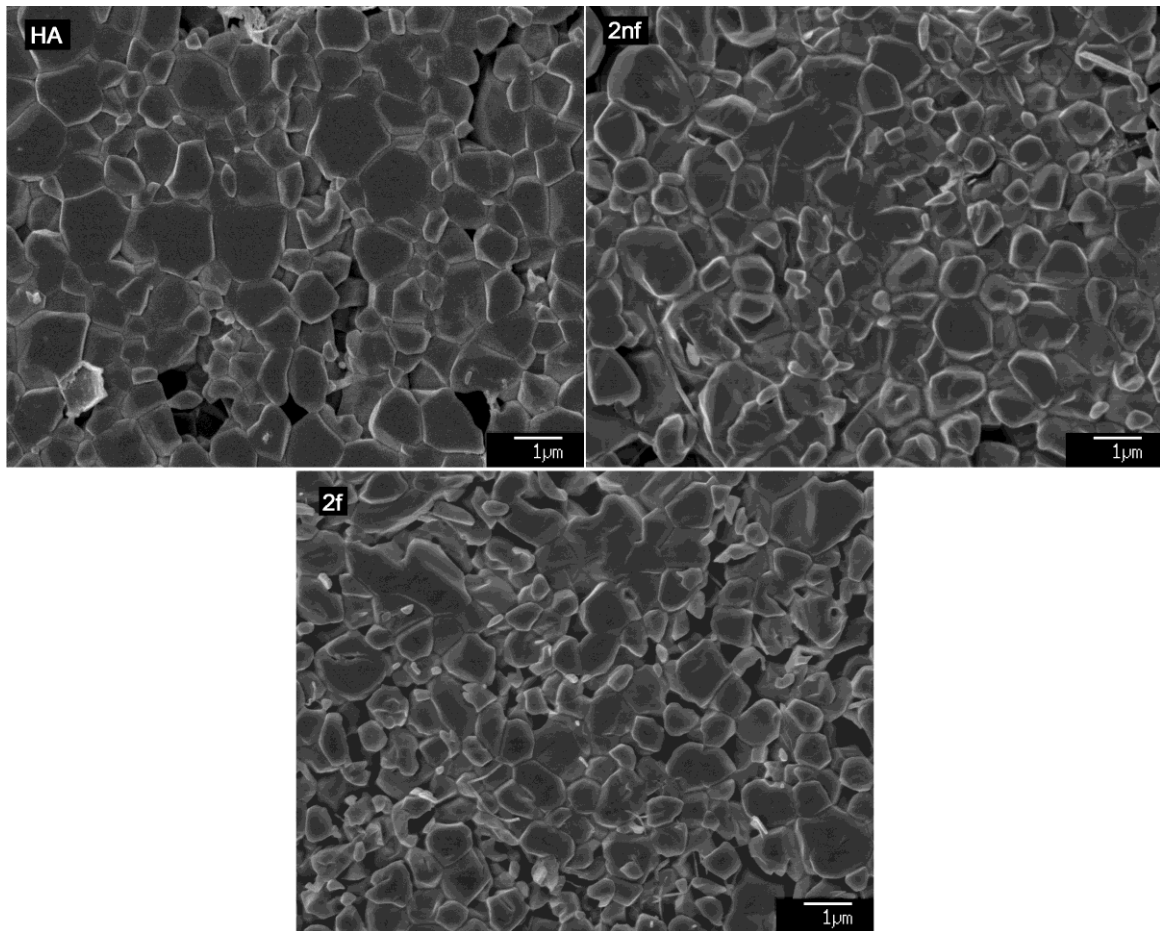


Figure 5.5: Microstructures of materials sintered at 1200°C for 1 hour.

Figure 5.5 compares the microstructures of the three materials sintered at 1200°C for 1 hour. The grain sizes of these samples were measured, and it was found that HA had an average grain size of  $860 \pm 120$  nm, 2nf had a grain size of  $780 \pm 200$ , and 2f had a grain size of  $690 \pm 180$ . While the variation in grain size was large, the presence of CNTs seemed to inhibit grain growth to some extent.

### 5.3.1.3 Choice of sintering profile

In choosing the optimal sintering profile, the two characteristics considered were grain size and porosity, as CNT loading, phase purity, and hydroxylation (particularly for the composites) was similar in most cases. The highest density (and thus lowest porosity) resulted from a sintering temperature of 1200°C for 1 hour. While the grain size was larger at 1200°C than at other temperatures, the additional porosity in the samples would

likely be detrimental to the mechanical properties. Juang *et al.* (1996) reported that above 95% density, grain size is the determining characteristic for mechanical properties, while below 95% density, porosity is dominant. Thus, the optimal profile was chosen as 1200°C for 1 hour.

### 5.3.2 Mechanical testing

The results of the material characterisation, including sintered density and CNT loading / loss, and mechanical testing, including tensile strength, Weibull moduli for the strength values, hardness, and indentation crack length are presented in Table 5.2.

Table 5.2: Summary of mechanical testing data.

Material	Sintered Density (% TD)	CNT Loading (wt.%)	CNT Loss	Tensile Strength (MPa)	Weibull Modulus	Hardness (H <sub>v</sub> )	Crack Length (µm)
HA	91.7 ± 0.8	---	---	28 ± 5	5.6	380 ± 30	163 ± 6
0.5nf	93.5 ± 0.3	0.32 ± 0.04	36%	29 ± 6	5.0	450 ± 40	151 ± 8
1nf	94.8 ± 0.5	0.51 ± 0.08	49%	25 ± 7	3.9	480 ± 60	NM
2nf	89.2 ± 0.6	0.65 ± 0.15	68%	29 ± 6	4.9	290 ± 50	NM
5nf	85.8 ± 1.2	1.3 ± 0.3	74%	21 ± 4	5.8	320 ± 50*	NM
0.5f	92.2 ± 1.4	0.33 ± 0.04	34%	19 ± 7	3.1	470 ± 30*	NM
1f	93.6 ± 1.2	0.67 ± 0.05	33%	23 ± 4	5.0	430 ± 30	165 ± 21
2f	87.8 ± 1.5	0.91 ± 0.08	55%	28 ± 5	6.3	300 ± 20	144 ± 26
5f	74.2 ± 1.6	2.5 ± 0.4	50%	14 ± 4	3.5	110 ± 30*	NM

'NM' indicates the crack length could not be measured. \*These hardnesses were measured with an indentation load of 500 gf rather than 1 kgf as for the other measurements.

### 5.3.2.1 Density and CNT loading

The relationship between the density and CNT loading of the samples following sintering is shown in Figure 5.6. From 0 wt.% to 0.51 wt.% (for nfCNT composite) and from 0 wt.% to 0.67 wt.% (for fCNT composite) there is a trend of increasing density with CNT loading. Past this point, an increase in CNT loading corresponds to a decrease in density.

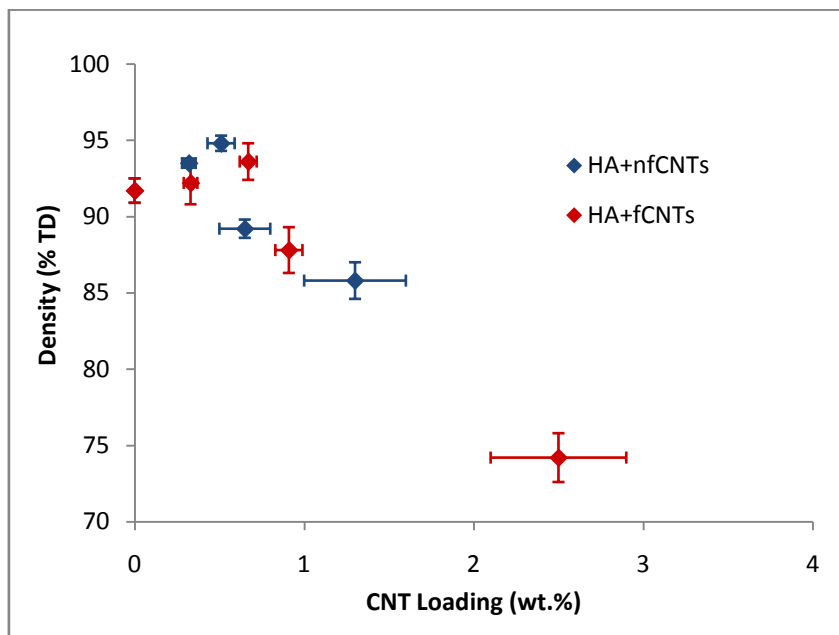


Figure 5.6: Relationship between density and CNT loading.

### 5.3.2.2 Tensile strength and CNT loading

Most samples were found to fail in triple cleft mode, while some failed in tensile mode and a few in shear mode (these were rejected). Figure 5.7 shows examples of the various failure modes.



Figure 5.7: Examples of failure modes for diametral compression specimens: shear (left), tensile (middle), triple cleft (right).

The relationship between tensile strength and CNT loading is shown in Figure 5.8. The data show no significant difference between most of the tensile strength values, regardless of CNT loading. While the mean values differed among the samples, the standard deviations were so large that there was no obvious trend in strength values. This was especially true of the nfCNT composites, which had a smaller range of CNT loadings and densities compared with the fCNT composites. The 5f composite, which had the lowest density (74.2%) and highest CNT loading (2.5 wt.%), was the only material whose data produced error bars which did not overlap with all of the samples.

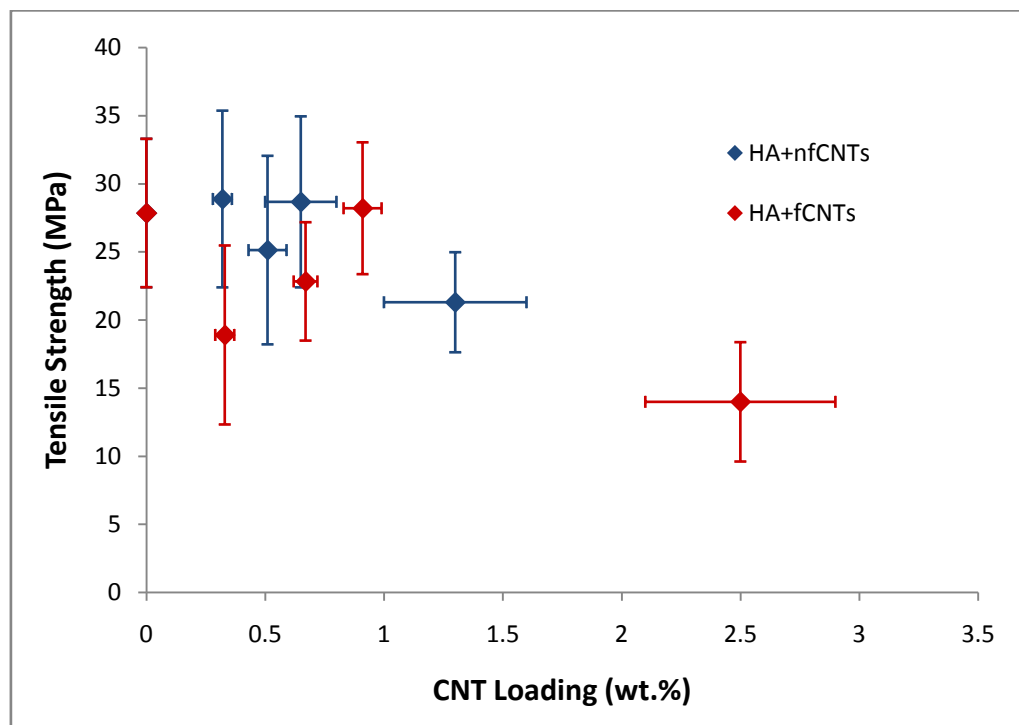


Figure 5.8: Relationship between tensile strength and CNT loading.

### 5.3.2.3 Weibull modulus calculations

The Weibull moduli calculated based on the diametral compression fracture strength measurements ranged from 3.1 for the 0.5f composite to 6.3 for the 2f composite. Some sample Weibull plots are shown in Figure 5.9. As the sample size ( $n=10$ ) from which the Weibull moduli were calculated was small, it is difficult to make accurate comparisons between moduli. However, all Weibull modulus values suggest a wide distribution of flaws in the materials, and suggest very brittle materials, as the typical range for brittle

materials is 5 -25. HA is particularly brittle, however, and these typical modulus values are more characteristic of engineering ceramics.

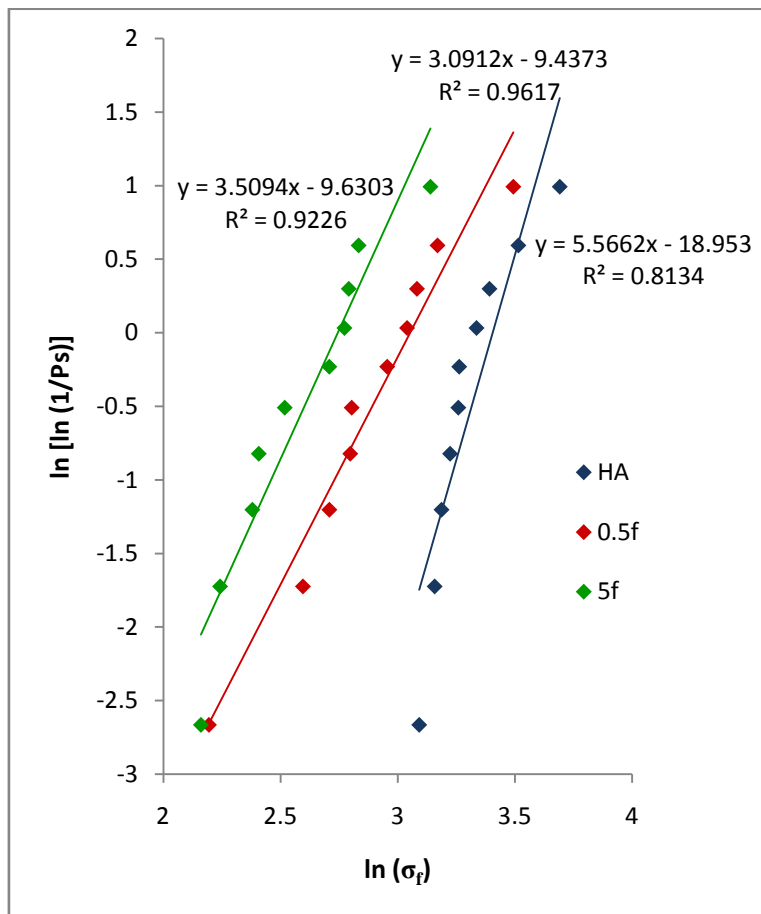


Figure 5.9: Sample Weibull modulus plots.

### 5.3.2.4 Hardness

While the tensile strength values did not show any obvious trends relating to CNT loading or density, due to large standard deviations, the hardness values showed a clearer relationship to other properties. As in the density vs. CNT loading data, the mean hardness increased with CNT loading from a value of 380 H<sub>V</sub> for HA to 480 H<sub>V</sub> for the nfCNT composite containing 0.51 wt.% CNTs, as shown in Figure 5.10. The fCNT composite peaks at a mean value of 470 H<sub>V</sub> for the composite containing 0.33 wt.% CNTs. At loadings above these points, the hardness decreases sharply. There was no significant difference between the two highest CNT loading materials for the nfCNT

composites. The fCNT composite, on the other hand, contained twice the amount of CNTs at its highest loading, and gave a hardness of just 110 H<sub>V</sub>, which was well below that of any other sample.

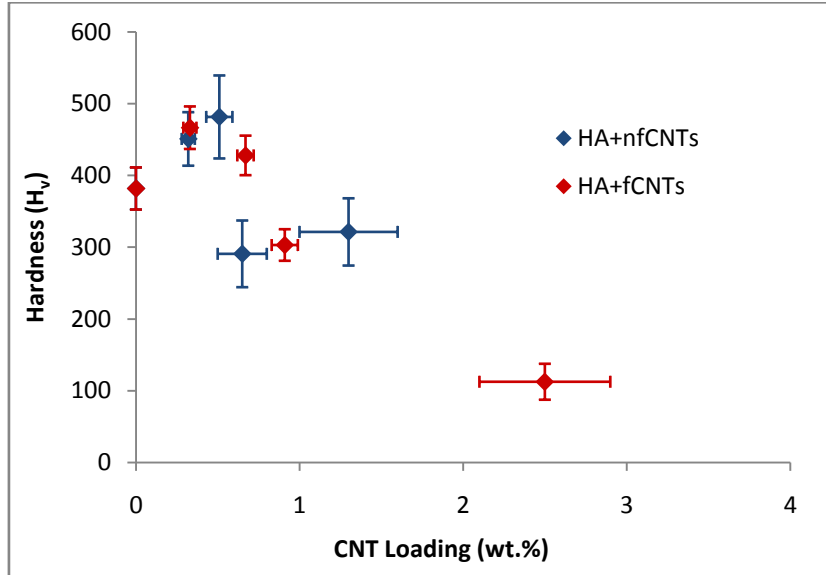


Figure 5.10: Relationship between hardness and CNT loading.

A plot of hardness vs. density shows that the two properties are correlated, with an R<sup>2</sup> value of 0.9022. Hardness increases as density increases and porosity decreases.

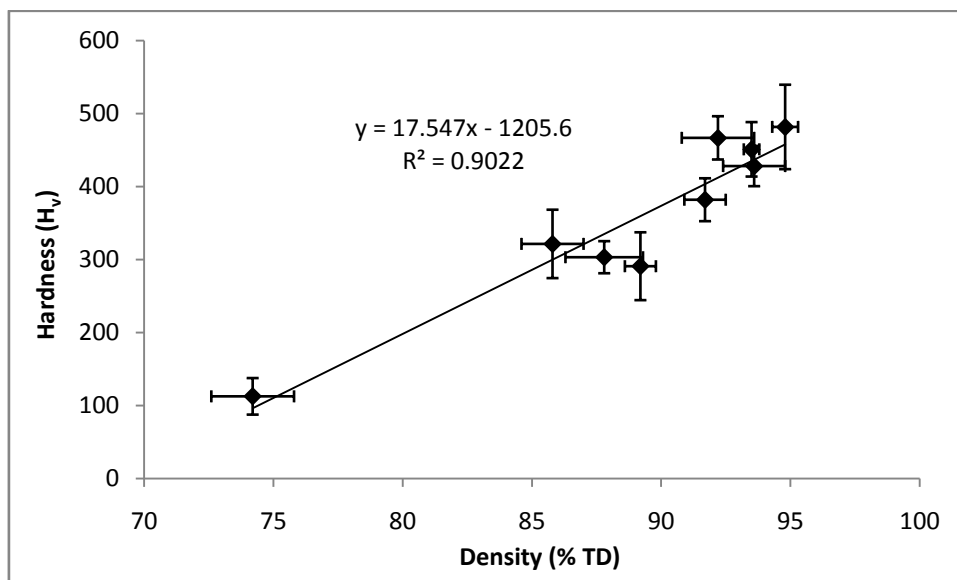


Figure 5.11: Relationship between hardness and density.

### 5.3.2.5 Evidence of toughening from crack length

The measured values of crack length emanating from Vickers microhardness indentations are shown in Table 5.2. For the majority of samples, however, no value could be obtained due either to a large amount of porosity preventing crack propagation or making it difficult to see, or due to large amounts of spalling around the indentation, making the values indeterminable and/or unreliable. The four mean values which were obtained were similar. The mean value of the 2f composite was lower than that of the other three values, but the standard deviation was large.

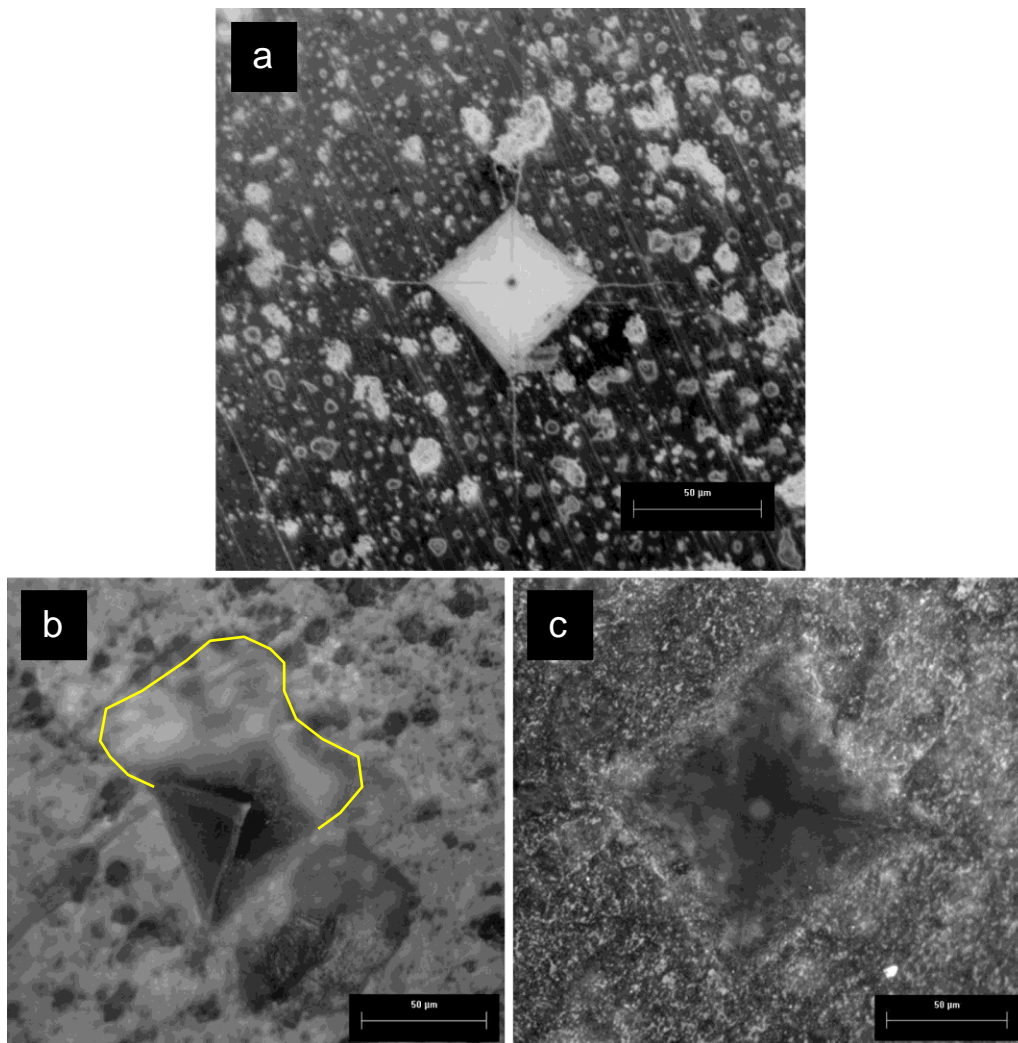


Figure 5.12: Hardness indentations on (a) 1f - showing cracks emanating from the indentation, b) 0.5f - showing spalling around the indentation (yellow), c) 5f - showing crack length difficult to determine. Scale bars = 50 µm.

### **5.3.3 Fracture surfaces**

The fracture surfaces of the composite materials are shown in Figure 5.13. HA's fracture surface was similar in appearance to the 0.5nf and 0.5f samples. The 0.5 wt.% and 1 wt.% composite samples all appeared to have a homogeneous dispersion of CNTs in the matrix. The 2 wt.% composites, on the other hand showed some inhomogeneities, with 2nf having fewer larger CNT clumps compared with the 2f material. The 5 wt.% materials had very different distributions of CNTs. The CNTs in the 5nf material seemed to clump in long, thin lines, forming crevices in the microstructure. The 5f material, on the other hand, did contain some small clumps of CNTs, but for the most part the dispersion was fairly homogeneous.

Differences in porosity could also be observed in the fracture surface micrographs. Most sample surfaces were fairly smooth, which is characteristic of transgranular fracture, with isolated areas of porosity which tended to be distributed with the same characteristic shape (marked in yellow). The 1 wt.% composites had slightly less porosity compared with the 0.5 wt.% composites. The 2 wt.% and 5 wt.% composite samples had a larger amount of porosity, as evidenced in the micrographs. The 5f sample, which had by far the lowest density (74%), displayed a very different microstructure from the other materials. No regions of relatively smooth surface were evident; the surface was instead very rough and homogeneously porous.

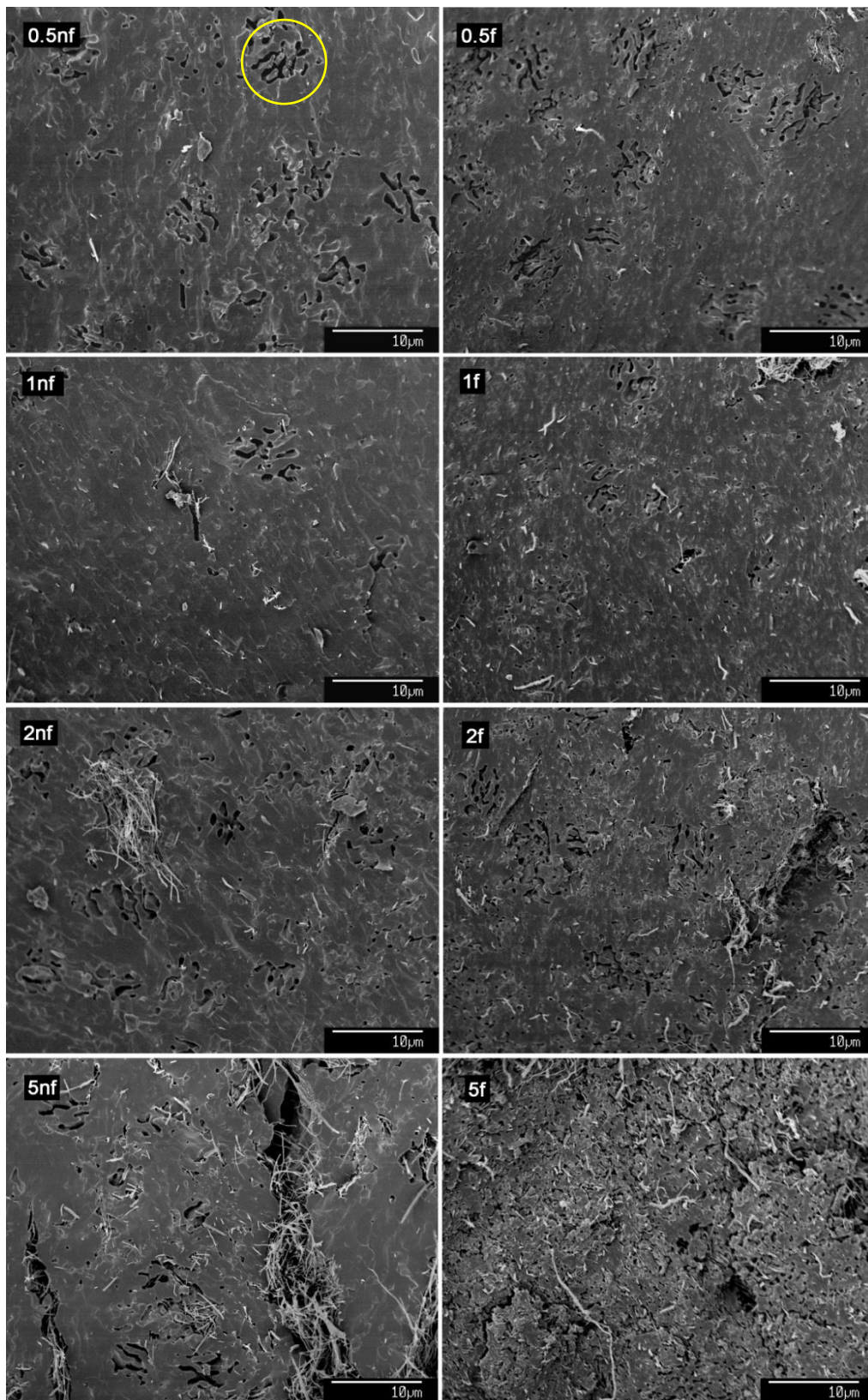


Figure 5.13: SEM images of fracture surfaces of composite materials. Characteristic porosity pattern is marked in yellow.

## 5.4 Discussion

### 5.4.1 Effect of sintering profile on phase purity and hydroxylation

As found in Chapter 4, HA consistently lost more OH groups compared with the composites and decomposed slightly when sintered in the CO + H<sub>2</sub> + H<sub>2</sub>O (ice) atmosphere. Some dependence of OH loss and phase purity on sintering time and temperature was found, with higher temperatures and longer sintering times tending to result in less hydroxylated and more decomposed HA. The composite samples followed a similar trend in hydroxylation compared to the HA samples, with increasing sintering time and longer sintering temperatures resulting in less hydroxylated materials. However, in all cases the composites were better hydroxylated than the HA. Small amounts of β-TCP were found in the composites at lower temperatures, but composites which were sintered at 1150°C for 3 hours and 1200°C for all times were purely HA.

It would appear, based on this data, that there was insufficient water in the heat treatment atmosphere to maintain HA's hydroxylation, and at higher temperatures and longer sintering times, this effect is enhanced. In Chapter 4, it was suggested that, since the HA was more dense than the composite samples, perhaps it underwent dehydroxylation and was then not able to rehydroxylate due to closed porosity forming in the samples. However, in the case of the profile 1200°C for 1 hour, the HA and 2f composites have the same density, yet HA has completely dehydroxylated and decomposed and 2f has not. This may indicate that the composite material has a higher affinity for the small amounts of water in the atmosphere, and so may preferentially adsorb this water. This topic warrants further investigation to fully explain these results.

### 5.4.2 Effect of sintering profile on CNT loss

The CNT loading data showed that loadings for three of the samples (2nf at 1100°C for 3 hours and both 2nf and 2f at 1150°C, 3 hours) had significantly higher CNT loadings after sintered compared with the other samples. The results in these cases may have been due to small amounts of differences in the green density of the samples, or experimental error (particularly in the case of 1150°C, 3 hours, as both composites experienced a similarly lower relative loss of CNTs).

This data could explain the observation that the grain size of the samples sintered at 1150°C for 3 hours was smaller than for those sintered for 2 hours. Grain size normally increases with sintering temperature and time, while this data showed the opposite. However, CNTs are known to inhibit grain growth, so the higher CNT loading (0.78 wt.% compared with 0.52 wt.%) may be responsible for the smaller grain size, despite the longer sintering time.

Additionally, the fact that most sintering atmospheres resulted in the same final CNT loading suggests that the full extent of CNT loss when sintering under these particular conditions may occur at temperatures below 1100°C. It may be that the critical temperature is approximately 1100°C and is slightly different for nfCNT composites and fCNT composites, which could explain the difference in CNT loss between the two samples sintered at 1100°C. As the partial pressure of water (which contributes to CNT oxidation) at high temperatures is very low for the  $C + H_2O = H_2 + CO$  system, and a high flow rate may be preventing full saturation of the gas with water, the amount of water in the system by 1100°C may be low enough to nearly prevent CNT oxidation altogether. However, this does not explain why longer sintering times would not result in more oxidation from gas impurities.

### 5.4.3 Effect of sintering profile on density

A general trend of increasing density with increasing sintering temperature and time was found over most of the data points. As sintering progresses, the contact area between particles increases and they coalesce, driven by the reduction of surface free energy. Then, as the gaps between particles close, the amount of porosity is reduced, raising the percentage theoretical density. While this explains the trend in data for five of the sintering atmospheres, it does not explain why the density of the samples sintered at 1200°C for two hours is lower than that for samples sintered at 1200°C for one hour.

Previous studies have found that at high temperatures, the presence of ‘blowholes’ may reduce the density of the samples (Ruys, A.J. *et al.* 1995). These features are created when dehydroxylation or other gaseous reactions continue after closed porosity has formed in the sample, blocking the gas bubbles’ escape by means of diffusion. Instead,

the excess pressure inside the bubbles builds up, eventually causing an eruption of sorts and creating micropores in the samples which reduce the density.

For these samples, there is no evidence that this is the case. The level of hydroxylation was similar for the materials for both sintering profiles, and no blowholes were observed on the samples' surfaces (although the amount of microporosity in the sample due to inhibited grain growth by the CNTs may have obscured these). It may be that another type of gaseous reaction occurs which results in blowholes, or the results may be explained by other means which are not obvious from the characterisation performed.

#### **5.4.4 Mechanical properties**

The main factor which seemed to inhibit CNTs reinforcing the HA was the general trend of increasing porosity with increasing CNT loading. As strength decreases with increasing porosity, according to the Ryshkewitch-Duckworth equation, this may account for the particularly low strength value of the 5f composite, which had a significantly higher porosity than the other materials. However, as the CNT loading decreased along with decrease in porosity, the potentially reinforcing phase was also lost.

Some data points went against the trend of decreasing density with increasing CNT loading at the lower end of the CNT loading spectrum. These differences may be attributable to variations between material batches. While the green materials were characterised for phase purity, hydroxylation, particle size, and surface area, and found to be similar, differences in characteristics after sintering were noted in Chapter 4 among various 5 wt.% fCNT composites batches.

The fracture surfaces were examined in SEM at high magnification for evidence of toughening mechanisms. The images are presented in Figure 5.14.

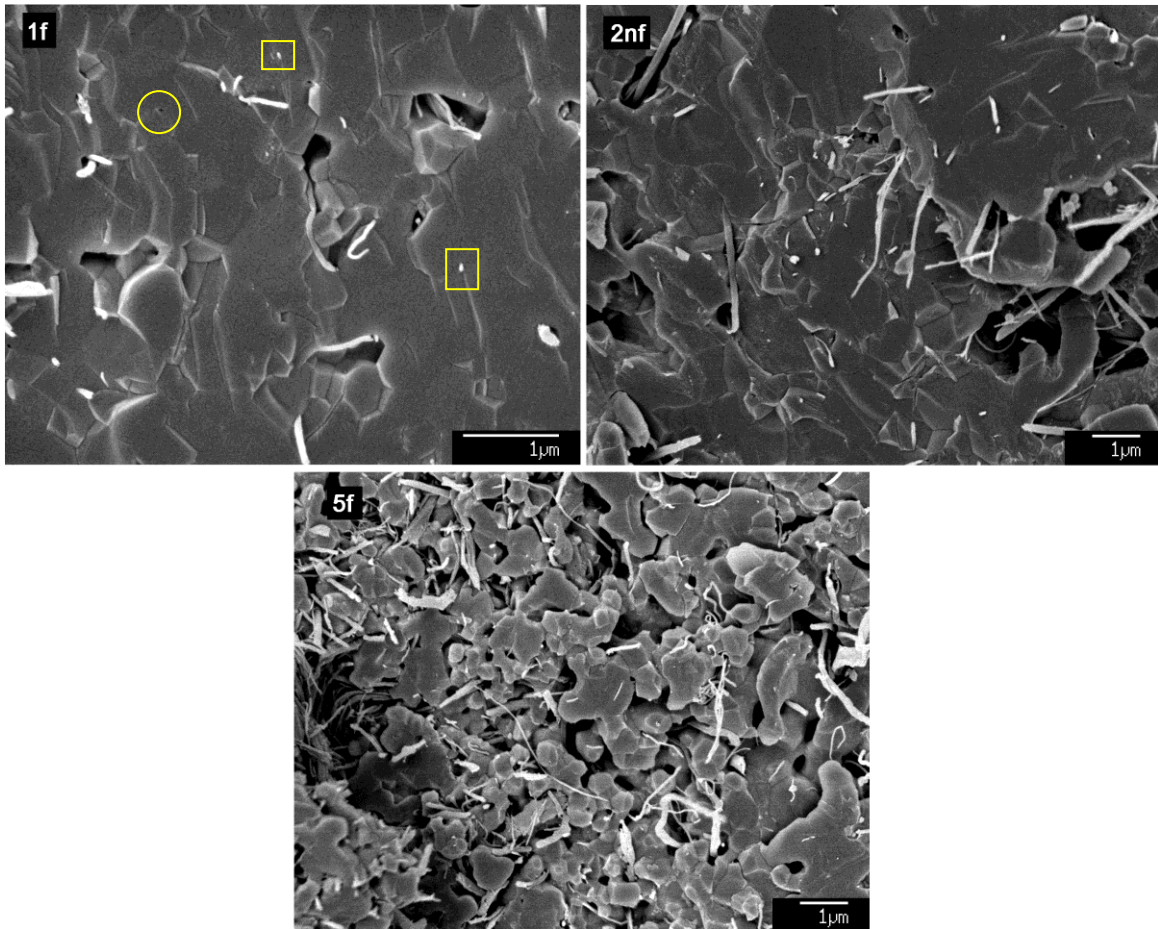


Figure 5.14: High magnification SEM images of fracture surfaces. Yellow circle indicates CNT hole, yellow rectangle indicates broken CNT end.

Toughening by crack bridging was not observed on the more dense samples, however CNTs did appear to bridge some of the grains in the more porous samples. Many of the CNTs appear to have broken off at the sample surface, appearing as a small white speck in the micrograph (marked in yellow). This would indicate that strength of the fibre was insufficient to overcome the interfacial bonding. Other samples, however, particularly at the higher CNT loadings, show longer bits of CNT protruding from the sample surface. It is possible these CNTs may have ‘pulled out’ from the opposite fracture face. There are small holes evident in the fracture face, as well, that may represent the holes from which CNTs on the opposite fracture face were pulled (circled in the image).

Other evidence of interfacial interaction may stem from how well the CNT seems to be ‘bonded’ to the matrix. In some cases, the CNTs can be found at grain boundaries, while in other cases they can be found within grains. When located at grain boundaries, the CNTs often appear to be accompanied by a small amount of porosity around the CNT, indicating poor cohesion. The CNTs within grains, however, appear intimately surrounded by the matrix. Thus, there may be some degree of interaction in these cases.

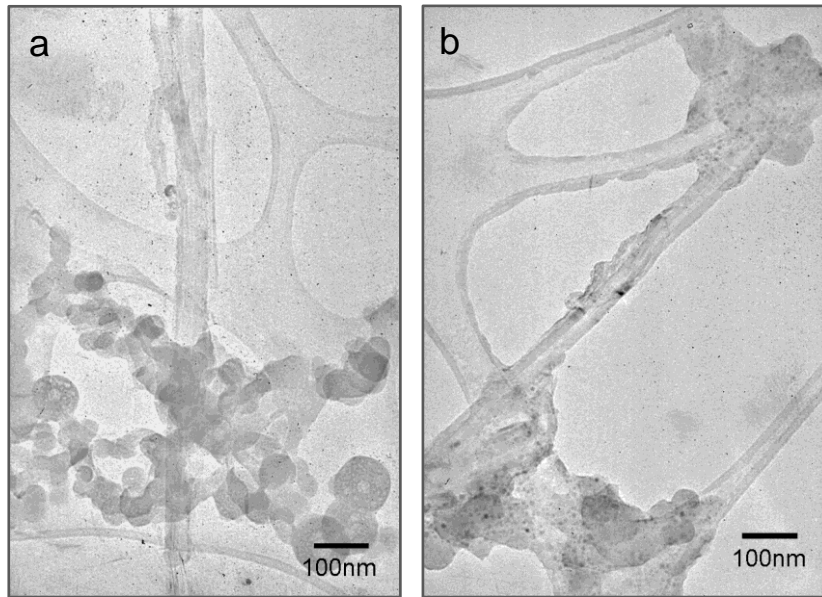


Figure 5.15: TEM images of fCNT composites, comparing areas of little HA-CNT interaction (a) and areas with more notable interaction (b).

To get a better idea of the amount of interaction between the two materials, the samples were viewed with TEM. Figure 5.15 shows two images, both from sintered 5f material. In Figure 5.15(a) there appears to be no interaction between the HA and CNTs. However, in Figure 5.15(b) the HA crystals appear concentrated around the CNT ends, where the concentration of functional groups is expected to be high.

## 5.5 Summary

The sintering profile for HA and composites containing nCNTs and fCNTs was optimised for the best combination of high density and low grain size. The optimal profile was found to be a sintering temperature of 1200°C and a sintering time of 1 hour.

HA and composites with loadings of 0.5 wt.% - 5 wt.% nCNTs and fCNTs were tested to determine values of tensile strength and hardness, and were examined for evidence of

toughening. Tensile strength values tended to be similar when the large error bars were taken into account. The exception to this was the 5f composite, which was particularly porous and had a significantly lower strength. Hardness values tended to scale with porosity, with denser samples giving higher hardness values.

The main limiting factor to strength in these materials was found to be porosity, and any mechanical reinforcement that could be offered by the CNTs may have been negated by the high porosity. However, as evidence was found that CNTs broke at the fracture surfaces, it may be that they would be too weak to result in much strengthening if the porosity were reduced. Occasional evidence of toughening was found in the form of fibre pull-out and some interaction between the HA and CNTs as observed in TEM. Further investigation is needed to determine further the mechanical reinforcing potential of these materials, with particular focus on reducing the porosity for materials with higher CNT loadings.

## 6 IN VITRO STUDIES

For a material to be used safely and successfully inside the body, an understanding of its interaction with human cells and tissues is necessary. At a basic level, this includes *in vitro* testing, such as cell culture on the material or incubation of the material in simulated body fluid. To assess the interaction of cells with the composite materials, human osteoblast-like cells were cultured on HA, 5 wt.% nfcCNT composite (5nf), 5 wt.% fcCNT composite (5f), and tissue culture plastic (as a control). Cell proliferation was measured at different time points over a twelve-day period using both the alamarBlue<sup>®</sup> and the CyQUANT<sup>™</sup> assays.

This chapter will give a brief overview of the basics of cell growth and the type of characteristics which affect cell response. The methods used for cell seeding and assays are then described in detail, and the results of the alamarBlue and CyQUANT studies are presented. An assessment of the material characteristics which influence cell behaviour is then shown. A comparison of the results from these two assays is then made, and possible explanations of the results are discussed.

### 6.1 *Background*

#### 6.1.1 Stages of cellular growth

Cells experience three main stages of growth (Figure 6.1). These stages can generally be observed in experiments to measure cell viability and cell proliferation, provided the experiment is long enough and the cells are healthy. During the ‘lag’ phase, the cells recover from subculture, attach to the surface of the material, and begin to spread; little to no growth is observed. The cells then enter the ‘log’ phase, where cell number increases exponentially and metabolic activity is high. The growth rate then slows or stops in the ‘plateau’ phase as the culture becomes confluent.

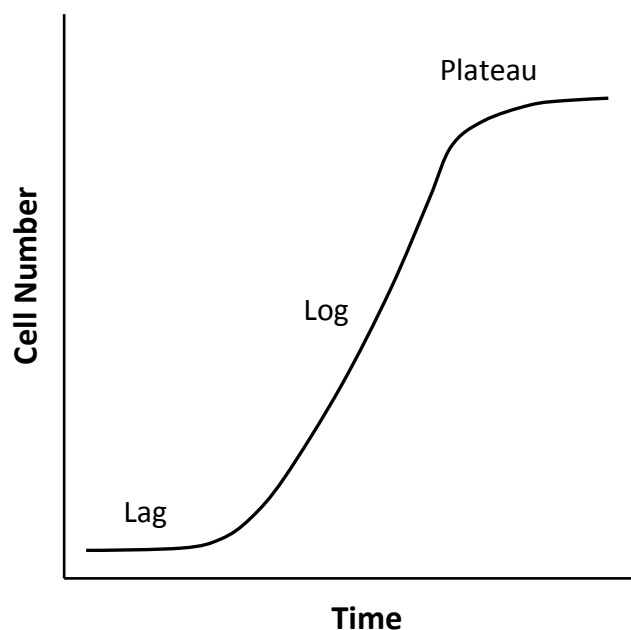


Figure 6.1: Cellular growth curve.

To measure cell number at different time points, cells may be directly counted (a labour-intensive process if there are many samples) or an assay may be used which indirectly measures cell number, for instance by using fluorescent or colorimetric dyes which interact in a measurable way with the cells. In some cases these dyes may change colour or fluorescence once they have been metabolised by the cell, thus the result given is a measure of metabolic activity rather than cell number. Other types of cellular response, such as cell differentiation, may also be assessed, for instance by measuring alkaline phosphatase activity.

### **6.1.2 Proliferation assays**

A wide range of cell proliferation assays are available, most involving organic dyes. For this study, alamarBlue was chosen to measure proliferation by cell metabolism, while CyQUANT was chosen to measure proliferation by cell number. The reasons for this choice are now explained.

#### **6.1.2.1 *alamarBlue* assay**

The alamarBlue assay has an advantage over other cell assays in that it allows the same samples to be measured at various time points. The dye can be added to samples for a

short period (~4 hours) at each time point and then removed. It has been shown to be non-toxic to all cell types tested and does not affect cell growth (AbDSerotec 2008).

Cells interact with the dye as they grow, causing a chemical reduction. The reduced dye is fluorescent and red, whereas the oxidised dye (inhibited growth) is non-fluorescent and blue. Either the fluorescence or absorbance of the dye can be measured following a few hours of incubation to give a measure of cell metabolism. The dye is also sensitive to pH and should only be used between pH 6.8 – 7.4 .

#### 6.1.2.2 *CyQUANT assay*

The CyQUANT assay measures the density of cells in culture through use of a green fluorescent dye which binds to cellular nucleic acids. As the assay does not rely on cellular metabolic activity, cells may be frozen before assaying (MolecularProbes *et al.* 2006).

### 6.1.3 Influence of material characteristics on cellular response

Cellular response, both *in vitro* and *in vivo*, is affected by a wide range of material characteristics. Surface topography, including roughness, both regularly- and irregularly-sized and spaced pits and grooves, and micro- and macro-porosity may affect cell attachment, orientation, proliferation, differentiation, and other responses (Recum *et al.* 1995; Curtis *et al.* 1997; Flemming *et al.* 1999). These topographical characteristics may be inherent to the material or introduced through machining, grinding, or other material preparation. A study on the response of osteoblast-like cells derived from rat osteosarcoma (ROS17/2.8) on HA surfaces found that topographical features introduced by microporosity did not affect cell attachment, but surfaces  $\leq 15\%$  porous favoured cell proliferation and differentiation (Rosa *et al.* 2002). Another study found that a large amount of surface topography increased differentiation of human osteoblast cells on HA, but lowered proliferation (Santos *et al.* 2009). In general, studies seem to agree that some degree of roughness promotes proliferation compared with a smooth surface (Boyan *et al.* 1996).

Surface chemistry and energy also play a role in cellular response. As described in Section 4.1.2.1, slight differences in the Ca/P ratio of calcium phosphates can affect the

solubility and dissolution rate of the material. These differences in chemistry may also affect cell attachment, proliferation, and differentiation. For example, one study found that  $\beta$ -TCP negatively affected adhesion, compared with HA, but positively affected proliferation and differentiation (Santos *et al.* 2009). The surface energy will determine the hydrophilicity of the material, with net negative or positive charges giving a hydrophilic surface and neutral charges giving a hydrophobic surface. The degree of hydrophilicity can change the cellular response significantly (Boyan *et al.* 1996).

## 6.2 *Methods*

*In vitro* studies were carried out on HA and composites containing nfCNTs and fCNTs. The cell response to HA was assessed and compared with the composites to determine the influence of the presence of CNTs. The nfCNT composites were also compared with fCNT composites to determine whether cells interact differently with the two types of CNTs.

### 6.2.1 **Sample preparation**

Twelve samples each of HA, 5 wt.% nfCNT composite (5nf), and 5 wt.% fCNT composite using the 5f-bio batch (5f) were used for cell culture. Powders of each material were pressed into discs of 0.5 g each and sintered. HA was sintered in wet, flowing Ar ( $0.5 \text{ L min}^{-1}$ ) and the composites were sintered in  $\text{CO} + \text{H}_2 + \text{H}_2\text{O(ice)}$  ( $1.2 \text{ L min}^{-1}$ ) according to the protocols outlined in Section 4.3.1 for the A/W and CO/H/W(ice) atmospheres. The sintering profile used was a dwell temperature of  $1200^\circ\text{C}$  for 1 hour with a heating and cooling rate of  $5^\circ\text{C min}^{-1}$ , as was found optimal in Section 5.3.1.3. Six samples of each type were used to measure cell proliferation by the alamarBlue assay and twelve were used to assess cell proliferation by the CyQUANT assay (six reserved just for CyQUANT and the six alamarBlue samples). Additionally, twelve tissue culture plastic discs were used as controls.

The samples were prepared for cell culture by first grinding one surface to 2400 grit with SiC paper. To clean the samples, they were ultra-sonicated in filtered, double-deionised water (Milli-Q), followed by 70% ethanol, then 100% ethanol, each for 2 minutes. The

samples were then sterilised in an oven at 200°C for 3 hours. The tissue culture plastic control discs were prepared by ultra-sonication in 100% ethanol for 5 minutes.

### 6.2.2 Cell seeding

The cells used in this study were human osteoblast-like cells isolated from trabecular bone fragments. To prepare the cells for study, they were seeded onto plastic flasks (surface area 75 cm<sup>2</sup>) and incubated at 37°C in a humidified atmosphere with 5% CO<sub>2</sub> until nearly confluent. The cell culture medium used throughout this study was McCoy's 5A (without phenol red, Gibco<sup>®</sup>, Invitrogen<sup>™</sup> Life Technologies, UK), supplemented with 10% (v/v) foetal calf serum and 1% (v/v) penicillin-streptomycin-glutamine.

To detach the cells, the cell culture medium was first aspirated, then 10 mL of Hank's balanced salt solution (HBSS, Gibco<sup>®</sup>) was introduced into each flask. After 5 minutes, the HBSS was aspirated and another 10 mL was added. After leaving about 2 minutes, the solution was aspirated again. Next, 5 mL of Trypsin-EDTA solution (0.5 g L<sup>-1</sup> Trypsin and 0.2 g L<sup>-1</sup> EDTA in Ca<sup>2+</sup> and Mg<sup>2+</sup> free HBSS) was added to each flask to detach the cells. To stop the trypsinisation, 5 mL of cell culture medium was added. To isolate the cells, the cell suspension was centrifuged at 250 rcf (1200 rpm) for 5 minutes. The supernatant was then removed and the cells were resuspended in 1 mL of cell culture medium.

To prepare the cells for counting, 20 µL of the cell suspension and 20 µL of 0.4% Trypan blue stain (Invitrogen) were combined. The cells were counted using a haemocytometer. The cell suspension was then diluted accordingly to give a concentration of 150,000 cells mL<sup>-1</sup>, which was calculated to give a cell concentration on each disc of approximately 20,000 cells cm<sup>-2</sup>.

The samples were placed in 24-well plates (Nunc), using only the inner wells. A 100 µL bead of cell solution was placed on each disc, taking care that it remained on the surface of the disc, and the samples were placed in the incubator for 3 hours to allow cell attachment. After 3 hours, 900 µL of culture medium was added to each sample well (1 mL was also added to two empty wells on each tray intended for cell proliferation study to serve as negative, background controls) and 1 mL HBSS was added to the remaining empty wells. The plates were then replaced in the incubator. Throughout the

experiment, the culture medium was changed at the time points of the alamarBlue readings – at 1, 3, 6, 9, and 12 days after seeding.

### 6.2.3 Cell proliferation by alamarBlue assay

The alamarBlue assay was used to measure cell proliferation at time points of 1, 3, 6, 9, and 12 days after seeding. A 10% [v/v] solution of alamarBlue in culture medium was prepared and filtered through an 0.2  $\mu\text{m}$  filter to remove any bacteria. The culture medium was then aspirated from each sample well and 500  $\mu\text{L}$  of alamarBlue solution was added to each well. After incubating for 4 hours, the samples were prepared for fluorescence reading.

To prepare samples for fluorescence readings, 100  $\mu\text{L}$  of each sample solution was transferred in duplicate to a 96-well black plate (Nunc). The samples included 6 each of HA, 5nf, 5f, the control culture plastic, and negative control wells which contained only culture medium. The fluorescence was measured with an EL 800 Universal microplate reader (Bio-tek Instruments, Inc., Winooski, USA) with an excitation of 544 nm and an emission of 590 nm. The mean values of the two fluorescent readings for each sample were averaged across all six mean sample values to give a final reading and standard deviation for each sample type.

To examine any possible interaction between the alamarBlue and the samples themselves, two negative control studies were carried out – one with the sample discs and one with CNTs alone – without any cells present. For the negative control study with sample discs, at day 3, two each of HA, 5nf, 5f, and culture plastic discs were placed in a 24-well plate and soaked for 15 minutes in 1 mL culture medium. The medium was then aspirated off and 500  $\mu\text{L}$  of 10% [v/v] solution of alamarBlue in culture medium was placed in each sample well and incubated at 37°C for 4 hours before reading the fluorescence. As with the samples containing cells, following alamarBlue preparation, the samples were given fresh culture medium and replaced in the incubator after each measurement. This was repeated at days 6, 9, and 12 of the alamarBlue study. As the negative control study of the discs only started on day 3, the adjusted time points were 0, 3, 6, and 9 days. The CNT negative control study involved four samples – fCNTs and nCNTs in water and fCNTs and nCNTs in cell culture medium. The CNT concentration used was 4  $\text{mg mL}^{-1}$ , and the

samples were prepared in duplicate. The samples were prepared for alamarBlue in the same way as the other samples. Only one measurement was made for each set of samples, but the experiment was repeated on two different days. Additionally, the pH of the CNT solutions was measured after 4 hours of incubation in alamarBlue.

#### **6.2.4 Cell proliferation by CyQUANT assay**

The CyQUANT assay was carried out on samples from day 1 and day 12. To prepare the samples at the specified time points, all medium was aspirated from the sample wells, the plates were sealed, and then they were frozen at -80°C for later analysis.

The CyQUANT buffer was prepared by diluting the '20x' buffer to '1x' buffer with DN/RNase-free water. The samples were allowed to thaw before 600 µL of diluted buffer was added to each sample well. The plates were then agitated for 5 minutes on an orbital shaker, followed by centrifuging at 1400 rpm for 6 minutes. For each sample, 100 µL of cell lysate was transferred to a 96-well black plate (Nunc) in duplicate. Just before measurements were made, 100 µL of CyQUANT GR dye solution (diluted 200-fold with '1x' CyQUANT buffer) was added to each well. After incubating for 5 minutes at room temperature, the fluorescence was measured with an EL 800 Universal microplate reader (Bio-tek Instruments, Inc., Winooski, USA) with an excitation of 480 nm and an emission of 520 nm.

To convert the readings to cell numbers, a standard curve was also made. A range of known concentrations of cells was seeded onto 24-well plates and prepared in the same manner as the samples.

#### **6.2.5 Statistical analysis**

The CyQUANT data were analysed using the SPSS 15.0 statistical software package. One-way analysis of variance (ANOVA) was used to determine significance in the data, while a *post-hoc* Bonferroni correction was applied to locate and assess significance. Differences of  $p \leq 0.05$  were considered significant. Due to inhomogeneous variation in the data, analysis was performed on data which had been logarithmically transformed. For all data reported, the values represent means, with error bars indicating standard deviations.

## 6.3 Results

### 6.3.1 alamarBlue assay

The alamarBlue assay study results are shown in Figure 6.2. One day after cell seeding, the cell metabolisms were at a similar level for all materials. Over the twelve day study, the metabolism of the cells on HA, 5nf, and the control plastic increased, while cell metabolism decreased for the 5f composite. HA and 5nf showed similar trends in the increase of cell metabolism over the twelve days, while the metabolism for the control increased more dramatically. The 5f composite showed a trend of decreasing metabolism over the twelve days, and by day 12 had roughly one-third the metabolism level compared with day 1.

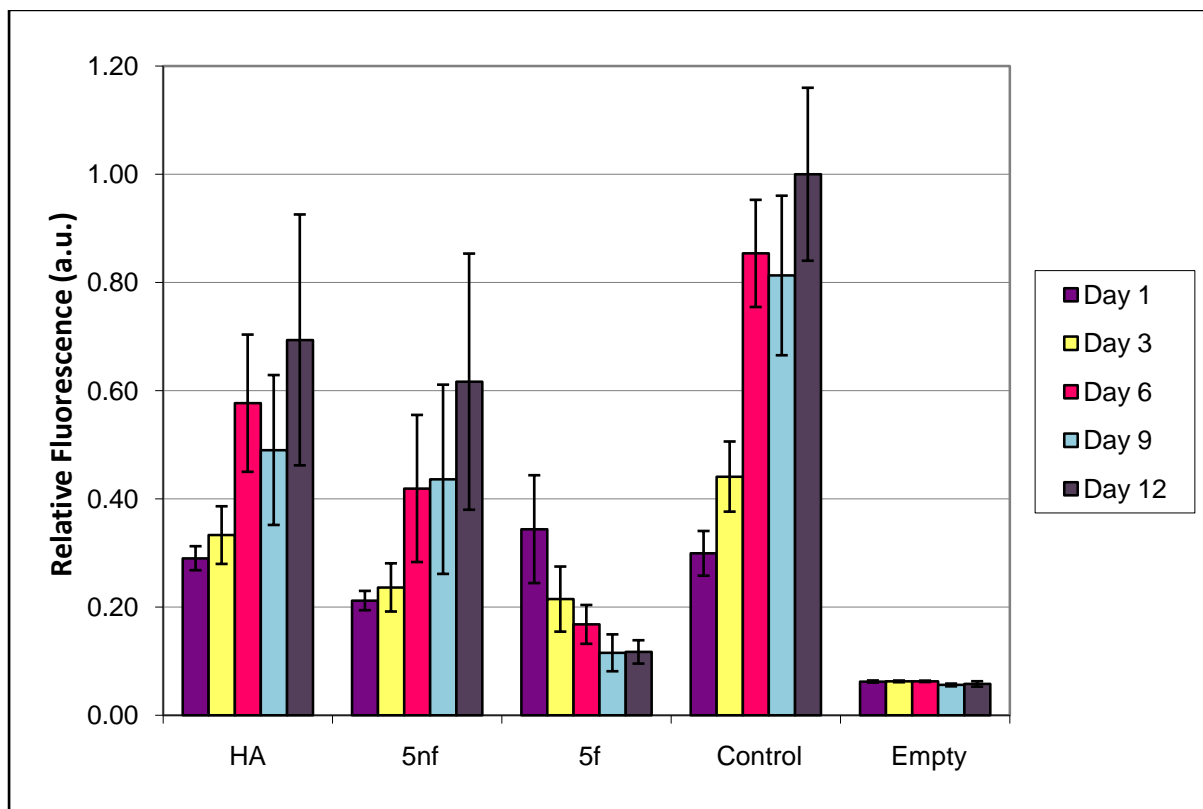


Figure 6.2: alamarBlue assay results.

To determine if the material itself was having any affect on the alamarBlue readings, the fluorescence was also measured for materials incubated in cell culture medium over a nine day period without cells. The results of these readings are shown in Figure 6.3. HA, 5nf, and the control plastic all showed similar fluorescence readings to those of the empty wells, indicating no interaction with the alamarBlue itself. The 5f composite, however, gave a fluorescence reading five times higher than the other materials at day 0. This interaction effect decreased over time, however, as by day 9 the fluorescence reading was only slightly higher compared with the other materials and empty wells. This brings into question whether the alamarBlue data from the cell study are accurate for the 5f composite. This effect will be discussed in more detail in Section 6.4.2.

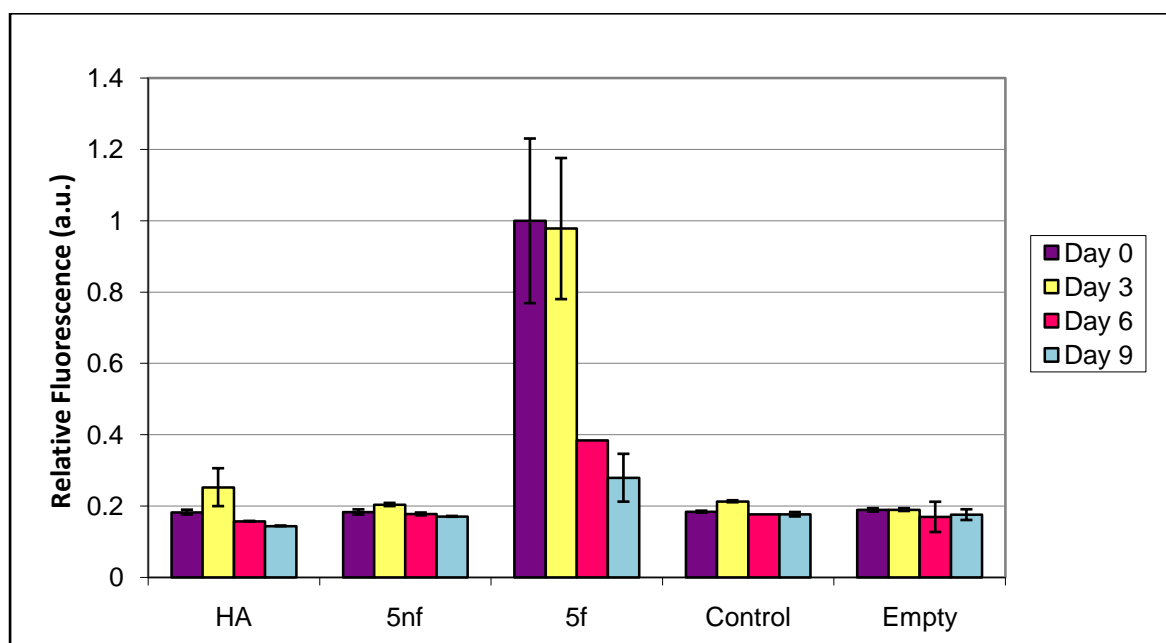


Figure 6.3: alamarBlue results for negative control samples.

To examine what role the CNTs themselves might be playing in this interaction, the fluorescence was measured for dispersions of CNTs in water and cell culture medium (Figure 6.4). The fluorescence readings for both the nfcNTs and fcNTs in water were far below that of the empty control wells and the CNTs in cell culture medium. A colour

change in the dye from blue to pink was noticed immediately upon adding the alamarBlue to the fCNTs + water and within a few minutes of adding the alamarBlue to the nfCNTs + water. After 4 hours of incubation, the dye had become nearly colourless. When the pH of these samples was measured, the fCNTs + water had a pH of ~3, while the nfCNTs + water had a pH of ~4. The CNTs in cell culture medium (particularly nfCNTs) showed only slightly lower fluorescences compared with the empty control, and the pH was measured as ~7.

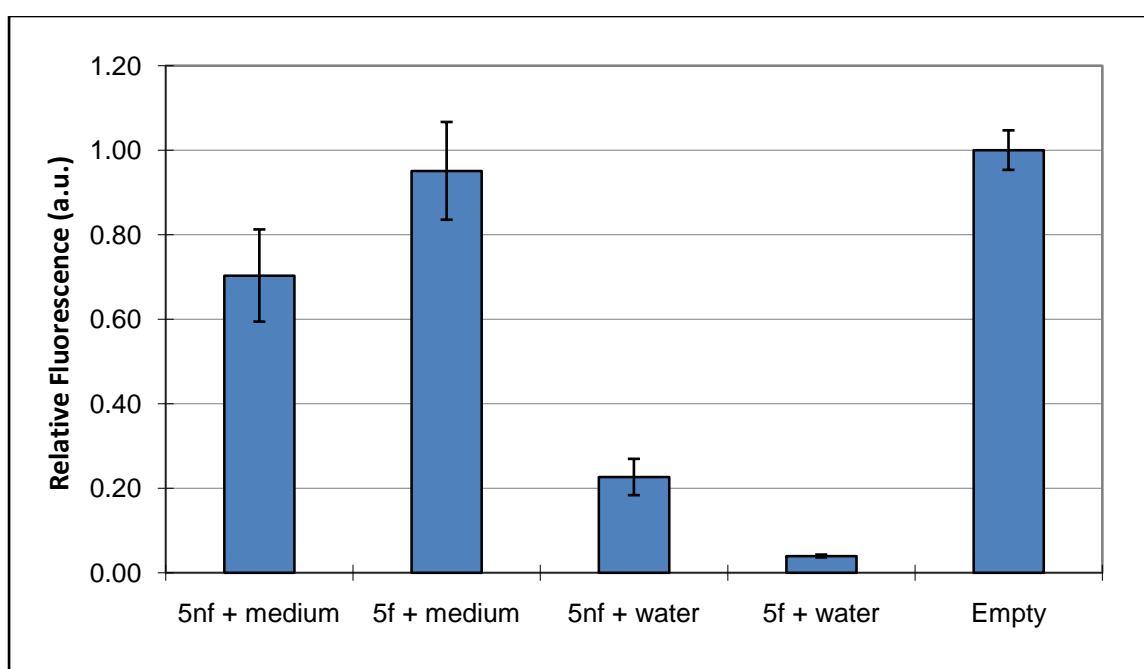


Figure 6.4: alamarBlue results for CNT samples.

### 6.3.2 CyQUANT assay

The results of the CyQUANT assay, for which fluorescence values were converted to cell numbers by means of a standard curve ( $R^2 = 0.9988$ ), are shown in Figure 6.5. At day 1, a significantly higher number of cells was found on the HA sample compared with the 5nf sample ( $p = 0.011$ ) and the 5f sample ( $p < 0.001$ ), while the amount found on the control plastic was not significantly different from the HA. Comparing 5nf, 5f, and the control, the cell numbers at day 1 were not significantly different.

By day 12, cell numbers increased on the HA, 5nf, and control material, and decreased on the 5f composite. The differences in cell numbers between day 1 to day 12 were all found to be statistically significant (HA:  $p = 0.029$ ; 5nf:  $p < 0.001$ ; 5f:  $p = 0.001$ ; control:  $p < 0.001$ ). Comparing the cell numbers at day 12, HA was not statistically different from 5nf or from the control, while 5nf had a significantly lower number when compared with the

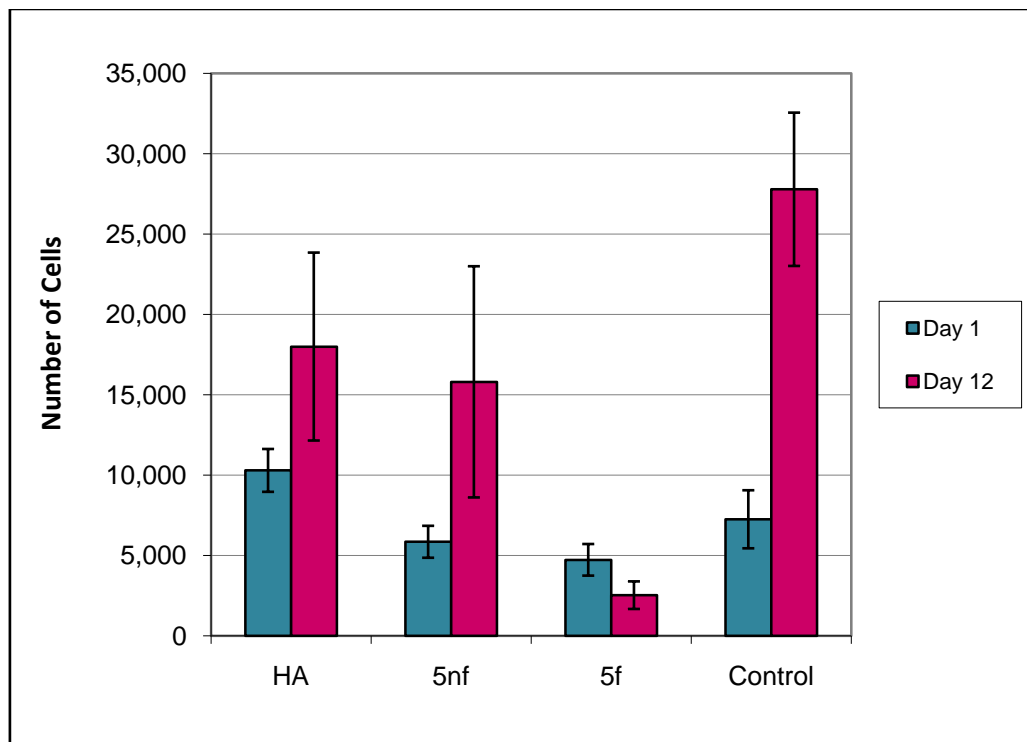


Figure 6.5: CyQUANT assay results.

control ( $p = 0.003$ ). The 5f composite had a significantly lower number of cells compared with the other day 12 materials, with  $p < 0.001$  in all cases.

As cells responded differently to the different types of materials, detailed characterisation was carried out to assess physical and physicochemical properties of the materials. Phase purity and hydroxylation were examined by XRD and FTIR, respectively. The CNT loading was measured by dissolving the HA in HCl acid and filtering, then weighing the remaining CNTs. The density of the samples was determined from sample dimensions and mass and an HA theoretical density of  $3.16 \text{ g cm}^{-3}$  and CNT theoretical density of  $2.00 \text{ g cm}^{-3}$ . All these characterisations were carried out according to the procedures

described in Section 3.2. Additionally, the surface topography of each sample type (ground surfaces in the case of HA, 5nf, and 5f-bio) was examined by SEM as described in Section 3.2.3.1.

### 6.3.3 Material characterisation

The results of the physical and physicochemical characterisation of the materials are summarised in Table 6.1. Plots of the XRD and FTIR data are shown in Figure 6.6 and Figure 6.7, respectively.

#### 6.3.3.1 Physical properties

The CNT loadings of the green materials were 2.8 wt.% and 4.5 wt.% for the 5nf and 5f material, respectively, which corresponds to a loss of 69% of the CNTs for the 5nf composite and only 27% for the 5f composite. The sintered densities of the materials ranged from 85.0% for the 5nf composite to 93.4% for HA. As observed previously, the composites have a greater amount of porosity than the HA. Despite the 5f composite having a higher loading of CNTs, its density is higher than that of the 5nf composite. This trend is the opposite of what was shown in Section 4.3.2.1.3, where higher loadings of CNTs were found to yield lower percent theoretical densities. However, the baseline loss of CNTs was found to vary with batch, and may be responsible for this observation in these materials, as well.

Table 6.1: Summary of physical and physicochemical properties of materials used for cell study.

Material	CNT Loading (wt.%)	XRD	FTIR	Sintered Density (% TD)
HA	---	HA (92%), $\beta$ (8%)	Significant dehydroxylation	$93.4 \pm 0.8$
5nf	$0.88 \pm 0.05$	HA (97%), $\beta$ (3%)	Good OH retention	$85.0 \pm 0.6$
5f	$3.3 \pm 0.2$	HA	Excellent OH retention	$87.5 \pm 1.0$

$\beta$  =  $\beta$ -TCP; TD = theoretical density

### 6.3.3.2 *Physicochemical properties*

The XRD data (Figure 6.6) show that all materials were composed primarily of HA. The calcium phosphate phase in the 5f composite was identified as pure HA, while the 5nf and HA were found to contain small amounts of  $\beta$ -TCP in addition to HA. The FTIR data (Figure 6.7) showed a range of hydroxylation for the materials. The HA was found to have completely dehydroxylated, while the 5nf and 5f composites remained hydroxylated to some degree.

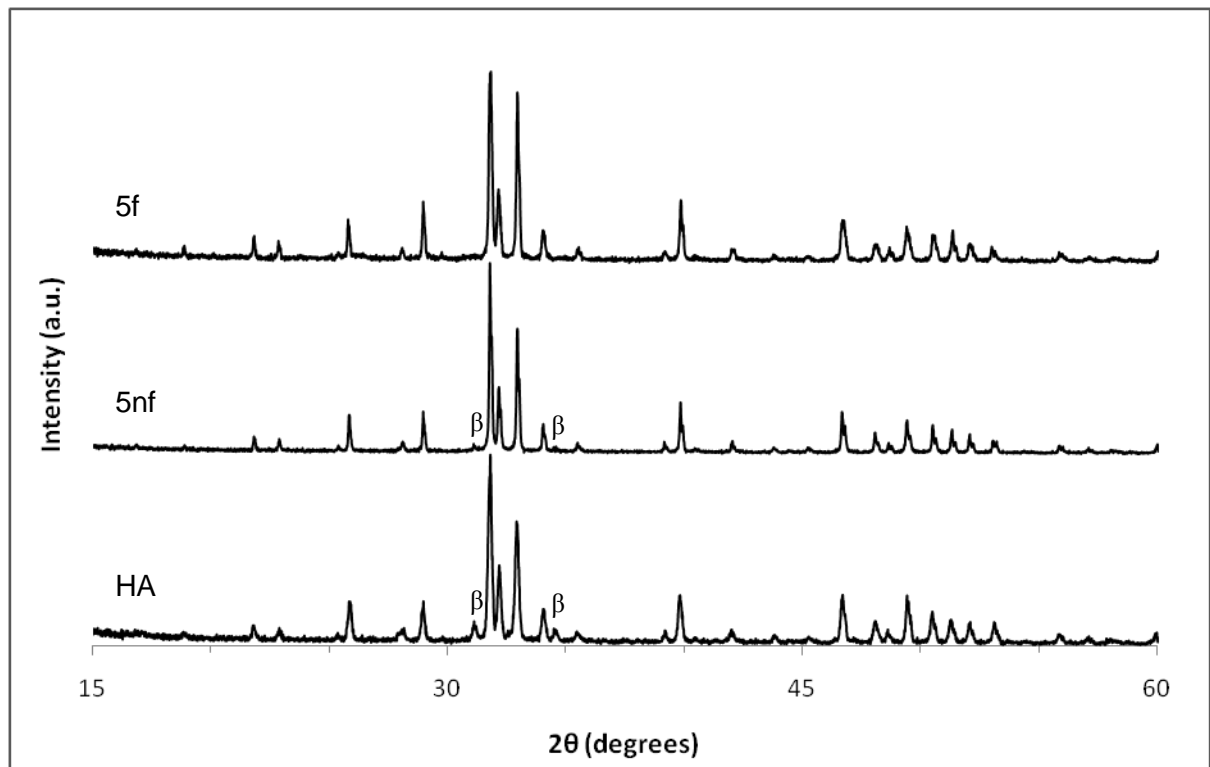


Figure 6.6: XRD traces of material used for cell study. 'β' indicates peaks for  $\beta$ -TCP; the remaining peaks belong to HA. For complete peak assignment, see Figure 3.13.

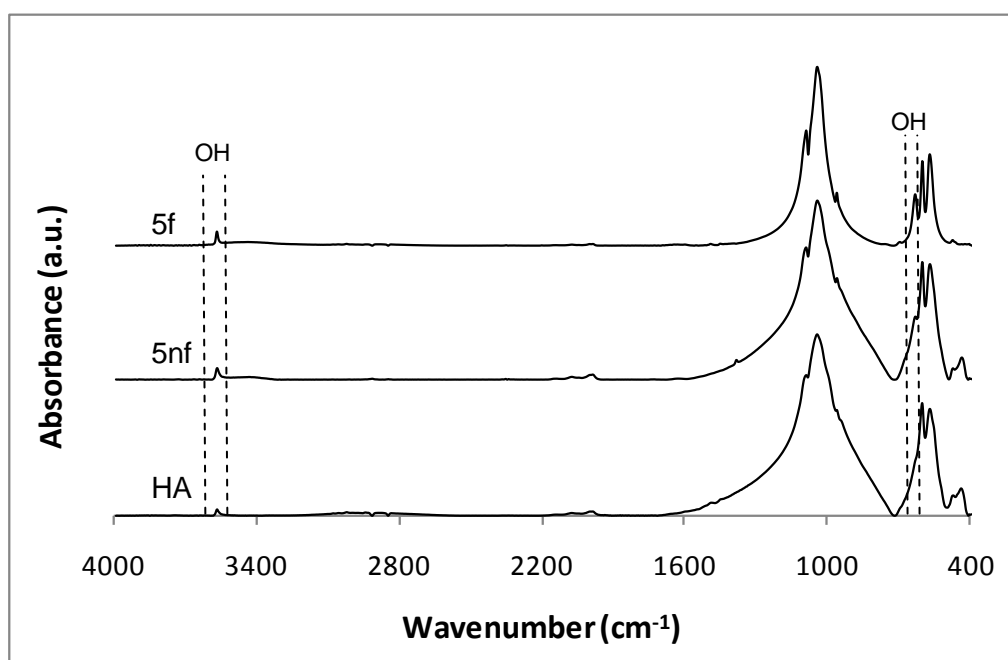


Figure 6.7: FTIR plots of materials used for cell study. Locations of OH peaks are indicated. For complete peak assignment, see Table 3.6.

### 6.3.3.3 *Surface topography*

SEM showed that the topography of the sample surfaces varied (Figure 6.8). HA had the smoothest surface, with only a few small bumps and pits. The tissue culture plastic also had a fairly smooth surface, compared with the composites, although it had more and slightly larger raised areas than the HA. The 5nf composite had the roughest surface, with some pitting, revealing CNT clumps, and some long crevices containing concentrated areas of CNTs. The 5f composite had areas of smooth surface along with some shallow cavities which exposed CNTs. These pits and cavities may have been artefacts from the grinding preparation.

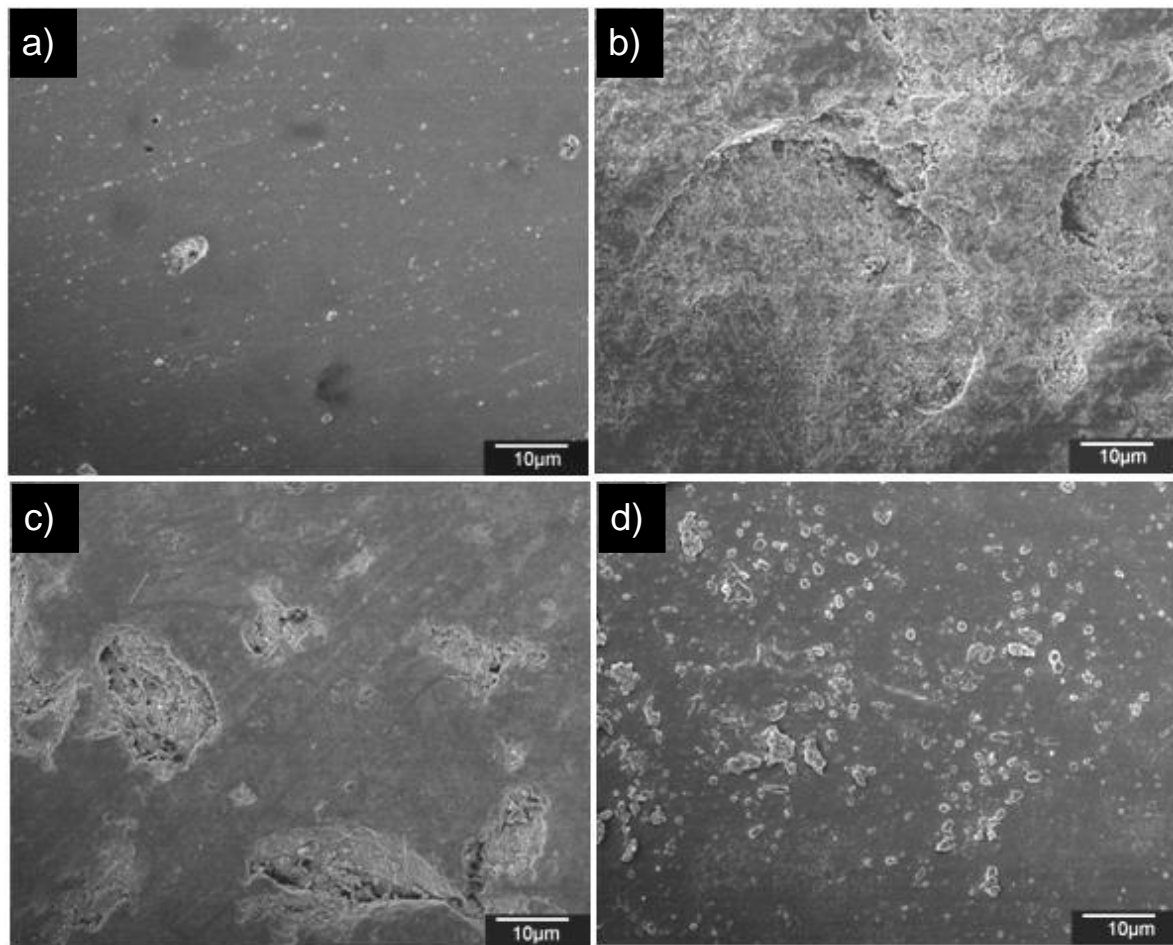


Figure 6.8: SEM micrographs of sample surfaces. (a) HA, (b) 5nf, (c) 5f, (d) tissue culture plastic.

Materials characterisation results have revealed some differences in the materials which may account for the differences in cell response. For instance, the CNT loading was higher in the 5f composites than the 5nf composites. The amount of porosity in the composites was also higher than for HA alone, and correspondingly the surface topography of the different samples varied. While the primary phase in all materials was HA, the HA and 5nf materials contained small amounts of  $\beta$ -TCP, as well. The possible effect of these differences in characteristics on cell response will be discussed in more detail in Section 6.4.5.

## 6.4 Discussion

### 6.4.1 Comparison of alamarBlue and CyQUANT results

In most cases, the alamarBlue and CyQUANT data showed similar trends in cell proliferation. The tissue culture plastic showed the best growth, which can be expected as it has been optimised to encourage cell attachment and proliferation. In comparing HA and 5nf composite, the HA showed slightly more cells and higher metabolic activity at day 1, but by day 12 the cell number and metabolic activity were similar. This may indicate that 5nf encourages more cell growth than HA, as the composite experienced a greater amount of growth over the period of the study.

The 5f composite, on the other hand, showed a decrease in both cell number and metabolic activity from day 1 to day 12. At day 1, the alamarBlue data indicated slightly more metabolic activity for the 5f composite compared with the other materials, whereas the CyQUANT data showed fewer cells compared with HA and a similar number compared with 5nf and the control. As the negative control data for early time points for the 5f composite show a higher fluorescence than for the other materials, the alamarBlue data presented in Figure 6.2 may be a falsely high fluorescence reading.

### 6.4.2 Possible role of CNT-dye and CNT-culture medium interactions

Previous studies have found that CNTs may interfere with various assay dyes and the cell culture medium, giving false cytotoxicity readings. Carbon black and SWNTs have been shown to adsorb Neutral Red dye and interact with the tetrazolium salts in the MTT assay dye, giving a false negative toxicity result for Neutral Red and a false positive result for MTT (Monteiro-Riviere *et al.* 2006; Worle-Knirsch *et al.* 2006). One study has also found that SWNTs adsorb the molecular components of cell culture medium, resulting in a reduced proliferative capacity of the cells (Casey *et al.* 2008). Studies thus far have been conducted with SWNTs and carbon black, but not with MWNTs. Much of the interference problem has been attributed to the high surface area of carbon black and the SWNTs.

From the results of this study, it is not clear whether dye interaction or culture medium depletion may have played a role. While MWNTs still have a large amount of surface area, it is considerably lower than that of SWNTs. For the MWNTs used in this study, the surface area is on the order of 100 times lower than that of commercial SWNTs. Large surface area also does not explain why this interaction would be observed with fCNTs but not with nfCNTs. On the other hand, the surface chemistry of the fCNTs is different from the nfCNTs, and thus they may tend to adsorb different species.

### 6.4.3 Possible role of catalyst residues

Another toxicity concern which has been raised relates to CNT catalyst residues. Pulskamp *et al.* (2007) found that iron catalyst residues had a negative impact on cell viability, while other research has found that catalyst residues did not affect the materials, as residues remained trapped in the interior of the CNTs (Cheng *et al.* 2009). While a small amount of iron catalyst residues was found in the characterisation reported in Section 3.3.1.2, there was much less iron in fCNTs compared with nfCNTs. Thus, it would seem that if residues played any role in the *in vitro* results, then cells would be less viable on the 5nf materials than the 5f materials, which is the opposite trend to what was observed here.

### 6.4.4 Possible role of CNT-induced pH changes

Another explanation for the observed results may lie in analysing the pH data collected and observations of the colour of the dye. According to the alamarBlue technical datasheet, alamarBlue should only be used at pHs between 6.8 – 7.4. The pH measured for suspensions of both nfCNTs and fCNTs in water was much lower than this, with the lowest being observed for the fCNTs (pH = 3 compared with pH = 4 for the nfCNTs). When the maximum buffering point of the dye is reached, the equilibrium between the oxidised and reduced forms is disrupted, and a colourless dye results. A colourless dye will, in turn, yield a lower fluorescence reading. As the suspension of CNTs had a low pH and was colourless after 4 hours of incubation, this is likely to explain the low fluorescence readings shown in Figure 6.4. As the fluorescence readings for the CNT suspensions in cell culture medium were much closer to that of the empty control wells,

this suggests that the cell culture medium has an enhanced buffering ability compared with water.

The lower pH of the fCNT suspension compared with the nfcCNT suspension may be due to insufficient washing of the CNTs after acid treatment to attach functional groups. While the fCNTs were washed until the pH of the filtrate was 7, some acid may have remained which only becomes apparent when the concentration of CNTs in a suspension is high. Additionally, acid may remain inside the tubes and slowly leach out. The data show that the fluorescence reading of the negative control 5f composite (Figure 6.3) decreases over several days, indicating either that acid is slowly leaching out of the CNTs or that it takes several days for acid from the interior of the tablet to leach out to the surface.

While a low pH was observed for the CNT suspensions in water, the pH was ~7 for the CNT suspensions in cell culture medium. As the cell culture samples were incubated in cell culture medium, a low pH would then not seem to explain the reduction in cell proliferation. It could be, however, that while the overall pH of the cell culture medium in all cases was ~7, there may have been localised reductions in pH which affected both the alamarBlue readings and/or the cells. This suggests the need for a more thorough washing process after the functionalisation treatment and perhaps also the need to soak the materials for several days in water or culture medium before seeding cells.

#### **6.4.5 Possible role of material characteristics**

The CNT loading data showed that the nfcCNT composites contained 0.88 wt.% CNTs, while the fCNT composites contained 3.3 wt.%. The reason for this difference is not clear. A possible explanation may be that at high loadings of CNTs, the nfcCNTs tend to form clumps, whereas the 5f composites have CNTs which are much more evenly dispersed. The clumps may allow for more easy oxidation of a sizeable amount of CNTs at once, and may lead to larger pores being formed which allow oxygen to more readily access further CNT clumps. A larger amount of CNT oxidation for 5nf material compared with 5f material was also found in the study of mechanical properties Section 5.3.2.

While the pH of the fCNT suspension in water was lower than the nfcCNT suspension in water, both were significantly lower than 7, suggesting that both should suffer some ill

effects from local pH changes. However, the 5nf material had a much lower CNT loading compared with the 5f composite. Thus, it may be that the CNT loading of the 5nf composite was simply too low to affect cell growth.

Other differences found in the material characterisation may also have played a role in the results. The composite samples had a larger degree of porosity compared with the HA, but as the two composites performed so differently from one another, effects from the differences in types of CNT or CNT loadings appear to have overridden any effects from porosity in that case. The somewhat better performance of the 5nf composite may be due partly to its higher porosity, or may also have to do with the rougher topography of its surface. Another possible factor is the difference in the level of phase purity and hydroxylation between the HA and 5nf.

#### **6.4.6 Additional observations**

An interesting observation was made when examining in SEM the 5f material from the negative control study after 9 days of incubation in cell culture medium. The size of the cavities observed on the surface before incubation had grown and the exposed CNTs were found to be covered with a thick coating (Figure 6.9). Further characterisation of this coating is needed, but it may be that a low local pH around the CNTs caused the dissolution of the surrounding HA, which then redeposited as an apatite layer on the CNTs.

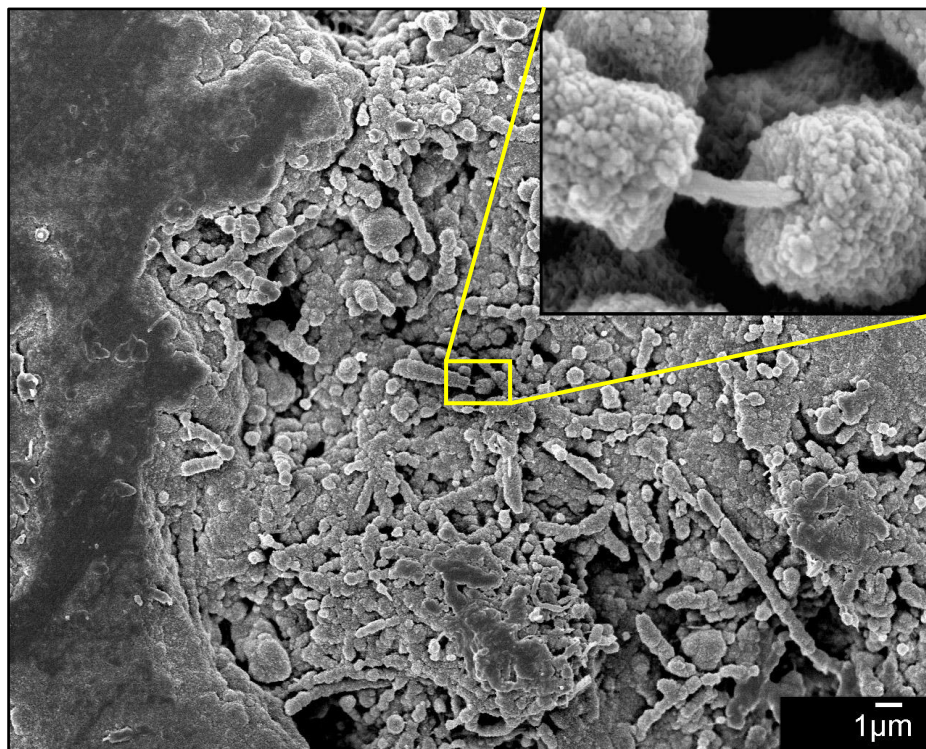


Figure 6.9: SEM micrograph of a cavity in the 5f sample after incubation in cell culture medium for 9 days. Insert shows a close-up image of a coating found on the CNTs.

## 6.5 Summary

Human osteoblast-like cells were cultured on HA, 5nf composite, 5f composite, and tissue culture plastic for 12 days. An alamarBlue proliferation assay was performed at time points of 1, 3, 6, 9, and 12 days and a CyQUANT assay was performed at time points of 1 and 12 days.

Material characterisation showed that all materials were composed primarily of HA and were hydroxylated to some degree. The porosity of the composites was higher than that of the HA, and the CNT loading for the 5nf composite (0.88 wt.%) was much lower than for the 5f composite (3.3 wt.%).

The cells were found to attach and grow well on HA, 5nf composite, and the control tissue culture plastic. The cells cultured on plastic showed the most dramatic growth between days 1 and 12. HA and 5nf performed similarly, but slightly more growth was observed for cells on the 5nf composite. The 5f composite, on the other hand, showed a

decrease in cell viability between days 1 and 12. Further analysis of the materials without cells and CNTs alone showed that the decrease in cell viability on the 5f composite may be due to changes in local pH. Additionally, the higher loading of CNTs for the 5f composite may have affected the results compared with the 5nf composite. The slightly better performance of the 5nf composite compared with HA may have been due to small differences in surface topography, porosity, and physicochemical properties.

## 7 CONCLUSIONS

This work focused on the investigation of HA-CNT composites in four main areas: 1) the production and characterisation of green materials, 2) the effects of sintering the materials in a wide range of atmospheres, 3) the evaluation of mechanical properties, and 4) *in vitro* cellular response. The main conclusions of the study are as follows:

- HA-MWNT composite powders with a range of CNT loadings (0.5 – 5 wt.%) were successfully prepared using a combination of *in-situ* precipitation and shear mixing techniques. Materials were found to be largely phase pure and hydroxylated as shown by XRD and FTIR.
- The optimal sintering atmosphere for balancing desirable physicochemical properties (e.g. phase purity, hydroxylation) and physical properties (e.g. high density and high CNT retention) was found to be CO + H<sub>2</sub> bubbled through ice water.
- Improvement in mechanical properties was limited by high porosity in the materials. The amount of porosity was found to linearly correlate with the CNT loading. Thus, any reinforcing effects the CNTs might have had were inhibited by the presence of porosity.
- Human osteoblast-like cells were found to grow well on HA, 5 wt.% nfcNT composite, and tissue culture plastic, with slightly more growth observed on the 5nf composite compared with the HA over a 12-day study. The 5 wt.% fcNT composite, on the other hand, experienced a decrease in cell viability over the 12-day period.

More detailed conclusions are provided under the relevant sub-headings below.

### **Green material production and processing**

- The HA and composite powders produced were largely phase pure, hydroxylated, had a bimodal particle size distribution with mean values ~10-20  $\mu\text{m}$ , and surface areas in the range of ~80-90  $\text{m}^2 \text{g}^{-1}$ .
- All HA and composite powders were suitable for uniaxial pressing to give mechanically-sound tablets with a green density of 45-50% of theoretical density.

- Functionalised CNTs resulted in better dispersion and interaction with the HA matrix than as-made CNTs as revealed by electron microscopy. However, the acid treatment to functionalise the CNTs was also found to yield shorter CNTs with poorer structural integrity, and possibly reduced mechanical properties.

### **Sintering atmosphere investigations**

- The sintering atmosphere which yielded the optimal combination of properties for the composite materials was CO + H<sub>2</sub> bubbled through ice water.
- Dry sintering atmospheres resulted in decomposed and dehydroxylated materials, although CNT retention was better than for other atmospheres.
- Sintering atmospheres with some inclusion of water resulted in improved retention of phase purity and hydroxylation than dry atmospheres, but at the expense of CNT loading.
- While the CO + H<sub>2</sub> + H<sub>2</sub>O (ice) atmosphere resulted in phase pure and hydroxylated material for the composites, HA decomposed and dehydroxylated in this atmosphere. Thus Ar bubbled through water was chosen as the optimal atmosphere for HA.
- Factors affecting CNT loading, density, and phase purity/hydroxylation included: tablet green density, atmosphere composition (including gas impurities), and batch variations (powder surface area, milling time, particle size, green CNT loading).

### **Sintering parameters**

- Increasing the mass of material sintered at once and increasing the gas flow rate when using the CO + H<sub>2</sub> + H<sub>2</sub>O (ice) atmosphere resulted in higher CNT loadings, good phase purity and hydroxylation, but lower densities.
- Sintering more than one type of material at once had little effect on the material properties compared to sintering each type separately.
- The optimal sintering profile (giving the best combination of low porosity and grain size) was found to be 1200°C with a dwell time of 1 hour and a heating and cooling ramp rate of 5°C min<sup>-1</sup>.

## Mechanical properties

- Tensile strength values measured using diametral compression tests ranged from 14 – 29 MPa. These strength values had large standard deviations and relatively low Weibull modulus values (3-6). The only material which had a significantly different strength value from the others was the 5 wt.% fCNT composite, which had the lowest tensile strength.
- Strength, hardness and CNT loading were found to correlate with porosity. Higher porosities yielded lower strength and hardness values, while materials with higher CNT loadings generally had more porosity.
- CNTs were found to inhibit grain growth, resulting in smaller grain sizes for composites compared with HA.
- Possible evidence of toughening was found in the form of HA-CNT interaction and fibre pull-out.

## *In vitro* cell response

- Human osteoblast-like cells were found to grow well on HA, 5nf, and the tissue culture plastic, with slightly more growth observed on the 5nf composite compared with the HA over a 12-day study.
- A decrease in cell viability was observed for the 5f composite over the 12-day study, which was attributed to decreases in local pH from residual acid left on the CNTs after the functionalisation process.
- Differences in surface topography, porosity, physicochemical properties, and CNT loading may contribute to the cell response, but further study is needed.

These investigations have resulted in a better understanding of how to synthesise and process HA-CNT composite materials and have yielded a great deal of information about the role the sintering atmosphere has in the final material characteristics. While no improvement in mechanical properties was measured in the preliminary investigation of these materials' mechanical behaviour, the porosity seems largely to blame and, if reduced, there is still evidence that the properties could be improved. The *in vitro* studies have also provided useful insights into the cell response to the different materials, which suggest some directions for future study.

## 8 FUTURE OUTLOOK

Five years after the publication of the first article on HA-CNT composites, many questions relating to these materials remain unanswered. Studies are divided on whether CNTs improve or worsen the mechanical properties of HA, and concern still remains regarding the *in vivo* impact of CNTs. Finding a cheap and efficient way to densify these composites to give a mechanically-sound material without CNT damage or loss, while preserving the phase purity and hydroxylation of the HA, is still a primary challenge.

### *8.1 Improvement through better CNTs*

Adding functional groups to the CNT surface to improve dispersibility and CNT-matrix interaction is most commonly achieved through the type of acid treatment used in this study. As shown in SEM images and TGA in this work, and reported widely in the literature, this functionalisation process is very damaging to the structural integrity of the CNTs, weakening their resistance to oxidation at high temperatures and likely weakening them mechanically. A primary focus of future investigations should be to find alternate functionalisation methods which are less damaging to the CNTs but still achieve the homogeneity and interaction necessary for good mechanical properties.

Another area of interest is using SWNTs rather than MWNTs to reinforce the HA. SWNTs tend to be stronger than MWNTs and have a larger aspect ratio and surface area. If bonded to the matrix, they would better be able to withstand load transferred from the matrix than MWNTs, as only the outermost graphene layer of a MWNT is likely to interact with a matrix. This type of interaction can result in a ‘sword-in-sheath’ type failure in which the outermost layer simply pulls away from the rest of the CNT, as the layers are only held together by weak van der Waals forces. In the past, SWNTs have been prohibitively expensive to produce in the volume needed for composite reinforcement. But as CNT synthesis techniques progress, using SWNTs becomes an increasingly viable option.

## ***8.2 Heat treatment techniques***

While pressureless sintering is a cheap and efficient method of sintering for large amounts of material, and thus is the industrial norm, it presents problems, particularly for ceramic-CNT composites. As shown in this study and reported often in the literature, the presence of CNTs hinders densification. Added pressure is normally required to achieve densities above 95%. Hot isostatic pressing and spark plasma sintering have already been shown to be useful for achieving dense HA-CNT composites; however, no extensive studies containing thorough characterisation of the materials have been reported. Thus, it is not clear how effective these techniques are both for retaining CNTs and for preserving the phase purity and hydroxylation of the HA. This should be explored further.

This study has made progress in developing further the potential of using pressureless sintering, as densities similar to and even higher than that of HA were achieved, albeit for very low CNT loadings. Thus pressureless sintering still warrants further investigation. In particular, understanding better how sintering progresses in the materials as temperature increases and how the physicochemical and physical properties are changing over the entire sintering profile would be helpful to improving further the sintering conditions. The effect of other sintering parameters, such as gas flow rate and the amount of material, still remain somewhat unclear and warrant further study.

## ***8.3 Mechanical properties***

As the results of HA studies and mechanical property studies have been shown to be dependent on the characteristics of the starting material, sample preparation, and measurement technique, it would be interesting to compare the mechanical properties of samples made by various methods of sintering using the same starting material. Only in this way can the most accurate comparisons be made regarding heat treatment and its effect on properties related to mechanical behaviour. In particular, it remains to be seen what effect the difference in the coefficients of thermal expansion between the two materials may have if a more dense material can be achieved with an alternative sintering technique. More detailed studies in this area should be carried out.

The mechanical property measurements performed in this study were only preliminary investigations. It would be useful to try a wider range of CNT loadings and to carry out a

more comprehensive range of mechanical tests on the materials (e.g. comparing diametral compression with 3-point bending and testing toughness by a notched beam technique). Other properties, such as fatigue life and modulus have not been studied at all for HA-CNT composites, nor has testing the samples under physiological conditions. These merit further investigation.

Another interesting parameter, which has not been investigated previously, is how aligning the CNTs may affect mechanical properties. Achieving alignment of CNTs would create an anisotropic material. As collagen is aligned longitudinally in bone, this structure may better mimic its mechanical properties.

Mechanical interest also lies in the final result presented in Chapter 6, in which CNTs were found to be coated with an apatite layer after soaking in cell culture medium for several days. This sort of intimate interaction between the apatite and the CNTs could be used to achieve more load transfer between the matrix and CNTs. On the other hand, it could be detrimental to the toughness, as too good an interface does not allow for fibre pull-out. This apparent apatite layer also has connotations for the potential *in vivo* response of the body to CNTs.

#### **8.4 *Biological properties***

Many questions still remain regarding the *in vivo* effects of CNTs. Even if the body's response to CNTs alone is better understood, the matrix in which CNTs are incorporated for a composite will likely alter this response. Thus more in depth *in vitro* and *in vivo* studies are needed to assess the potential of HA-CNT composites for bone graft or other *in vivo* applications.

While the results of this study suggest that fCNTs may negatively affect cell viability, it may simply be that a more thorough washing process after the acid functionalisation treatment would change this response. Longer cell studies are needed and a wider range of techniques should be used, including alkaline phosphatase production assessment. Electron microscopy would also help elucidate the cell interaction with materials, and particularly the interaction of the cells with CNTs.

Even if the biological community eventually rules CNTs toxic and prohibits their use in the body, this study and further investigations are still useful to understanding how CNTs may reinforce other ceramics for use in a wide range of applications.

## REFERENCES

- AbDSerotec. (2008). "BUF012A/B alamarBlue product datasheet." from <http://www.ab-direct.com>.
- Ajayan, P. M. (1999). "Nanotubes from carbon." Chem. Rev. **99**: 1787-1799.
- Ajayan, P. M. and S. Iijima (1993). "Single-shell carbon nanotubes of 1-nm diameter." Nature **361**: 333-334.
- Akao, M., H. Aoki and K. Kato (1981). "Mechanical properties of sintered hydroxyapatite for prosthetic applications." J. Mater. Sci. **16**: 809-812.
- Akazawa, T. (1953). "Tension test method for concrete." Intl. Assoc. of Testing and Res. Lab. for Mater. and Struct. **13**.
- Antis, G. R., P. Chantikul, B. R. Lawn and D. B. Marshall (1981). "A critical evaluation of indentation techniques for measuring fracture toughness: I, Direct crack measurements." J. Am. Ceram. Soc. **64**: 533-538.
- Babushkin, O., T. Lindback, A. Holmgren, J. Li and L. Hermansson (1994). "Thermal expansion of hot isostatically pressed hydroxyapatite." J. Mater. Chem. **4**: 413-415.
- Balani, K., R. Anderson, T. Laha, M. Andara, J. Tercero, E. Crumpler and A. Agarwal (2007a). "Plasma-sprayed carbon nanotube reinforced hydroxyapatite coatings and their interaction with human osteoblasts in vitro." Biomater. **28**: 618-624.
- Balani, K., Y. Chen, S. P. Harlinkar, N. B. Dahotre and A. Agarwal (2007b). "Tribological behavior of plasma-sprayed carbon nanotube-reinforced hydroxyapatite coating in physiological solution." Acta Biomater. **3**: 944-951.
- Benard, A. and E. C. Bos-Levenbach (1953). "The plotting of observations on probability paper." Statistica Neerlandica **7**: 163-173.
- Best, S. M., B. Sim, M. Kayser and S. Downes (1997). "The dependence of osteoblastic response on variations in the chemical composition and physical properties of hydroxyapatite." J. Mater. Sci.: Mater. Med. **8**: 97-103.
- Bezzi, G., G. Celottie, E. Landi, T. M. G. LaToretta, I. Sopyan and A. Tampieri (2003). "A novel sol-gel technique for hydroxyapatite preparation." Mater. Chem. Phys. **78**: 816-824.

- Bonfield, W., M. D. Grynps, A. E. Tully, J. Bowman and J. Abram (1981). "Hydroxyapatite reinforced polyethylene - a mechanically compatible implant material for bone replacement." Biomater. **2**: 185-186.
- Bouyer, E., F. Gitzhofer and M. I. Boulous (2000). "Morphological study of hydroxyapatite nanocrystal suspension." J. Mater. Sci.: Mater. Med. **11**: 523-531.
- Bowen, H. K. (1980). "Basic research needs on high temperature ceramics for energy applications." Mater. Sci. Eng. **44**: 1-56.
- Boyan, B., T. Hummert, D. Dean and Z. Schwartz (1996). "Role of material surface in regulating bone and cartilage cell response." Biomater. **17**: 137-146.
- Carneiro, F. L. L. B. and A. Barcellos (1953). "Tensile strength of concretes." RILEM Bull. **13**: 103-107.
- Casey, A., E. Herzog, F. M. Lyng, H. J. Byrne, G. Chambers and M. Davoren (2008). "Single walled carbon nanotubes induce indirect cytotoxicity by medium depletion in A549 lung cells." Toxicol. Lett. **179**: 78-84.
- Chappell, H. (2006). Atomistic simulations of hydroxyapatite. Cambridge, U.K., University of Cambridge, Ph.D.
- Chen, Y., C. H. Gan, T. N. Zhang, G. Yu, P. C. Bai and A. Kaplan (2005). "Laser-surface-alloyed carbon nanotubes reinforced hydroxyapatite composite coatings." Appl. Phys. Lett. **86**: 251905.
- Chen, Y., T. H. Zhang, C. H. Gan and G. Yu (2007). "Wear studies of hydroxyapatite composite coating reinforced by carbon nanotubes." Carbon **45**: 998-1004.
- Chen, Y., Y. Q. Zhang, T. H. Zhang, C. H. Gan, C. Y. Zheng and G. Yu (2006). "Carbon nanotube reinforced hydroxyapatite composite coatings produced through laser surface alloying." Carbon **44**: 37-45.
- Cheng, C., K. Muller, K. Koziol, J. Skepper, P. Midgley, M. Welland and A. Porter (2009). "Toxicity and imaging of multi-walled carbon nanotubes in human macrophage cells." Biomater. **30**: 4152-4160.
- Chlopek, J., B. Czajkowska, B. Szaraniec, E. Frackowiak, K. Szostak and F. Beguin (2006). "In vitro studies of carbon nanotubes biocompatibility." Carbon **44**: 1106-1111.
- Choi, J. W., Y. M. Kong and H. E. Kim (1998). "Reinforcement of hydroxyapatite bioceramic by addition of Ni<sub>3</sub>Al and Al<sub>2</sub>O<sub>3</sub>." J. Amer. Ceram. Soc. **81**: 1743-1748.

- Clark, J. S. (1955). "Solubility criteria for the existence of hydroxyapatite." Can. J. Chem. **33**: 1696-1700.
- Curtin, W. A. and B. W. Sheldon (2004). "CNT-reinforced ceramics and metals." Mater. Today **7**: 44-49.
- Curtis, A. and C. Wilkinson (1997). "Topographical control of cells." Biomater. **18**: 1573-1583.
- deGroot, K. (1980). "Bioceramics consisting of calcium phosphate salts." Biomater. **1**: 47-50.
- deGroot, K., C. P. A. T. Klein, J. G. C. Wolke and J. M. A. deBlieck-Hogervorst (1990). Chemistry of calcium phosphate bioceramics. CRC Handbook of bioactive ceramics, Vol. II: Calcium phosphate and hydroxylapatite ceramics. T. Yamamuro, L. L. Hench and J. Wilson. Boca Raton, FL, CRC Press: 3-16.
- Delgado, J. A., L. Morejon, S. Martinez, M. P. Ginebra, N. Carlsson, E. Fernandez, J. A. Planell, M. T. Clavaguera-Mora and J. Rodriguez-Viejo (1999). "Zirconia-toughened hydroxyapatite ceramic obtained by wet sintering." J. Mater. Sci.-Mater. Med. **10**: 715-719.
- Denissen, H., C. Mangano and G. Cenini (1985). Hydroxylapatite implants, Piccin Nuova Libreria, S.P.A., India.
- deWith, G. and A. J. Corbijn (1989). "Metal fiber reinforced hydroxy-apatite ceramics." J. Mater. Sci. **24**: 3411-3415.
- deWith, G., H. J. A. van Dijk, N. Hattu and K. Prijs (1981). "Preparation, microstructure and mechanical properties of dense polycrystalline hydroxyapatite." J. Mater. Sci. **16**: 1592-1598.
- Donaldson, K., X. Y. Li, S. Dogra, B. G. Miller and G. M. Brown (1992). "Asbestos-stimulated tumor necrosis factor release from alveolar macrophages depends on fiber length and opsonization." J. Pathol. **168**: 243-248.
- Dorozhkin, S. V. (2009). "Calcium orthophosphates in nature, biology and medicine." Mater. **2**: 399-498.
- Driessen, A. A., C. P. A. T. Klein and K. DeGroot (1982). "Preparation and some properties of sintered B-whitlockite." Biomater. **3**: 113-116.
- Duckworth, W. H. (1953). "Discussion of Ryshkewitch paper by Winston Duckworth." J. Am. Ceram. Soc. **36**: 68.

- Eitan, A., K. Jiang, D. Dukes, R. Andrews and L. S. Schadler (2003). "Surface modification of multiwalled carbon nanotubes: toward the tailoring of the interface in polymer composites." Chem. Mater. **15**: 3198-3201.
- Fahad, M. K. (1996). "Stresses and failure in the diametral compression test." J. Mater. Sci. **31**: 3723-3729.
- Falvo, M. R., G. J. Clary, R. M. T. II, V. Chi, J. F.P. Brooks, S. Washburn and R. Superfine (1997). "Bending and buckling of carbon nanotubes under large strain." Nature **389**: 582-584.
- Fischer, G. R., P. Bardhan and J. E. Geiger (1983). "The lattice thermal expansion of hydroxyapatite." J. Mater. Sci. Lett. **2**: 577.
- Flahaut, E., M. C. Durrieu, M. Remy-Zolghadri, R. Bareille and C. Baquey (2006). "Investigation of the cytotoxicity of CCVD carbon nanotubes towards human umbilical vein endothelial cells." Carbon **44**: 1093-1099.
- Flemming, R., C. Murphy, G. Abrams, S. Goodman and P. Nealey (1999). "Effects of synthetic micro- and nano-structured surfaces on cell behavior." Biomater. **20**: 573-588.
- Fogden, S., R. Verdejo, B. Cottam and M. Shaffer (2008). "Purification of single walled carbon nanotubes: the problem with oxidation debris." Chem. Phys. Lett. **460**: 162-167.
- George, J. H., M. S. Shaffer and M. M. Stevens (2006). "Investigating the cellular response to nanofibrous materials by use of a multi-walled carbon nanotube model." J. Exp. Nanosci. **1**: 1-12.
- Gibson, I. R., S. Ke, S. M. Best and W. Bonfield (2001). "Effect of powder characteristics on the sinterability of hydroxyapatite powders." J. Mater. Sci.: Mater. Med. **12**: 163-171.
- Gross, K. A., C. S. Chai, G. S. K. Kannangara and B. Ben-Nissan (1998). "Thin hydroxyapatite coatings via sol-gel synthesis." J Mater Sci: Mater Med **9**: 839-843.
- Hayek, E. and H. Newesely (1963). "Pentacalcium monohydroxyorthophosphate." Inorg. Synth. **7**: 63-65.
- Hench, L. L. (1991). "Bioceramics: from concept to clinic." J. Amer. Ceram. Soc. **74**: 1487-1510.

- Hirsch, A. (2002). "Functionalisation of single-walled carbon nanotubes." Angew. Chem. Int. Ed. **41**: 1853-1859.
- Hong, L., H. C. Xu and K. deGroot (1992). "Tensile strength of the interface between hydroxyapatite and bone." J. Biomed. Mater. Res. **26**: 7-18.
- Hull, D. (1981). Strength of short fibre composite materials. An introduction to composite materials. Cambridge, Cambridge University Press: 199-219.
- Iijima, S. (1991). "Helical microtubules of graphitic carbon." Nature **354**: 56-58.
- Jarcho, M., C. H. Bolen, M. B. Thomas, J. Bobick, J. F. Kay and R. H. Doremus (1976). "Hydroxylapatite synthesis and characterization in dense form." J. Mater. Res. **11**: 2027-2035.
- Jiang, H., B. Liu, Y. Huang and K. C. Hwang (2004). "Thermal expansion of single wall carbon nanotubes." J. Eng. Mater. Technol. **126**: 265-270.
- Jillavenkatesa, A. and S. R.A. Condrate (1998). "Sol-gel processing of hydroxyapatite." J. Mater. Sci. **33**: 4111-4119.
- Juang, H. Y. and M. H. Hon (1996). "Effect of calcination on sintering of hydroxyapatite." Biomater. **17**: 2059-2064.
- Kay, M. I., R. A. Young and A. S. Posner (1964). "Crystal structure of hydroxyapatite." Nature **204**: 1050-1052.
- Kaya, C. (2008). "Electrophoretic deposition of carbon nanotube-reinforced hydroxyapatite bioactive layers on Ti-6Al-4V alloys for biomedical applications." Ceram. Inter. **34**: 1843-1847.
- Kealley, C., M. Elcombe, A. van Riessen and B. Ben-Nissan (2006). "Development of carbon nanotube-reinforced hydroxyapatite bioceramics." Physica B **385**: 496-498.
- Kealley, C. S., B. A. Latella, A. van Riessen, M. M. Elcombe and B. Ben-Nissan (2008). "Micro- and nano-indentation of a hydroxyapatite-carbon nanotube composite." J. Nanosci. Nanotechnol. **8**: 3936-3941.
- Keller, E. E. and W. W. Triplett (1987). "Iliac bone grafting: Review of 160 consecutive cases." J. Oral Max. Surg. **45**: 11-24.
- Kendall, K. (1989). "Influence of powder structure on processing and properties of advanced ceramics." Powder Technol. **58**: 151-161.

- Kiricsi, I., Z. Konya, K. Niesz, A. A. Koos and P. Biro (2003). Synthesis procedures for production of carbon nanotube junctions. SPIE-Int. Soc. Opt. Eng. 280-287.
- Klein, C. P. A. T., J. M. A. Deblieckhogervorst, J. G. C. Wolke and K. Degroot (1990). "Studies of the solubility of different calcium-phosphate ceramic particles in vitro." Biomater. **11**: 509-512.
- Klein, C. P. A. T., P. Patka, H. B. M. van der Lubbe, J. G. C. Wolke and K. de Groot (1991). "Plasma-sprayed coatings of tetracalcium phosphate, hydroxyl-apatite and B-whitlockite on titanium alloy. An interface study." J. Biomed. Mater. Res. **25**: 53-65.
- Knepper, M., S. Moricca and B. K. Milthorpe (1997). "Stability of hydroxyapatite while processing short-fibre reinforced hydroxyapatite ceramics." Biomater. **18**: 1523-1529.
- Kroto, H. W., J. R. Heath, S. C. O'Brien, R. F. Curl and R. E. Smalley (1985). "C60: Buckminsterfullerene." Nature **318**: 162-163.
- Kruzic, J. J., D. K. Kim, K. J. Koester and R. O. Ritchie (2009). "Indentation techniques for evaluating the fracture toughness of biomaterials and hard tissues." J. Mech. Beh. Biomed. Mater. **2**: 384-395.
- Lakes, R. S. (1993). "Materials with structural hierarchy." Nature **361**: 511-514.
- Lam, C. W., J. T. James, R. McCluskey and R. L. Hunter (2004). "Pulmonary toxicity of single-wall carbon nanotubes in mice 7 and 90 days after intratracheal instillation." Toxicol. Sci. **77**: 126-134.
- Lau, K. T. and D. Hui (2002). "Effectiveness of using carbon nanotubes as nano-reinforcements for advanced composite structures." Carbon **40**.
- LeGeros, R. Z. (1974). "The unit-cell dimensions of human enamel apatite: effect of chloride incorporation." Arch. Oral. Biol. **20**: 63-71.
- LeGeros, R. Z. and J. P. LeGeros (1993). Dense hydroxyapatite. An introduction to bioceramics. L. L. Hench and J. Wilson. Singapore, World Scientific: 139-180.
- Levitt, S. R., P. H. Crayton, E. A. Monroe and S. R.A. Condrate (1969). "Forming method for apatite prostheses." J. Biomed. Mater. Res. **3**: 683-684.
- Lewandrowski, K. U., J. D. Gresser and D. L. Wise (2000). "Bioresorbable bone graft substitutes of different osteoconductivities: a histologic evaluation of osteointegration of poly(propylene glycol-co-fumaric acid)-based cement implants in rats." Biomater. **21**: 757-764.

- Li, A. M., K. N. Sun, W. F. Dong and D. M. Zhao (2007). "Mechanical properties, microstructure and histocompatibility of MWCNTs/HAp biocomposites." Mater. Lett. **61**: 1839-1844.
- Li, G. Y., P. M. Wang and X. Zhao (2005). "Mechanical behavior and microstructure of cement composites incorporating surface-treated multi-walled carbon nanotubes." Carbon **43**: 1239-1245.
- Li, H. P., N. Q. Zhao, Y. Liu, C. Y. Liang, C. S. Shi, X. W. Du and J. J. Li (2008). "Fabrication and properties of carbon nanotubes reinforced Fe/hydroxyapatite composites by in situ chemical vapor deposition." Compos. Pt. A-Appl. Sci. Manuf. **39**: 1128-1132.
- Li, J., H. Liao and L. Hermansson (1996). "Sintering of partially-stabilized zirconia and partially-stabilized zirconia-hydroxyapatite composites by hot isostatic pressing and pressureless sintering." Biomater. **17**: 1787-1790.
- Liao, C. J., F. H. Lin, K. S. Chen and J. S. Sun (1999). "Thermal decomposition and reconstitution of hydroxyapatite in air atmosphere." Biomater. **20**: 1807-1813.
- Lin, C. J., H. J. Han, F. Zhang and A. M. Li (2008). "Electrophoretic deposition of HA/MWNTs composite coating for biomaterial applications." J. Mater. Sci.-Mater. Med. **19**: 2569-2574.
- Lin, T., V. Bajpai, T. Ji and L. Dai (2003). "Chemistry of carbon nanotubes." Aust. J. Chem. **56**: 635-651.
- Liu, D. M., T. Troczynski and W. J. Tseng (2001). "Water-based sol-gel synthesis of hydroxyapatite: process development." Biomater. **22**: 1721-1730.
- Liu, Z. J., Z. Y. Yuan, W. Zhou, L. M. Peng and Z. Xu (2001). "Co/Carbon-nanotube monometallic system: the effects of oxidation by nitric acid." Phys. Chem. Chem. Phys. **3**: 2518-2522.
- Ma, R. Z., J. Wu, B. Q. Wei, J. Liang and D. H. Wu (1998). "Processing and properties of carbon nanotube-nano-SiC ceramic." J. Mater. Sci. **33**: 5243-5246.
- Matthews, F. L. and R. D. Rawlings (1994). Ceramic matrix composites. Composite materials: Engineering and science. London, Chapman & Hall: 118-167.
- Meng, Y. H., C. Y. Tang, C. P. Tsui and D. Z. Chen (2008). "Fabrication and characterization of needle-like nano-HA and HA/MWNT composites." J. Mater. Sci.-Mater. Med. **19**: 75-81.
- MolecularProbes and Invitrogen (2006). "CyQUANT cell proliferation assay kit technical datasheet MP 07026."

- Monteiro-Riviere, N. A. and A. O. Inman (2006). "Challenges for assessing carbon nanomaterial toxicity to the skin." Carbon **44**: 1070-1078.
- Niyogi, S., M. A. Hamon, H. Hu, B. Zhao, P. Bhowmik, R. Sen, M. E. Itkis and R. C. Haddon (2002). "Chemistry of single-walled carbon nanotubes." Acc. Chem. Res. **35**: 1105-1113.
- Nygren, M. and Z. Shen (2004). "Spark plasma sintering: possibilities and limitations." Key Eng. Mater. **264-268**: 719-724.
- Osaka, A., Y. Miura, K. Takeuchi, M. Asada and K. Takahashi (1991). "Calcium apatite prepared from calcium hydroxide and orthophosphoric acid." J. Mater. Sci.: Mater. Med. **2**: 51-55.
- Ovri, J. E. O. and T. J. Davies (1987). "Diametral compression of silicon nitride." Mater. Sci. Eng. **96**: 109-116.
- Palmqvist, S. (1962). "Occurrence of crack formation during Vickers indentation as a measure of the toughness of hard metals." Arch. Eisenhuettenwes **33**: 629-633.
- Pantarotto, D., M. Prato and A. Bianco (2004). "Translocation of bioactive peptides across cell membranes by carbon nanotubes." Chem. Commun. **1**: 16-17.
- Patel, N., I. R. Gibson, S. Ke, S. M. Best and W. Bonfield (2001). "Calcining influence on the powder properties of hydroxyapatite." J. Mater. Sci.: Mater. Med. **12**: 181-188.
- Peigney, A. (2003). "Tougher ceramics with nanotubes." Nat. Mater. **2**: 15-16.
- Perdok, W. G., J. Christoffersen and J. Arends (1987). "The thermal lattice expansion of calcium hydroxyapatite." J. Crystal Growth **80**: 149.
- Posner, A. S., A. Perloff and A. F. Diorio (1958). "Refinement of the hydroxyapatite structure." Acta Crystallogr. **11**: 308-309.
- Price, R. L., M. C. Waid, K. M. Haberstroh and T. J. Webster (2003). "Selective bone cell adhesion on formulations containing carbon nanofibers." Biomater. **24**: 1877-1887.
- Pulskamp, K., S. Diabate and H. Krug (2007). "Carbon nanotubes show no sign of acute toxicity but induce intracellular reactive oxygen species in dependence on contaminants." Toxicol. Lett. **168**: 58-74.

- Radin, S. R. and P. Ducheyne (1992). "Plasma spraying induced changes of calcium phosphate ceramic characteristics and the effect on in vitro stability." J. Mater. Sci.: Mater. Med. **3**: 33-42.
- Rao, R. and T. S. Kannan (2002). "Synthesis and sintering of hydroxyapatite-zirconia composites." Mater. Sci. and Eng. C **20**: 187-193.
- Recum, A. v. and T. v. Kooten (1995). "The influence of micro-topography on cellular response and the implications for silicone implants." J. Biomater. Sci. - Polymer Ed. **7**: 181-198.
- Rosa, A., M. Beloti, R. vanNoort, P. Hatton and A. Devlin (2002). "Surface topography of hydroxyapatite affects ROS17/2.8 cells response." Pesqui Odontol. Bras. **16**: 209-215.
- Roy, D. M. and S. K. Linneham (1974). "Hydroxyapatite formed from coral skeletal carbonate by hydrothermal exchange." Nature **247**: 220-227.
- Ruoff, R. S. and D. C. Lorents (1995). "Mechanical and thermal properties of carbon nanotubes." Carbon **33**: 925-930.
- Ruys, A. J., A. Brandwood, B. K. Milthorpe, M. R. Dickson, K. A. Zeigler and C. C. Sorrell (1995). "The Effects of Sintering Atmosphere on the Chemical Compatibility of Hydroxyapatite and Particulate Additives at 1200-Degrees-C." J. Mater. Sci.-Mater. Med. **6**: 297-301.
- Ruys, A. J., N. Ehsani, B. K. Milthorpe and C. C. Sorrell (1993). "Effects of nonoxide additions on the decomposition and densification of hydroxyapatite." J. Aust. Ceram. Soc. **29**: 65-69.
- Ruys, A. J., B. K. Milthorpe and C. C. Sorrell (1994). "Preparation of fibre-reinforced hydroxylapatite." Interceram. **43**: 7-9.
- Ruys, A. J., M. Wei, C. C. Sorrell, M. R. Dickson, A. Brandwood and B. K. Milthorpe (1995). "Sintering effects on the strength of hydroxyapatite." Biomater. **16**: 409-415.
- Ruys, A. J., K. A. Zeigler, B. K. Milthorpe and C. C. Sorrell (1992). Ceramics: adding the value. Austceram 92, Australia, CSIRO. 591, 598-604.
- Salvetat, J. P., A. J. Kulik, J. M. Bonard, G. A. D. Briggs, T. Stockli, K. Metenier, S. Bonnamy, F. Beguin, N. A. Burnham and L. Forro (1999). "Elastic modulus of ordered and disordered multiwalled carbon nanotubes." Adv. Mater. **11**: 161-165.

- Santos, E. D., M. Farina, G. Soares and K. Anselme (2009). "Chemical and topographical influence of hydroxyapatite and B-tricalcium phosphate surfaces on human osteoblastic cell behavior." J. Biomed. Mater. Res. A **89**: 510-520.
- Sargin, Y., M. Kizilyalli, C. Telli and H. Guler (1997). "A new method for the solid-state synthesis of tetracalcium phosphate, a dental cement: X-ray powder diffraction and IR studies." J. Eur. Ceram. Soc. **17**: 963-970.
- Sayes, C. M., J. D. Fortner, W. Guo and D. Lyon (2004). "The differential cytotoxicity of water-soluble fullerenes." Nano Lett. **4**: 1881-1887.
- Sayes, C. M., F. Liang, J. L. Hudson, J. Mendez, W. Guo, J. M. Beach, V. C. Moore, C. D. Doyle, J. L. West, W. E. Billups, K. D. Ausman and V. L. Colvin (2006). "Functionalization density dependence of single-walled carbon nanotubes cytotoxicity in vitro." Toxicol. Lett. **161**: 135-142.
- Shi, D. and W. Xuejun (2006). Bioactive ceramics: structure, synthesis, and mechanical properties. Introduction to biomaterials. D. Shi. Beijing, Tsinghua University Press: 13-28.
- Siegel, R. W., S. K. Chang, B. J. Ash, J. Stone, P. M. Ajayan, R. W. Doremus and L. S. Schadler (2001). "Mechanical behavior of polymer and ceramic matrix nanocomposites." Scripta Mater. **44**: 2061-2064.
- Singh, R., D. Pantarotto, L. Lacerda, G. Pastorin, C. Klumpp, M. Prato, A. Bianco and K. Kostarelos (2006). "Tissue biodistribution and blood clearance rates of intravenously administered CNT radiotracers." Proc. Natl. Acad. Sci. **103**: 3357-3362.
- Slosarczyk, A., C. Paluszkiwicz, M. Gawlicki and Z. Paszkiewicz (1987). Ceram. Inter. **23**: 297-304.
- Smart, S. K., A. I. Cassady, G. Q. Lu and D. J. Martin (2006). "The biocompatibility of carbon nanotubes." Carbon **44**: 1034-1047.
- Suchanek, W. and M. Yoshimura (1998). "Processing and properties of hydroxyapatite-based biomaterials for use as hard tissue replacement implants." J. Mater. Res. **13**: 94-117.
- Takagi, M., M. Mochida, N. Uchida, K. Saito and K. Uematsu (1992). "Filter cake forming and hot isostatic pressing for TZP-dispersed hydroxyapatite composite." J. Mater. Sci.: Mater. Med. **3**: 199-203.

- Tancred, D. C., A. J. Carr and B. A. O. McCormack (2001). "The sintering and mechanical behavior of hydroxyapatite with bioglass additions." J. Mater. Sci.: Mater. Med. **12**: 81-93.
- Tasis, D., N. Tagmatarchis, A. Bianco and M. Prato (2006). "Chemistry of carbon nanotubes." Chem. Rev. **106**: 1105-1136.
- Thomas, M. B., R. H. Doremus, M. Jarcho and R. L. Salsbury (1980). "Dense Hydroxylapatite - Fatigue and Fracture Strength after Various Treatments, from Diametral Tests." J. Mater. Sci. **15**: 891-894.
- Thostenson, E. T., Z. Ren and T. W. Chou (2001). "Advances in the science and technology of carbon nanotubes and their composites: a review." Comput. Sci. Technol. **61**: 1899-1912.
- Trombe, J. C. and G. Montel (1978). "Some features of the incorporation of oxygen in different oxidation states in the apatitic lattice, I: On the existence of calcium and strontium oxyapatites." J. Inorg. Nucl. Chem. **40**: 15-21.
- vanAnduyt, P., F. Li, J. P. Keustermans, J. M. Streydio, F. Delannay and E. Munting (1995). "The influence of high sintering temperatures on the mechanical properties of hydroxylapatite." J. Mater. Sci.: Mater. Med. **6**: 8-13.
- Vijayalakshmi, U. and S. Rajeswari (2006). "Preparation and characterization of microcrystalline hydroxyapatite using sol gel method." Trends Biomater. Artif. Organs **19**: 57-62.
- Wagner, H. D., O. Lourie and Y. Feldman (1998). "Stress-induced fragmentation of multi walled carbon nanotubes in a polymer matrix." Appl. Phys. Lett. **72**: 188-190.
- Wang, M. and W. Bonfield (2001). "Chemically coupled hydroxyapatite-polyethylene composite: structure and properties." Biomater. **22**: 1311-1320.
- Wang, P. E. and T. K. Chaki (1993). "Sintering Behavior and Mechanical-Properties of Hydroxyapatite and Dicalcium Phosphate." J. Mater. Sci.-Mater. Med. **4**: 150-158.
- Wang, T., A. Dorner-Reisel and E. Muller (2004). "Thermogravimetric and thermokinetic investigation of the dehydroxylation of a hydroxyapatite powder." J. Eur. Ceram. Soc. **24**: 693-698.
- Wang, Z. W., M. D. Shirley, S. T. Meikle, R. L. D. Whitby and S. V. Mikhalovsky (2009). "The surface acidity of acid oxidised multi-walled carbon nanotubes and the influence of in-situ generated fulvic acids on their stability in aqueous dispersions." Carbon **47**: 73-79.

- Warren, R. (1992). Fundamental aspects of the properties of ceramic-matrix composites. Ceramic matrix composites. R. Warren. New York, Chapman & Hall: 64-114.
- Weng, W. and J. L. Baptista (1998). "Sol-gel derived porous hydroxyapatite coatings." J. Mater. Sci.: Mater. Med. **9**: 159-163.
- White, A. A., S. M. Best and I. A. Kinloch (2007). "Hydroxyapatite-carbon nanotube composites for biomedical applications: A review." Intl. J. Appl. Ceram. Technol. **4**: 1-13.
- Wong, E. W., P. E. Sheehan and C. M. Lieber (1997). "Nanobeam mechanics: elasticity, strength, and toughness of nanorods and nanotubes." Science **277**: 1971-1975.
- Worle-Knirsch, J. M., K. Pulskamp and H. F. Krug (2006). "Oops they did it again! Carbon nanotubes hoax scientists in viability assays." Nano Lett. **6**: 1261-1268.
- Wu, J. M. and T. S. Yeh (1988). "Sintering of Hydroxylapatite Zirconia Composite-Materials." J. Mater. Sci. **23**: 3771-3777.
- Xia, Z., L. Riester, W. A. Curtin, H. Li, B. W. Sheldon, J. Liang, B. Chang and J. M. Xu (2004). "Direct observation of toughening mechanisms in carbon nanotube ceramic matrix composites." Acta Mater. **52**: 931-944.
- Xu, J. L., K. A. Khor, J. J. Sui and W. N. Chen (2009). "Preparation and characterization of a novel hydroxyapatite/carbon nanotubes composite and its interaction with osteoblast-like cells." Mater. Sci. Eng. C-Biomimetic Supramol. Syst. **29**: 44-49.
- Yao, N., V. Lordi, S. X. C. Ma, E. Dujardin, A. Krishnan, M. M. J. Treacy and T. W. Ebbesen (1998). "Structure and oxidation patterns of carbon nanotubes." J. Mater. Res. **13**: 2432-2436.
- Ye, J., X. Shi, W. Jones, N. Rojanasakul, N. Cheng and D. Cheng (1999). "Critical role of glass fiber length in TNF-alpha production and transcription factor activation in macrophages." Amer. J. Physiol. **276**: 426-434.
- Yu, M. F., O. Lourie, M. J. Dyer, K. Moloni, T. F. Kelly and R. S. Ruoff (2000). "Strength and breaking mechanism of multiwalled carbon nanotubes under tensile load." Science **287**: 637-640.
- Yu, R., L. Chen, Q. Liu, J. Lin, K. L. Tan, S. C. Ng, H. S. O. Chan, G. Q. Xu and T. S. A. Hor (1998). "Platinum deposition on carbon nanotubes via chemical modification." Chem. Mater. **10**: 718-722.

- Yubao, L., C. P. A. T. Klein, Z. Xingdong and K. d. Groot (1993). "Relationship between the colour change of hydroxyapatite and the trace element manganese." Biomater. **14**: 969-972.
- Zanello, L. P., B. Zhao, H. Hu and R. C. Haddon (2006). "Bone cell proliferation on carbon nanotubes." Nano Lett. **6**: 562-567.
- Zhan, G. D., J. D. Kuntz, J. Wan and A. K. Mukherjee (2003). "Single-wall carbon nanotubes as attractive toughening agents in alumina-based nanocomposites." Nat. Mater. **2**: 38-42.
- Zhang, X., G. H. M. Gubbels, R. A. Terpstra and R. Metselaar (1997). "Toughening of calcium hydroxyapatite with silver particles." J. Mater. Sci. **32**: 235-243.
- Zhao, B., H. Hu, S. K. Mandal and R. C. Haddon (2005). "A bone mimic based on the self-assembly of hydroxyapatite on chemically functionalized single-walled carbon nanotubes." Chem. Mat. **17**: 3235-3241.
- Zhao, L. P. and L. Gao (2004). "Novel in situ synthesis of MWNTs-hydroxyapatite composites." Carbon **42**: 423-426.